THE UNIVERSITY *of* EDINBURGH

THE UNIVERSITY *of* EDINBURGH

Additive manufacturing of carbon fibre reinforced polyphenylene sulphide composites

Yahui Lyu

A thesis submitted in accordance with the requirements for the degree of

Doctor of Philosophy

The University of Edinburgh

Institute for Materials and Processes, School of Engineering

February 2024

Declaration

I hereby declare that this submission is my own work, and it contains no material written by another person, nor material which to a substantial extent has been accepted for the award of any other degree or diploma of any other educational institution. Any contribution made to the research by others, with whom I have worked at this or any other educational institution, is explicitly acknowledged in the thesis. I also declare that the intellectual content of this thesis is the product of my own work, except where work which has formed part of jointly authored publications has been included. In these cases, I have clearly identified my contribution to the joint work.

The work presented in Chapter 3 was previously published in *Journal of Composite Materials: Effects of thermal process conditions on crystallinity and mechanical properties in material extrusion additive manufacturing of discontinuous carbon fibre reinforced polyphenylene sulphide composites* by Lyu, Y. (author of the declaration), Wu, J., Zhang, H., Brádaigh, C. M. Ó., & Yang, D. (supervisor). This study was conceived by the author of the declaration and her supervisor. I carried out all the experiment, characterisation, data analysis and writing in this work.

The work presented in Chapter 4 was previously published in *Journal of Cleaner Production: Improving the interfacial adhesion between recycled carbon fibres and polyphenylene sulphide by bio-inspired dopamine for advanced composites manufacturing* by Lyu, Y. (author of the declaration), Koutsos, V., Brádaigh, C. M. Ó., & Yang, D. (supervisor). This study was conceived by the author of the declaration and her supervisor. I carried out all the experiment, characterisation, data analysis and writing in this work.

Signed:

Acknowledgements

First and foremost, I would like to give my deepest gratitude to my principal supervisor, Dr. Dongmin Yang, for his unwavering support and guidance throughout my doctoral journey. His innumerable insightful comments and steadfast encouragement have been invaluable. I am also grateful to my co-supervisors, Prof. Conchúr M. Ó Brádaigh and Prof. Vasileios Koutsos, for their constructive feedback and guidance on my doctoral projects.

I owe a debt of gratitude to the University of Edinburgh for the financial assistance provided through the Edinburgh Global Research Scholarship and the Principal's Career Development Scholarship. This support was crucial in the successful completion of my PhD studies and the crafting of this thesis.

Special appreciation is extended to Dr. Chun Wang at the University of Leeds for her assistance with the nanoindentation experiments detailed in Chapter 5. My sincere thanks go to my peers Aonan Li, Haoqi Zhang, Jiang Wu, Junaid Qayyum, and Shuai Wang, for their invaluable assistance throughout my PhD project. I am also grateful to Colin Robert, John Blackhurst, Fergus Dingwall, and Andrew Brown for their indispensable support in the laboratory.

I wish to acknowledge the assistance of Stephen Mitchell from the School of Biological Sciences Electron Microscopy unit at Edinburgh, supported by the Wellcome Multi User Equipment Grant (WT104915MA), for the electron microscopy work. My thanks also to Andrey Gromov at the School of Chemistry for the Raman Spectroscopy assistance, and to Stephen Francis at the University of St Andrews for his help with XPS.

Last but not least, I must express my heartfelt gratitude to my family. Their enduring love and presence have been a pillar of strength and inspiration throughout my PhD journey, significantly contributing to the fruition of my project.

Abstract

The emergence of high-performance carbon fibre reinforced thermoplastic (CFRTP) manufactured through material extrusion-based additive manufacturing (AM) techniques has gained special attention for its geometric flexibility, cost-effectiveness, and elimination of multiple processing tools. This thesis investigates the material extrusion-based AM of carbon fibre reinforced polyphenylene sulphide (CF/PPS) composites, focusing on thermal process conditions, fibre-matrix adhesion, interlaminar properties and sustainable printing, to produce high-performance CF/PPS composite parts suitable for high-end applications.

Initially, this study examines the thermal behaviour of discontinuously reinforced CF/PPS, manufactured additively through material extrusion. It centres on how thermal process conditions affect the degree of crystallinity, oxidation crosslinking, and mechanical properties of CF/PPS from filament fabrication and material extrusion to annealing treatment. Adjusting thermal treatment conditions allows for the design, control, and tailoring of crystallinity and mechanical properties in the printed CF/PPS composites.

Secondly, the study introduces an innovative one-step bio-inspired method, employing the copolymerisation of dopamine to graft silica nanoparticles onto carbon fibre surfaces. Extensive experimentation was conducted to fabricate these modified fibres and characterise the treated samples, assessing surface morphology and functional groups. The findings indicate that the polydopamine/silica nanoparticle (PDA/NPs) network significantly enhances interlaminar shear strength by 28.4% in the resultant composites. Additionally, dynamic mechanical analysis confirms robust interfacial bonding at the fibre-matrix interface, exhibiting impressive thermal cycling resistance.

Furthermore, this study explores the combined effects of pre-processing continuous carbon fibre (CCF) treatment with PDA/NPs network and post-processing printed parts with hot press

compaction on the intralaminar attributes of 3D printed CCF/PPS. Results reveal marked improvements in interlaminar properties, with flexural strength and interlaminar shear strength (ILSS) increasing by 27% and 172%, respectively, compared to untreated samples. Molecular dynamics (MD) simulations and nano-indentation tests elucidate the mechanisms underlying the enhanced interfacial adhesion, attributed from PDA/NPs network on CCF. Differential scanning calorimetry (DSC) and microscopic analysis are employed to evaluate improvements in crystallinity and void content following post-processing. Additionally, this study introduces an innovative post-processing technique that utilises a salt bath, which is particularly advantageous for complex structures.

Lastly, this study establishes a basis for a sustainable in-situ remanufacturing system, integrating with 3D overprinting techniques. It examines the mechanical properties of reclaimed carbon fibre from commercial thermosetting composites and reshaped carbon fibre from printed thermoplastic composites, both with and without surface treatment. Moreover, reshaped short carbon fibre reinforced PPS composites, exhibiting enhanced performance, were repurposed in an in-situ repair process alongside original continuous carbon fibre filaments. The efficacy of in-situ bonding patches was tested on damaged open-hole PA6 laminates through tensile tests, with real-time failure analysis conducted using digital image correlation (DIC).

Overall, this thesis provides a comprehensive exploration into the additively manufactured CF/PPS composites, addressing critical aspects such as low degree of crystallinity of PPS polymer during the printing process, weak interfacial adhesion between carbon fibre and polymer matrix and poor interlaminar properties of printed CCF/PPS laminates. These approaches demonstrate significant improvements in mechanical properties and structural integrity, fulfilling the potential of additive manufacturing in producing high-quality, sustainable composites for engineering applications.

Keywords:

Material extrusion additive manufacturing; carbon fibre; polyphenylene sulphide; interfacial property; interlayer property; sustainable printing.

Lay summary

This thesis explores the 3D printing of carbon fibre reinforced thermoplastic (CFRTP) composites. CFRTP is a type of material that is lightweight yet strong, and it has been widely used in industries such as automotive and aerospace. 3D printing technology offers the advantages in manufacturing CFRTP, including flexible design, cost reduction and less material waste. The main focus of this study is on a specific type of CFRTP, combining carbon fibres with a polymer known as polyphenylene sulphide (PPS). PPS is a high-performance polymer with superior mechanical strength and better printability, due to its relatively low viscosity compared to other high-performance polymers. The goal of this study is to additively manufactured high-quality carbon fibre reinforced polyphenylene sulphide (CF/PPS) composites for high-end applications.

The study first focused on how heating factors affect the material properties under different thermal process conditions, included the extrusion process, 3D printing process and annealing process. By adjusting the temperature, the polymer composites could become more crystalline, leading to higher mechanical strength. Next, this study applies a bio-inspired approach to modify the surface of commercial carbon fibre (CF). This approach involves the deposition of a new layer containing polydopamine (PDA) and silica nanoparticles (SiO_2) onto the CF surface. The interfacial laminar strength (ILSS) could be increased by nearly 30%. Furthermore, the study examined the combined effect of a pre-processing method with the bio-inspired structures and a post-processing method involving hot press compaction on the 3D printed continuous carbon fibre reinforced polyphenylene sulphide (CCF/PPS). As a result, the ILSS could be increased up to 172% stronger. Lastly, this research explored sustainable options in CFRTP repair. The mechanical properties of 3D printed PPS composites reinforced by recycled CF (rCF/PPS) were tested and evaluated. A novel in-situ composite repair approach using 3D overprinting technology with rCF/PPS and CCF/PPS was also explored.

Table of Contents

List of Figures

List of Tables

Chapter 1 **Introduction**

1.1 **Research motivation**

The utilisation of carbon fibre reinforced thermoplastic (CFRTP) is increasingly widespread, attributed to its distinct advantages such as shorter cycle times, enhanced impact resistance, recyclability, and an indefinite shelf life. These benefits sharply contrast with the limitations inherent in thermoset composites. A prime example is the Gulfstream G650 aircraft, which employs lightweight and cost-effective carbon-fibre reinforced polyphenylene sulphide (PPS) in its tail parts, resulting in a weight reduction of 10% and a cost reduction of 20% (shown in Figure 1-1) [1]. PPS polymer is recognised for its semi-crystalline matrix, characterised by high service temperatures, superior mechanical strength, excellent chemical resistance, and effective flame retardation. Additionally, it is more commercially accessible than other high-performance semi-crystalline polymers like PEEK or PEKK, or amorphous polymers such as PEI.

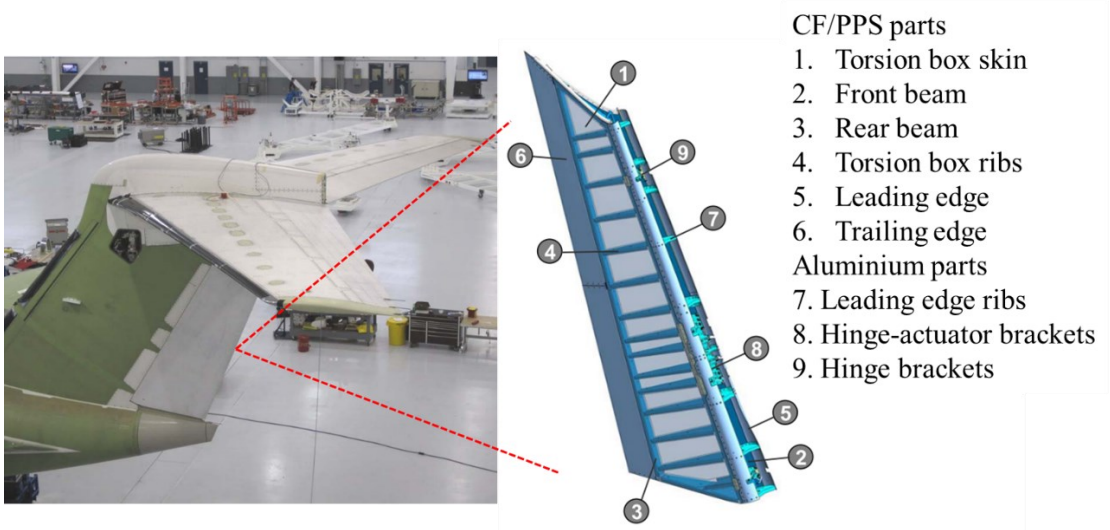

Figure 1-1 G650 Elevators and rudder assembled on the prototype aircraft and G650 rudder design [1].

The fabrication of thermoplastic composites via additive manufacturing (AM) methods, especially using the fused deposition modelling (FDM) technique, has recently seen a surge in popularity. This growing interest stems from its exceptional flexibility in crafting complex geometries and its cost-effectiveness. The growing field of AM with high-performance CFRTP offers potential opportunities for research, particularly in optimising the mechanical properties for high-end applications while maximising the advanced capabilities of AM technologies.

Four primary knowledge gaps were found upon reviewing the recent literature on this research topic. First, the influence of thermal history on the behaviour of CF/PPS materials remains inadequately explored. Second, the weak interface between carbon fibres and thermoplastic polymers presents a significant challenge. Third, there is a need for an intensified focus on refining pre-processing and post-processing techniques. Lastly, the advancement of 3D overprinting techniques offers promising prospects for the in-situ fabrication of repair patches.

The thermal history is crucial in determining the degree of the crystallinity within semi-crystalline polymers. The complexity of thermal conditions, encompassing melting and deposition associated with thermal history, is likely to affect the entanglement of polymer chains in the printed components. This, in turn, may play an important role in crystal formation and the establishment of three-dimensional networks within the polymer chains. While extant studies have focused on the various aspects of AM concerning CF/PPS composites including printing parameters, as well as rheological and thermal properties [2–4], there is a requirement for future research to probe the impacts of thermal history, spanning extrusion, printing, and post-printing treatments, on polymer crystallinity and oxidation dynamics. This study aims to get a comprehensive understanding how thermal history influences the mechanical behaviour of deposited polymers through a variation of process parameters.

Moreover, the insufficient interfacial adhesion between carbon fibre and thermoplastic matrix significantly hampers the broader application of CF/PPS composites. Many researchers have reported the utilisation of conventional chemical modifications and physical treatments or a combination to alter the inherently non-polar carbon fibre surface [5–7]. Existing approaches typically involves oxidising the surface or applying plasma treatment to introduce functional group, followed by the grafting coupling agents or the addition of compatibilisers. While these techniques have proven effective, they frequently depend on organic solvents like chloroform and dichloromethane [8], or strong oxidising agents such as hydrochloric acid (HCL) [9], nitric acid (HNO_3) [10], and sodium hydroxide (NaOH) [11]. In addition, these approaches may also require energy-consuming equipment and cause the potential reduction in the mechanical strength of carbon fibre. Therefore, some scholars have increasingly shifted their attention to green solutions, such as advanced nanoparticles and bio-inspired constructs like polydopamine (PDA). Although many studies have focused on the application of PDA to attach functional groups onto the carbon fibre [12–14], there remains a gap in the literature regarding the application of this innovative, sustainable method to recycled carbon fibres and high-temperature thermoplastics such as PPS. To address this, our research is committed to develop a more environmentally sustainable, single-step treatment method that substantially enhances interfacial adhesion.

Furthermore, the defects between interlayers, perpendicular to the print direction, is another critical issue that needs to be addressed in the printed parts. The bulk of the previous research have focus on the in-situ interference methods, including optimising the printing parameters and consolidation during the printing process [15–17]. However, the optimisation of the layer thickness, fibre orientation and printing speed is generally limited to certain printing materials, and in-situ consolidation introduce excessive pressure, potentially damaging the print path and harming surface quality. Therefore, there is a need for more research to focus on the versatile

pre-processing and post-processing method. Pre-processing methods consist of new layer sizing and pre-impregnation, as well as innovative combination of these methods, to greatly improve the interlaminar shear strength [18–20]. Post-processing techniques, such as thermal annealing and hot press compaction, are subsequently employed to mitigate the void formation and strengthen inter-layer bonding [21–23]. This work aims to further integrate the pre-processing approach of commercial carbon fibre by bio-inspired PDA and post-processing techniques through hot press compaction. Additionally, the exploration in the hot pressing for the complex structures is warranted to fully align with the strengths of 3D printing.

Lastly, 3D printing has been investigated as a novel approach for repairing damaged composites. While most studies involve the separate manufacturing of carbon fibre patches [24–26], this technology holds great potential for in-situ repairs using the overprinting techniques on the existing structures. This process involves depositing repair material on a heated surface of the damaged structures. This study aims to establish a basic foundation for an in-situ remanufacturing system by investigating the recovered tensile strength of repaired composites through overprinting of hybrid patches comprising recycled and virgin composites. The process window for in-situ repairs is also defined by examining thermal characteristics.

1.2 Aims and objectives

1.2.1 Aims

This thesis aims to additively manufacture the high-performance CF/PPS composites by optimising the thermal process conditions for the polymer matrix, developing a surface modification strategy for carbon fibres and further enhancing the interlaminar properties for the composites. Subsequent to these developments, the thesis investigates the mechanisms underpinning these improvements and the applications of these advanced CF/PPS composites in in-situ composite repair.

1.2.2 **Objectives**

(1) Study on effects of thermal process conditions on crystallinity and mechanical properties in extrusion-based additive manufacturing of discontinuous carbon fibre reinforced PPS composites (sCF/PPS).

(2) Develop a one-step treatment method to enhance the interfacial bonding between carbon fibre and PPS matrix by mussel-inspired dopamine for advanced composites manufacturing.

(3) Enhance the interlaminar properties of printed dopamine treated continuous carbon fibre reinforced polyphenylene sulphide composites

(4) Overprinting of continuous carbon fibre reinforced PPS (CCF/PPS) filament and reshaped discontinuous carbon fibre reinforced PPS (rCF/PPS) filament with a stable surface treatment for in-situ composites repair.

1.2.3 **Thesis structures**

The thesis is structured into seven chapters, encompassing Chapter 1: Introduction, Chapter 2: Literature Review, four chapters detailing the main research topics, and a final chapter presenting conclusions. The overall structure is depicted in Figure 1-2.

Chapter 1 introduces the research motivations, aims, and objectives. It provides a background on CFRTP composites and an overview of AM technologies, emphasising their relevance in the context of CF/PPS composites.

Chapter 2 offers a comprehensive literature review on topics related to polymers in 3D printed filaments, reinforced carbon fibres in 3D printed composites, fibre-matrix interface improvements, printing performance enhancements, and sustainable in-situ remanufacturing systems. Key knowledge gaps are identified in the summary section.

Chapter 3 details the investigation into the thermal behaviour of additively manufactured PPS composites reinforced with discontinuous carbon fibre. This chapter evaluates the impact of varying thermal conditions on the crystallinity and mechanical properties of the composites.

Chapter 4 introduces a bio-inspired method for carbon fibre surface treatment. Comprehensive investigations were undertaken to produce the treated carbon fibre and analyse the modified samples, focusing on surface morphology and functional groups. The effects of a polydopamine/silica nanoparticle network on interlaminar shear strength and thermal cycling resistance are assessed.

Chapter 5 studies the effects of pre-processing CF treatment with bio-inspired structures and the impact of post-processing techniques involving hot press compaction on the intralaminar properties of 3D printed CCF/PPS composites. Molecular dynamics (MD) simulations and nano-indentation tests were conducted to elucidate the mechanisms of interfacial adhesion.

Chapter 6 delves into the sustainable in-situ manufacturing approach combined with 3D overprinting technology. This chapter analyses the mechanical properties of 3D printed composites reinforced with reclaimed carbon fibre from commercial thermosetting resins and reshaped composites from additively manufactured thermoplastics. It also assesses the in-situ repair processes involving 3D overprinting of reshaped rCF/PPS and CCF/PPS on damaged laminates.

Chapter 7 provides a comprehensive presentation of the key findings and their significance. Recommendations for further research are also outlined in this chapter.

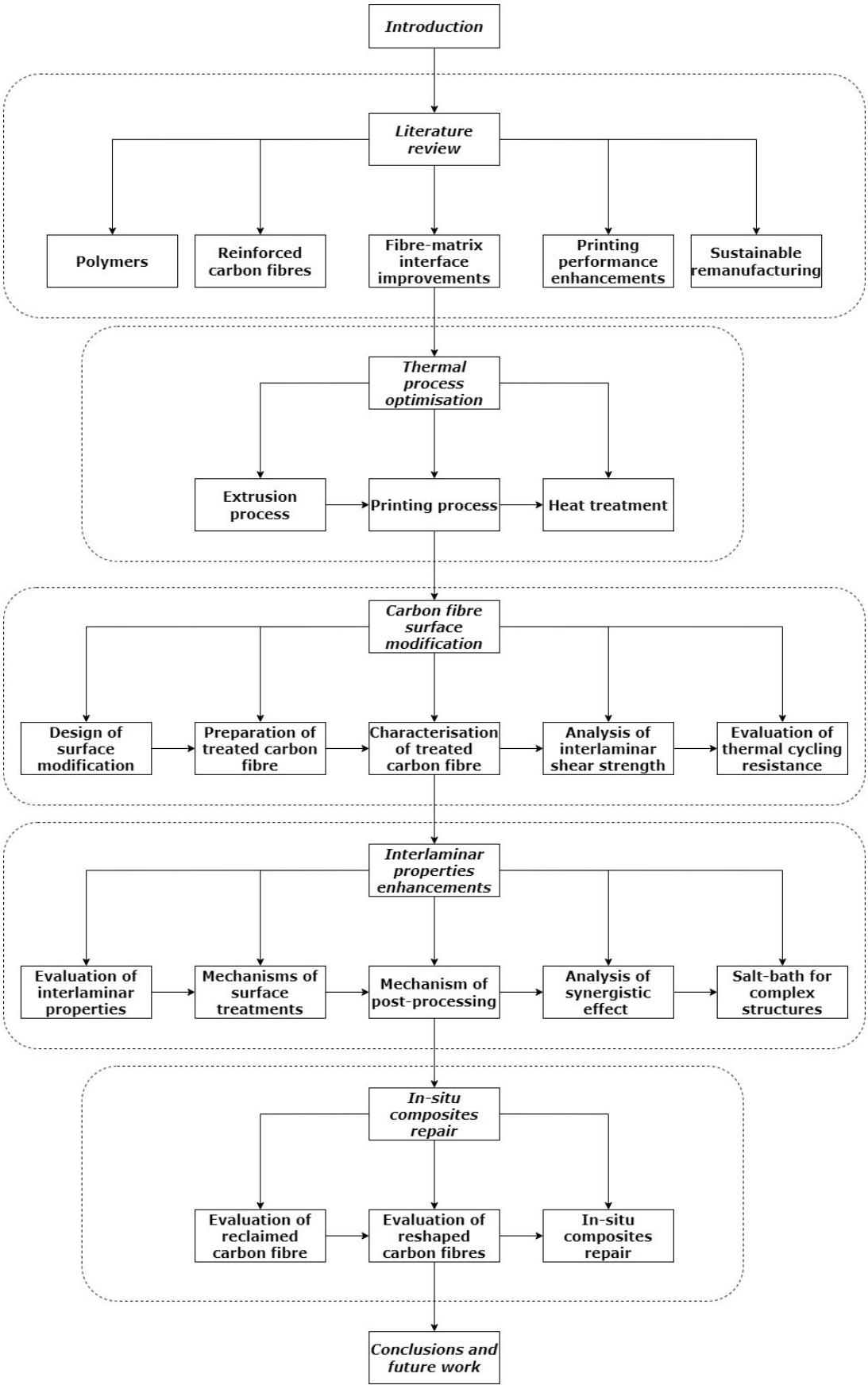

Figure 1-2 Overall structure of the thesis.

Chapter 2 Literature Review

2.1 Polymers for 3D printing filaments

2.1.1 Molecular chains and arrangements

3D printing technology, an additive manufacturing (AM) technique, constructs a variety of structures and complex geometries layer by layer from a three-dimensional (3D) geometric model. Charles Hull first developed this technology in 1986, pioneering the technique known as stereolithography (SL) [27]. Subsequently, inspired by Hull's innovation, several methods emerged, including Digital Light Processing (DLP), Laminated Object Manufacturing (LOM), Selective Laser Sintering (SLS), and Fused Deposition Modelling (FDM, also known as Fused Filament Fabrication, FFF). Of these AM techniques, FDM 3D printing, as a material extrusion (MEX) technique, has become the most prevalent, particularly for manufacturing polymeric products and their composites [28,29].

Polymers, the most common feedstock materials for FDM 3D printing, have been extensively explored in both industrial and academic settings. These polymers can be categorised into three types based on their molecular chains: linear, branched, and 3D networks of polymers, as depicted in Figure 2-1(a). In FDM 3D printing filaments, typical thermoplastic polymers such as polylactic acid (PLA), polyamide 6 (PA6), polyphenylene sulphide (PPS), and polyether ether ketone (PEEK) are classified as linear or semi-linear polymers. Conversely, commonly used polymers like atactic polypropylene (PP) and branched polyvinyl alcohol (PVA) are categorised as branched polymers (refer to Figure 2-1(b)). Linear polymers generally exhibit higher density, greater strength, a higher melting point, and a tendency to be semi-crystalline or crystalline. They are less soluble in solvents due to the close alignment and bonding of molecular chains. However, they pose processing challenges due to higher intermolecular

forces, often requiring higher melting temperatures. Additionally, linear polymers demonstrate better flow characteristics when melted, advantageous for the FDM process, where the polymer is extruded through a heated nozzle. In contrast, branched polymers display less predictable flow properties, potentially affecting the precision and quality of FDM printing.

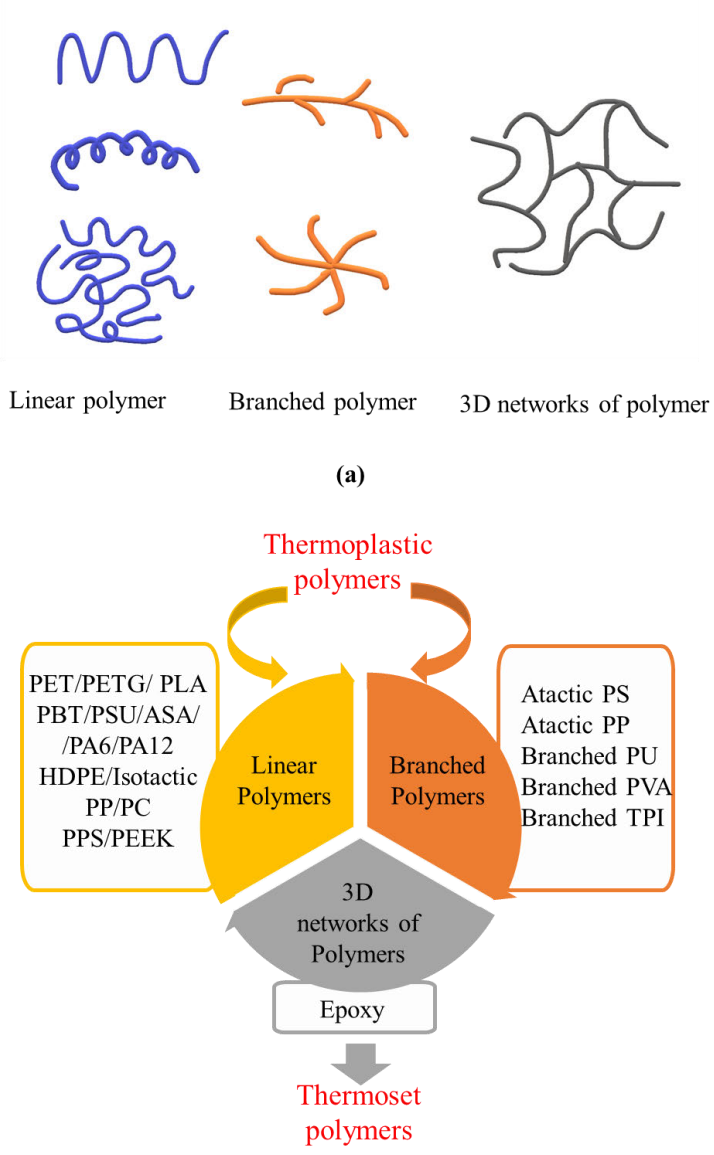

Figure 2-1 (a) Three types of molecular chains for polymers; (b) classification of polymers for FDM 3D printing based on molecular chains [30].

Figure 2-2 categorises FDM 3D printing polymers based on molecular arrangements into amorphous and semi-crystalline polymers. The molecular chains in amorphous polymers are randomly arranged, whereas semi-crystalline polymers contain both amorphous (randomly arranged chains) and crystalline regions (ordered and closely packed chains). Generally, semi-crystalline polymers exhibit higher mechanical strength, greater rigidity, and enhanced chemical resistance compared to their amorphous counterparts, though amorphous polymers have superior impact resistance [31]. Additionally, semi-crystalline polymers are more resistant to creep and deformation under load. Amorphous polymers, lacking a sharp melting point, are easier to process in AM techniques. Conversely, semi-crystalline polymers necessitate more precise control of thermal processing temperatures.

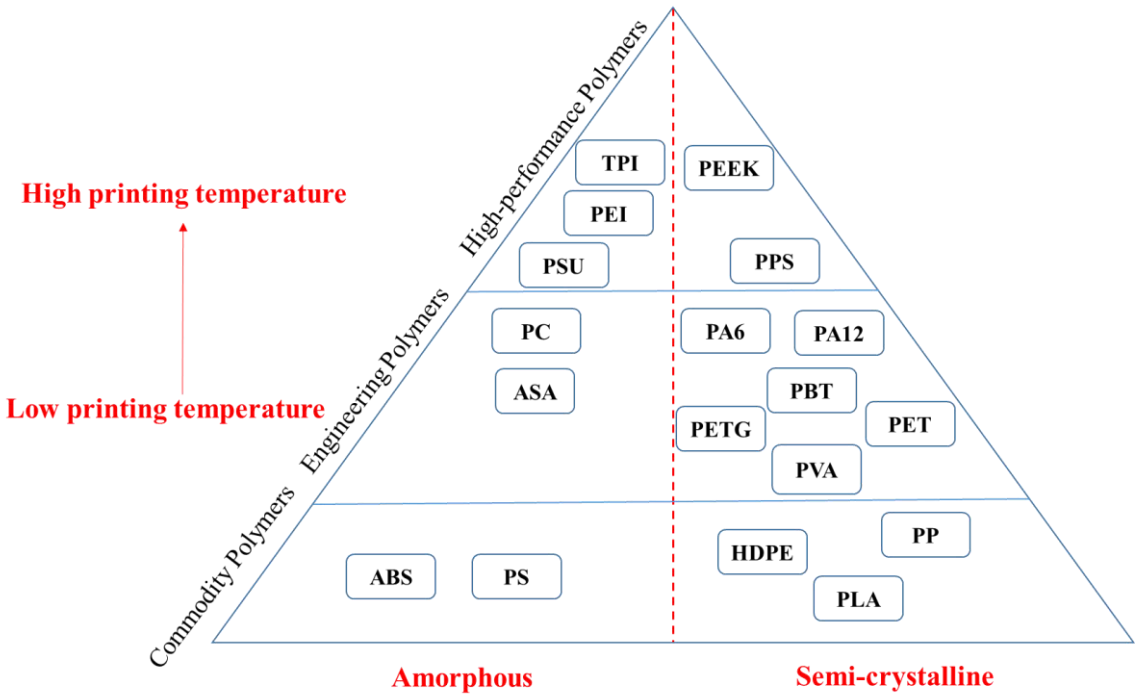

Figure 2-2 Classification of polymers for FDM 3D printing based on molecular arrangements [32].

2.1.2 **High performance semi-crystalline polymers**

PPS and PEEK are two principal high-performance semi-crystalline polymers, notable for their remarkable thermal and chemical properties. These attributes render them as intriguing feedstock materials for FDM printing. As a semi-crystalline polymer, the degree of crystallinity in material extrusion and 3D printing processes is influenced by complex thermal conditions, including melting and crystallisation processes. These conditions subsequently impact the tensile strength, fracture toughness, impact properties, and other mechanical properties [33]. Consequently, numerous studies have examined the effect of processing parameters on the final part crystallinity and the resulting mechanical properties of high-performance semi-crystalline materials such as PPS, as illustrated in Table 2-1.

Most previous studies on the material extrusion of PPS polymers have centred on investigating printing parameters. Kishore *et al*. [3] conducted experimental studies on the rheological and thermal properties of short CF/PPS composite, successfully extruding and printing the filament via a desktop printer. Fitzharris *et al*. [34] studied the fast scanning calorimetry (FSC) on FDM conditions and gained a deeper understanding of the as-processed structure of semi-crystalline polymers based on a three-phase model, including a mobile amorphous region (MAF), a rigid amorphous region (RAF), and a crystalline region. EI Magri *et al*. [35] reported that layer thickness was the most influential printing parameter on Young's modulus and the degree of crystallinity, suggesting an optimal thickness of 0.17 mm. Additionally, annealing treatment can significantly enhance the thermal, structural, and mechanical properties. Furthermore, Yeole *et al*. [36] investigated the processability, microstructure, and mechanical performance of twin-screw compound CF/PPS and compared it with other traditional processing methods. Geng *et al*. [37] found that thermal history profoundly affects the properties of printed PPS samples by studying the crystallinity and oxidative crosslinking. They noted that appropriate selection of heat treatment conditions could improve the mechanical properties of the printed

pure PPS samples. These scholars found that 3D printed composites could exhibit comparable properties to extrusion-compression moulding due to highly aligned fibres, but inferior mechanical properties compared to injection moulding, attributed to relatively higher porosity.

Recently, a Composites Additive Manufacturing Research Instrument (CAMRI) system was developed for printing high-performance PPS with 42.6 vol% carbon fibres. This system utilised a single screw extrusion system to replace the traditional molten extrusion system and used CF/PPS pellets as feedstock, significantly enhancing printing efficiency in large-scale deposition [38,39]. The CF/PPS with high carbon fibre loading by volume (33.1% to 52.7%) were investigated by thermal analysis, mechanical tests, rheological analysis and investigation of the crystal structures [40,41]. In addition, heat transfer, melting and crystallisation, layer adhesion, thermo-viscoelasticity and shrinkage process was modelled and characterised in extensive works to develop a fundamental understanding of the Extrusion Deposition Additive Manufacturing (EDAM) process for fibre reinforced PPS composites [4,42–44].

In addition, several studies have been reported on other semi-crystalline polymers such as PEEK and poly(ethylene terephthalate) (PET). Yang *et al*. [45] illustrated the relationship between the thermal processing conditions and the crystallinity and mechanical properties of pure PEEK materials. Results show that printed parts with different degrees of crystallinity or different crystallinity regions in the same part can be designed and realised by controlling the heat treatment process. Voorde *et al*. [46] optimised the extrusion parameters by conducting a thermal analysis of PET filaments. They investigated the effect of the degree of crystallinity on the mechanical properties of semi-crystalline PET, which proved that the printing parameters had a large effect on the degree of crystallinity and therefore on the mechanical properties of the printed PET samples.

Table 2-1 Summary of the reported FDM printed PPS polymers and their composites.

Source	Materials/Methods	Printing settings	Mechanical testing	Degree of crystallinity
Kishore, 2020 [3]	Neat PPS	327 ℃	1.49 GPa (G')	48.7/66.7(anneal)
	CF/PPS (33.1 vol%)	327 ℃	2.46 GPa (G')	43.9/67.1(anneal)
	CF/PPS (42.6 vol%)	337 ℃	2.61 GPa (G')	32.1/63.7(anneal)
	CF/PPS (52.7 vol%)	337 ℃	3.36 GPa (G')	51.7/61.7(anneal)
Fitzharris, 2019 [34]	As-printed PPS in monofilament	290℃/80℃	/	15.1
	Annealing 85℃/90℃/95℃			27.2/28.5/28.4
	Annealing 100℃/110℃/120℃			30.7/30.3/37.7
EI Magri, 2020 [35]	PPS from FILOALFA	320℃-340℃	51.6 MPa (Tensile)	38.6
	Annealing 180℃-1hr		61.1 MPa (Tensile)	43.4
	Annealing 200℃-1hr		63.1 MPa (Tensile)	51.3
	Annealing 220℃-1hr		60.1 MPa (Tensile)	40.3
Yeole, 2020 [36]	CF/PPS (42.6 vol%)	305℃-338℃	Tensile: 56.02 MPa Flexural:63.23 MPa ILSS:8.34 MPa	/
Geng, 2018 [37]	PPS A900-Air forced cooling/Natural cooling	285℃	※Tensile:28 MPa/39 MPa	19.13/35.43
	Heat treatment at 130℃/150℃		Tensile:40MPa/39MPa	42.28/42.75
	Heat treatment at 200℃/240℃		Tensile:45MPa/57MPa	50.04/64.08

2.1.3 **Polymer chain reptation mechanisms**

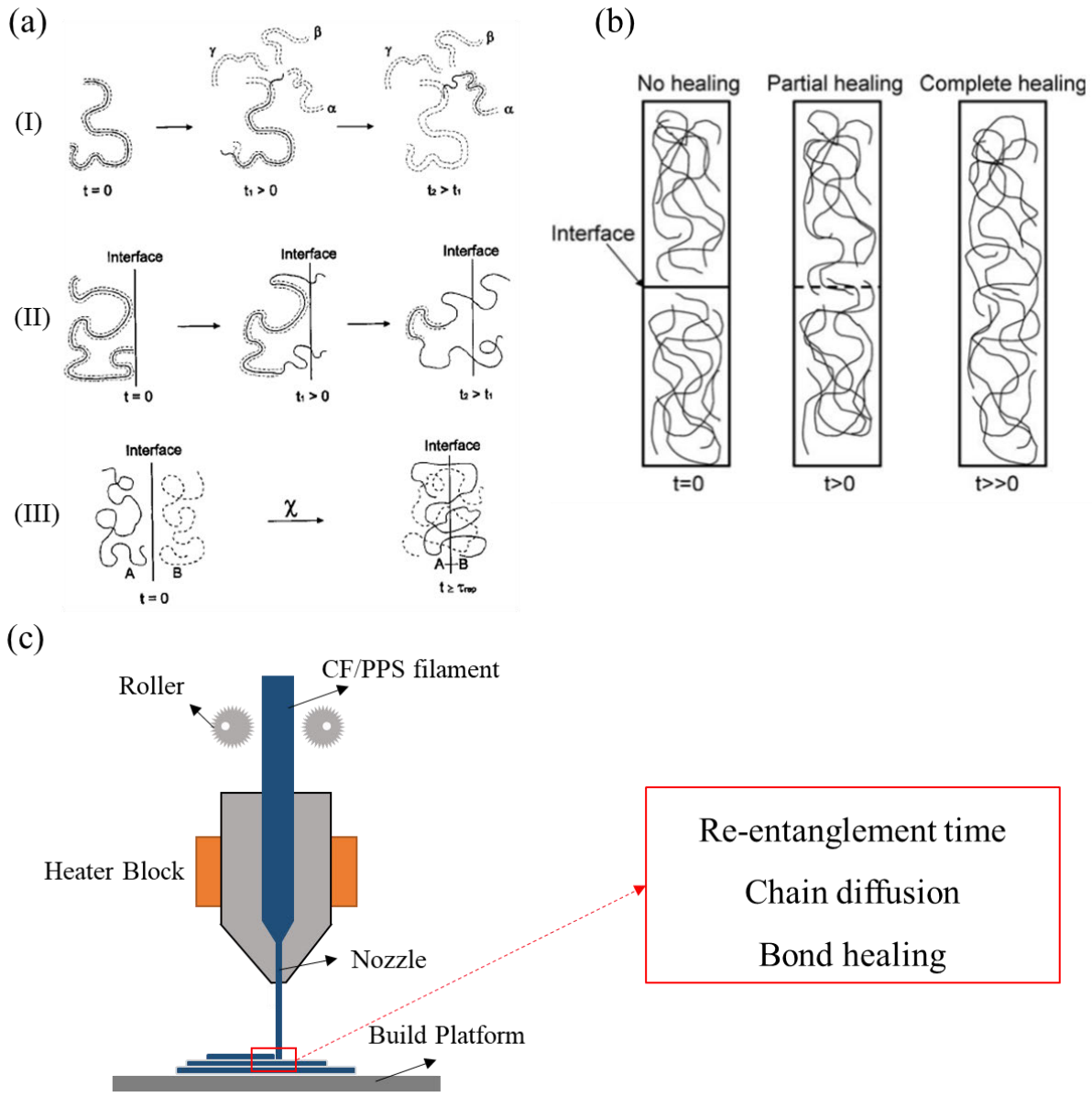

Figure 2-3 (a) Reptation mechanism illustrating molecular diffusion and chain randomisation at the interface during healing, with χ indicating the segment distance from the interface [47]; (b) detailed view of the polymer chain network and interlayer interactions during interface healing [48]; (c) analysis of data sets describing polymer melt behaviour during the deposition phase of the FDM process.

In the FDM printing, polymer layers solidify rapidly due to high cooling rates in the postdeposition process, a critical factor in shaping the mechanical properties along the axis perpendicular to the printing direction. Studies have shown that in this orientation, performance tends to be significantly lower compared to parts produced using conventional manufacturing techniques [23,49]. The lack of strong interfacial adhesion along the z-axis often leads to early failure when these parts are subjected to mechanical stress perpendicular to the printing direction.

The quality of interlayer bonding is determined by the dynamics of polymer chain movement, known as reptation, which affects how the polymers diffuse across the interfaces of the deposited layers [47]. Figures 2-3 depicts this process, highlighting that for complete bonding, polymer chains must first reorient and approach the surface (influenced by surface tension) before wetting the surface, diffusing across the interface, and ultimately achieving a state of equilibrium and randomisation. This final, healed state results from a combination of factors including surface wetting, the growth of the contact area (neck growth), and the diffusion and entanglement of polymer chains across the interface.

Pokluda *et al.* have developed a model to predict the expansion of the bond width, encapsulated by the following equations [50]:

The rate of change of the bond width, θ , over time is given by:

$$\frac{\mathrm{d}\theta}{\mathrm{d}t} = \frac{\frac{\Gamma}{a_0\mu}(2^{-5/3}\cos\theta\sin\theta(2-\cos\theta)^{1/3})}{(1-\cos\theta)(1+\cos\theta)^{1/3}} \tag{2-1}$$

Here θ is the bond width, and it is described as the inverse sine of the ratio of the neck radius x, to the particle radius, a:

$$\theta = \sin^{-1}\frac{x}{a} \tag{2-2}$$

In these equations, x denotes the radius of the neck time at the time t, μ stands for viscosity, a_0 is the initial particle radius, and Γ signifies the surface tension.

The final mechanical properties of the printed composites can be inferred from the welding strength as illustrated in the equation below [51]:

$$\frac{\sigma_{\text{weld}}}{\sigma_{UTS}} = \left(\frac{t_{\text{weld}}}{\overline{\tau}_{\text{rep}}}\right)^{1/4} = \left(\frac{t_{\text{weld}} \times D_s}{{R_g}^2}\right)^{1/4} \quad (2\text{-}3)$$

Here, σ_{weld} is the welding strength, σ_{UTS} is the ultimate tensile strength of the polymer, t_{weld} is the welding time, $\overline{\tau}_{\text{rep}}$ represents the time-averaged reptation time, and R_g is the radius of gyration.

In the standard FDM process, there is a limited time span, typically 2-3 seconds, for neck growth to occur when temperatures exceed the glass transition temperature (T_g) [52]. Consequently, the interdiffusion length remains shorter than the radius of gyration (R_g). This brief period for polymer chain diffusion leads to only partial healing, resulting in an incomplete restoration of the bulk properties of polymers.

Adjusting printing parameters that influence thermal history can markedly impact the formation of interlayer bonds. Expanding the duration for which the temperature remains above T_g is a frequent approach in the FDM process to enhance bonding. To better predict the rheological behaviour over an extended range of temperatures and times, we can refer to the Williams-Landel-Ferry (WLF) equation as detailed here [53]:

$$a_T(T) = \exp\left[\frac{-c_1(T - T_{ref})}{c_2 + (T - T_{ref})}\right] \quad (2\text{-}4)$$

The reptation time at a given temperature $\tau_{\text{rep}}(T)$ is related to the reptation time at a reference temperature by the shift factor:

$$\tau_{\text{rep}}(T) = \tau_{\text{rep}}(T_{\text{ref}}) \times a_T(T) \quad (2\text{-}5)$$

Where the $a_T(T)$ is the temperature-dependent shift factor that adjusts for changes in temperature, T is the current temperature under consideration, and the T_{ref} is the reference temperature where the shift factor equals one.

To quantify the require time to achieve the complete healing of polymer chains, a two-step shearing test with a specified relaxation time is conducted. The recovery rate could be calculated using the formula [51]:

$$\%\text{recovery} = \frac{[\tau_m(\dot{\gamma},t_r)-\tau_{ss}]/\tau_m(\dot{\gamma},t_r)}{[\tau_m(\dot{\gamma},\infty)-\tau_{ss}]/\tau_m(\dot{\gamma},\infty)} \quad (2\text{-}6)$$

In this equation, $\tau_m(\dot{\gamma},t_r)$ represents the stress overshoot after a given relaxation time, $\tau_m(\dot{\gamma},\infty)$ denotes the stress overshoot after infinite relaxation time, and τ_{ss} is the steady stress value.

These equations are essential for understanding the thermal and mechanical behaviour of polymers under different temperature conditions, especially relevant for polymers processed through FDM printing. The healing process and, consequently, the strength of interlayer bonding are influenced by the thermomechanical properties, rheological characteristics, and the specific thermal history imparted by the printing conditions. Research indicates that the printing temperature, the printing speed and annealing treatment can significantly affect the extent of polymer chain movement in the deposited layers, impacting the overall mechanical integrity of the finished product [54,55].

2.2 Reinforcing fibres for 3D printing filaments

2.2.1 Discontinuous fibres

Discontinuous carbon fibre, typically less than 1 mm in length, has been mixed into polymer matrices to fabricate 3D printed filaments, enhancing the mechanical properties for high-end

applications. Incorporating short carbon fibres into the polymer feedstock can increase thermal conductivity and mechanical strength and stiffness, while reducing thermal expansion and residual stress in the printed composites [46]. Moreover, short carbon fibres can improve friction and wear resistance, even compared to their continuous carbon fibre counterparts [47]. Extensive studies have investigated polymer composites reinforced with discontinuous carbon fibre for common thermoplastics, as listed in Table 2-2.

Ning *et al.* [56] were the first to prepare filaments from the extrusion of carbon fibre and acrylonitrile butadiene styrene (ABS), investigating the effect of carbon fibre on the mechanical properties of FDM printed ABS. It was found that adding discontinuous carbon fibre could enhance tensile strength and Young's modulus but might decrease toughness, yield strength, and ductility compared to pure polymer, with the highest flexural value at 3.8 vol% carbon fibre volume fractions (carbon fibre length is 150 μm). Additionally, composites with longer carbon fibre (150 μm) exhibited better tensile performance, while maintaining yield strength between longer and shorter carbon fibre (100 μm). It was also mentioned that porosity in the fabrication process was a major issue in decreasing mechanical properties in 9.1 vol.% carbon fibre composites.

Similarly, Jiang *et al.* [57] observed that carbon fibre addition significantly enhanced the elastic modulus for all four commercial filaments, including ABS, PLA, polyethylene terephthalate glycol (PETG) and Amphora. This study also considered printing orientation, reporting that printing at 0° orientation can align the carbon fibre mostly in the printing direction, leading to the greatest improvement. Interestingly, the addition of carbon fibre decreased the tensile properties of ABS and Amphora in other directions.

Table 2-2 Summary of the reported mechanical data of polymers composites with discontinuous carbon fibres.

Source	Samples	Tensile Modulus (GPa)	Tensile Strength (MPa)	Other Properties
Ning, 2015 [56]	CF/ABS			Porosity %
	Neat ABS	1.90	34.0	2.7
	CF/ABS (150 μm) 1.7/2.9/4.4/5.9/9.1 vol%	2.07/2.46/2.50 /2.15/2.27	40.7/42.5/42.0 /34.0/35.0	0.5/0.9/1.3/9/3.3
	CF/ABS (100 μm) 2.9 vol%	1.28	39.1	/
Jiang, 2017 [57]	CF/ABS-PLA-PETG-Amphora	0/45/90	0/45/90	Elongation %
	ABS	2.3/2.1/2.1	38.2/34.7/32.4	9.71/15.7/7.1
	CF/ABS (10.3 vol%)	7.15/3.09/3.03	50.9/29.2/27.3	1.36/2.54/1.64
	PLA	3.5/3.3/3.2	60/52.2/49.6	4.94/2.28/2.18
	CF/PLA (7.6 vol%)	9.28/5.2/4.61	68.4/54.6/43.7	1.28/1.69/1.29
	PETG	2.05/1.91/1.89	46.1/41.3/41.4	>25
	CF/PETG (13.8 vol%)	8.47/4.23/3.19	68.3/50.9/42.6	2.99/3.63/2.92
	Amphora	2.01/1.96/1.9	46.9/44.4/44.4	>25/17/13.7
	CF/Amphora (8.4 vol%)	3.93/2.63/2.45	49.3/42/40.5	2.95/6.28/2.61

	CF/PLA	0/45/90	0/45/90	
Ferreira, 2017 [58]	PLA	3.37/1.09/3.12	54.7/18/37.1	/
	CF/PLA (11.6 vol%)	7.54/1.27/3.92	53.4/18.9/35.4	
	CF/PA12			Thermal conductivity
Liao, 2018 [59]	PA12	0.96	48	0.22
	CF/PA12 (1.1/2.3/3.5/4.7/6.0 vol%)	1.43/1.96/2.79/3.35/3.59	52/58/78/84/86	0.25/0.42/0.62/0.70/0.85

Ferreira *et al.* [58] also concluded similar findings about fibre orientation. They noted that discontinuous carbon fibre tended to stay oriented in the material extrusion orientation during the FDM printing process. Furthermore, this study found that while tensile strength did not differ significantly, stiffness was greatly improved, primarily due to the very short length of chopped carbon fibres.

Liao *et al.* [59] also investigated the effect of carbon fibre with different volume fractions on 3D printed polyamide 12 (PA12) composites. The results indicated that the addition of 6.0 vol% CF could enhance flexural performance by 251.1%. Additionally, thermal conductivity was remarkably increased by discontinuous carbon fibre.

The tensile strength in fibre-reinforced composites is significantly influenced by the characteristics of discontinuous carbon fibres including length, volume fraction, and orientation [60,61]. The predicted tensile strength of composites (σ_t) can be expressed using modified Kelly-Tyson equation [62]:

$$\sigma_t = \nu_f \cdot \sigma_f \left[\left(\sum_{l_i=l_{min}}^{l_c} \left(\frac{l_i}{2l_c} \right) \right) + \sum_{l_c}^{l_c=l_{\max}} \left(1 - \frac{L_c}{2l_i} \right) \right] + \sigma_m (1 - \nu_f) \quad (2\text{-}7)$$

Where v_f is the fibre volume fraction, σ_f is the tensile strength of carbon fibre, l_c is the critical fibre length, and σ_m is tensile strength of the polymer matrix.

Regarding fibre length, the critical fibre length (l_c) is the minimum length required for the fibres to utilise their full-strength potential. This length can be determined by the equation [61]:

$$l_c = \frac{\sigma_f d}{2\tau_y} \tag{2-8}$$

Where d is the fibre diameter and τ_y is the shear strength of polymer matrix.

Fibre orientation also significantly impacts the tensile strength of composites. The relationship is calculated using the modified Tsai-Hill criterion, expressed as an angle ply lamina with off-axis tensile strength ($\sigma(\theta)$) [63]:

$$\sigma(\theta) = \left[\frac{cos^4\theta}{{\sigma_{11}}^2} + \left(\frac{1}{{\tau_{12}}^2} - \frac{1}{{\sigma_{22}}^2}\right) sin^2\theta\, cos^2\theta + \frac{sin^4\theta}{\sigma_{22}}\right]^{-\frac{1}{2}} \tag{2-9}$$

Where θ is the angle between fibre orientation and loading direction, σ_{11}, σ_{22} represent the longitudinal and transverse tensile strengths, respectively.

The shear strength of composites (τ_{12}) was calculated using the equation [64]:

$$\tau_{12} = \frac{\tau_m}{\left(1+v_f\right)^2} \tag{2-10}$$

Where τ_m is the shear strength of matrix.

In general, longer fibre length, higher fibre content and better alignment of short fibres in additive manufacturing led to improved thermal and mechanical properties of printed composites [48]. Therefore, material extrusion of high-performance polymer composites with a high volume of discontinuous carbon fibre is likely to grow in industries such as automotive, electronics, and aerospace, as well as other fields, due to its relatively low cost, accessible printing process, and feasible recycling process.

2.2.2 **Continuous fibres**

Continuous fibre filament represents a promising advancement in FDM 3D printing technology. Markforged developed its first version of a printer, the MarkOne, designed to deposit continuous fibre reinforced Nylon filaments. This technology has reported superior mechanical strengths of 700 MPa and a stiffness of 50 GPa in the printed parts. In this method, a continuous carbon fibre-reinforced polymer filament is anchored to the printing bed and fed through a heated nozzle. The filament is guided along the designed trajectory throughout the printing process. During printing, the filament transitions from a round to a rectangular cross-section. This change is accompanied by compression pressure to enhance the intralaminar in-fill degree and improve interlaminar adhesion. Table 2-3 summarises the reported mechanical data for continuous fibre composites. In 2016, Klift *et al.* [65] utilised this printer to manufacture CFRTP, recording a tensile strength of 464.4 MPa for specimens containing 6 CFRTP layers.

Matsuzaki *et al.* [66] and Li *et al.*[67] investigated the FDM printing of continuous carbon fibre-reinforced PLA filaments through in-nozzle impregnation. In their studies, a thermoplastic filament and continuous fibres were separately supplied to the 3D printer, with the fibres being impregnated with the filament within the heated nozzle immediately before printing. Compared to their pure polymer counterparts, these continuous carbon fibre-reinforced materials exhibited dramatic improvements in mechanical properties.

Table 2-3 Summary of the reported mechanical data for continuous fibre composites.

Source	Samples	Tensile Modulus (GPa)	Tensile Strength (MPa)	Other Properties	
Matsuzaki, 2016 [66]	CF/PLA			Strain to failure %	
	PLA	3.25	42.6	1.45	
	CF/CFRTP (6.6 vol%)	294/19.5	5880/185.2	2/0.95	/
	Jute fibre/JFRTP (6.1 vol%)	27.4/5.11	417/57.1	2.81/1.81	
Li, 2016 [67]	CF/PLA			Flexural strength (MPa)	Storage modulus (GPa)
	PLA	/	28	53	1.22
	CF/PLA (34 vol%)	/	80	59	0.72
	surface modified CF/PLA (34 vol %)	/	91	156	3.25
Klift, 2016 [65]	CF/PA6			Elongation %	
	PA6	0.9	85	5	
	2CFRTP layers (6 vol%)	14	140	/	/
	6CFRTP layers (1.8 vol%)	35.7	464.4	1.3-2	

	PA6 and PPS		UTS (filament)	Crystallinity (310 ℃)	Crystallinity (330 ℃)	Crystallinity (345 ℃)
Parker, 2022 [68]	CF/PA6 (28 vol%)	/	1485	/	/	/
	CF/PPS (36/43/53 vol%)	/	1410/1920/ 1940	31/29/32	20/21/25	20/19/27
	PA6 and PPS		UTS (Filament) Stage 1/2/3/4			
	CF/PA6 (28 vol%)	/	1410/1215/ 960/725			
Parker, 2023 [69]	KF/PA6 (56 vol%)	/	875/855/ 710/600		/	
	CF/PPS (40 vol%)	/	1845/1690/ 1685/1700			
	CF/PPS (50 vol%)	/	2035/1940/ 1630/1600			

In the context of high-performance polymers, several recent studies have also explored FDM printing of continuous carbon fibre-reinforced PPS composites for high-end applications. Parker *et. al* [68] studied the effect of fibre volume fraction on the ultimate strength of continuous carbon fibre (CCF) filaments. This study compared commercial Markforged Nylon filament and experimental Toray PPS filaments ranging from 30% to 50% fibre volume. The results demonstrated the printability of CCF/PPS materials using FDM printing technology, and it was noted that crystallinity could be altered by decreasing nozzle temperature, achieving a maximum value of more than 30%. It was suggested that the thermograms have a larger peak area of cold crystallisation at higher nozzle temperature as a result of more rapid cooling. They further assessed the printing process of these filaments by evaluating the ultimate tensile

strength for a single path [69]. It was found that the most significant reduction in strength occurs during the deposition of the filament from the nozzle onto the print bed. Compared to commercial nylon filament, CCF/PPS showed a lower reduction in strength and higher reliability. However, these studies only investigated the mechanical performance of a single printed path. The overall mechanical performance of printed CCF/PPS composites needs further exploration.

Continuous fibres are matched in performance for high-stress applications but come with higher costs and processing complexity. Short fibres offer more versatility and cost-effectiveness with sufficient performance for many standard applications. In addition, short fibres reinforced polymer composites offer higher impact resistance than their continuous counterparts due to random fibre orientation. In the practical industrial application, the type of carbon fibres is selected based on the specific requirements.

2.2.3 **Recycled carbon fibres**

Presently, it is projected that over 6000 aircraft will reach the end of their service life by 2030. This scenario presents a significant challenge in managing the resultant composite waste, which poses environmental risks and exacerbates the issue of limited landfill space. Moreover, the accumulation of waste carbon fibre, originating from expired prepreg rolls and off-cuts during manufacturing, has already raised public awareness and concern. Repurposing this more cost-effective carbon fibre for other applications, such as in the automotive industry as next-generation composites, would not only benefit industrial manufacturing but also contribute positively to environmental conservation.

There are principally three methods for reclaiming carbon fibre from composites: mechanical, thermal, and chemical. The mechanical method, encompassing shredding, crushing, and milling, is the simplest approach for recycling carbon fibres, offering labour cost savings and

minimal capital investment. This process breaks down waste into a powdered form for reuse as filler or secondary reinforcement. Chemical recycling represents another method for separating carbon fibres from their matrix. Utilising specific solvents, this technique can nearly cleanse the fibre surfaces while maintaining good mechanical performance. However, scaling up this method poses challenges, and chemical agents require sufficient time to dissolve the matrix. Pyrolysis is a more complex yet efficient method, degrading the matrix into lower molecular weight compounds using heat energy. This process can effectively clean the carbon fibre surface, albeit with some residual contamination.

Numerous studies have focused on the remoulding of thermoplastic matrices and reclaimed carbon fibres to fabricate next-generation composites. As listed in Table 2-4, Caltagirone *et al*. [70] concentrated on the injection moulding compound of recycled carbon fibre and polyamide 66 for automotive applications. They recycled expired epoxy prepreg through chemical treatment and resized the fibre surface to enhance interfacial adhesion with the PA66 matrix. Stoeffler *et al.* [71] examined CF/PPS composites made using PPS matrix and carbon fibre reinforcement recycled from the aerospace industry. They first characterised the morphology and cumulative frequency distribution of recycled carbon fibres from prepregs and finished parts. PPS composites with 15.7 vol% and 33.1 vol% fibre contents were integrated using a twin-screw extruder and then manufactured into specimens via injection moulding. Results indicated that composites reinforced with recycled carbon fibre exhibited similar or better mechanical properties compared to industrial-grade virgin carbon fibres.

In general, recycled CF offer considerable mechanical strength and are increasingly favoured in applications where environmental impact considerations and cost reduction are critical, although they may not reach the high-performance thresholds reserved for virgin CF. However, challenges persist, particularly in the poor adhesion between thermoplastic matrices and recycled fibres, as observed on fracture surfaces. Debonding phenomena observed during

mechanical testing remain a primary challenge that needs addressing to further enhance interfacial strength, thereby improving the overall structural properties for secondary structures in automotive or other industrial applications.

Table 2-4 Summary of the reported mechanical data for rCF/PPS composites.

Source	Samples	Tensile Modulus (GPa)	Tensile Strength (MPa)	Other Properties
Caltagirone, 2021 [70]	CF/PA66			Impact strength (MPa)
	Commercial CF/PA66 (29.6 vol%)	36.3±1.59	269±7.85	9.57±0.446
	Recycled CF/PA66 (27.9 vol%)	33.2±2.56	298±9.12	8.39±0.399
Stoeffler, 2013 [71]	CF/PPS			Flexural modulus (GPa)
	PPS	3.9±0.2	24±6	4.5±0.2
	vCF/PPS (15.7 vol% CF)	14.7±0.5	107±3	12.6±0.1
	rCF/PPS from prepregs (15.7 vol%)	16.8±0.2	133±5	16.3±0.4
	rCF/PPS from finished parts (15.7 vol%)	17.4±0.5	146±4	16.9±0.5
	vCF/PPS (33.1 vol% CF)	30.5±3.1	174±2	24.3±0.5
	rCF/PPS from prepregs (33.1 vol%)	30.3±1.6	200±5	28.6±1.0
	rCF/PPS from finished parts (33.1 vol%)	30.3±0.3	191±3	28.7±0.4

2.3 Fibre-matrix interface improvements

2.3.1 Interfacial adhesion mechanisms

The interface between the thermoplastic matrix and recycled carbon fibre is crucial for the mechanical integrity of composites, as the bonding area often represents the weakest point in composite structures. The main interfacial adhesion mechanisms include molecular entanglement, interdiffusion, chemical bonding, physical attractions and mechanical interlocking [72]. These mechanisms are detailed in Figure 2-4.

The interdiffusion mechanism at the CFRTP interface is characterised by the diffusion of atoms and molecules from the fibre material into the polymer material, aiming for thermodynamic equilibrium [73]. Polymer diffusion involves the movement of polymer chains across the interface, creating a region of molecular entanglement. The gradual change in elastic modulus across the fibre/matrix interface, measurable by nanoindentation tests, serves as evidence of interdiffusion between the relatively stiffer carbon fibre and the polymer matrix [74].

Chemical bonding at the interface occurs through the formation of covalent or non-covalent bonds between the polymer matrix and carbon fibres. This can happen when the fibre/matrix materials are chemically compatible or can be facilitated through surface treatments or sizing agents that introduce specific functional groups. Chemical modifications on carbon fibres, such as grafting coupling agents [5] and compatibilisers [75], aim to enhance chemical bonding by introducing functional groups.

Physical attractions, including electrostatic attraction and physical attraction between electrically neutral bodies, can occur before the fibre and matrix contact each other during the formation of interfacial bonding, whereas other mechanisms typically occur post-contact. Wettability is commonly used to characterise physical attraction. The interface energy (γ_{int}) can be determined by the following equations, based on the Young – Dupré equation [73]:

$$\gamma_{int} = \gamma_f + \gamma_m - \beta_{int} \quad (2\text{-}11)$$

$$\beta_{int} = \gamma_m(1 + \cos\theta) \quad (2\text{-}12)$$

Where γ_f and γ_m are the surface energies of carbon fibres and the polymer matrix, respectively, and θ is the contact angle at the interface.

Enhancing wettability between the fibre and polymer is an effective method to improve interfacial bonding. Plasma treatment, for example, can enhance surface wettability by introducing carboxyl and hydroxyl groups, thereby increasing γ_f in Equation 2-11 [76].

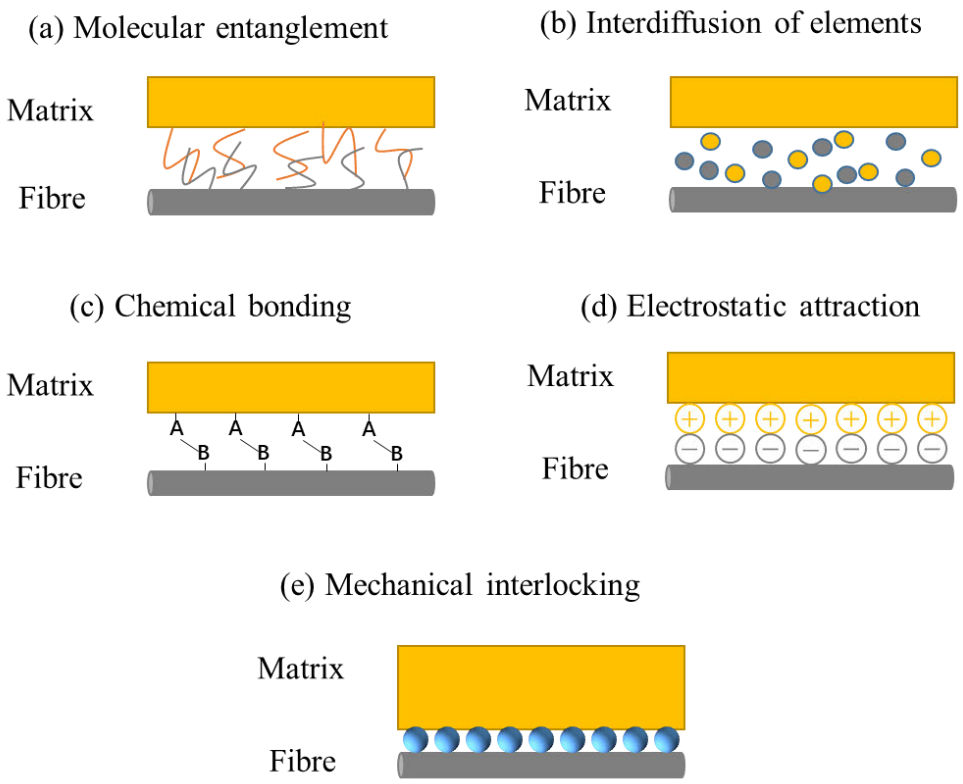

Figure 2-4 Interfacial adhesion mechanisms: (a) molecular entanglement; (b) interdiffusion of elements; (c) chemical bonding; (d) electrostatic attraction; (e) mechanical interlocking [73,77].

Mechanical interlocking occurs between the polymer matrix and roughened carbon fibres. The roughness of the fibre surface, which may include regular or irregular valleys, protuberances,

and crevices, can be increased by grafting nanoparticles such as silica nanoparticles or carbon nanotubes [78]. This increased roughness enhances mechanical interlocking by expanding the bonding area between the carbon fibre and polymer matrix, leading to stronger bond strength. Additionally, the residual clamping stress resulting from differences in thermal expansion during cooling can further enhance mechanical interlocking [73].

2.3.2 **Chemical modification**

The lack of functional groups in pure thermoplastic resin and non-polar carbon fibres typically leads to poor interfacial adhesion with the matrix, potentially resulting in a higher risk of fractures at the interface. This limitation could impact the broader industrial application of CF/PPS composites. To address these challenges, previous studies have predominantly employed chemical modifications, physical treatments and combined methods. Table 2-5 gives the summary of the reported enhanced interfacial adhesion for matrix and carbon fibre.

Grafting coupling agents are an effective means to improve interfacial adhesion by introducing chemical groups onto the non-polar carbon fibre surface. Wong *et al.* [5] explored the impact of three different maleic anhydride-grafted polypropylene (MAPP) coupling agents on the mechanical properties of PP composites reinforced with recycled carbon fibre. They discovered that the tensile, flexural, and impact strengths of the specimens were significantly improved due to higher compatibility, which depended greatly on the molecular weight and anhydride groups of the coupling agents. Moreover, the interfacial shear strength, measured by a micro-bond test, increased, with less fibre pull-out observed on the fracture surface, indicating improved interfacial bonding.

Adding compatibilisers is another efficient method to introduce functional groups, enhancing the bonding with the matrix and reducing interfacial stress, thereby mitigating crack initiation and propagation. Zhang *et al.* [75] studied the effect of PPS-NH_2 on the mechanical properties

of short carbon fibre-reinforced PPS composites. They observed enhanced mechanical properties, including tensile strength, flexural strength, and modulus, by adding the compatibiliser PPS-NH_2. The morphologies of fracture surfaces revealed fewer carbon fibre pull-outs and more severe fibre breakage in the CF/PPS/PPS-NH_2 composites. Dynamic mechanical properties and interfacial shear strength (IFSS) also indicated that the compatibiliser improved interfacial adhesion of PPS and carbon fibres, particularly at a DCA concentration of 1.0% in the polymerisation. However, the compatibiliser's role in increasing interfacial and impact strengths was limited to approximately 13.3% and 12%, respectively.

In conclusion, chemical modification proves to be an effective method for enhancing the interfacial adhesion between carbon fibre and polymers, thereby improving their compatibility and various mechanical properties. Nonetheless, this modification process often requires the use of toxic chemicals and harsh reaction conditions, posing significant challenges for its application on a large scale.

2.3.3 **Physical treatment**

Physical treatment is one of the most efficient methods for activating the surface of carbon fibre, with plasma treatment being a notable example [79]. Plasma treatment can be categorised based on the use of oxidative and non-oxidative gases, encompassing both low-pressure [80] and atmospheric conditions [7]. Low-pressure plasma (LPP) techniques including Microwave (MW) [81], Radio frequency (RF) [82], Plasma immersion ion implantation [83], Direct current (DC) [84] have been deployed for the surface treatment of commercial carbon fibres, all conducted under vacuum gas pressure. Atmospheric plasma includes Dielectric barrier discharge (DBD) [85] and corona discharge (CD) [84], offer convenience for the continuous carbon fibre production.

Tiwari *et al.* [80] employed cold remote nitrogen plasma for carbon fibre surface treatment. Three high-performance polymers—PEI, polyether sulfone (PES), and PEEK—were compounded to create treated CF reinforced composites. The results indicated improvements in most mechanical properties, varying across different plasma types and polymer matrices. X-ray Photoelectron Spectroscopy (XPS) revealed the inclusion of oxygen and nitrogen on the surface, thereby enhancing interfacial adhesion. Similarly, Fourier Transform Infrared Reflectance Spectroscopy (FTIR) confirmed the presence of ether, carboxylic, and carbonyl functional groups on the treated surface.

In conclusion, LPP techniques exhibit considerable potential for introducing functional groups onto the surface of carbon fibre. These treatments are versatile and capable of achieving effective plasma-surface interaction through the optimisation of processing parameters. However, these techniques primarily modify the surface chemistry of the outermost layer. Unlike wet chemical modifications, no functional groups were detected beneath the surface of the carbon fibre bundle. Additionally, the potential degradation of functional groups exposed to the atmosphere post-LPP treatment presents a challenge for practical application. Lastly, this technique often requires complex vacuum equipment and significant energy, potentially increasing costs.

2.3.4 **Combined methods**

Some researchers have employed multiple chemical modification treatments or combined that with physical treatments in modifying the surface of the non-polar carbon fibre. The initial step involves roughening the smooth surface of carbon fibres through methods such as oxidation and plasma treatment. The subsequent step introduces a new layer between the fibre and matrix by grafting coupling agents or adding compatibilisers.

Hu *et al.* [10] enhanced the interfacial adhesion of CF/PPS by combining liquid-phase oxidation with grafting of silane coupling agents. They initially desized commercial carbon fibre using acetone, then oxidised it with HNO_3 to introduce oxygen-containing groups. Subsequently, the treated CF was grafted with different SCFs to introduce a siloxane network between the matrix and fibre. This approach led to increases in tensile strength, flexural strength, and interlaminar shear strength (ILSS) of 5.96%, 36.18%, and 21.73%, respectively, compared with desized CF. Fracture surface images indicated a shift in the failure mechanism from interface debonding to deformation and break- up of the polymer matrix. Thus, this study revealed that a combination of roughness enhancement and interlayer introduction is more effective for improving interfacial adhesion than a single oxidation treatment. However, the study did not consider samples prepared solely from grafting silane coupling agents (SCAs).

Dong *et al.* [9] improved interfacial shear strength in CF/PPS composites by combining sizing processes with plasma treatment. They activated the inert surface of virgin carbon fibre via plasma and then used synthesized PPS-COOH as a sizing agent, enhancing the wettability and bonding between fibre and matrix. This resulted in a significant increase in tensile strength and IFSS by 43.81% and 27.71%, respectively.

Extensive recent research has delved into a variety of chemical agents or plasma treatments to improve interfacial strength [9,10,86]. Despite the effectiveness, however, these traditional methods often depend on toxic chemicals, are energy-intensive, and require harsh operational conditions, as previously highlighted.

Table 2-5 Summary of the reported enhanced interfacial adhesion for matrix and carbon fibre.

Methods	Source	Treatments	Tensile strength (MPa)	Flexural Strength (MPa)	Interfacial shear strength (MPa)
Coupling agents	Wong, 2012 [5]	PP	28.94±0.44	44.15±0.30	/
		CF/PP (18.1 vol%)	50.62±2.00	91.34±1.82	2.36
		CF/PP+2.3 vol%E43	108	190	4
		CFPP+5.7 vol%G3003	122	210	4.5
		CF/PP+5.7 vol%G3015	120	210	6
Compatibiliser	Zhang, 2014 [75]	CF/PPS/PPS-NH_2 (15.7 vol%)	80	87	/
		CF/PPS	105	155	30
		CF/PPS/PPS-NH_2 (0.6 DCA%)	107	162	/
		CF/PPS/PPS-NH_2 (0.7 DCA%)	110	160	/
		CF/PPS/PPS-NH_2 (0.8 DCA%)	112	165	/
		CF/PPS/PPS-NH_2 (0.9 DCA%)	113	164	/
		CF/PPS/PPS-NH_2 (1.0 DCA %)	115	166	32.5
		CF/PPS/PPS-NH_2 (1.2 DCA%)	113	164	34

		CF/PPS (HNO_3+SCAs)			
	Hu, 2020 [10]	RSA-CF	639.73	725.32	67.68
		ATS-CF	659.64	781.13	69.05
		GTS-CF	658.53	856.02	75.10
Two-step combination strategy		MTS-CF	677.86	987.74	82.39
		Plasma + Sizing			
	Dong, 2020 [9]	PPS	80	/	/
		VCF/PPS(7.6 vol %)	100	/	29.1
		PCF/PPS (7.6 vol%)	100	/	32.3
		ACF/PPS (7.6 vol%)	115.2	/	37.2

2.3.5 **Bio-inspired structures for fibre/matrix interface**

Consequently, there has been a shift towards environmentally friendly alternatives, including the use of advanced nanomaterials [87–91] and the development of bioinspired structures (shown in Figure 2-5) [92–96].

Among these eco-friendly solutions, the ability of mussels to adhere to a wide range of substrates, including superhydrophobic surfaces, has been particularly noteworthy. Scientists have attributed this remarkable adhesive capability to the presence of dihydroxyphenylalanine (DOPA) near the plaque-substrate interface. In 2007, it was established that polydopamine (PDA), which shares a similar structure with DOPA, can strongly adhere to virtually any surface, ranging from inorganic to organic substrates [97]. The main advantages of PDA as a coating material are of green synthesis in the water solution with a self-polymerization process

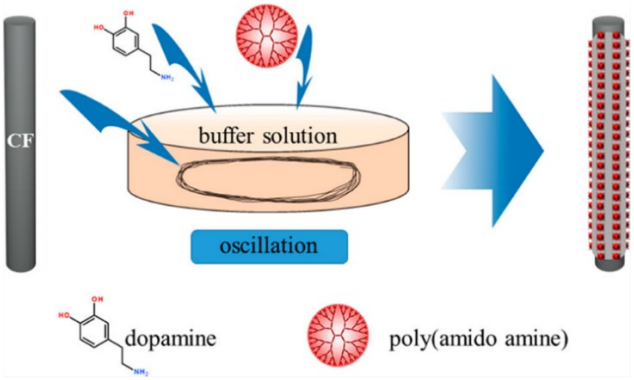

(a)

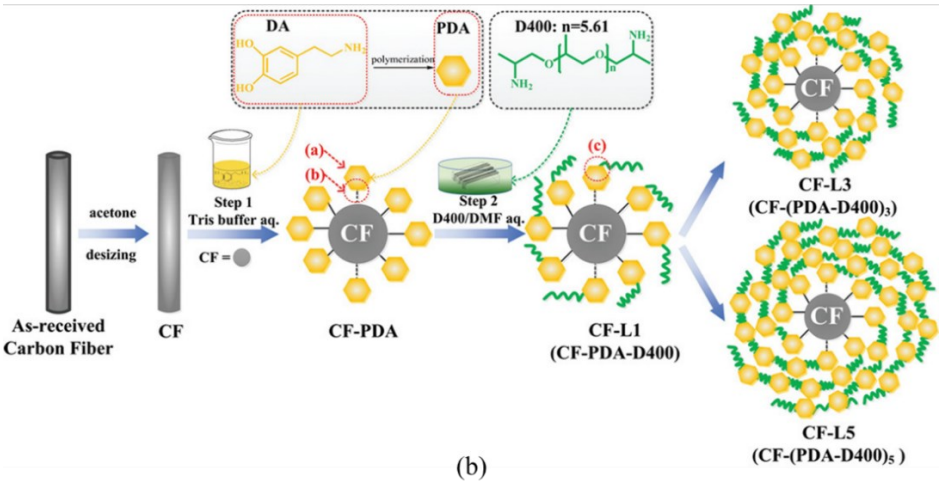

(b)

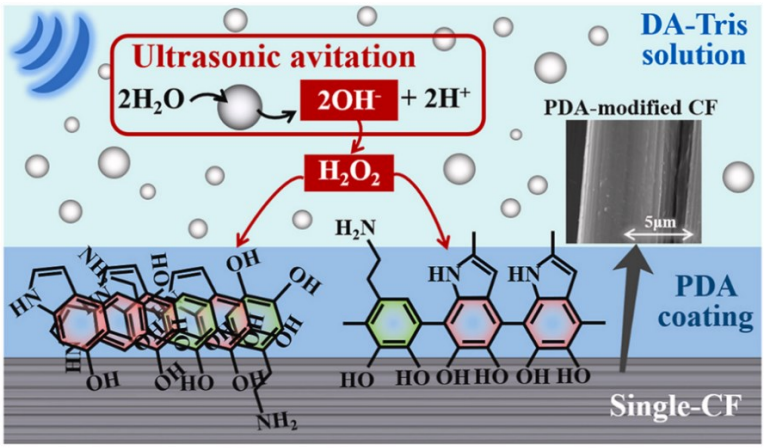

(c)

Figure 2-5 (a) Schematic of copolymerisation of DA/PAMAM on carbon fibre surfaces at room temperature [96]; (b) schematic illustration of dip coating assembly of PDA/D400 multilayers onto surface of carbon fibre [93,94]; (c) the oxidation process of DA and the polymerization and assembly of PDA on CF surface [98].

and can easily deposit on the all types of surfaces. The primary benefits of PDA as a coating material lie in its environmentally friendly synthesis in aqueous solutions and its capacity for self-polymerisation, enabling easy deposition on various surfaces. To tackle the challenge of interfacial adhesion, some researchers have focused on PDA-assisted nanoparticle modifications of carbon fibres in composite manufacturing.

Gao *et al.* [96] were the first to report on the one-step copolymerisation of dopamine and poly(amidoamine) (PAMAM) on carbon surfaces. They harnessed the synergistic effects of PDA and PAMAM to attach ample functionalisation groups onto the fibre surface, significantly enhancing the interfacial properties between carbon fibre and epoxy matrix. As a result, the IFSS and impact strength of the composites increased by 78.57% and 75.12%, respectively. This promising method, featuring a green synthesis process, holds potential in the production of products with high mechanical properties.

Wu *et al.* [93,94] also investigated a nacre-like hybrid network by depositing both rigid PDA and flexible polyether amine. They observed a 39.2% increase in optimal interfacial strength and a 99.8% enhancement in toughness compared to untreated fibre composites. The significant improvements were attributed to the synergistic interaction of covalent bonds, hydrogen bonding, and π-π stacking between the fibre and matrix. This multilayered structure, based on the uniform dispersion of nanoparticles on a polymer platform, effectively transfers stress and bridges cracks across the cross-sectional area, mitigating the effects of internal and external forces. This bioinspired strategy offers a sustainable approach to fabricating high-performance composite materials.

Recently, Sun *et al.* [98] explored an ultrasound-assisted PDA polymerisation process on CF, which accelerated PDA production to less than one hour and facilitated the permeation of PDA molecules into the fibre bundle. Their findings indicated a 21.07% improvement in interfacial

shear properties for PDA-modified CF reinforced PA6 composites compared to desized CF reinforced PA6 composites. This study also highlighted the phenolic hydroxyl and amino groups as key functional groups forming strong bonds with CF, thus ensuring compatibility with the PA6 matrix.

Furthermore, it was reported that catechol, another bioinspired material, could serve as an alternative to PDA in surface treatment [92]. The results showed that catechol-coated composites exhibited increases of 51.9% in flexural strength and 51.7% in ILSS compared to desized carbon fibre composites. The uniformly coated Cc-PEI significantly enhanced the diffusion and entanglement of matrix molecular chains, forming chemical bonds and π-π stacking between the fibre and matrix, thereby improving interfacial adhesion.

2.4 Printing performance enhancement

In the FDM printing of thermoplastic composite filaments, key manufacturing defects have been identified, including void formation and poor inter-layer bonding, as highlighted in numerous studies [68,99,100]. Figure 2-6 illustrates the typical three types of voids observed in printed composites: (a) voids within a single printed track, which result from inadequate impregnation of the carbon fibre bundle with the thermoplastic matrix; (b) inter-bead voids and strip gaps, caused by the in-situ consolidation process and improper geometry of the printed bead; and (c) voids between deposited layers, which are attributed to insufficient thermomechanical consolidation due to temperature differences between the deposition layers.

To address these manufacturing defects in FDM printing process, many researchers have developed a variety of improvement methods. These methods can be categorised into three distinct stages based on the printing procedure: pre-processing methods, in-situ interference techniques and post-print processing.

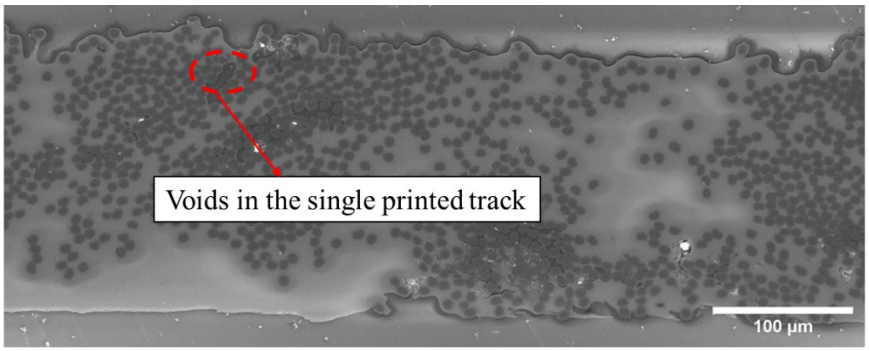

(a)

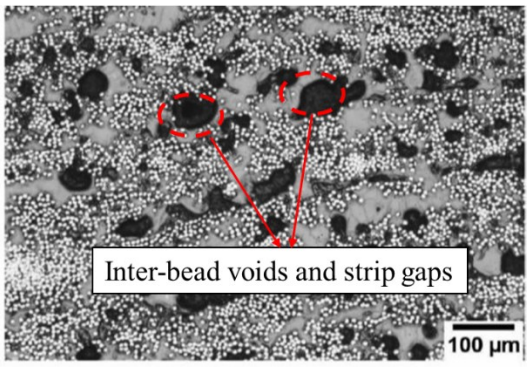

(b)

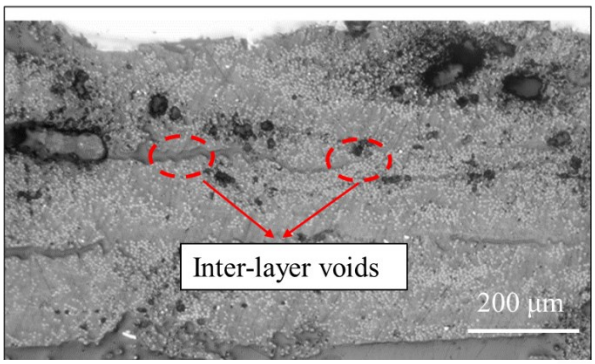

(c)

Figure 2-6 Typical three types of voids observed in printed composites: (a) voids in the single printed track; (b) inter-bead voids and strip gaps; (c) voids between deposited layers [68,99,100].

2.4.1 **Pre-processing methods**

The primary aim of pre-processing methods in FDM printing of thermoplastic composites is to optimise the impregnation between the thermoplastic matrix and carbon fibre bundle prior to the initiation of the printing process. This enhancement plays a crucial role in determining the mechanical properties of the final printed parts, as extensively reviewed in the literature [101]. Within this context, two predominant methodologies (refer to Figure 2-7) emerge: new layer sizing and pre-impregnation.

The application of a new layer for sizing carbon fibre significantly transforms the surface properties of commercial CF, customising the surface components to promote adhesion with

the thermoplastic matrix. For instance, Li *et al.* [67] employed a methylene dichloride solution to dissolve PLA resin, thereafter coating a continuous carbon fibre bundle with a PLA sizing layer (refer to Figure 2-7(a)). This adjustment in the carbon fibre surface properties resulted in a remarkable improvement in tensile strength – increases of 13.8% and 164% were observed in comparison to original CF-reinforced samples. Similarly, Heidari *et al.* [20] treated carbon fibre surfaces with a PVA solution before the printing process (see Figure 2-7(c)), passing the continuous carbon fibre tow through a solution bath and then through a 1mm die.

The pre-impregnation strategy, on the other hand, involves the integration of the thermoplastic matrix and carbon fibre into prepregs. Luo *et al.* [102] pioneered a pre-impregnation technique for dry carbon fibre and PLA matrix, as illustrated in Figure 2-7(b). In their process, a continuous carbon fibre tow is immersed through a container housing heated PLA resin at its melting point, subsequently extruded through a 0.6 mm nozzle. Adopting a comparable approach, Mosleh *et al.* [18] facilitated the impregnation of carbon fibre in an ABS solution bath (depicted in Figure 2-7(d)), creating ABS/CCF prepregs by allowing the carbon fibre tow to permeate through an ABS-infused acetone solution.

Furthermore, an innovative combination of these two pre-processing methods was explored by Liu *et al.* [19], who applied a PA6 sizing layer to carbon fibres. This treatment was aimed at enhancing the compatibility between the commercial carbon fibre and the PA matrix, as represented in Figure 2-7(e). Their findings indicated that the PA6 composites reinforced with sized carbon fibre exhibited a 42.2% improvement in interlaminar shear strength (ILSS) compared to composites reinforced with virgin carbon fibre.

In summary, the new layer sizing and pre-impregnation in the pre-processing methods significantly enhance the interfacial adhesion of the fibre/matrix, improving the impregnation

of matrix materials into dry carbon fibre tow. This enhancement contributes to superior interlaminar bonding, resulting in a higher load transfer capacity in the printed parts.

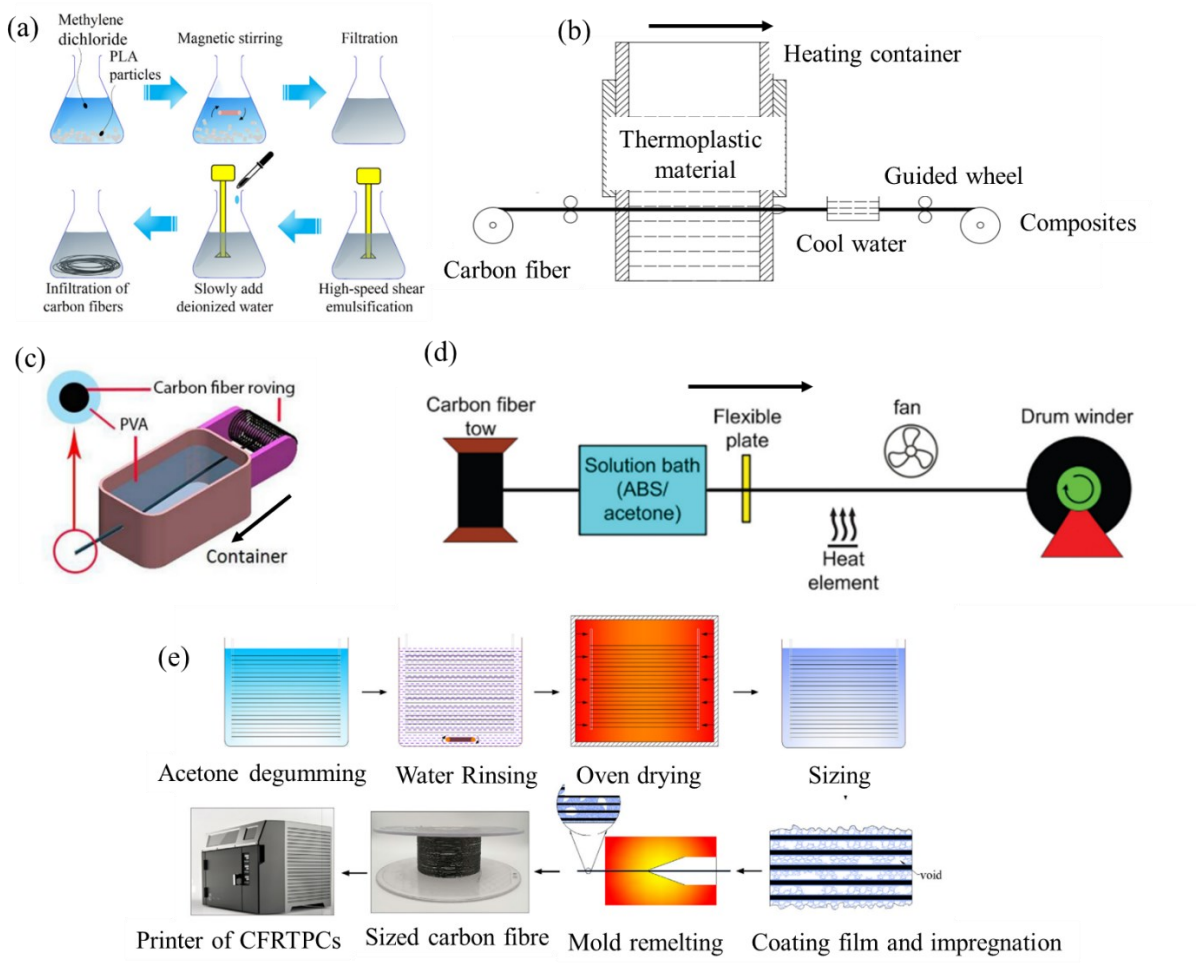

Figure 2-7 Summary of the pre-processing methods in the literature [18–20,67,102].

2.4.2 **In-situ interference techniques**

The majority of research in CFRTP FDM printing has predominantly concentrated on in-situ interference, as opposed to pre-processing or post-processing methods. Optimisation of printing parameters and in-situ consolidation represent the two principal areas of focus within these works. The processing factors play a vital role in determining the tensile, flexural and shear properties of printed composites.

With respect to the optimisation of printing parameters, the literature [101] commonly identifies layer thickness [15,16], fibre orientation [17,103], and printing speed [16] as the three most critical variables. Following closely are variables such as printing temperature [15] and infill pattern and density [104,105]. Other optimised printing parameters include printing path [106], filament feed rate [15,19], hatch spacing [15], and build orientation [16].

Another significant in-situ interference condition is the incorporation of consolidation during the printing process. It has been observed that applying pressure during FDM printing can enhance the mechanical properties of composites. Ueda *et al.* [107] modified an FFF printer to incorporate a hot-compaction module equipped with a 10 mm compaction roller, and adapted the printer bed to be movable and rotatable around the z-axis. Their results indicated improvements in tensile and bending properties of the printed parts, attributed to reductions in void content and enhancements in layer adhesion. Similar findings are in the Zhang *et al.* [108] research, which also introduce a pressure roller in the 3D printer. They reported a significant increase in mechanical properties, with tensile strength reaching 644.8 MPa and bending strength reaching 401.24 MPa. However, it was also noted that excessive pressure could pose a challenge by potentially damaging the print path and diminishing surface quality during the in-situ consolidation process.

In conclusion, optimising printing parameters is beneficial for improving fibre orientation and polymer diffusion, which can enhance the bulk properties of composites. Moreover, consolidation during the printing process primarily works to reduce inter-layer voids. Both methods can significantly improve the mechanical performance of printed composites.

2.4.3 **Post-print processing**

Post-print processing (or usually post processing) techniques are employed subsequent to FDM 3D printing to further mitigate void formation and promote inter-layer bonding. These

techniques primarily include hot press compaction for thermoplastic polymer matrices and post-print curing for thermoset polymer matrices. Although the literature on hot press compaction is somewhat limited, its impact on the mechanical properties of printed composite parts, particularly those with continuous carbon fibre reinforcement, is significant. Table 2-6 summarised applications of hot press compaction in the literature.

Mei *et al.* [21] optimised hot press parameters: a pressure of 200 kPa, a temperature of 200 °C, and a duration of 30 minutes for printed CCF/PA6 composites. The resultant highest tensile strength and modulus were recorded at 106 MPa and 4.27 GPa, respectively, marking improvements of 36.7% and 63.0% over the unpressed samples. He *et al.* [22] reported similar enhancements, with increases of 32.8% and 63.0% in flexural strength and modulus, respectively, after hot press compaction of printed CCF/PA6 composites. Ueda *et al.* [107] compared the mechanical performance of PA6 composites subjected to in-situ consolidation and hot press compaction. The samples were heated and compressed at 230 °C and 0.1 MPa for 10 minutes. They found that the flexural strength of the composites post hot-press compaction was comparable to that achieved through in-situ consolidation. Furthermore, Pascual-González *et al.* [23] explored the effects of hot-pressing parameters on the microstructure, interlaminar properties, and thermal stability of printed CFRTP. The hot press temperature was optimised based on the thermal characterisation of the printed composites. Their findings indicated a reduction in void content by 87% and an enhancement in interlaminar strength by 145%.

In summary, the application of pressure during hot press compaction for 3D printed composites can significantly reduce voids and improve interlayer bonding, leading to the enhanced interlaminar properties of post-processed parts. However, this method requires specific moulds for complex geometries, potentially limiting its applicability. This challenge necessitates further research to harmonise FDM printing design with high-temperature and high-pressure

post-processing techniques. Moreover, most existing studies focus on commercial Markforged Nylon filaments, indicating a need for expanded research into FDM high-performance polymer composites.

Table 2-6 Summary of applications of hot press compaction in the literature.

Source	Samples	Hot press conditions	Mechanical properties	Other properties
Mei, 2019[21]	CF/PA6 (Markforged)	200 ℃/200 kPa/30min	Tensile strength: +36.7%	Tensile modulus: +21.7%
Ueda, 2020[107]		230 ℃/0.1 MPa/10 min	Flexural strength: +32.8%	Flexural modulus: +63.0%
He, 2020[22]		230 ℃/5 MPa/10 min	Tensile strength: +22.5%	Flexural strength: +92.6%
Pascual-González, 2021[23]		70-270 ℃/5 MPa/10 min	Interlaminar strength: +145%	Void content: -87%

2.5 Sustainable in-situ remanufacturing system

2.5.1 3D overprinting techniques

3D overprinting technique involves bonding 3D-printed structures directly onto laminates, eliminating the need for additional joining steps. This technique has been explored in various studies with both commodity and engineering thermoplastics (see Figure 2-8). Boros *et al*. [109] compared the bonding strength of PLA parts manufactured through overprinting and overmoulding (see Figure 2-8(a)). They examined the tear-off strength in cases where overprinted ribs were applied to injection-moulded plates, discovering that deactivating the cooling fan during the printing process yielded better results than keeping it on. Morales *et al.*

[110] extended this approach by overprinting PA6 onto an organo-sheet (shown in Figure 2-8(b)). Their study focused on the impact of the organo-sheet temperature on the shear strength of the bond. They found that the bonding strength could be significantly enhanced if the interface temperature exceeded the melting point of the substrate layer. Additionally, there is a need for further investigation into printing parameters such as temperature and pressure, and surface treatments like texturing or the application of hot-melt adhesives.

In another study, Maier *et al.* [111] fabricated specimens by overprinting PA6 onto a continuous woven glass fibre-reinforced PA6 (GF/PA6) substrate (presented in Figure 2-8(c)). Their findings indicated that both the printing and platform temperatures influenced the bonding strength and corresponding failure. They also demonstrated that surface treatments, such as plasma treatment, could improve interfacial adhesion in hybrid manufacturing.

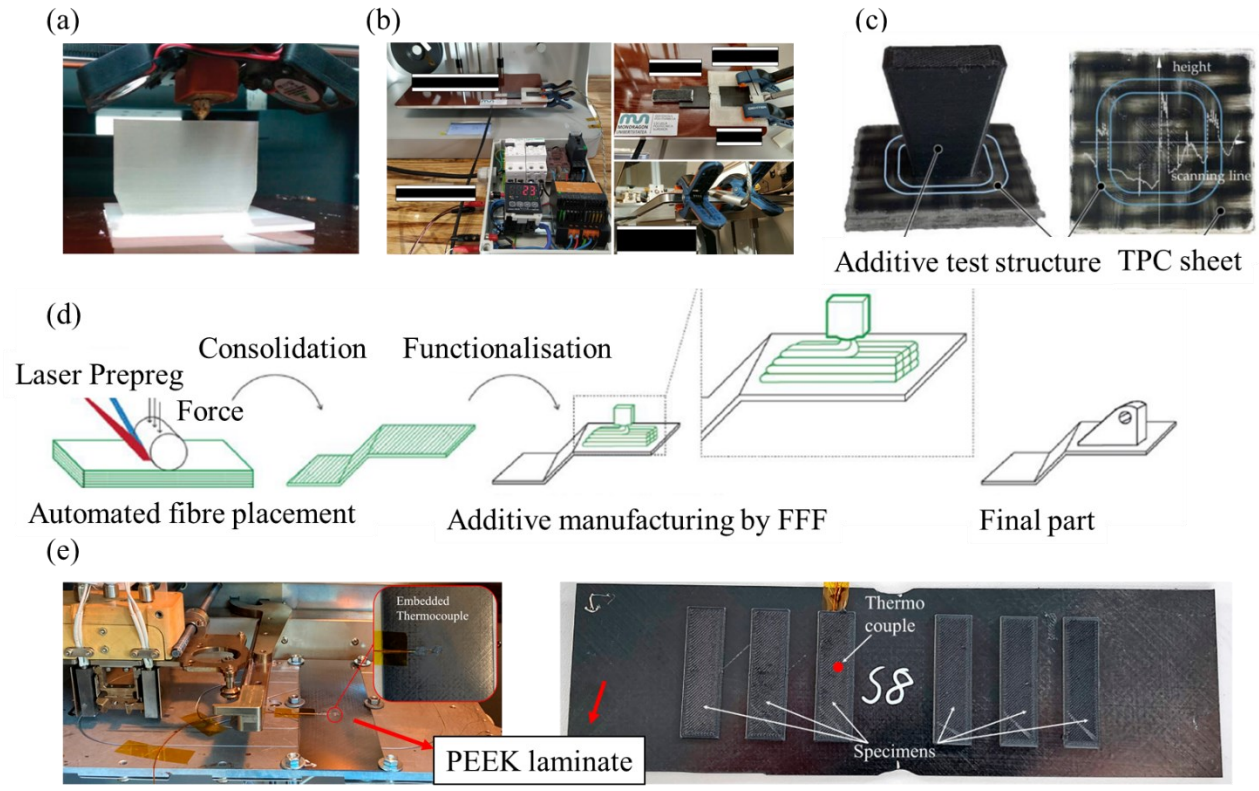

Figure 2-8 Summary of 3D overprinting technology involves FDM printing [109–114].

Although previous research on overprinting techniques has been limited to high-temperature polymers, Caprais *et al.* [112,113] were pioneers in extending this technique to PEEK polymers. They reported that thermal history is a critical factor in bonding 3D printed PEI onto continuous carbon fibre reinforced PEEK substrates manufactured by automated fibre placement (AFP) (illustrated in Figure 2-8(d)). They underscored the importance of adequate thermal energy to facilitate macromolecular chain diffusion. Most recently, Hümbert *et al.* [114] investigated the feasibility of in-situ bonding between PEEK laminates and 3D printed short carbon fibre reinforced PEEK during the overprinting process (depicted in Figure 2-8(e)). They highlighted the significance of additional printing parameters such as layer height and chamber heating above 200 °C, in addition to interface temperatures, for optimising bonding strength.

2.5.2 **Repair thermoplastic composites by 3D printing**

Traditional repair methods for thermoplastic composites typically involve mechanical fastening, adhesive bonding, and three notable fusion bonding techniques: induction, resistance, and ultrasonic welding. Mechanical fastening can introduce additional stress concentrations in the repaired parts due to damage to the continuous fibres [115]. Adhesive bonding, while effective, requires surface treatments with specialised instruments before the repair process, which may not be practical for industrial applications [116]. Fusion bonding, developed primarily for joining thermoplastic structures, involves heating the interface above the glass transition temperature for amorphous polymers or the melting temperature for semi-crystalline polymers. This method is highly promising for maintaining structural integrity in repairs [117–119].

Additive manufacturing offers unique advantages in the repair of thermoplastic laminates. FDM 3D printing technology, in particular, has been linked to composite repairs in several

studies (see Figure 2-9). In 2018, Justo *et al.* [24] proposed a new automated repair system for manufacturing repair patches via 3D printing, aiming to enhance the quality of the final part while saving time and cost (refer to Figure 2-9(a)). They printed two-part repair patches, which were later bonded to the parent panels. The results demonstrated that adhesive bonding with printed repairs could restore the original mechanical performance of the panel. Similar recent work was conducted by Joosten *et al.* [25]. They utilised the additively manufactured patches to repair damaged sandwich structures (see Figure 2-9(c)). In all cases, the repaired structures were able to regain the full mechanical performance of the undamaged parts. Likewise, Li *et al.* [26] developed an adhesively bonded repair method using FDM printed patches. They fabricated multiple patch types and adhered them to two different stacking sequence laminates (refer to Figure 2-9(b)). During tensile testing, digital image correlation (DIC) techniques were applied to monitor the damage process and analyse strain distribution during failure. Compared to traditional patches, the 3D printed patches exhibited enhanced repair performance with reductions in time and cost.

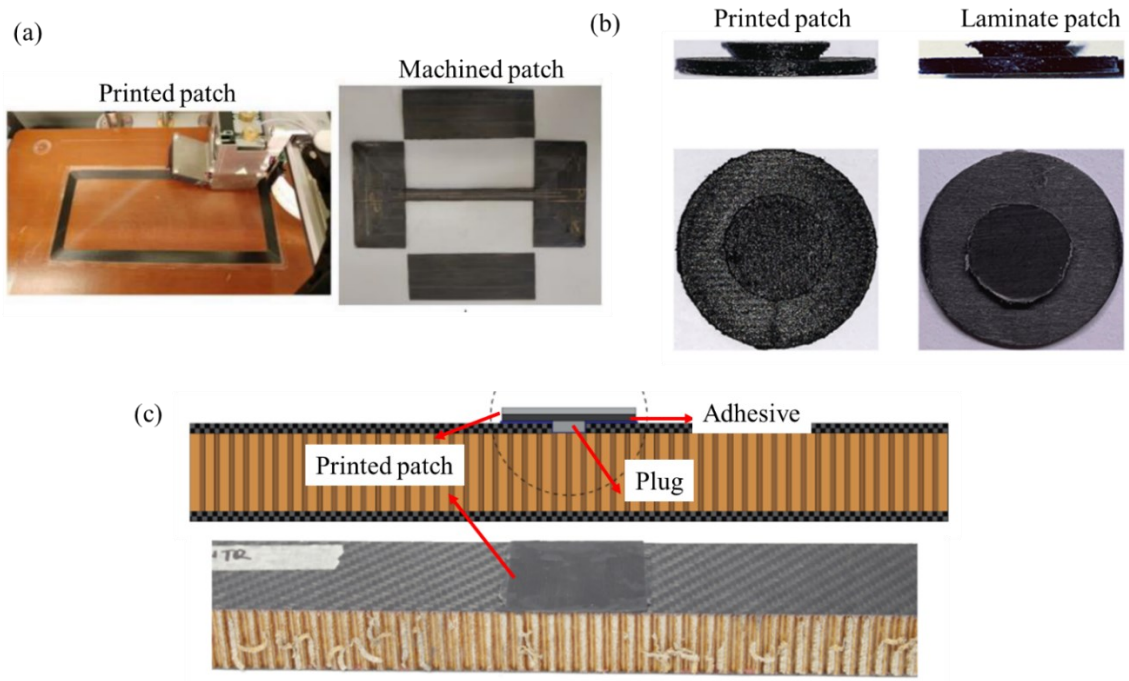

Figure 2-9 Summary of the additively manufactured repair patch for damaged CFRP [24–26].

In summary, previous studies have primarily focused on the separate manufacturing of repair patches via 3D printing. Moreover, this technique shows potential for performing in-situ repairs by heating the surface when the extruding nozzle is in intimate contact with the parent structure. Additionally, the repair path for fibre orientation can be customised according to stress distributions in the damaged area.

2.5.3 **Customised printing paths**

Compared to traditional composites manufacturing, additive manufacturing of continuous carbon fibre reinforced thermoplastic filament (1-2 mm in width) presents a distinct advantage in fibre alignment along curved trajectories. This advantage facilitates the transfer of loads in structures along the longitudinal direction of the fibre, owing to the layer-by-layer deposition of smaller fibre tows. This capability, inherent in 3D overprinting, allows for controlled fibre arrangement and minimises material waste in in-situ composites repair systems.

There has been considerable research focused on optimising fibre orientation through numerical modelling within the additive manufacturing process, although direct application in overprinting for composite repair patches is less common. Among the various numerical simulation methods, the stress-lines method has been shown to achieve higher stiffness and improved stress distribution in anisotropic materials. This approach aligns the continuous carbon fibre with the principal stress trajectories in the additive manufacturing process to maximise stiffness. In 2018, Zhang *et al.* [120] introduced a novel concept for placing continuous curved fibres in CFRP composites. They employed finite element analysis (FEA) to generate principal stress trajectories, guiding fibre placement for potential additive manufacturing applications. This method was then applied to design various 3D printed cases, including open-hole laminates [121,122], Messerschmitt-Bolkow-Blohm (MBB) beams [123] and single-notched samples [124]. Both numerical and experimental results demonstrated

higher stiffness, reduced stress concentration, and superior mechanical performance using this performance-driven optimisation approach.

In conclusion, this innovative performance-driven optimisation method holds significant potential for customising fibre paths in overprinting continuous carbon fibre filaments for in-situ repair systems, thereby enhancing the mechanical performance of 3D printed patches. However, future applications of these repaired patches should also consider additional simulation steps, including progressive interfacial failure and the potential for patch debonding.

2.6 Summary of literature review

This literature review provides a comprehensive background and highlights state-of-the-art research in FDM printed thermoplastic composites, with a particular focus on high-performance semi-crystalline polymers. The review initially addresses crucial factors in composite materials, including the inherent properties of polymer matrices, reinforcing fibres, and the fibre-matrix interface. It then discusses three methods aimed at enhancing printing performance to improve inter-layer bonding, specifically in continuous carbon fibre reinforced thermoplastic composites. Lastly, it covers recent research on sustainable in-situ remanufacturing systems through the application of 3D overprinting technology for thermoplastic repairs.

Key knowledge gaps identified are as follows:

(1) Thermal history and mechanical performance: The thermal history is crucial in processing high-performance semi-crystalline polymers, impacting their mechanical performance significantly. Analysing the effects of thermal process conditions on the crystallinity of 3D printed semi-crystalline composites is essential. Furthermore, the sensitivity of PPS polymers to oxidation during material extrusion at varying temperatures (310 ℃-340 ℃) remains insufficiently understood and requires deeper investigation.

(2) Interface challenges between thermoplastics and carbon fibre: The interface between PPS polymer and commercial carbon fibre is a major challenge in high-end applications of composites. Although mussel-inspired polydopamine emerges as a promising candidate for carbon fibre surface treatment in the impregnation process with thermoplastic polymers, the gap between this eco-friendly approach and its practical application to carbon fibres and high-temperature thermoplastic resins like PPS is yet to be bridged. Clarification and further research into the mechanisms of these improvements are needed.

(3) Enhancing interlaminar properties: In comparison to the numerous in-situ interference activities, more research should be focused on the pre-processing methods and post-processing methods. These methods are vital for enhancing interlaminar properties, particularly in 3D printing of continuous carbon fibre reinforced high-performance thermoplastic polymers, which exhibit higher viscosity at the melting temperature during carbon fibre impregnation. Additionally, addressing the limitations in geometry for hot press compaction post-3D printing is an area that warrants further exploration.

(4) In-situ repairs and overprinting techniques: While most studies have concentrated on the separate manufacturing of repair patches via 3D printing, this technology also holds potential for in-situ repairs. This involves heating the surface as the extruding nozzle comes into direct contact with the parent structure. In overprinting techniques, interface temperature is a critical factor influencing bonding performance with 3D printed composites and substrate laminates, deserving more detailed exploration and control. Furthermore, the development of customised printed paths, guided by principal stress trajectories, is another avenue to enhance the performance of printed patches and merits further research.

Chapter 3 **Effects of thermal process conditions on crystallinity and mechanical properties in material extrusion additive manufacturing of discontinuous carbon fibre reinforced polyphenylene sulphide composites**

Abstract

This study investigates the thermal behaviour of discontinuous carbon fibre reinforced polyphenylene sulphide (CF/PPS), additively manufactured by material extrusion, with a focus on the effects of thermal process conditions on the degree of crystallinity, oxidation crosslinking and mechanical properties of CF/PPS from filament fabrication, material extrusion to annealing treatment. The screw extrusion parameters are optimised by performing a thermal analysis of the fabricated filaments. The effect of crosslinking reactions on the crystallinity process in determining the mechanical properties of the printed samples is illustrated by investigating the influence of the printing conditions. Furthermore, the effect of annealing treatment on the semi-crystalline polyphenylene sulphide (PPS) is studied by measuring the degree of crystallinity and viscoelasticity behaviours. Results demonstrate that the flexural properties of the printed CF/PPS composites at elevated processing temperatures (above 320 ℃) are mainly determined by the oxidation crosslinking between PPS chains. The oxidation crosslinking reaction between polymer chains enhances the crystallisation process of semi-crystalline polymers by acting as the nucleating agent first but negatively affect the mechanical properties at higher temperatures because of the detrimental effects of the polymer inter-chain bonding. The maximum flexural strength of printed CF/PPS reached 164.65 MPa when processing at an extrusion temperature of 280 ℃, a printing temperature of 320 ℃, and an annealing temperature of 130 ℃ for 6 hours. By adjusting the thermal treatment conditions,

the degree of the crystallinity and the mechanical properties of the printed CF/PPS composites can be designed, controlled and tailored.

Keywords

material extrusion additive manufacturing; carbon fibre; polyphenylene sulphide; thermal process condition; crystallinity.

3.1 Introduction

Thermoplastic composites have increasing applications due to their advantages of rapid cycle time, improved impact strength, recyclability, and unlimited shelf life as compared to thermoset composites[125]. For instance, the G650 business jet from Gulfstream adopts the lightweight carbon fibre/polyphenylene sulphide (CF/PPS) to form the tail section, which reduces 10% of the structural weight and 20% of the cost [1]. Polyphenylene sulphide (PPS) is a semi-crystalline matrix with a relatively high service temperature (200℃-220℃), exceptional mechanical strength, great chemical resistance, and good flame retardation [126], and it is less expensive than other high-performance semi-crystalline polymers like polyetheretherketone (PEEK) [127]. Thermoplastic composites manufactured by additive manufacturing (AM) such as material extrusion technique recently emerged due to their high flexibility in geometry, cost-effectiveness, and being free of multiple processing tools [28]. The most common polymers used in material extrusion-based printing are acrylonitrile butadiene styrene (ABS) [128], polylactic acid (PLA) [58], polyamide (PA) [124], and polyethylene terephthalate (PET) [129]. Short carbon fibre reinforced polymers offer the most accessible pathway toward large-scale, affordable and functional AM composites [130]. Mixing short carbon fibres in the PPS feedstock can increase the thermal conductivity and mechanical strength and stiffness while reducing the thermal expansion and residual stress in the printed composites [131].

Furthermore, short carbon fibres can improve friction and wear resistance, even compared with their continuous carbon fibre counterparts [132]. In general, higher fibre content and better-aligned short fibres in additive manufacturing lead to improved mechanical properties of printed composites [133]. Therefore, material extrusion of discontinuous CF/PPS composites with a high fibre volume is likely to grow in the automotive, electronics, and aerospace industries as well as other fields, due to its relatively low cost, accessible printing process, and feasible recycling process.

As semi-crystalline polymer, the degree of crystallinity of PPS during the extrusion and printing processes is influenced by complex thermal conditions, including melting and recrystallisation. These conditions subsequently influence the tensile strength, fracture toughness, impact properties and other mechanical properties [33]. Previous studies on material extrusion of PPS focused on the printing parameters [134], heat transfer [44], layer adhesion [2,43], rheological and thermal properties [3,34] of CF/PPS composites [4]. They found that the 3D printed composites could present a comparable property to extrusion-compression moulding due to highly aligned fibres but a poorer mechanical property to the injection moulding. Material extrusion additive manufacturing still faces challenges, however, to produce high-performance short CF/PPS composite parts for high-end applications because of the formation of the densely packed and ordered crystalline regions as well as thermal and oxidative responses [31]. Although there is limited literature on the thermal history in material extrusion of CF/PPS, several studies have been reported on pure PPS [37,135] and other semi-crystalline polymers such as PEEK [45] and PET [46]. Results show that printed parts with different degrees of crystallinity or different crystallinity regions in the same part can be designed and realised by controlling the heat treatment process. The above literature demonstrated that it is essential to analyse the thermal conditions on the performance of 3D printed semi-crystalline composites.

Previous studies have focused on various aspects of CF/PPS composites in material extrusion, including printing parameters, rheological and thermal properties, and mechanical performance [2–4,136]. However, few studies explore the effect of the thermal history of CF/PPS filament on the material behaviour of printed parts. Therefore, there is a need for further research to specifically investigate the different thermal conditions in processing thermoplastics and their effects on the degree of crystallinity and oxidative reaction of CF/PPS composites. The present study addresses this gap by investigating the thermal conditions, optimising the mechanical properties, and exploring potential applications of CF/PPS composites in material extrusion. Firstly, this study aims to understand how the thermal history influences the resulting composites performance by examining the impact of different thermal processing conditions on the degree of crystallinity and mechanical properties of CF/PPS composites. Secondly, by systematically varying these conditions, we aim to optimise the mechanical properties of CF/PPS composites. By controlling the thermal parameters, such as filament fabrication temperature and annealing treatment parameters, we seek to tailor the degree of crystallinity and enhance the mechanical performance of printed parts. Lastly, this study is to identify potential applications for CF/PPS composites in high-end industries, such as aerospace, automotive, and electronics. By demonstrating the enhanced mechanical properties achieved through thermal optimisation, we aim to display the suitability of CF/PPS composites for lightweight and high-performance components in these industries. Overall, the study contributes to the knowledge and understanding of the thermal behaviour and performance of CF/PPS composites in material extrusion additive manufacturing, which can have implications on optimising processing parameters and improving the mechanical properties of printed parts. The aerospace, automotive, electronics and general manufacturing industries can benefit from the optimised CF/PPS composites produced through material extrusion, while the recyclability aspect aligns with sustainable manufacturing practices.

3.2 Materials and methods

In this study, the commercial product polyphenylene sulphide (PPS) pellets filled with 30 wt. % short carbon fibres (Torayca A630T-30V, Toray Industries Inc., Tokyo, Japan) were used to fabricate the 3D printing filament. The length of carbon fibre is around 200 μm. The PPS powder used in the Fourier transform infrared spectroscopy (FTIR) characterisation was ground from the PPS pellets (Torelina A900, Toray Industries Inc., Tokyo, Japan).

3.2.1 Filament fabrication

The CF/PPS pellets were dried before extrusion in a furnace at 100 ℃ for at least 3 hours, using a lab-scale single screw extruder (Noztek Pro HT). In the extrusion process, the pellets were fed into the hopper and then processed through the heated nozzle, as shown in Figure 3-1. An extrusion speed of 2.5 m/min was applied, and a winding spool was placed at the end of the extruder to receive the filament. The diameter of the extruded filament was 1.6 ± 0.1 mm.

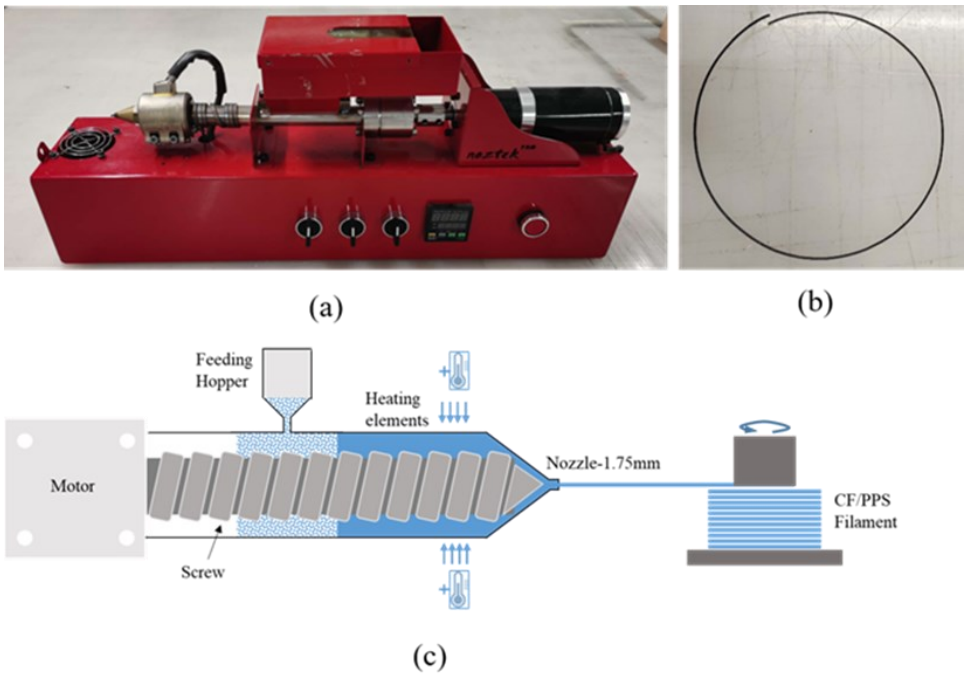

Figure 3-1 (a) Noztek Pro HT Desktop extruder; (b) CF/PPS filament; (c) Schematic diagram of the single screw extrusion process.

3.2.2 **Material extrusion**

A Creatbot F430 printer (420 ℃ version, Henan, China) was used to print the CF/PPS filament, as shown in Figure 3-2. To optimise the printing conditions for the CF/PPS filaments, a range of nozzle temperatures between 310 ℃ and 340 ℃ were selected. It is noted that only the printing temperature was altered in this study. The build platform temperature was set to 90 ℃. The nozzle diameter is 0.8 mm and the printing speed was 20 mm/s. The printing direction was set along the longitudinal direction. All specimens were printed to a 100% infill degree. In addition, the G-code was created by the slicer software Creatware, developed by Creatbot.

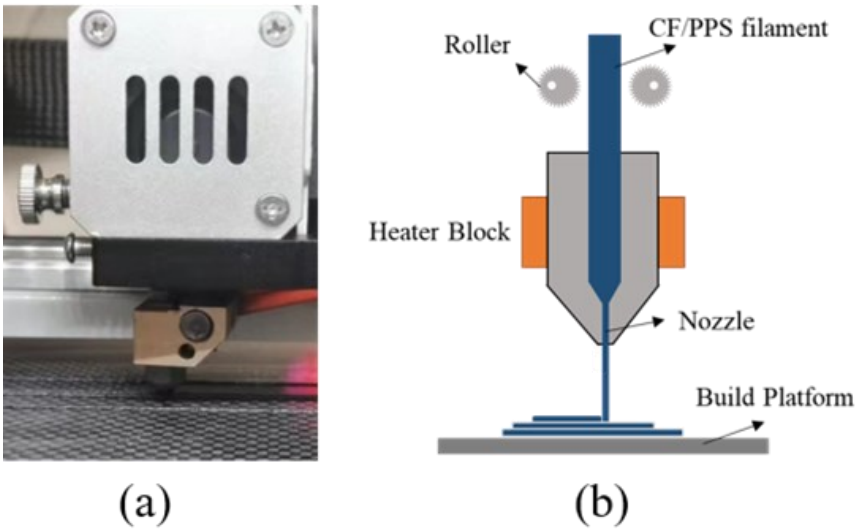

Figure 3-2 (a) Extrusion head of Creatbot F430 printer; (b) Deposition process of the CF/PPS filament.

3.2.3 **Three-point bending test**

All the three-point bending tests on the printed parts were based on the ASTM D7264 standard. The tests were performed using an Instron 3369 machine with a 10 kN load cell. Each test was conducted under displacement control at a crosshead rate of 1.0 mm/min. According to the standard, rectangular parts with dimensions 80 mm × 13 mm × 4 mm were printed. This study

tested three coupons within one group to mitigate the randomness. Figure 3-3 shows the three-point bending test set-up.

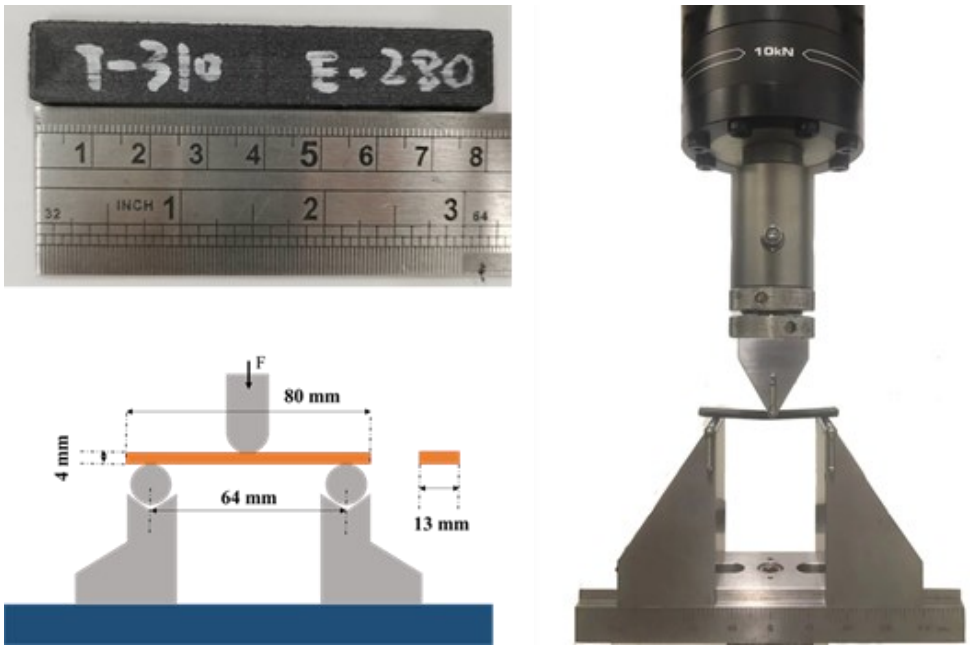

Figure 3-3 Printed CF/PPS sample and three-point bending test set-up.

3.2.4 **Thermal characterisation**

Thermal analysis of the CF/PPS composites was performed by Differential Scanning Calorimetry (DSC, PerkinElmer 8000). All non-isothermal tests were carried out under a 20 ml/min nitrogen flow. The samples were heated up from 30 ℃ to 300 ℃ at a ramp rate of 20 ℃/min and then cooled down to 30 ℃ at the same rate. After that, the samples were heated again based on the same program. Heat flows were measured in the first and second heating cycles for all the samples placed in the alumina crucibles. The melting temperature (T_m) was obtained from the second heating curve according to the heat capacity components, such as the reversing heat flow, while the total enthalpy of reaction in the melting process of the DSC curve was calculated automatically using the Pyris software to determine the crystallinity of the printed composites. The degree of crystallinity (X_c) of PPS is calculated by:

$$X_c(\%) = \frac{\Delta H_m}{\Delta H_f(1-x)} \times 100\% \quad (3\text{-}1)$$

Where ΔH_m is the melting enthalpy, ΔH_f is the melting enthalpy of PPS with 100% crystallinity (80 J/g) and both of which were obtained from the first heating run of the heat flow. x represents the weight fraction of carbon fibre [137]. Note that the cold crystallisation process would not exist in the heating process based on the curves presented in the results section. Therefore, it was not necessary to consider this peak in the calculation.

3.2.5 **Dynamic mechanical analysis**

Dynamic mechanical analysis (DMA) is a technique to characterise the viscoelastic properties of a material by subjecting the sample to a sinusoidal oscillating stress [138]. The viscoelastic properties of untreated printed CF/PPS parts and annealed printed CF/PPS parts were measured on a TA Instruments Discovery DMA 850, with specimen dimensions of 55 mm × 12 mm × 3 mm. Samples in each group were printed in a row to mitigate the errors in the printing process. Two groups were studied to check the repeatability. Each DMA test was performed with a temperature sweep from 40 ℃ to 250 ℃ in the dual cantilever mode, using a frequency of 1 Hz and an amplitude of 30 μm. A ramp rate of 2 ℃/min was used in a nitrogen environment to avoid any degradation.

3.2.6 **Microstructure characterisation and morphology analysis**

Morphology of the raw pellets extruded CF/PPS filament and printed composites were observed using a Scanning Electron Microscope (SEM, HITACHI TM4000Plus) and an optical microscope (Zeiss Axioskop 2). The SEM images were observed to compare the volume fraction of carbon fibres, while the optical microscopic images were used to calculate the void content [139]. Specimens were extracted from raw pellets, from CF/PPS filaments extruded at different temperatures, and from 3D printed composites, which were subsequently sanded and

polished. Images obtained from SEM and optical microscopy were analysed using ImageJ software. The area of carbon fibres and air voids was measured and averaged. To process the images in the software, a threshold was applied according to the pixel difference between carbon fibres and PPS as well as the air voids. Cross-sectional images of five samples were observed and analysed to minimise the uncertainty.

3.2.7 **Fourier transform infrared spectroscopy**

Fourier Transform Infrared (FTIR) spectroscopy was used to characterise the presence of the functional groups in the original pellets, the extruded filament and the annealed parts for PPS materials. A Perkin-Elmer Frontier spectrometer with a universal ATR accessory was used for the FTIR scan. CF/PPS composites were replaced by pure PPS part with natural colour for this work, as it was very difficult to obtain accurate FTIR results using this machine due to the inclusion of black carbon fibres. To ensure a good contact between the samples with the probe, thin PPS parts were used in the scan and each sample was scanned 32 times for wavenumbers between 4000 cm^{-1} and 500 cm^{-1}.

3.3 Results and discussion

3.3.1 **Filament fabrication of CF/PPS pellets**

Firstly, the thermal properties of the as received PPS and CF/PPS materials were characterised by the DSC machine. The results are shown in Figure 3-4. The melting temperature of the PPS polymer matrix was 273 ℃, while the melting temperature of the CF/PPS composites was 283 ℃. The melting temperature of a polymer is the point at which it transitions from a solid to a liquid state. Carbon fibres, which do not degrade at high temperatures, can distribute thermal energy more efficiently than the polymer alone. Additionally, carbon fibres can act as barriers to heat flow within the material. Moreover, by restricting the mobility of polymer chains during the transition, carbon fibres effectively raise the melting temperature of the

composite. The degrees of crystallinity of the as-received PPS and CF/PPS composite are calculated to be 41.1% and 37.6%, respectively. Based on the previous studies related to the extrusion of semi-crystalline polymers, increased chain entanglements and a lower degree of crystallinity in the extruded filament would be more desirable to enable a better printability during the 3D printing [46]. In those cases, the viscosity of the material would become lower and thus more easily extruded through the nozzle of the printer. To optimise the extrusion temperature for the CF/PPS filament, DSC testing was carried out to determine the degree of crystallinity of the filament extruded at different temperatures, ranging from 280 ℃ to 330 ℃. In order to promote the chain entanglements of PPS, the molar mass reduction during the extrusion needed to be mitigated by reducing the water adsorption. Therefore, all the pellets were dried at 100 ℃ for at least 3h in a furnace prior to the extrusion.

The degree of crystallinity versus extrusion temperatures and the first heating running in DSC is plotted in Figure 3-5. The results illustrate that as the extrusion temperature increased from 280 ℃ to 320 ℃, the degree of crystallinity increased from 28.3% to 51.4% accordingly and then showed a slight drop at 330 ℃. Generally, a more brittle filament with a higher crystallinity was obtained at a higher extrusion temperature. This is explained by more polymer chains folding and aligning themselves with each other as the temperature increases. The inter-chain bonding showed a slight decrease, however, when the filament was extruded at an elevated temperature, possibly because of oxidation. Therefore, the lowest extrusion temperature of 280 ℃ was preferably selected to produce a more ductile and flexible filament for later 3D printing. A further decrease of the temperature below 280 ℃ was impossible since the CF/PPS pellets could not be extruded at a temperature that is below the melting point of the PPS polymer. Overall, the optimal thermal conditions for the extrusion of CF/PPS pellets were identified as drying the pellets at 100 ℃ for at least 3h and then extruding at 280 ℃.

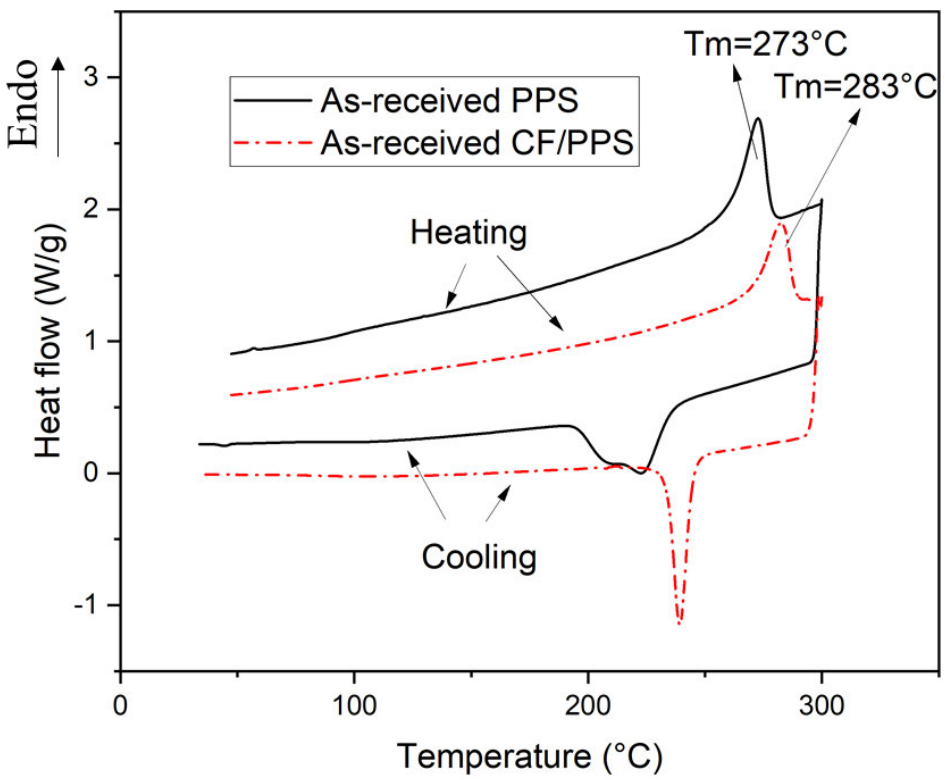

Figure 3-4 DSC curves of as-received PPS and CF/PPS.

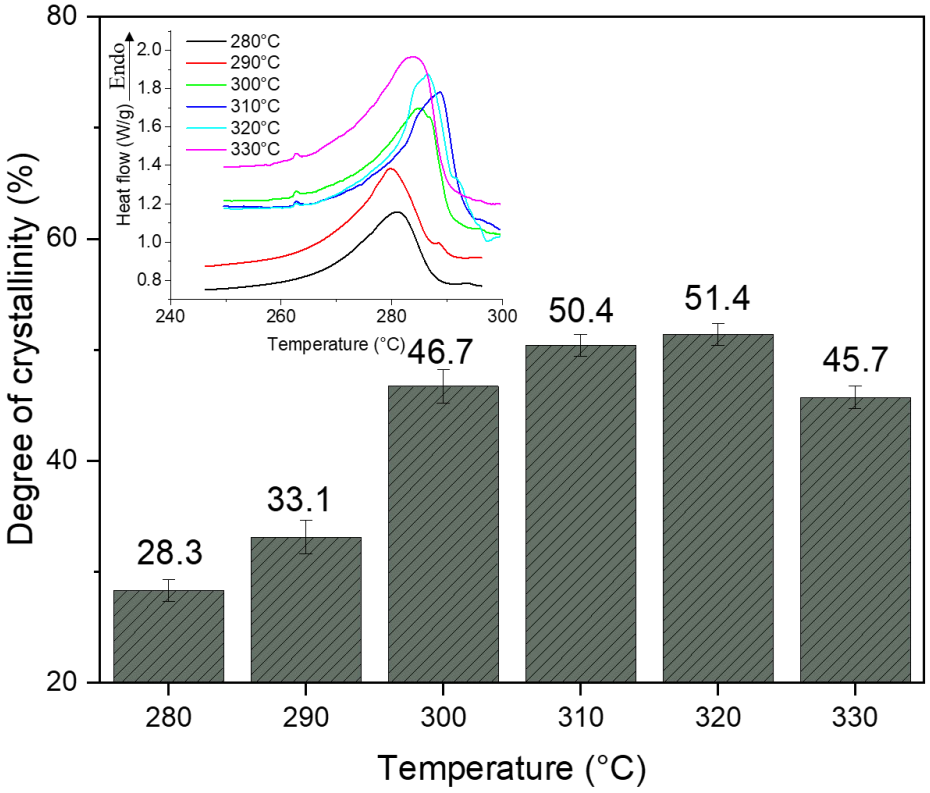

Figure 3-5 Degree of crystallinity of filaments extruded at different temperatures.

3.3.2 **Material extrusion of CF/PPS filament**

The printing parameters in material extrusion have a significant effect on the crystallisation behaviour of semi-crystalline polymers [45]. To investigate the optimal printing temperatures for the CF/PPS filament, the mechanical properties, as well as the crystallinity of the parts printed at 310 ℃, 320 ℃, 330 ℃ and 340 ℃ were studied. The crystallinity and DSC peaks of printed CF/PPS parts in the first heating process and the crystallinity temperatures at different printing temperatures are plotted in Figure 3-6. The relationship between the printing temperature and the mechanical properties in terms of flexural strength and modulus is presented in Figure 3-7.

As shown in Figure 3-6(a), when the temperature was increased from 310 ℃ to 340 ℃, the crystallinity first increased from 48.7% to 51.5% at 320 ℃ and then started to reduce until 340 ℃. At the same time, in the first cooling process shown in Figure 3-6(b), the crystallisation temperature of the CF/PPS reached a peak at 238.8 ℃ first and then interestingly went down to 237.1 ℃. Correspondingly, the mechanical properties show the same trend, increasing from 125.3 MPa to 155.1 MPa for the flexural strength and from 10.64 MPa to 14.23 MPa for the flexural modulus and then decreasing to minimum values at 340 ℃ (Figure 3-7). On one hand, the higher nozzle temperature provides more energy to melt all crystals in PPS material and allows more time for it to recrystallise in the cooling process during the 3D printing. In addition, PPS material tends to crosslink when the temperature is higher. This crosslinking may change the crystallisation process of uncross-linked PPS as a nucleating agent, which could provide the reaction point for the crystallisation process. The parts with higher crystallinity also manifest higher flexural strength and greater flexural modulus. On the other hand, when the nozzle temperatures are above 320 ℃, the effect of the nozzle temperature is more complicated.

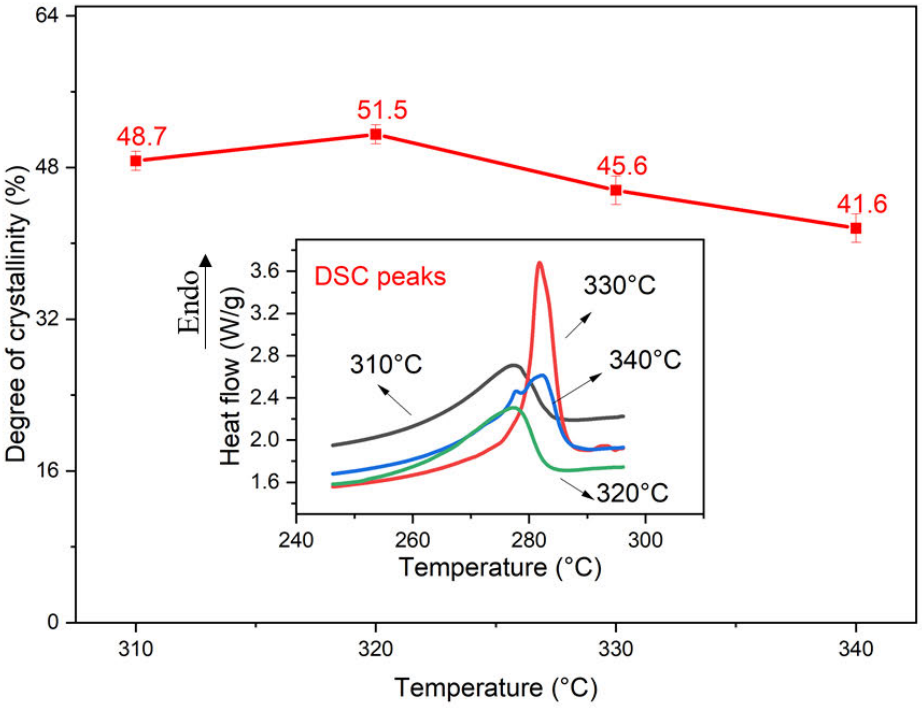

(a)

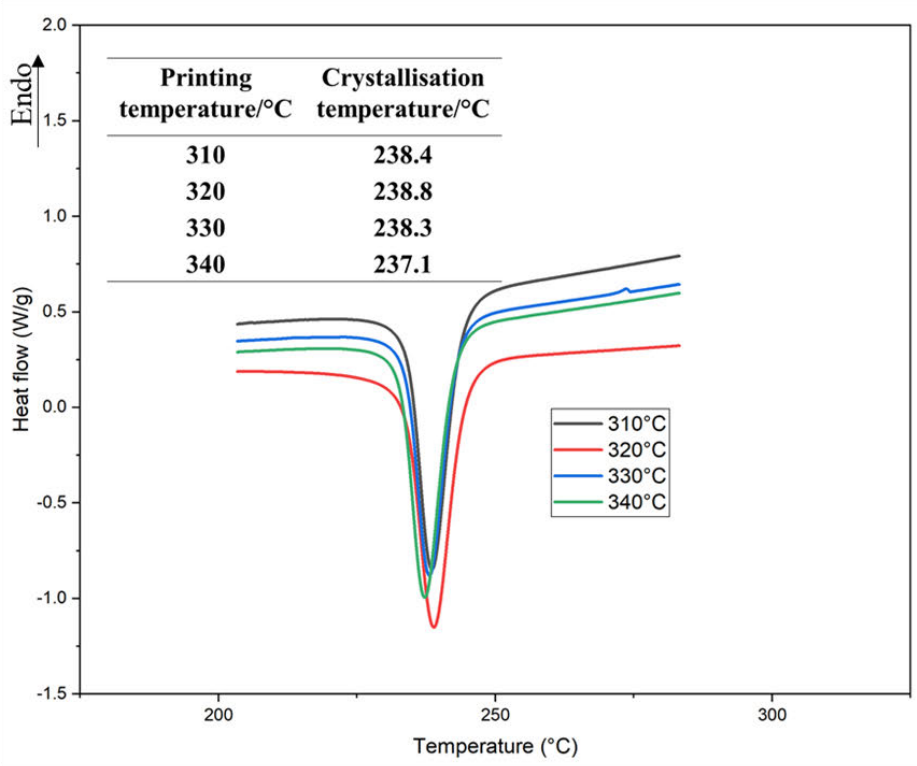

Printing temperature/°C	Crystallisation temperature/°C
310	238.4
320	238.8
330	238.3
340	237.1

(b)

Figure 3-6 (a) Degree of crystallinity and melting peaks of printed CF/PPS parts at different printing temperatures in the first heating process; (b) Crystallisation temperatures and DSC peaks of printed CF/PPS parts at different printing temperatures in the first cooling process.

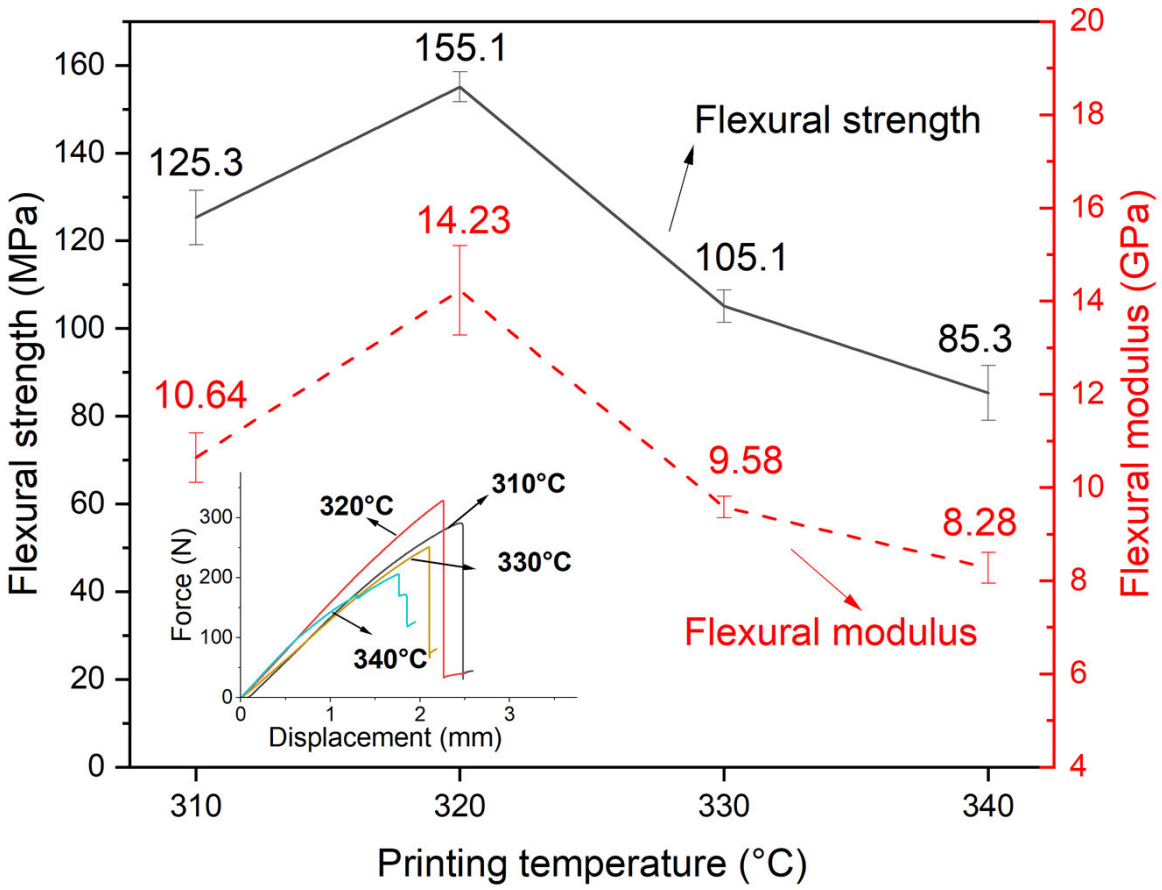

Figure 3-7 Flexural strength and modulus of printed CF/PPS parts at different printing temperatures.

PPS is known to be sensitive to oxidative reactions at process temperatures, which changes the behaviour of the polymer chains [37]. At high temperatures, particularly in the presence of oxygen, PPS can undergo oxidative degradation. This process involves the breaking of C-S-C bonds in the polymer backbone, leading to the formation of aryl ether group (C-O), sulfoxide group (-S=O) and other oxidative species [140]. To better understand the chemical reactions between the PPS chains at higher temperatures, PPS parts printed at different nozzle temperatures were subjected to FTIR analysis. As seen in Figure 3-8, a new peak at 1042 cm^{-1} corresponding to the presence of aryl ether (C-O) bonding occurred at printing temperatures of 320 ℃, resulting from the oxidation reactions. And, its intensity rose as the printing temperature increased. It is interesting to note that the cross-linking structure in the polymer

acts as the nucleating agent first and then hinders the formation of the crystalline structure if the linkages become dominant at elevated temperatures [141,142]. These crosslinking chains could cause the deterioration phenomenon of polymer materials and then have a negative impact on crystallinity, thus reducing the mechanical properties of the printed parts. Results proved that the crosslinking effects performed a key role in determining the crystallinity in a higher nozzle temperature environment, and the degree of crystallinity indicated the mechanical properties. Overall, the optimal thermal process condition for this CF/PPS filament in material extrusion was found to be 320 ℃.

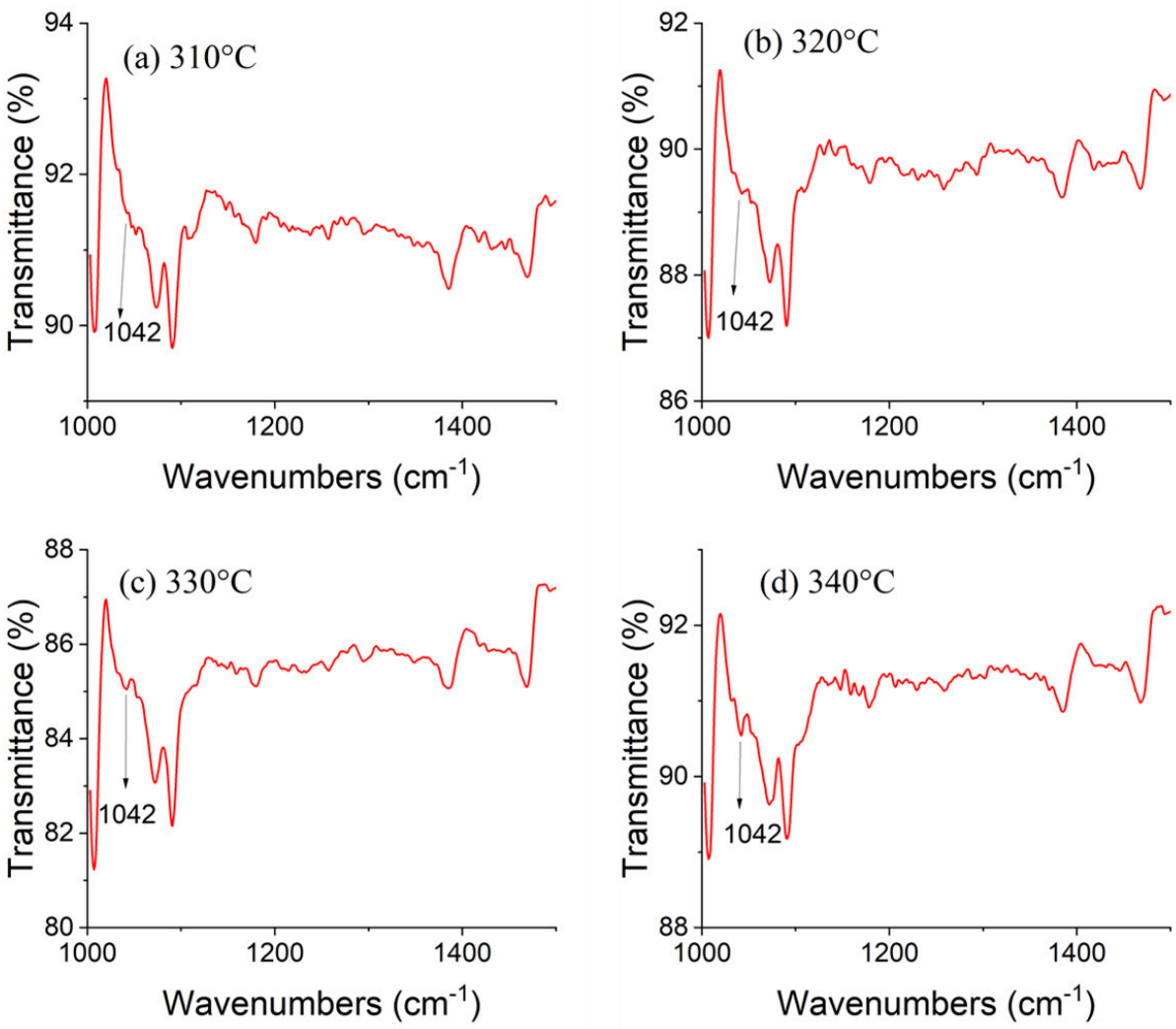

Figure 3-8 FTIR analysis of PPS parts at different printing temperatures: (a) 310 ℃; (b) 320 ℃; (c) 330 ℃; (d) 340 ℃.

3.3.3 **Heat treatment of 3D printed CF/PPS composites**

It has been reported that heat treatment methods could have a significant effect on the degree of crystallinity of PPS polymers [3]. Therefore, furnace annealing could be an efficient method to enhance the crystallinity of the 3D-printed CF/PPS composites. The samples were heated in a muffle furnace at 100 ℃ for 45 min (heating rate: 5 ℃/min) first and then annealed at 130 ℃ for 6 hours. After annealing the samples were cooled down in the furnace naturally by air. The annealing temperature was selected between glass transition temperature (around 100 ℃) and melting temperature (around 280 ℃) of CF/PPS composites. Samples were 3D-printed at 320 ℃, the optimal printing temperature, and 340 ℃ for comparisons. Half of the samples in each group were heat treated by annealing, and all samples were printed at one time to mitigate the uncertainties in the 3D printing process. The results were plotted in Figure 3-9.

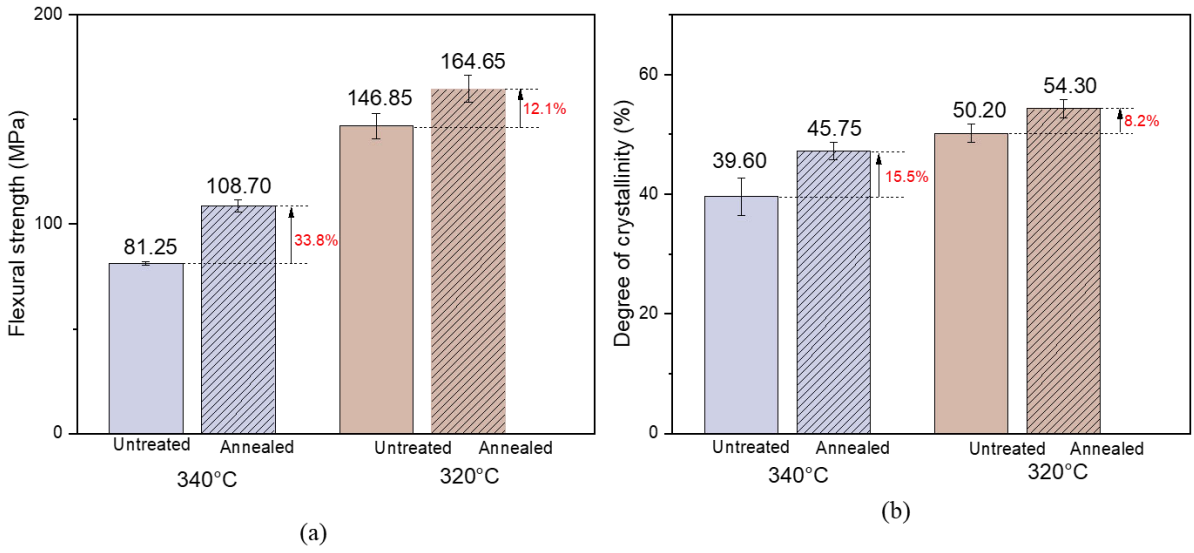

Figure 3-9 (a) Flexural strength and (b) degree of crystallinity of printed CF/PPS before and after annealing.

As seen in Figure 3-9(a), the samples in both groups show an increase in flexural strength after the annealing treatment. When printing at 340 ℃, the annealed part showed an increase in flexural strength of 33.8%, in contrast to an increase of 12.1% for printing at 320 ℃. This is

also confirmed by the curves in Figure 3-9(b) which show a higher degree of crystallinity after the annealing treatment. Annealed part printing at 320 ℃ manifested the highest crystallinity of 54.3% after the treatment. It is known that the annealing method has a substantial impact on the crystallisation process, crystal structure, and size of the semi-crystalline polymers, resulting from the increase of chain mobility when heat is applied at temperatures above glass transition temperature and below melting temperature. In addition, isothermal annealing could also lead to structural changes in the form of chain extension, branching, or crosslinking (curing), especially in an oxidising environment.[3,143,144] Therefore, the post-process heating treatment could increase the degree of crystallinity, trade off the printing defects and consequently improve the flexural properties of printed parts in this work. Annealing was found useful in improving the CF/PPS mechanical properties, especially for the parts with poorer mechanical performance.

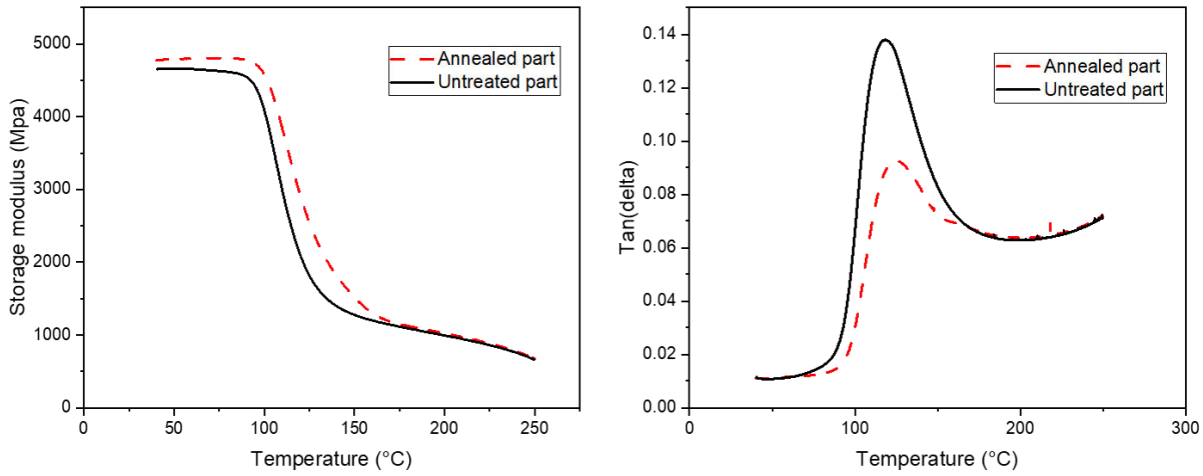

Figure 3-10 Comparison of (a) storage modulus and (b) tan δ for untreated printed parts and annealed parts.

DMA tests of two groups of the printed parts were conducted to measure the variation in viscoelastic properties with temperature for untreated and annealed samples of the printed

CF/PPS composites to further understand the effect of the annealing treatment on the CF/PPS materials. The nozzle temperatures for these two samples are set to 320 ℃. Figure 3-10 depicts the storage modulus (*G'*) as well as the damping factor (tan δ), which is the ratio of the loss modulus (*G''*) to the storage modulus (*G'*). It can be seen that the CF/PPS sample subjected to the annealing treatment shows an increased storage modulus from room temperature until 150 ℃. The *G'* was increased by 34.1%, the maximum value at *Tg* temperature (112 ℃) for annealed sample (Figure 3-10(a)). The storage modulus is indicative of the elastic energy stored in the material, which is related to the morphology changes of the material. In addition, the damping factor (tan δ) showed a reduction caused by annealing treatment in the same temperature range, which indicates that higher energy is used to deform the annealed materials that are directly dissipated into heat. These variations in storage modulus and damping factor are most likely to be generated by increasing crystallisation [137]. Greater constraints of polymer chains are imposed by more crystal domains and thereby reduce their mobility and increase the resistance to deformation caused by oscillating stress. As a result, the elasticity of the materials was improved [143]. Furthermore, Figure 3-10(b) shows that the *Tg* of the annealed samples has slightly increased by 8 ℃, resulting from this heating treatment method, which also is an indication of improved crystallinity in semi-crystalline PPS.

To confirm the presence of the oxidative groups in printing materials after annealing, untreated PPS and annealed PPS were characterised using FTIR, as shown in Figure 3-11. The peaks at 1572, 1470, and 1385 cm^{-1} were assigned to benzene ring stretching (C-C) in S–C_6H_4–S. The peaks at 1090 and 1072 cm^{-1} were attributed to ring-S stretching (C-S) in S–C_6H_4–S. The characteristic bands at 1008 cm^{-1} were attributed to C–H bending modes [145,146]. Compared with PPS raw material, there is a new peak at 1042 cm^{-1} generated by the aryl ether (C-O) linkage in the annealed sample, which indicates the oxidation reactions in the annealing process. In addition, the peak at 1178 cm^{-1} was broadened by the annealing treatment, corresponding to

the stretching vibration adsorption of the sulfoxide group (–S=O). That indicates that the oxidation level was increased in the form of oxidative branching as well. In summary, the annealing treatment introduces the oxidative groups and increases the degree of crystallinity to the PPS material.

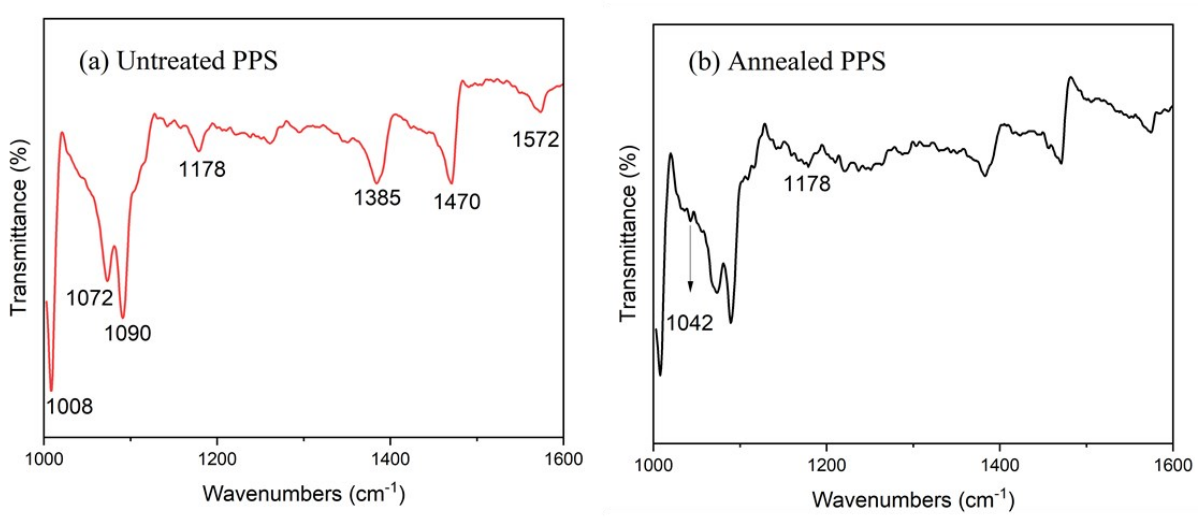

Figure 3-11 FTIR analysis of (a) untreated and (b) annealed PPS powders.

In order to compare the 3D printed CF/PPS in this study with previous work and PPS composites reinforced by random-oriented discontinuous carbon fibres in the literatures, Figure 3-12 summarises published studies on the flexural strength and modulus of CF/PPS composites from both traditional manufacturing methods and material-extrusion additive manufacturing methods at different carbon fibre fractions [36,71,75,126,132,147–149]. Although there are limited studies on the material extrusion based additive manufacturing of short CF/PPS composites, there is a huge improvement (150%) in the flexural strength of PPS composites with 24.1 vol% (calculated) fibres in this work compared with the previous 3D printed pure PPS parts, thanks to the carbon fillers. Meanwhile, the results in this work are comparable with the CF/PPS composites manufactured by the hydraulic press and injection moulding with the same carbon fibre content.

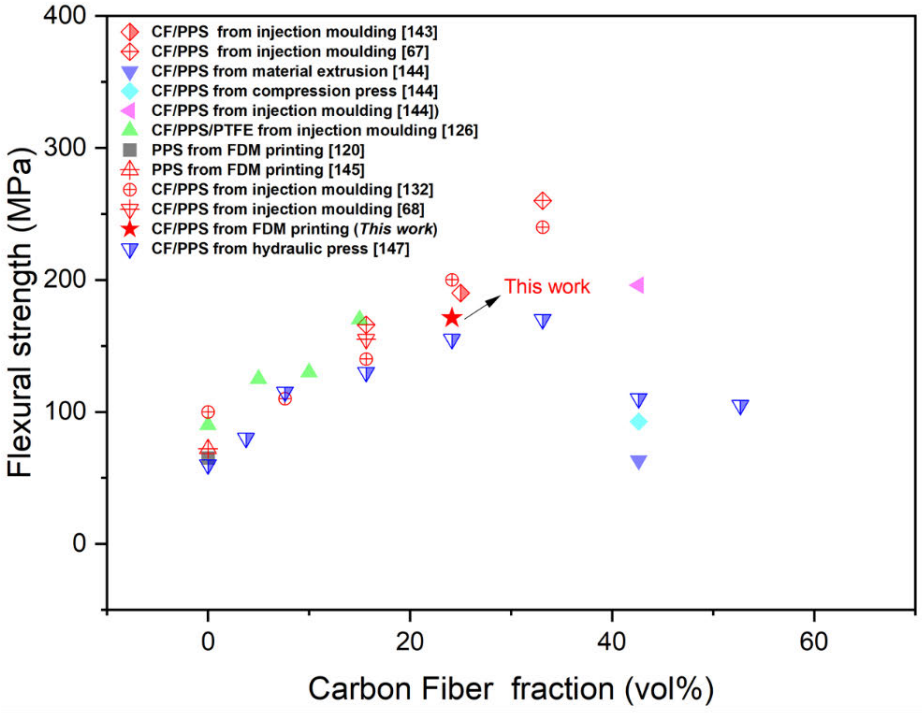

(a)

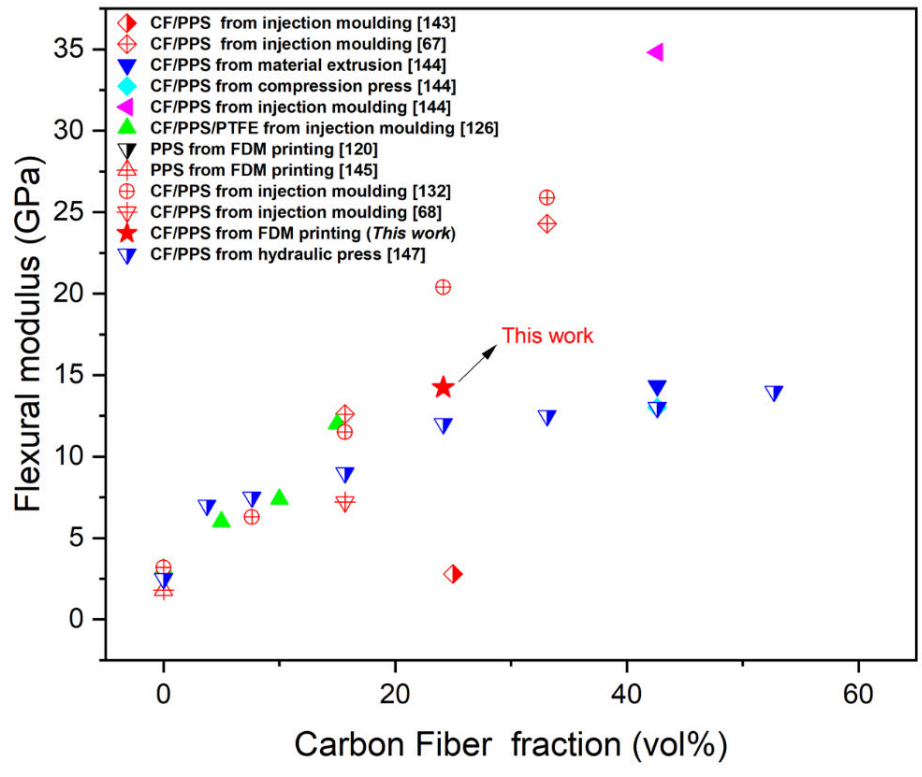

(b)

Figure 3-12 Comparison of (a) flexural strength and (b) flexural modulus in this work with previous studies.

This comparison highlights the effectiveness of the material extrusion additive manufacturing method in producing CF/PPS composites with enhanced mechanical properties. The results from this study indicate that the 3D printed CF/PPS composites exhibit competitive performance when compared to traditionally manufactured CF/PPS composites. The use of carbon fibre fillers in the material process enhances the flexural strength of CF/PPS composites, making them a promising alternative for various applications requiring lightweight, high-strength and cost-effective materials. Overall, this study provides a comprehensive overview of the performance of the 3D printed CF/PPS composites and establishes their competitiveness in terms of flexural strength and modulus, which facilitates the development of high-performance CF/PPS composite parts with improved reliability and durability for demanding applications.

3.3.4 **Microstructure characterisation and morphology analysis**

The microstructure of the CF/PPS material, in terms of fibre volume fraction, fibre length, and air void contents, before and after 3D printing was measured. This was to check whether the microstructure has evolved in addition to the crystallinity of the PPS matrix, as they both could affect the mechanical properties of the printed CF/PPS composite. Optical microscopic images of the raw pellet, the filament, and the printed composite are shown in Figure 3-13 (a), (c), and (e), respectively. Fibre volume fraction and air void contents were measured using ImageJ software and listed in Table 3-1. The fibre volume fraction was then calculated and found to be slightly reduced from 28.6% in the raw pellet to 26.1% in the filament and further to 25.3% in the printed composite. It is shown that the void contents in both the raw pellets and the printed composites are around 5% although it becomes slightly higher (6.37%) in the extruded filaments. This is possibly due to voids between the printed beads, even though the printer nozzle diameter (0.8 mm) was smaller than the extruder nozzle diameter (1.75 mm).

Nevertheless, the orientation angle of the discontinuous carbon fibres remains the same (18˚in average) after being deposited through the 3D printer nozzle, as shown in Figure 3-13(e).

Table 3-1 Summary of the carbon fibre length and carbon fibre volume and void content in raw pellets, extruded filaments, and printed composites.

	Average carbon fibre length (μm)	Carbon fibre volume (%)	Void content (%)
Raw pellets	206.9	28.6±1.5	4.00±0.80
Extruded filaments	209.5	26.1±1.2	6.37±0.60
Printed composites	198.2	25.3±1.4	5.71±0.64

Samples of raw pellet, extruded filament, and printed composite were burned off in a furnace to thermally decompose the PPS matrix to measure the fibre length. The pyrolysis conditions were set up to 500 ℃ for 2 hours to achieve a full decomposition of the PPS polymer. The optical microscopic images of individual carbon fibres after burn-off experiments are shown in Figure 3-13(b), (d), and (f). The average fibre length of approximately 250 fibres, with a range of 200-300 fibres was measured and calculated by ImageJ software. The results are listed in Table 3-1. As observed, there is no noticeable change in fibre length during the filament fabrication and material extrusion. The average fibre length remains around 200 μm in the CF/PPS filament and the printed CF/PPS composite.

Overall, in the final printed composites, there is no substantial alteration of length and volume fraction of the discontinuous carbon fibres through the extrusion and printing processes, thus the effect of these parameters on the comparison of the flexural strength in each group is negligible.

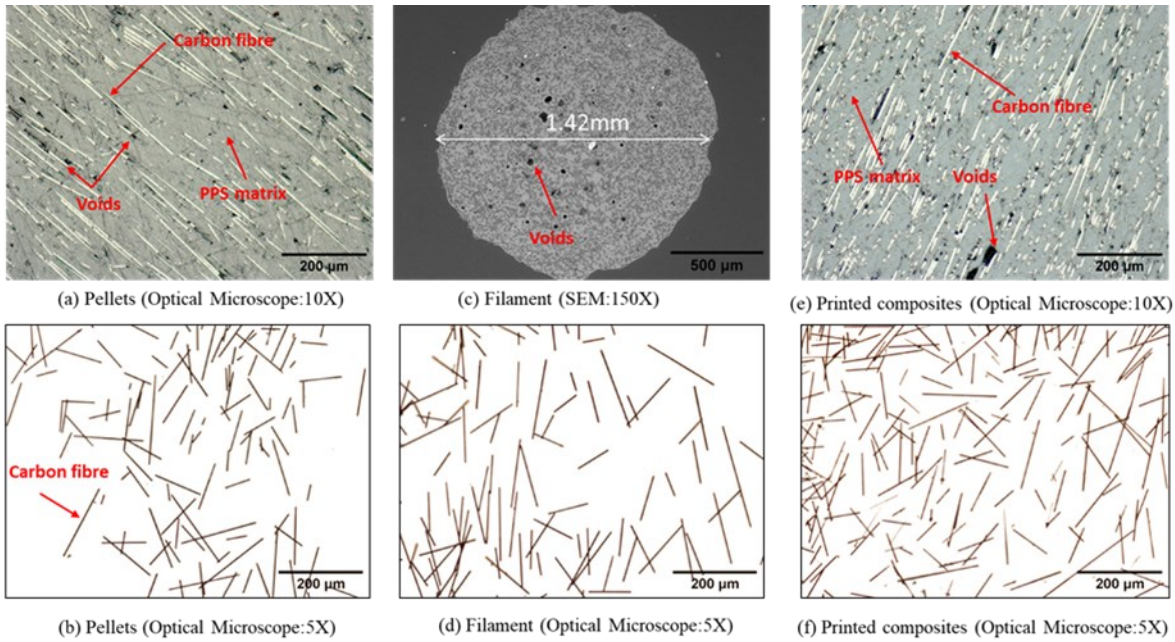

Figure 3-13 Cross-sectional images of (a) pellets, (c) filament and (e) printed composites and optical microscope images of carbon fibre in (b) pellets, (d) filament and (f) printed composites after burn-off experiment.

3.4 Conclusions

The results highlight the significant role of oxidation crosslinking reactions in altering the crystallinity and mechanical strength of CF/PPS composite at elevated temperatures. The findings indicate that oxidation crosslinking acts as a nucleating agent, enhancing the degree of crystallisation in uncross-linked polymers. However, at higher temperatures, the dominant effect of the crosslinking of the polymer chains hinders crystallisation.

Furthermore, the annealing treatment was found to influence the crystallisation process, thereby impacting the mechanical properties of the printed parts. Remarkably, the annealing thermal treatment showed a larger improvement in the mechanical properties of the printed CF/PPS composites with initially poorer properties.

In summary, this research provides a deeper scientific understanding of the relationship between thermal conditions, crystallinity, and mechanical performance in CF/PPS composites. The insights can guide future research in optimising processing parameters and further enhancing the performance of CF/PPS composites in applications requiring lightweight, high-strength, and cost-effective materials.

Chapter 4 **Improving the interfacial adhesion between recycled carbon fibres and polyphenylene sulphide by mussel-inspired dopamine for advanced composites manufacturing**

Abstract

Polyphenylene sulphide composites with recycled carbon fibres are of high interest due to their promising mechanical properties. Poor interfacial adhesion between recycled carbon fibre and thermoplastic matrix, however, remains a major problem in composite manufacturing. Herein, a novel one-step method using bio-inspired copolymerisation of dopamine to graft silica nanoparticles onto the carbon fibre surface is reported. Comprehensive investigations were conducted to fabricate the treated carbon fibre and characterise the modified samples by analysing the surface morphology and functional groups. The experimental results reveal that the network of bio-inspired adhesive polydopamine and nanoparticles adhering to the fibres can improve inter-laminar shear strength by 28.4% in the resulting composites. In addition, dynamical mechanical analysis results prove that the interfacial bonding at the fibre/matrix interface provides good resistance to thermal cycling. This novel approach introduces the functional groups on the recycled carbon fibre surface, leading to an improvement of surface energy and wettability between the carbon fibres and polyphenylene sulphide matrix and constitutes a robust and green approach to the manufacturing of advanced composites.

Keywords

Recycled carbon fibres; Fibre/matrix bonding; Bio-inspired dopamine; Advanced composites manufacturing; Polyphenylene sulphide; Sustainability

4.1 Introduction

Fibre-reinforced polymers (FRPs) have been widely used in aircraft structures due to their enhanced mechanical strength and light-weight for reduced fuel consumption [71,131]. It was reported that the use of carbon fibres has increased from 48,500 tons in 2013 to 140,000 tons in 2020, expected to grow several times in size in the next decade [150]. One of the most significant growth sectors is in the aerospace industry. Currently, more than 6,000 aircraft will end their lives by 2030, thus there will be a big challenge to deal with the end-of-life composite materials because of the detrimental environmental impact and landfill area shortage. Furthermore, a large amount of waste carbon fibres from out-of-life rolls of prepreg and off-cut the manufacturing process has already attracted public concern [151,152]. Technological breakthroughs in pyrolysis or fluidised bed process for recycling carbon fibre from thermoset composites, mainly epoxy resin, have recently made this product commercially available [70,153,154]. This study is motivated by the pressing need to manufacture sustainable next-generation composites that not only mitigate the environmental impact but also maximise the economic value of recycled carbon fibre (rCF). By focusing on the integration of rCF into secondary structural components for the aerospace industry and extending its application to the automotive sector [155], our research aims to contribute significantly to the development of green manufacturing processes, highlighting the critical role of innovative surface treatment strategies in the transition towards more sustainable industrial practices.

It is well known that the interface between carbon fibre and matrix is vital to the mechanical properties of composites because the bonding area is usually the weakest part of the whole structure [94,156,157]. However, non-polar carbon fibres lacking functional groups often lead to poor interfacial adhesion with thermoplastic matrices, which could result in severe fracture risks at the interface. The primary challenge includes the reduced mechanical properties,

delamination, reduced fatigue resistance and compromised thermal resistance. Therefore, the weak interface properties limit the industrial application of carbon fibre/polyphenylene sulphide (CF/PPS) composites. Traditional surface modification methods include chemical modifications, physical treatments, and their combinations. Chemical modifications effectively enhance interfacial adhesion by introducing chemical groups onto the non-polar carbon fibre surface. Techniques such as grafting coupling agents [6] and adding compatibilisers [75] have been widely documented, increasing compatibility between carbon fibre and polymer to improve mechanical properties. Nonetheless, traditional chemical modifications often involve oxidation processes, organic solvents, and harsh reaction environments, potentially weakening the original carbon fibre and posing challenges for scaling up.

Plasma treatment, a key physical method, activates the carbon fibre surface efficiently. Low-pressure plasma techniques are promising for introducing functional groups such as ether, carboxylic, and carbonyl onto the carbon fibre surface, thereby enhancing interfacial adhesion [80]. Despite their versatility and effective plasma-surface interaction through processing condition optimisation, these techniques have limitations, including inability to modify the carbon fibre bundle's inner surface, potential functional group degradation, and the requirement for complex vacuum equipment and high energy [158].

Some researchers have utilised multiple chemical modification treatments or combined that with physical treatments in modifying the surface of the non-polar carbon fibre. Existing solutions generally follow a two-step approach: the first step is to roughen the smooth surface of carbon fibres, mainly including oxidation or plasma treatment, and the next step is to introduce a new layer between the fibre and matrix by adding compatibiliser and grafting coupling agents [9,10,157,159]. Previous research has explored various modification methods to enhance the interfacial strength. Despite the effectiveness, these conventional methods often rely on toxic chemicals, energy-intensive process, or harsh operating conditions.

Increasingly, attention has shifted towards green solutions including advanced nanomaterials [87–91] and building green networks through bioinspired structures [92–96,160,161]. The mussel's adhesion capability to various substrates, attributed to dihydroxyphenylalanine (DOPA), has inspired the use of polydopamine (PDA) for strong adherence to diverse surfaces, from inorganic to organic [97]. PDA's green synthesis in aqueous solutions and self-polymerisation process facilitate easy deposition on various surfaces [162].

Recent research has focused on enhancing interfacial adhesion between commercial carbon fibre and thermosetting resins using PDA-assisted carbon fibre modifications. Gao *et al.* [96] reported a one-step copolymerisation of dopamine and poly(amidoamine) on carbon surfaces, markedly improving interfacial properties between carbon fibre and epoxy matrix. Wu *et al.* [93,94,160,161] further explored this bioinspired strategy to deposit various layers (silane coupling agent, polyether amine or graphite oxide) on carbon fibre, offering a sustainable approach to fabricate enhanced-performance composites. Similarly, polydopamine assists in depositing silica nanoparticles [12] and Ni $(OH)_2$ nanosheets [13]. This strategy has also been applied to thermoplastic resins, with hybrid sizing of carbon nanotube and polydopamine significantly enhancing the creep resistance of CF/PEI composites [14]. Recently, to expedite PDA production, Sun *et al.* [98] investigated an ultrasound-assisted PDA polymerisation process on CF, also facilitating PDA molecule permeation into the fibre bundle and highlighting the crucial role of phenolic hydroxyl and amino groups for compatibility with the PA6 matrix.

While numerous studies have focused on using PDA to modify the surface of carbon fibres and to graft polymer or nanomaterials onto them [12–14,93,94,160,161], existing literature has not yet bridged the gap between this novel, environmentally friendly approach, and its application to recycled carbon fibres and high-temperature thermoplastic resins like polyphenylene sulphide. In response, this work develops a more sustainable one-step surface modification

strategy that employs PDA as an adhesive agent for recycled carbon fibres. This PDA layer forms a hybrid network with silica nanoparticles on the fibre surface, acting as a multi-functional interface. This interface not only enhances adhesion but also introduces new mechanical and chemical pathways for stress distribution, thereby improving the performance of rCF/PPS composites. Our work takes a significant step toward lowering the environmental footprint of composite manufacturing.

4.2 Materials and methods

4.2.1 Materials

Carbon fibre (Plain weave 3K woven fabric cloth, areal weight of 210 g/m^2) was purchased from Easy Composites Ltd, Stoke on Trent, United Kingdom. Tetraethoxysilane (TEOS), Dopamine hydrochloride (DP) and Tris (hydroxymethyl)-aminomethane (Tris) were purchased from Merck Life Sciences Ltd, United Kingdom. Polyphenylene sulphide (PPS, Torelina A900) was manufactured by Toray Industries, Japan. Acetone used in the desizing process was obtained from Fisher Scientific Ltd, Leicestershire, UK. All chemicals were used as received unless stated otherwise.

4.2.2 Fabrication of CF-PDA/NPs

Colloidal silica nanoparticles (NPs) were synthesised using TEOS as the precursor following a specified route [163]. Initially, a mixture of ethanol and TEOS was prepared to form Solution A, while Solution B comprised a mixture of ethanol, deionised water, and ammonia solution. Subsequently, Solution B was gradually added to Solution A at a temperature of 60 °C. Ammonia served as a catalyst to expedite the hydrolysis and condensation reactions. The concentration of ammonia dictated the pH of the solution, which in turn significantly influenced the size and distribution of the silica nanoparticles. Upon introduction to water, TEOS promptly undergoes hydrolysis catalysed by ammonia, resulting in the formation of

silicic acid ($Si(OH)_4$). These silicic acid molecules then undergo polycondensation to form silica nanoparticles. The resultant colloidal silica nanoparticles purified through centrifugation, followed by concentration using a rotary evaporator. Transmission Electron Microscopy (TEM) image for silica nanoparticles shows that the average diameter of a single particle is around 50 nm (Figure 4-1(c)), which is dispersed uniformly in the buffer solution.

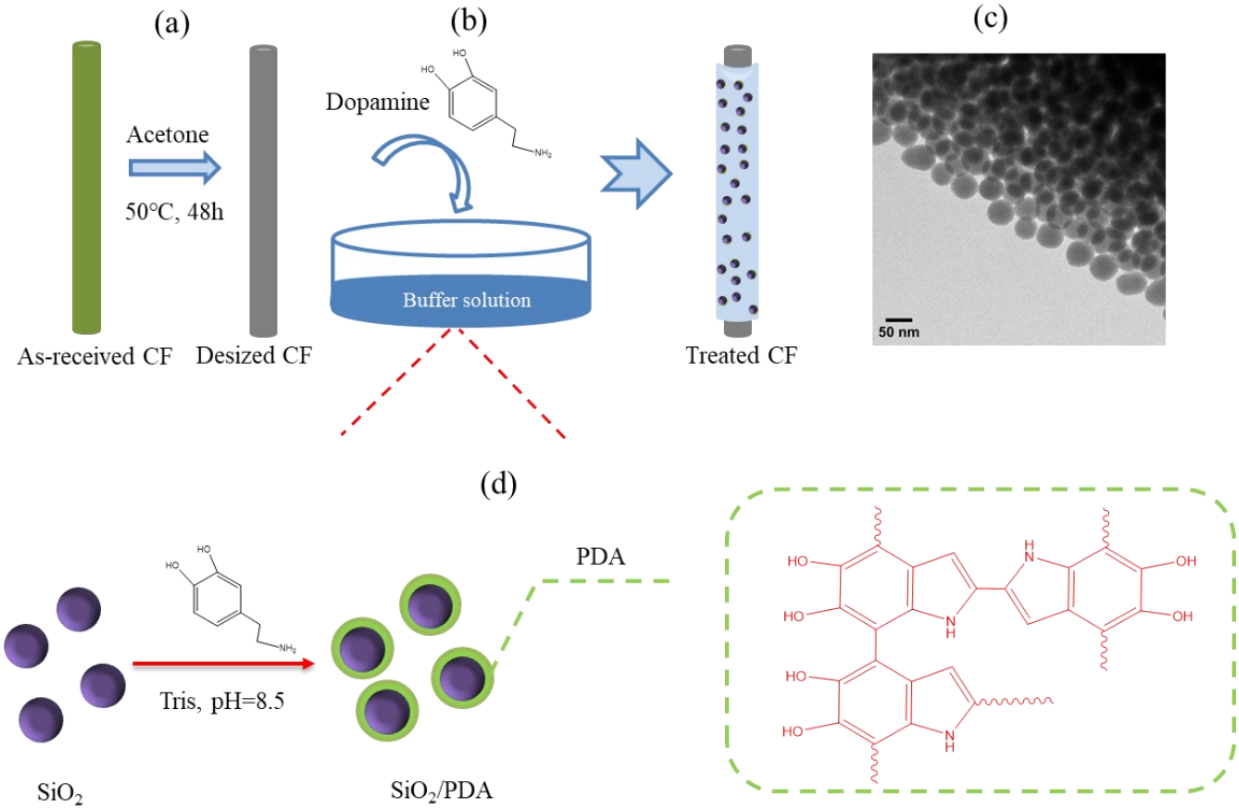

Figure 4-1 Fabrication scheme of the treated carbon fibre: (a) desizing procedure; (b) dopamine/silica nanoparticles treatment; (c) silica nanoparticles; (d) reaction scheme in buffer solution.

Untreated (as-received) carbon fibre was desized by acetone first to remove any contaminants or sizing agents (Figure 4-1(a)), and then the concentrated silica nanoparticles were dispersed in the buffer solution (0.1% Tris solution, pH=8.5), which is suitable for the self-polymerisation reaction of dopamine. The carbon fibre and dopamine hydrochloride were added to the buffer

solution simultaneously at room temperature with an ultrasound instrument to produce the treated carbon fibre CF-PDA/NPs, as illustrated in Figure 4-1(b). After immersing the fabric cloth in the modification solution, it was removed and rinsed three times with deionised water and then dried at 60 ℃ in the oven for 48 hours to obtain the treated CF. As seen in Figure 4-1(d), nanoparticles were coated through the self-polymerisation of dopamine reacting in the buffer solution, followed by depositing themselves on the carbon fibre surface, to ensure the PDA layer and silica nanoparticles are securely attached.

4.2.3 **Characterisation of carbon fibres**

Scanning Electron Microscope (SEM) instrument (JEOL, JSM-IT100) was applied in observing the surface morphology of the desized carbon fibre and treated carbon fibre. Samples were initially dispersed in ethanol and subsequently evaporated onto stubs at room temperature. Following this, the sample underwent sputter-coating with a conductive material, specifically gold, to enhance conductivity. SEM images were captured at magnifications of ×4000 to meticulously assess the distribution, density, and adherence of silica nanoparticles on the carbon fibre surface.

Transmission Electron Microscopy (TEM), employing a JEOL JEM1400 Plus instrument, facilitated detailed observations of the polydopamine and nanoparticle coatings on individual fibres. Carbon fibres were dispersed in ethanol, evaporated onto a mesh for TEM examination. This allowed for an in-depth analysis of the coatings' cross-sections and the interface between the desized carbon fibre, polydopamine layer, and silica nanoparticles.

Raman spectroscopy was employed to assess near-surface structural variations across different fibres. A Renishaw inVia Raman microscope was applied to generate the Raman spectra of the different carbon fibre surfaces. The spectra were obtained using excitation laser lines of 514 nm, with a spectral resolution of 1 cm^{-1}.

X-ray photoelectron spectroscopy (XPS, Scienta 300) spectra were performed to determine the elemental composition and chemical states of atoms within the carbon fibre surface. The X-ray source is a SPECS monochromated Al Ka source (photon energy 1486.6 eV) operating at approx. 12 KV and 200 watts power. For all spectra, the instrument maintained a pass energy set to 150 eV. Survey scans were collected with a dwell time of 133 msec, a step size of 200 meV, and 2 scans aggregated for enhanced accuracy.

4.2.4 **Preparation of the CF/PPS composite laminates**

Single carbon fibre woven sheet was desized and then immersed in the buffer solution containing PDA and NPs to allow the NPs to penetrate and deposit on the surface of carbon fibre (refer to Figure 4-2(a)). After rinsed and dried, they were hot pressed into the PPS matrix to form CF/PPS laminates using a PEI Lab 450 press (Figure 4-2(b)). The PPS pellets were milled into powders (70 μm in average) first and then pressed at elevated temperatures in a mould to fabricate PPS films. Then the PPS film was compounded with carbon fibre using the film stacking method to produce CF/PPS sheets (thickness: 0.5 mm; carbon fibre volume fraction: 42.6%). Lastly, 8 plies of CF/PPS composite sheets were placed in the mould again to complete the consolidation process by hot press to produce the laminates in 3PB bending (thickness: 4 mm). As observed from Figure 4-2(c), the average void content in the CF/PPS laminates was calculated to be around 5%. The time-temperature-pressure cycle of the hot press is shown in Figure 4-3 and was plotted with parameters referenced in [164]. Higher pressure (5 MPa) was used in the fabrication process of CF/PPS sheets to promote the impregnation quality. Lower pressure (1 MPa) in the consolidation process to reduce the void.

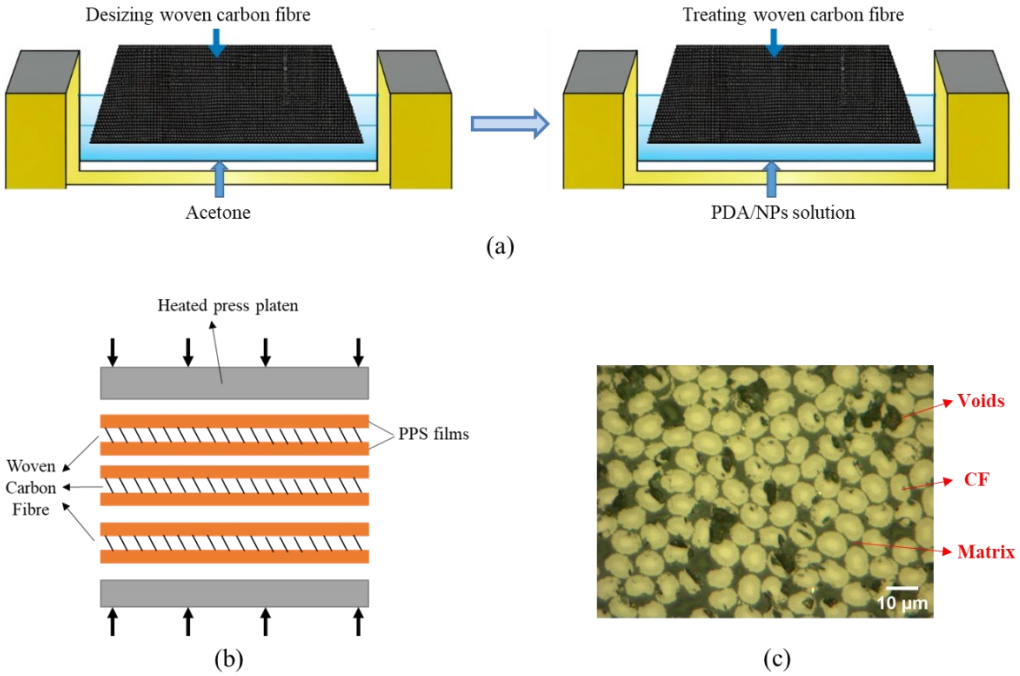

Figure 4-2 (a) Desized process and treatment process of woven carbon fibre; (b) set-up of hot press in producing CF/PPS laminates; (c) Optical microscopic image of cross-section for CF/PPS laminates.

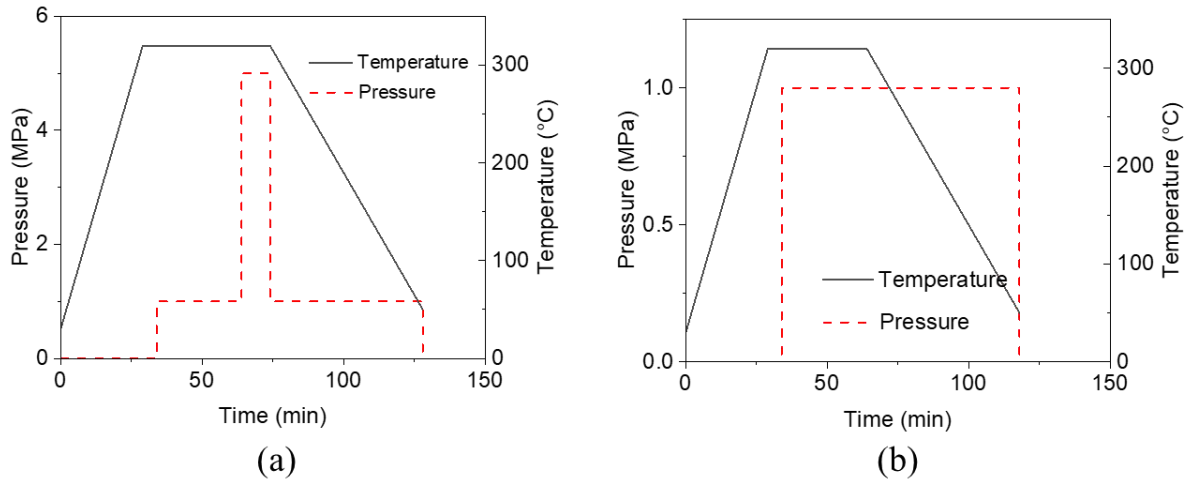

Figure 4-3 Time-temperature-pressure cycle in (a) hot-pressing of CF/PPS sheets; (b) consolation process of CF/PPS laminates.

4.2.5 Interlaminar shear strength of CF/PPS composite laminates

Interlaminar shear strength (ILSS) and interfacial shear strength (IFSS) both provide insights into the performance of composite materials, yet they measure different aspects of material behaviour. While ILSS primarily assesses the shear strength of the resin matrix and its ability to hold layers of composite together, IFSS evaluates the strength of the bond at the interface between the fibres and the matrix.

We chose ILSS testing in this chapter because it provides a comprehensive evaluation of composite performance, including detecting defects crucial for aerospace and automotive applications. Although ILSS is influenced mainly by the resin, the fibre/matrix interface still contributes to the overall shear strength, enhancing load transfer.

To investigate the interfacial adhesion between woven carbon fibres and PPS matrix, ILSS was measured by the short beam test according to the ASTM D2344 standard. The short beam specimens were cut from the hot-pressed CF/PPS composite laminates with the dimensions of 24 mm × 8 mm × 4 mm. The tests were carried out on an Instron 3369 universal testing machine, where the span length was 16 mm and the crosshead rate was 1.0 mm/min. Three tests were repeated for each type of composite laminate.

4.2.6 Dynamic mechanical analysis (DMA) of CF/PPS composite laminates

The thermal-mechanical behaviours of resulting CF/PPS laminates were investigated using the methodology outlined in Section 3.2.5.

4.3 Results and discussion

4.3.1 Surface morphology of carbon fibres

To observe the copolymerisation process of dopamine and nanoparticles in the modification process, SEM was used to characterise the surface morphology of desized carbon fibre (Figure

4-4(a)) and treated carbon fibre. Samples were prepared at different coating times, *i.e.*, 2 hours (Figure 4-4(b)), 4 hours (Figure 4-4(c)), 14 hours (Figure 4-4(d)), 16 hours (Figure 4-4(e)) and 18 hours (Figure 4-4(f)), respectively. In this study, the nanoparticles concentration is set to 2% and the dopamine concentration is 0.1%. As expected, Figure 4-4 shows that as the treating time increased, the surface topography of functionalised carbon fibres was distinctly different from the smooth and neat surface of desized carbon fibres. Also, the surface roughness increased over time. A uniform layer with many nanoparticles was formed on the carbon fibre surface after 16 hours of treatment. It is interesting to note that the surface morphology of the carbon fibre surface no longer changed when the modification time reached 18 hours. Results illustrate that the self-polymerisation process of dopamine continuously reacts as the coating time increases and remains stable for more than 16 hours under these conditions. Therefore, the optimal modification time is set as 16 hours, which is applied in the following experiments.

In addition, the synergistic effect of the polydopamine (PDA) and nanoparticles (NPs) plays a key role in the interfacial properties of carbon fibre and PPS polymer matrix. For comparisons, the specimens treated by 0.1%PDA solution (CF-PDA), 2%NPs solution (CF-NPs), 0.1%PDA-1%NPs solution (CF-PDA/NPs1), 0.1%PDA-2%NPs solution (CF-PDA/NPs2) and 0.1%PDA-4%NPs solution (CF-PDA/NPs4), respectively, were also prepared to evaluate the difference in surface morphologies by TEM. Figure 4-5 displays the surface morphologies of carbon fibres treated by these different solutions. Figure 4-5 (a) shows the clean surface for the desized carbon fibre. Compared with the sole CF-PDA (Figure 4-5(b)), a distinct layer of nanoparticles (around 50 nm) was observed on the carbon fibre surface in the CF-PDA/NPs2 (Figure 4-5(e)) as well as CF-PDA/NPs4 (Figure 4-5(f)). Furthermore, a more homogenous deposition layer of nanoparticles was obtained in CF-PDA/NPs1 (Figure 4-5(d)) than CF-NPs (Figure 4-5(c)). They were likely deposited and grafted on the surface with the assistance of the PDA. Interestingly, as the concentration of nanoparticles continuously increases, however,

the surface morphologies did not show significant differences between the 0.1%PDA-1%NPs (Figure 4-5(d)), 0.1%PDA-2%NPs (Figure 4-5(e)) and 0.1%PDA-4%NPs (Figure 4-5(f)) solution. For the 1% NPs, the layer does not distribute uniformly due to the lower concentration of silica nanoparticles, whereas at a higher concentration of 3% NPs, particle aggregates occur.

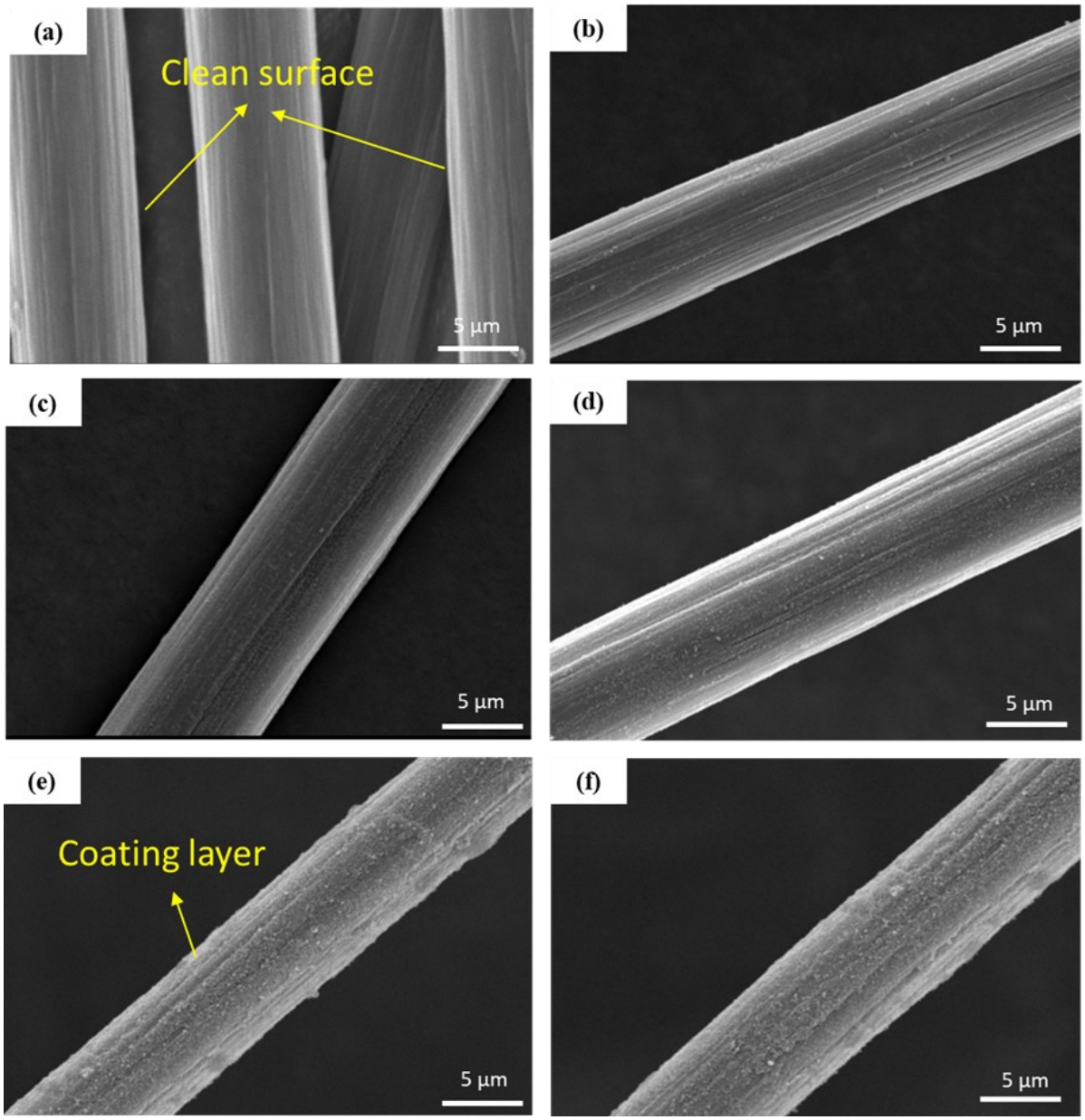

Figure 4-4 Surface morphology of carbon fibre at different treatment times: (a) 0 hours (b) 2 hours; (c) 4 hours; (d) 14 hours; (e) 16 hours; (f) 18 hours. The nanoparticles concentration is set to 2% and the dopamine concentration is set to 0.1%.

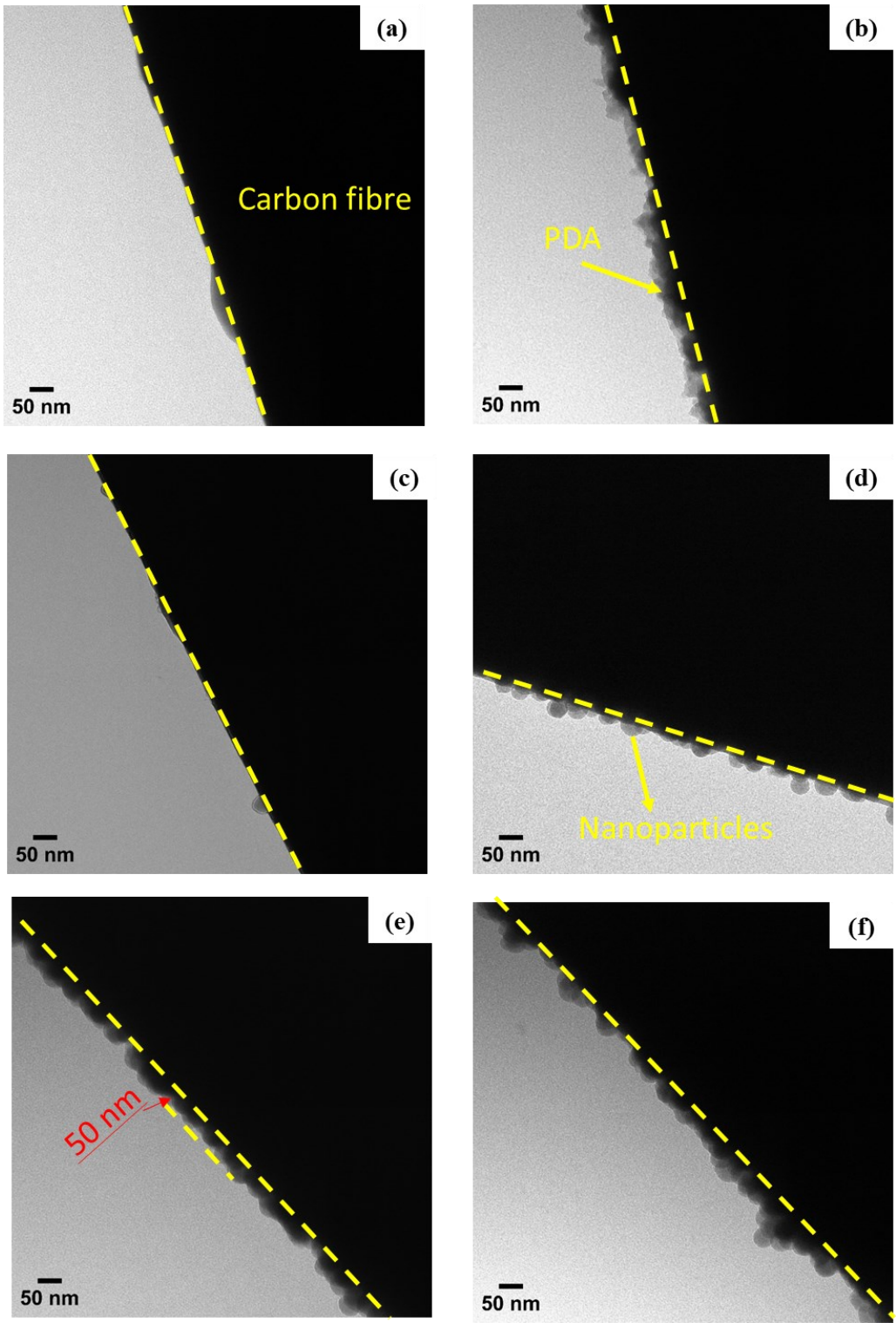

Figure 4-5 Surface morphology of carbon fibre with different treated solutions (treatment time: 16 h): (a) Desized carbon fibre; (b) 0.1%PDA solution (CF-PDA); (c) 2%NPs solution (CF-NPs); (d) 0.1%PDA-1%NPs solution (CF-PDA/NPs1); (e) 0.1%PDA-2%NPs solution (CF-PDA/NPs2); (f) 0.1%PDA-4%NPs solution (CF-PDA/NPs4).

Results indicate that a solution concentration of 0.1% PDA and 2% colloidal nano-SiO_2 solution is most suitable for treatment of carbon fibres due to its ability to create a uniform adhesive layer on the CF surface, offering an ideal balance between morphological enhancement and cost-effectiveness, which was selected in the following experiments. Overall, in the modification process, the polydopamine acting as an efficient and robust platform could support the grafting of the nanoparticles. The mechanism of the possible copolymerisation process is explored in the later section.

4.3.2 **Chemical analysis of modified carbon fibres**

(1) Raman spectroscopy

Raman Spectroscopy was used to evaluate the surface structural variations because it is sensitive to the order structure. Figure 4-6 shows the Raman spectra of desized CF, CF-PDA, CF-NPs, CF-PDA/NPs2 and CF-PDA/NPs4. There are two distinct peaks displayed in the spectroscopy D band (around 1370 cm^{-1}) and G band (around 1600 cm^{-1}), respectively. As it is well known, the D band is a result of the structure disorder or defects in graphite, while the G band is due to in-plane vibration of sp2 bonded carbon atoms corresponding to ordered graphite structure (crystallinity) [94]. Compared to the desized carbon fibre, the peak intensity of D and G band for carbon fibres treated by PDA and NPs solely show minor difference. However, the peak intensity of D and G band was obviously increased by the incorporation of both polydopamine and nanoparticles (refer to Figure 4-6(a)). CF-PDA/NPs2 exhibits the highest intensity of the D peak and G peak.

The intensity ratio of the D band and G band reveals the functionalisation degree and the extent of structural defects or disorders. A higher ID/IG ratio indicates more defects or disorder in the carbon material. For desized CF (Figure 4-6(b)), the ID/IG ratio is 1.973, which is relatively high, suggesting a significant level of disorder, which is common in carbon fibre that have been

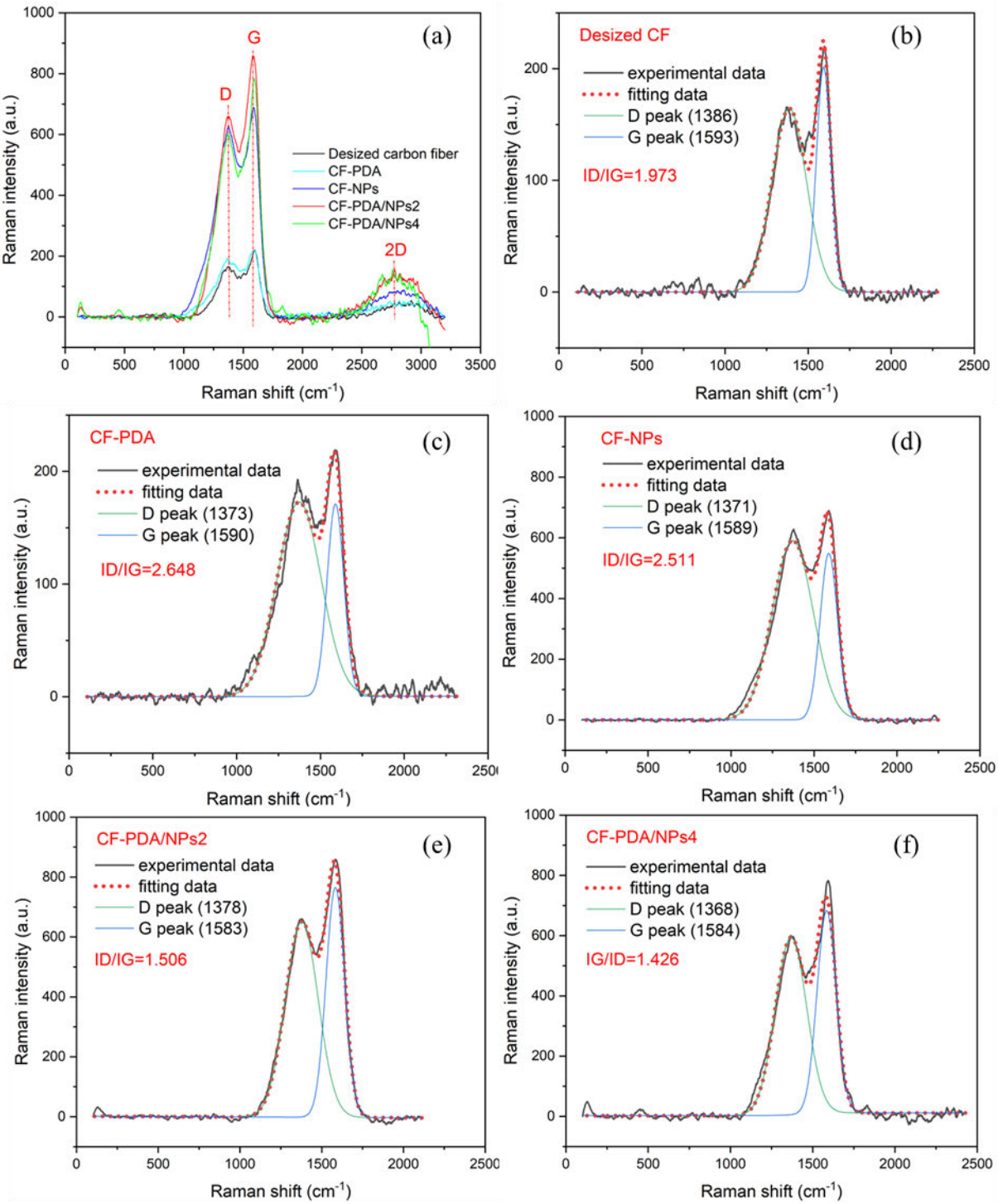

Figure 4-6 (a) Raman spectroscopy and (b-f) peak fitting results of carbon fibres: (b) desized carbon fibre; (c) 0.1%PDA solution (CF-PDA); (d) 2%NPs solution (CF-NPs); (e) 0.1%PDA-2%NPs solution (CF-PDA/NPs2); (f) 0.1%PDA-4%NPs solution (CF-PDA/NPs4).

desized to remove the sizing agents during the manufacturing process. For CF-PDA (Figure 4-6(c)), this sample has been treated with polydopamine, presenting a highest ID/IG ratio (2.648), which indicates PDA treatments could introduce additional defects or disorder into the carbon surfaces, due to the functionalization or roughening of the surface as a result of the PDA coating. For the CF-NPs (Figure 4-6(d)), the ID/IG ratio of 2.511 is also higher than desized carbon fibre, suggesting a higher disorder on the carbon fibre surface, which could result from the non-unform deposition of a few nanoparticles aggregates on the surface of carbon fibre. Once PDA is introduced, the ID/IG ratios are lower at 1.508 and 1.425 for CF-PDA/NPs-2 (Figure 4-6(e)) and CF-PDA/NPs-4 (Figure 4-6(f)), respectively.

This decrease in the ID/IG ratio compared to the CF-NPs sample could indicate that the combined treatment creates a stronger π-orbital hybridisation with a more ordered structure than nanoparticle treatment alone, supporting the assertion that PDA could increase the intact graphitic domains [93]. As expected, the result shows evidence that nanoparticles were successfully grafted onto the surface of the treated CF assisting with polydopamine to produce the CF-PDA/NPs. Further analysis of chemical groups will be combined with XPS in the later section.

(2) X-ray photoelectron spectroscopy

XPS was applied to measure the changes in the binding energy of the ejected photoelectrons in order to elucidate the modifications in chemical compositions of the treated CF, compared to desized CF. Figure 4-7 depicts the results of survey scans for desized CF and fabricated CF-PDA/NPs2. Three peaks assigned to C, N and O elements were found in the survey spectra of desized CF, while one extra Si element was observed in the treated CF sample (enlarged peak). To get more detailed information, the peak fitting results in the C 1s spectrum and N 1s spectrum of desized CF and fabricated CF-PDA/NPs2 were also displayed in Figure 4-8. These

core-level spectra were fitted with several peak components separately based on the binding energies.

In Figure 4-8(a), there are four peaks assigned to C-C bonding (284.6 eV), C-N bonding (285.7 eV), C-O bonding (286.6 eV) and O=C-O bonding (288.0 eV) respectively in C 1s spectra of desized CF [165,166]. Compared with the desized sample, there emerged a new peak attributed to C=O bonding (287.6 eV) [96,166] in the spectra of the treated sample, as shown in Figure 4-8(b).

Additionally, the peak area fraction of the nitrous carbons C-N and oxygenated carbons C-O shows a great increase from 27.1% of desized CF to 50.2% of fabricated CF-PDA/NPs2. Further, the detailed information on differences of N 1s core-level spectra between the desized CF and treated CF. As presented in Figure 4-8(c), two fitted peaks represent the N-H bonding and C-N bonding with the binding energy of 397.8 and 400.1 eV respectively [165]. As for CF-PDA/NPs2 (Figure 4-8(d)), the spectra are decomposed into three peaks with a new peak position with the binding energy of 402.5 eV arising from the N-SiO_2 structure [167]. In addition, the content N-H increased from 7.6% of desized CF to 12.7% of fabricated CF-PDA/NPs2. By the introduction of the PDA/NPs network, these polar nitrogen-containing functional groups, especially for $–NH_2$, play an important role in activating the carbon fibre surface [96], which could further react with the matrix to increase the interfacial strength between carbon fibre and PPS matrix in the resulting composites.

The reaction mechanism is further analysed in Section 4.3.4.

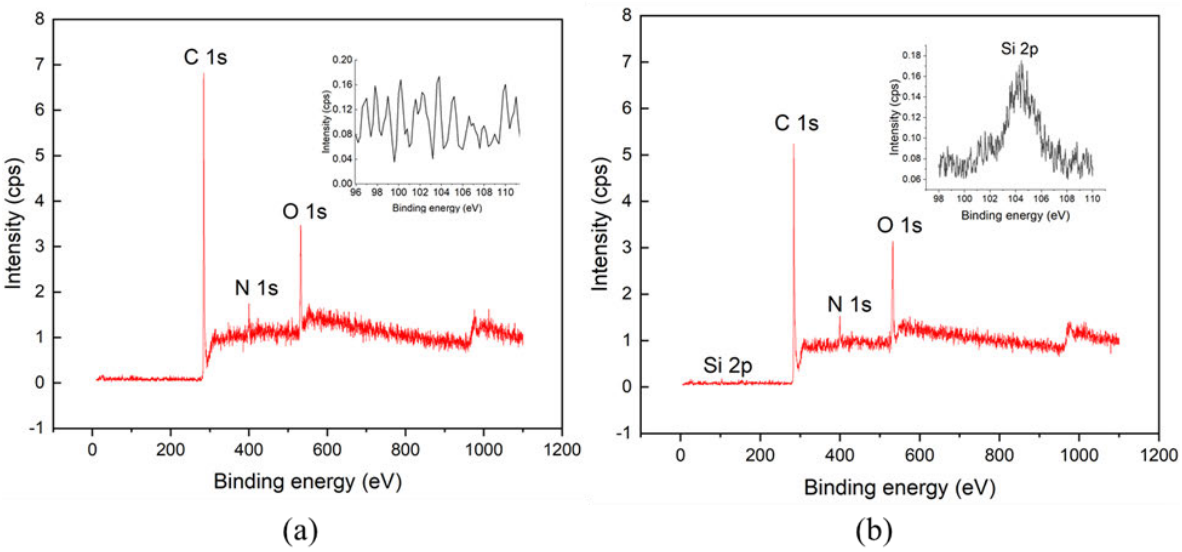

Figure 4-7 Survey scans of (a) desized CF and (b) fabricated CF-PDA/NPs2.

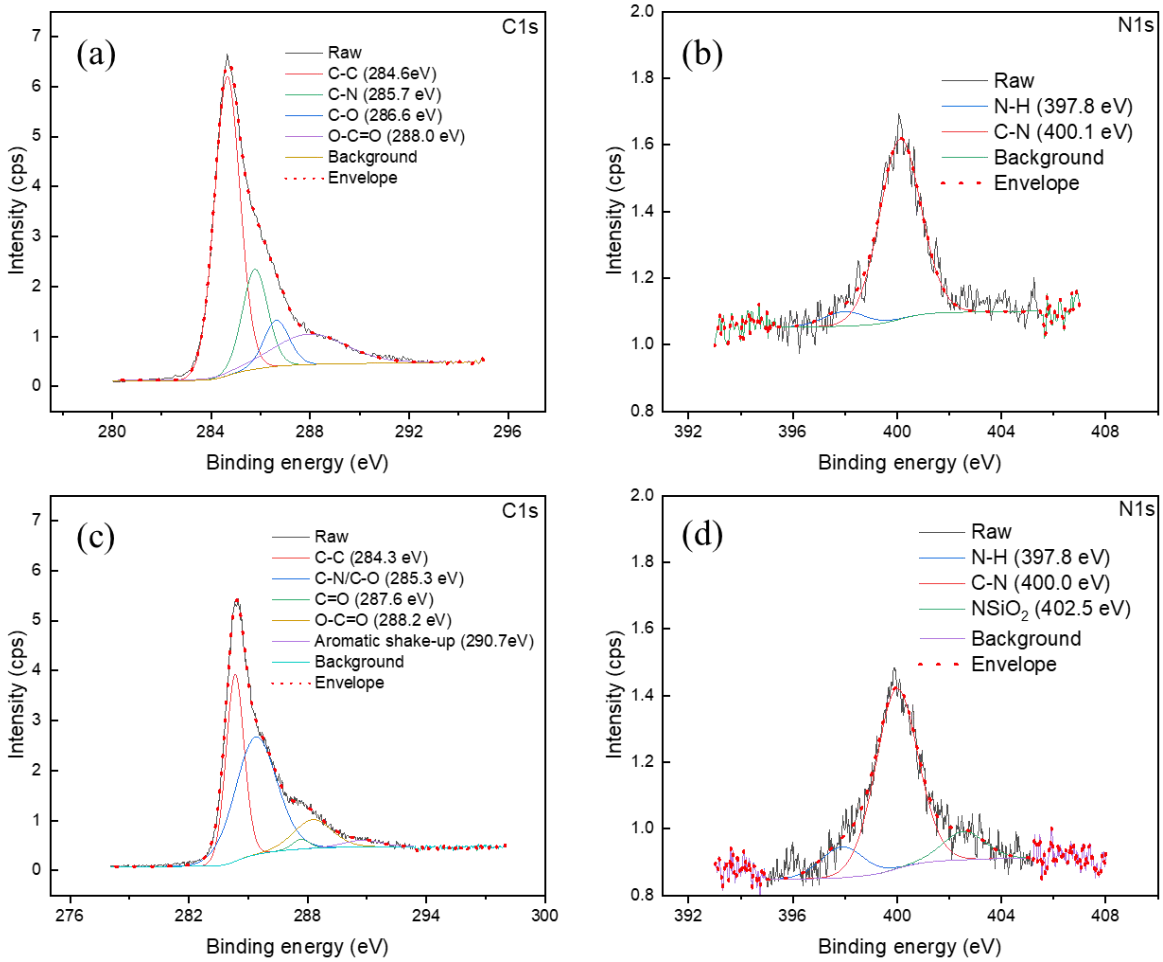

Figure 4-8 C1s and N1s spectra of desized CF (a & b) and fabricated CF-PDA/NPs2 (c & d).

4.3.3 **Mechanical performance of the resulting CF/PPS composites**

(1) Interlaminar shear strength (ILSS)

The short-beam test is an effective way to evaluate the interfacial properties of fibre-reinforced composites. In Figure 4-9, the ILSS values of composites with untreated CF and desized CF are quite close (17.50 MPa and 18.43 MPa, respectively), which indicates that the interfacial bonding between the carbon fibre and PPS matrix is almost the same before and after the desizing of the carbon fabrics. The untreated carbon fibre was desized first and then treated with a solution containing 0.1% PDA and 2% colloidal nano-SiO_2 to obtain the treated CF. After the establishment of the network of CF-PDA/NPs on the carbon fibre surface, the ILSS value reaches 23.66 MPa with a 28.4% increase compared to that of desized CF composites. The ILSS was calculated from the maximum force observed in the force-displacement curves based on the standard. The typical failure mode observed in the ILSS tests for all samples is delamination after reaching peak force.

By comparison with the previous studies which shows increases of between 15% and 40% [10,87–89,91], this one-step modification strategy has advantages in low cost, low energy consumption and is also free of toxic chemicals. Overall, the figure effectively demonstrates that the treatment of carbon fibres with polydopamine and nanoparticles leads to a substantial improvement in their mechanical performance, as evidenced by the increased ILSS values. This treated CF exhibits not only better performance compared to the untreated and desized counterparts but also shows significant potential for use in advanced composite materials where higher mechanical strength is required.

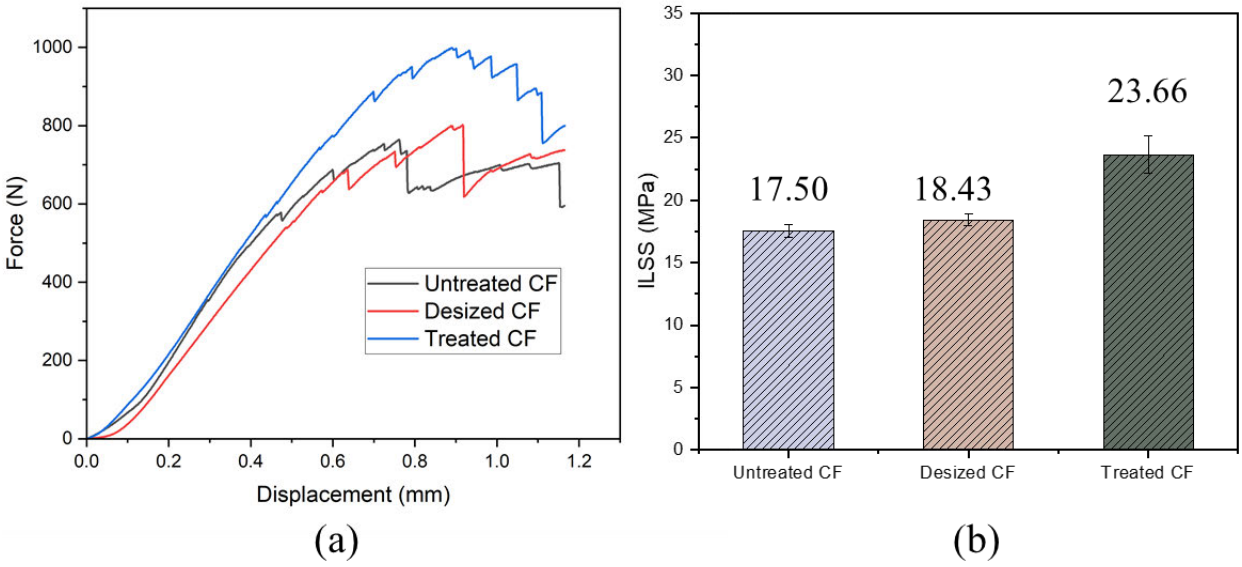

Figure 4-9 (a) Representative force-displacement curves (b) ILSS values of the resulting composites manufactured with untreated CF, desized CF and treated CF.

(2) Dynamic mechanical analysis

To enhance our understanding of the thermo-mechanical behaviour of the treated CF/PPS composites, dynamic mechanical analysis (DMA) was conducted over a temperature range of -60 °C to 250 °C. Figure 4-10 presents the storage modulus (G') alongside the damping factor (tan δ) for both untreated and treated CF composites. Notably, the treated composites exhibit consistently superior G' values across the entire temperature spectrum, with an improvement of 15% in G' at ambient temperatures post-treatment, rising from 4687 MPa for untreated CF to 5380 MPa for treated CF in the initial cycle.

Moreover, the damping factor (tan δ) reveals an obvious difference between the treated and untreated samples. This factor is a recognised indicator of the energy dissipation mechanisms within a material [168]. Reduced damping factor in the treated composites suggests that higher energy is used to deform the treated composites, indicative of an improved fibre/matrix interface. The results demonstrate that the PDA/NPs network could play an important role in improving the elastic modulus of the resulting composites.

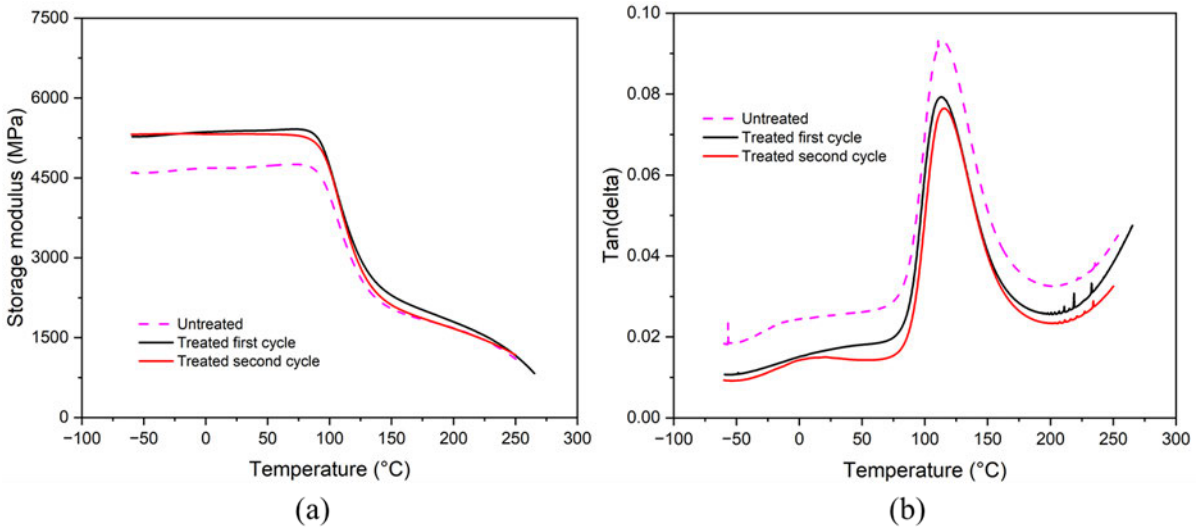

Figure 4-10 DMA results of the resulting composites manufactured with untreated CF and treated CF: (a) storage modulus and (b) damping factor.

Furthermore, the robustness of the interfacial bonding at the matrix/fibre interface was put to the test through a second series of thermal heating-cooling cycles. The subsequent findings, also depicted in Figure 4-10, confirm the exceptional thermal resistance of treated composites, particularly between -60 °C and 100 °C. Remarkably, even under thermal cycling for extreme conditions, the treated interface retains 99% of its initial performance at 100 °C, to be superior to the virgin interface. This result shows that the thermal cycles have negligible effect on the storage modulus of the resulting CF/PPS composites at serviced temperatures, which is important for potential applications in environments where materials are subjected to extreme and fluctuating temperatures.

In conclusion, the DMA results clearly reveal that the PDA/NPs treatment enhances fibre/matrix bonding, as evidenced by increased storage modulus (G'), leading to stiffer composites with superior load handling. Moreover, the composites exhibit remarkable resilience to thermal cycling, preserving most of their original storage modulus after repeated cycles. These findings are particularly relevant for applications in harsh thermal environments,

where material performance and longevity are of utmost importance. These properties are crucial for high-performance applications requiring materials that can withstand harsh operating conditions during repeated heating and cooling cycles without compromising their structural integrity or performance.

4.3.4 Mechanism for the improvement of interfacial properties by the PDA/NPs network

Figure 4-11 presents the FTIR spectra of dopamine hydrochloride, polydopamine, silica nanoparticles (NPs), and polydopamine-functionalised silica nanoparticles (PDA/NPs). The spectral analysis in Figure 4-11(a) highlights the variances in functional groups between dopamine and its polymerised form, polydopamine. The polydopamine spectrum exhibits an obvious broad peak between 3000-3500 cm^{-1}, reflective of O-H and N-H stretching vibrations. Additionally, peaks around 2900 cm^{-1} correspond to the C-H stretching vibrations, a feature also present in dopamine hydrochloride spectra. Notably, new peaks at 1627 cm^{-1} and 1552 cm^{-1}, which appear from the 1616 cm^{-1} band, are attributable to the C=C and C=N stretching vibrations in aromatic rings. The emergence of another peak at 1400 cm^{-1} is identified with the indole ring CNC stretching modes, corroborating the existence of 5,6-dihydroxyindole units within the structure [169,170].

Figure 4-11(b) exhibits FTIR spectrum of NPs, and PDA/NPs. For both structures, the peaks observed at 798 cm^{-1} and 960 cm^{-1} are characteristic of the Si-O-Si bending vibrations, and the peak at approximately 1100 cm^{-1} is indicative of Si-O-Si stretching vibrations. These peaks are typical for silica and confirm the presence of Si-O bonds [171]. After functionalisation with PDA, additional peaks at 2924 cm^{-1} and 2856 cm^{-1} attributed to the C-H stretching vibrations from the PDA, and the appearance of the characteristic peak at 1400 cm^{-1} confirms that the PDA layer has been successfully grafted onto the silica nanoparticles.

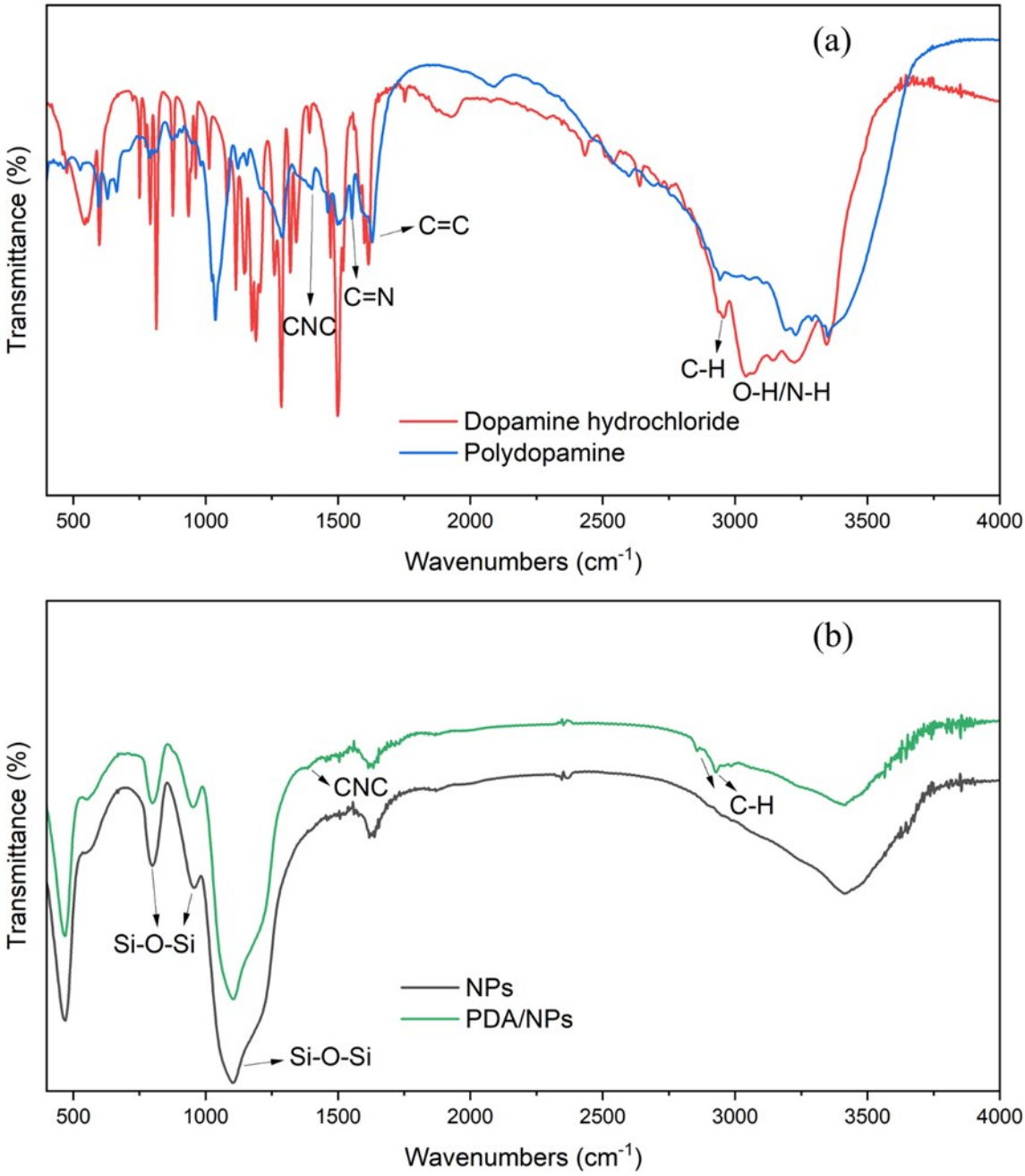

Figure 4-11 FTIR spectrum of (a) dopamine hydrochloride and polydopamine; (b) silica nanoparticles (NPs) and polydopamine functionalised silica nanoparticles (PDA/NPs).

Figure 4-12 presents the fabrication process of PDA-assisted silica nanoparticles coated on the carbon fibre surface and the following reaction pathway in the resulting composites, to understand the possible reaction mechanism between the CF-PDA/NPs and PPS matrix. Based on previous studies, the typical polymerisation process of the PDA is presented for the in-situ

polymerisation of its monomer, dopamine, which can be oxidised by oxygen and self-polymerised in the alkaline solution (Figure 4-12(a)) [95,172]. This spontaneous polymerisation reaction is green and mild without any harsh reaction conditions. When dopamine hydrochloride is dissolved under alkaline conditions (pH>7.5), this chemical reaction immediately occurs in the buffer solution. The colourless solution turns yellow-brown first and finally change to dark brown. The dopamine suffers from oxidation first to form dopamine-quinone, followed by intramolecular cyclisation through Michael Addition to produce leucodopaminechrome, which is further oxidised to 5,6-dihydroxyindole. This reaction product can be easily oxidised into 5,6-indolequinone, forming the cross-linked polymer.

It has been reported that polydopamine has strong adhesion to almost all types of surfaces [97]. Overall, the mechanisms are generally divided into two types of bonding: covalent bonding and non-covalent bonding [162]. Typically, covalent bonding can be formed on substrates containing some specific groups, such as the amine group via Michael addition or Schiff base. In most cases, however, PDA tends to diffuse into the surface to form non-covalent bonding including chelating, hydrogen bonding, π-π stacking, and quinhydrone complex, especially for the interactions under ambient conditions. In this study, the copolymerisation of dopamine on the carbon fibre surface introduces a variety of functional groups, including amine and catechol groups. These functional groups serve multiple roles, including acting as binding sites for silica nanoparticles. the catechol group of PDA is possible to form the hydrogen bonding with the hydroxyl groups in silica nanoparticles. The presence of these functional groups enhances the chemical affinity between the carbon fibres and silica nanoparticles, facilitating a stronger bond. This polydopamine layer coated on the silica nanoparticles provides an active surface for further deposition on the carbon fibre surface. As

a result, the PDA-coated nanoparticles could be easily adhered to the smooth and inert surface of carbon materials by the non-covalent interactions.

Polydopamine forms a cohesive and adhesive layer on the surface of carbon fibres, consisting of an interconnected network of dopamine monomer units that have undergone oxidative polymerisation. The PDA layer acts as a foundation for nanoparticles attachment, through various types of chemical interactions, such as hydrogen bonding. Nanoparticles can be embedded into or layered onto the PDA layer. The resulting structure is a cross-linked network where the PDA binds the nanoparticles to the carbon fibre surface, enhancing the topography and increasing the functional group density. The PDA/NPs network could significantly enhance the adhesion between carbon fibres and the matrix material in composites. The presence of various functional groups like catechol and amine groups allows for strong interfacial bonding with PPS matrix molecules (Figure 4-12(b)). Specifically, catechol can interact with the polar sites on the PPS, while amine group can form hydrogen bonds with oxygen-containing groups. The aromatic rings present in both PDA and PPS can engage in π-π stacking interactions.

Moreover, the integration of nanoparticles within the PDA layer increases the surface roughness of the carbon fibres, amplifying van der Waals forces with increased contact area and promoting mechanical interlocking with the matrix material. These stronger bonding, in turn, potentially enhances load transfer and mechanical properties of the composite material. The polydopamine and nanoparticle treatment creates a structurally complex and chemically active interface on the carbon fibres, which translates into composites with enhanced mechanical properties and durability.

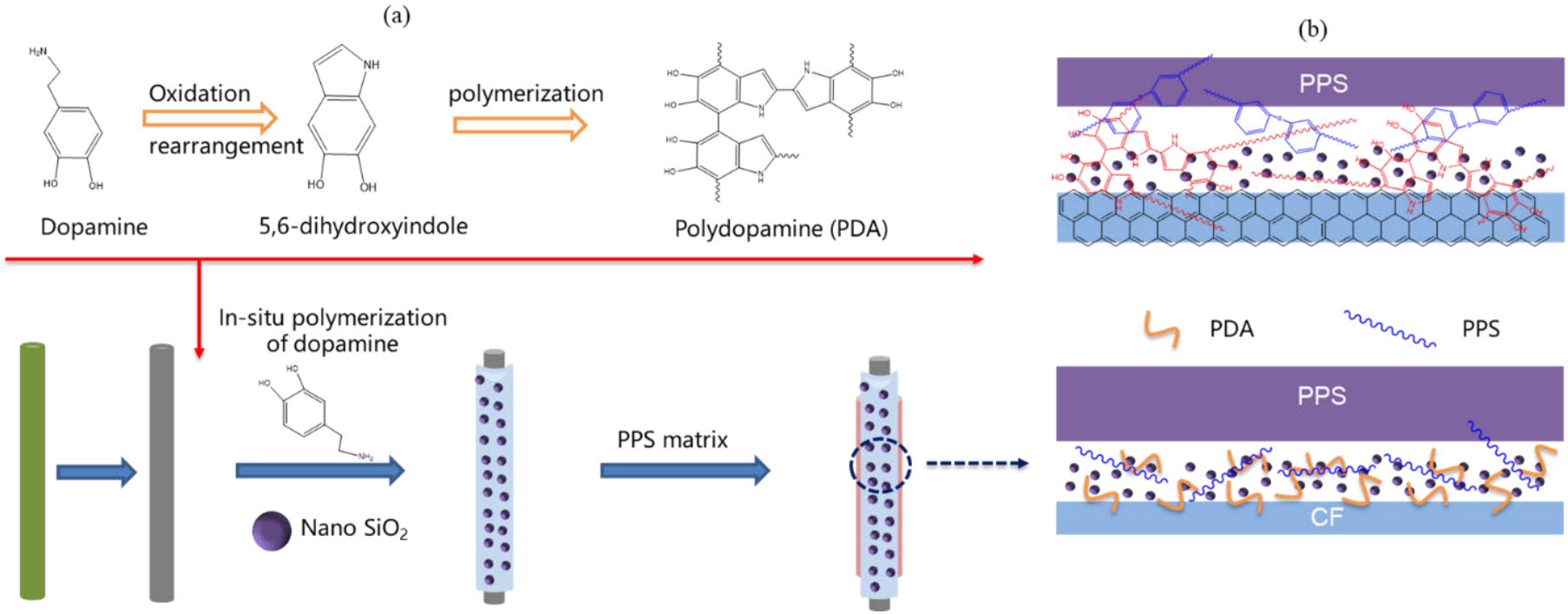

Figure 4-12 (a) Functionalisation of PDA/NPs on the carbon fibre surface; (b) possible reaction mechanism between CF-PDA/NPs and PPS matrix in the resulting composites

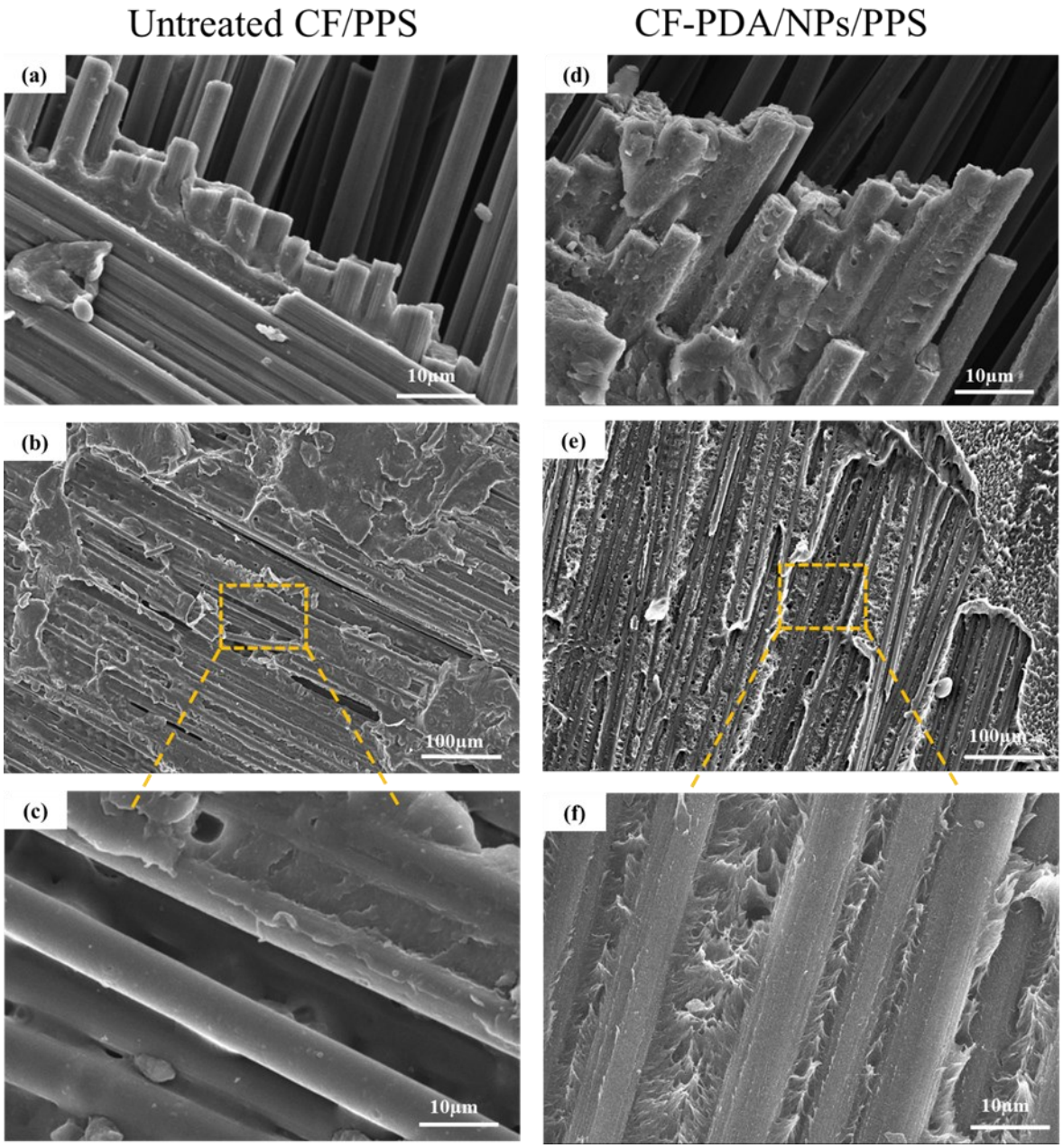

Figure 4-13 Interlaminar shear fracture surface morphology of CF/PPS composites with untreated CF (a-x1000; b-x200; c-x1000) and CF-PDA/NPs (d-x1000; e-x200; f-x1000).

To investigate the mechanisms in improving the fibre/matrix interfacial properties by the network of PDA/NPs, the specimens were completely teared between the failed layers after the ILSS tests [173], and the morphologies of the fractured surface were observed by SEM (refer to Figure 4-13). Figure 4-13(a) and Figure 4-13(d) were obtained from the edge area of the

fractured surface. By comparing Figure 4-13(a) and Figure 4-13(d), as expected, the PPS matrix could be completely separated from the untreated carbon fibres in most edge areas on the fractured surface due to relatively weak interfacial adhesion. After the introduction of the PDA/NPs network, a thick layer of PPS resin was found on the fractured surface. As shown in Figure 4-13(b) & (c), in the absence of PDA/NPs network, the clean and smooth fibre bundles and gaps were captured along CF direction, which indicates that the crack propagates rapidly through the interface of CF/PPS. Figure 4-13(e) & (f), however, shows that the rougher CF surface and zigzag patterns were observed. On one hand, the silica particles function as spacers, which could induce more smaller cracks in the cross-sectional area, instead of directly extending to the surfaces of carbon fibre. This contributed to the improved shear yield stress of the interface layer.

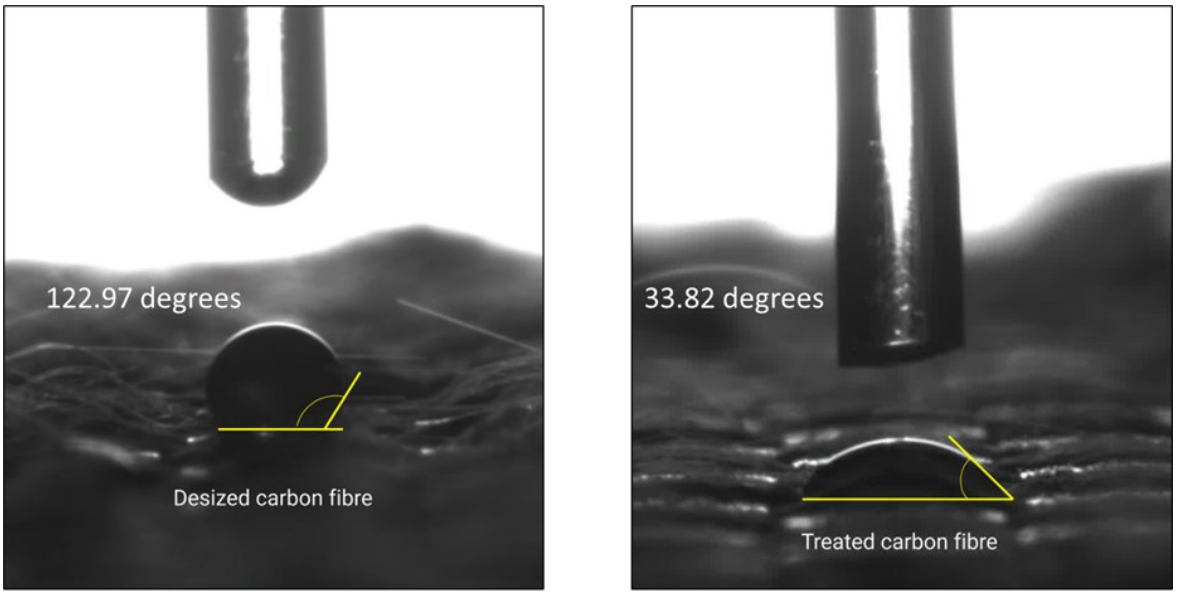

Figure 4-14 Contact angle measurement of (a) desized carbon fibre cloth and (b) treated carbon fibre cloth.

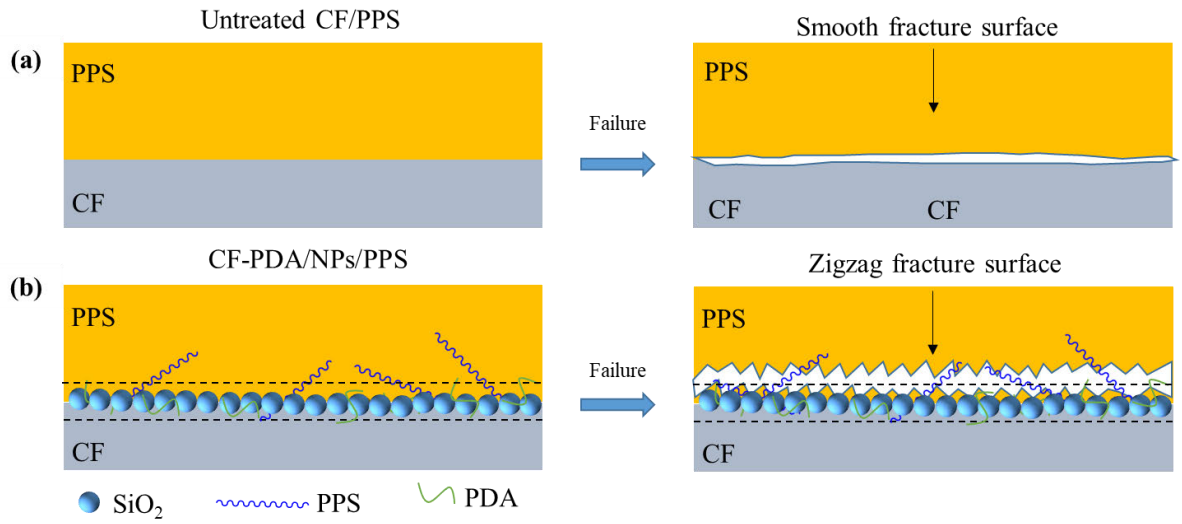

Figure 4-15 Schematic diagram of the failure mode for CF/PPS composites: (a) untreated CF/PPS; (b) CF-PDA/NPs/PPS.

The comparative analysis of desized and treated carbon fibres via contact angle measurements is depicted Figure 4-14. The contact angles were determined by depositing a water droplet onto the carbon fibre cloth, yielding a measurement of 122.97 degrees for desized fibre and 33.82 degrees for treated fibre respectively. This variation in contact angles indicates the wettability change induced by surface modifications. The elevated contact angle observed in the desized carbon fibre is indicative of a hydrophobic surface, which can be detrimental to the composite's mechanical integrity due to poor interfacial adhesion. In contrast, the treated carbon fibre significantly decreases contact angle, suggesting a transition to a more hydrophilic nature. This shift is primarily due to the introduction of polar groups on the carbon fibre surface, including hydroxyl groups from the silica nanoparticles and amine groups from the PDA layer.

Surface energy, governed by thermodynamic principles, influences the spreading and adhesion properties of a liquid on a solid substrate. A high contact angle is generally associated with low surface energy, indicating a surface's limited adhesive potential. For carbon fibres, enhanced surface energy following treatment suggests improved wetting properties and the likelihood of

stronger chemical bonding with the matrix material. Conversely, reduced surface energy implies lesser wetting and potentially weaker interfacial bonding. It can be concluded that the application of a PDA/NPs layer to desized carbon fibres not only improves wettability but also is likely to elevate the surface energy, thereby facilitating stronger interfacial adhesion within composites.

According to the above results, Figure 4-15 presents the schematic diagram of the failure mode of CF/PPS composites for untreated CF and CF treated with PDA/NPs. Because of the formation of interactive network of the PDA-coated silica nanoparticles, the tougher interface layer around the CFs consisting of spherical shaped nanoparticles can dissipate the strain energy and transfer the stress to the interface region, which prevents the fibre-matrix de-bonding and therefore retard the propagation of cracks in the interlayer. As a result, the smooth fracture surface changes to a zigzag-like fracture surface with larger surface areas, thus leading to an enhanced ILSS strength.

In conclusion, the PDA layer has been successfully grafted onto the silica nanoparticles, introducing amine groups and catechol groups onto the non-polar carbon fibre surface. These groups enhance the potential for chemical bonding. The introduction of these polar groups improved the surfaces energy of the treated surfaces. Additionally, the nanoparticles aid in increasing the mechanical interlocking and roughness of the interface.

4.4 Conclusions

Recycling and reuse of waste carbon fibres from end-of-life composites is a timely and important priority because of the detrimental environmental impact and landfill area shortage. This study demonstrates a one-step treatment that increases the ILSS of resulting CF/PPS composites by 28.4% through the establishment of a PDA/NPS network by the self-polymerisation of dopamine on the carbon fibre surface. The interfacial bonding between fibre

and matrix exhibits great thermal stability in DMA results, which indicates that the network remains effective at service temperatures. Additionally, the network is proven to be reliable by thermal cycling, which indicates that this method could be widely applied in complicated conditions. By grafting the polar functional groups on the carbon fibre surface, the roughness and wettability could be altered, leading to the improvement in fibre/matrix impregnation in the resulting composites. This process is free of toxic chemicals and easy to use, and thus constitutes a promising treatment for recycling and recovering carbon fibre for end-of-life advanced composites. The proposed method aligns with several key sustainability goals, including waste reduction, resource efficiency, and the minimisation of hazardous substances, while also promoting energy conservation and the development of durable and sustainable materials.

Chapter 5 **3D printing of dopamine treated continuous carbon fibre reinforced polyphenylene sulphide composites with enhanced interfacial and interlayer properties**

Abstract

This study investigates the impact of dopamine-treated carbon fibre reinforcement and post-processing techniques in polyphenylene sulphide (PPS) composites, with a focus on improving interfacial and interlayer properties. The synergistic effects of continuous carbon fibre (CCF) treatment with polydopamine and silica nanoparticles (PDA/NPs) and post-processing on the mechanical performance of 3D printed composites are explored. The findings demonstrate that treated composites exhibit significant improvements in interlaminar properties, with increases in flexural strength by 27% and interlaminar shear strength (ILSS) by 172%, compared to untreated specimens. Molecular dynamics (MD) simulations and nano-indentation tests reveal the mechanisms behind the improved fibre/matrix interfacial adhesion attributing to PDA/NPs network on the fibre. Differential scanning calorimetry (DSC) and microscopic analyses are utilised to assess enhancements in crystallinity, void content, and fibre orientation after post-processing. Furthermore, we introduce a novel post-processing method involving a salt bath, which aligns with the unique advantages offered by 3D-printed complex composites. This approach is validated with two complex demonstrative geometries, confirming its effectiveness in maintaining structural integrity while enhancing material properties. The integration of pre-processing with the PDA/NPs network and post-processing techniques with a salt bath offers particular benefits for additively manufactured high-performance materials.

Keywords

Continuous carbon fibre reinforced thermoplastic composites; Additive manufacturing; Polydopamine; Post-processing; Interlaminar properties.

5.1 Introduction

Continuous carbon fibre reinforced thermoplastics (CCFRTPs) have emerged as a cornerstone in modern aerospace and automotive industries, mostly attributed to their unique combination of light weight, superior strength, high modulus and improved recycling feasibility. These CCFRTP composites are increasingly replacing traditional metal materials, leading to advancements in fuel efficiency and structural integrity in various applications. The manufacturing of CCFRTP involves processes like compression moulding, thermoforming and automated tape/fibre placement [30]. Each of these methods comes with its own set of limitations while effective in certain applications. The shortcomings include complex procedural requirements, prolonged production cycles, and elevated costs, particularly when it comes to manufacturing of parts with complex shapes and geometries [174].

In recent years, additive manufacturing (AM) or 3D printing, has been gaining momentum in manufacturing fibre-reinforced polymer composites [125,131,175]. This technology stands out for its ability to fabricate components with complex geometry that were previously challenging or impossible to create using conventional methods. Moreover, AM offers remarkable control over fibre orientation, streamlined manufacturing processes, and significant cost reductions, especially in low-volume or custom production runs [28,40,176,177]. Among the various AM techniques, material extrusion (MEX) is the most widespread technology due to its versatility in creating thermoplastic composites [20,178–180]. This method is particularly adept at

working with both discontinuous or continuous reinforcements, making it a versatile option for a wide range of applications.

The incorporation of continuous fibres in polymer composites is a notable advancement over short fibre reinforcements [69,181,182]. Continuous fibres provide a substantial enhancement to the mechanical properties of composites, including tensile strength and durability. However, the full potential of 3D printing of CCFRTP is yet to be achieved, primarily due to challenges in impregnation during pre-processing and consolidation during post-processing [101]. Commonly used commercial carbon fibre tows often struggle to bond effectively with thermoplastic matrices. The poor interfacial adhesion leads to heightened risks of fracture at the interface under loading, which is the critical vulnerability in the composites structure [8,11,94]. Additionally, the inherent principle of MEX, involving the extrusion of materials at high temperature followed by rapid cooling and solidification upon contact with cooler surfaces, present additional challenges [4,22,183]. The rapid temperature change can lead to weak adhesion between successive layers and increased porosity within the composites, adversely affecting its overall integrity and performance. Although the mechanical properties along the printing direction may be comparable with those produced by traditional manufacturing methods, the response of these materials under transverse or interlaminar loads is significantly compromised due to the inherent defects of weak adhesion on the fibre/matrix interface and insufficient thermal consolidation of the layers during the layer deposition process [23,129].

In response to these limitations, this work introduces an innovative approach that involves treating the commercial carbon fibre with silica nanoparticles and polydopamine hybrid network [184]. This treatment aims to enhance fibre/matrix adhesion significantly. We then use this treated fibre to fabricate continuous carbon fibre reinforced polyphenylene sulphide (CCF/PPS) filament, designed for optimised performance in 3D printing application.

Additionally, we propose a post-processing method that applies high temperature and pressure to mitigate layer adhesion defects. The mechanical performance under flexural loads and interlaminar shear loads are measured to investigate the synergistic effect of pre-processing and post-processing. The improvement mechanisms are thoroughly investigated using a multifaceted approach. For the pre-processing, we employ molecular dynamic (MD) simulation and single fibre push-out test to elucidate the underlying mechanisms contributing to the enhanced interfacial adhesion. For the post-processing, we analyse the microstructure and crystallinity to gain insights into the structural evolution. Further, X-ray computed tomography (XCT) scanning is utilised to explore the synergetic effects of combined pre-treatment and post-processing methods on improving the interlaminar performance, particularly under short beam bending conditions. The comprehensive analysis helps in understanding the interfacial and interlayer properties of the composites materials and guides the optimisation of our processes. Ultimately, we propose and validate an optimised post-processing method involving a salt bath. This method demonstrates its feasibility to process the complex 3D printed structures, including two-dimensional lightweight perforated designs and intricate three-dimensional integrated structures. Our findings open new avenues for the advanced manufacturing of CCFRTP, setting a new benchmark for the fabrication of high-performance composites in aerospace, automotive, and other demanding industries

5.2 Experimental setup

5.2.1 Materials

Continuous carbon fibre tow (3K) was procured from Easy Composites Ltd, Stoke on Trent, UK. Tetraethoxysilane (TEOS), Dopamine hydrochloride (DP) and Tris (hydroxymethyl)-aminomethane (Tris) were sourced from Merck Life Sciences Ltd, UK. Polyphenylene sulphide (PPS, Torelina A900) was produced by Toray Industries, Japan. Acetone, employed

in the desizing process, was acquired from Fisher Scientific Ltd, Leicestershire, UK. All chemicals were utilised as received, except reported otherwise.

5.2.2 Modification of continuous carbon fibre

The process of modifying the continuous carbon fibre tow began with the synthesis of colloidal silica nanoparticles (NPs), employing TEOS as the precursor [163]. The initial step involved the desizing of the as-received carbon fibre tow using acetone. Following this, we prepared a reaction medium by dispersing the silica nanoparticles in a 0.1% Tris-buffered solution (pH=8.5), an environment conducive to dopamine's self-polymerisation. The next stage of the process involved the simultaneous introduction of the carbon fibre and dopamine hydrochloride into this buffered nanoparticle solution (see Figure 5-1(a)). This step was conducted at ambient room temperature, using an ultrasonic device to facilitate the uniform coating of the carbon fibre with the PDA/NPs hybrid network. The carbon fibre tow was then left immersed in this modification solution for a duration of 16 hours, ensuring thorough treatment. Post-immersion, the carbon fibre tow underwent a rinsing process, being washed three times with ultra-pure water to remove any unreacted components or residues. The final step in the pre-treatment process was the drying of the carbon fibre tow. This was achieved by placing it in an oven and maintaining a consistent temperature of 60 °C for a prolonged period of 48 hours, resulting in the acquisition of the modified, pre-treated continuous carbon fibre.

5.2.3 Filament fabrication of CCF/PPS composites

Continuous carbon fibre reinforced PPS composites were fabricated using an-house developed filament-line, modified from our previous work [122]. The equipment is shown in Figure 5-1(b). Initially, the continuous carbon fibre tow was held under tension using a wind-up spooler. This setup was critical for ensuring uniform fibre alignment and tension during the subsequent impregnation process. For the formation of pristine continuous carbon fibre reinforced PPS

composites (p-CCF/PPS), PPS powder was evenly distributed onto the surface of the carbon fibre. The coated fibres were then passed through a nozzle, where the powder was melted at high temperatures to create a resin bath. The pultrusion temperature was precisely controlled and set at 320 °C to facilitate optimal melting and impregnation. As the carbon fibre tow was drawn through this resin bath, it became thoroughly impregnated with the PPS resin, forming the p-CCF/PPS. For the production of the treated composites (t-CCF/PPS), dry continuous carbon fibre was first subjected to a treatment involving a modification solution containing polydopamine and silica nanoparticles. This pre-treatment involved immersing the carbon fibre in the solution, followed by a thorough rinsing and drying process. Once prepared, the treated carbon fibres were compounded with PPS powder through the filament-line following the same process as above. This step was crucial for ensuring the even distribution and integration of the PPS powder with the modified carbon fibre, resulting in the formation of the t-CCF/PPS composites.

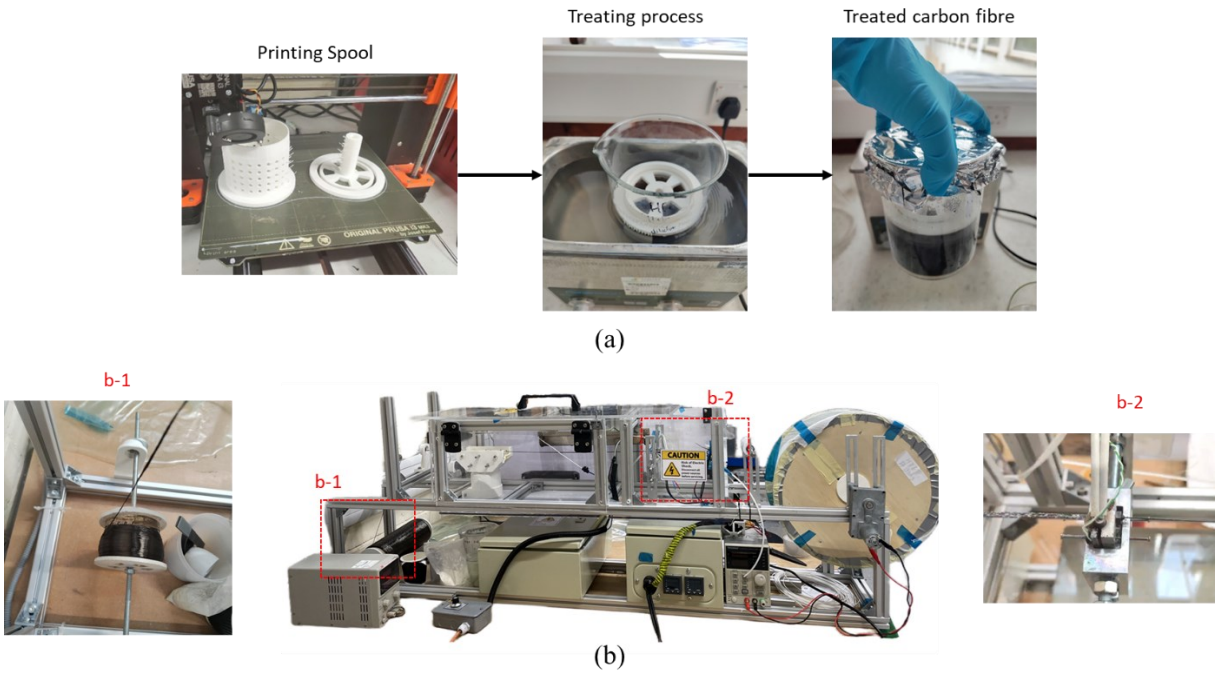

Figure 5-1 (a) Surface treatment procedure of continuous carbon fibre tow; (b) set-up of a house developed filament-line.

5.2.4 **3D printing and post-processing of CCF/PPS composites**

The fabrication process progressed to the 3D printing stage, where both types of the previously fabricated continuous filaments were utilised. A circular-similar cross-section, possessing a diameter of approximately 600 μm, was observed for the 3K continuous carbon fibre/polyphenylene sulphide (CCF/PPS) filament, featuring an average fibre volume fraction of around 50% (refer to Figure 5-2(a)). As shown in the cross-sectional image of manufactured filament, a non-uniform distribution of fibres results from our in-house developed filament fabrication process. Despite this, the quality of filament remains acceptable for the printing process when compared with commercial filaments [122].

Table 5-1 Printing parameters for CCF/PPS filament.

Printing parameters	**Values**
Bed temperature	90 ℃
Nozzle temperature	320 ℃
Chamber temperature	25 ℃
Print speed	150 mm/s
Raster width	1.5 mm
Layer height	0.2 mm
Nozzle diameter	1.3 mm

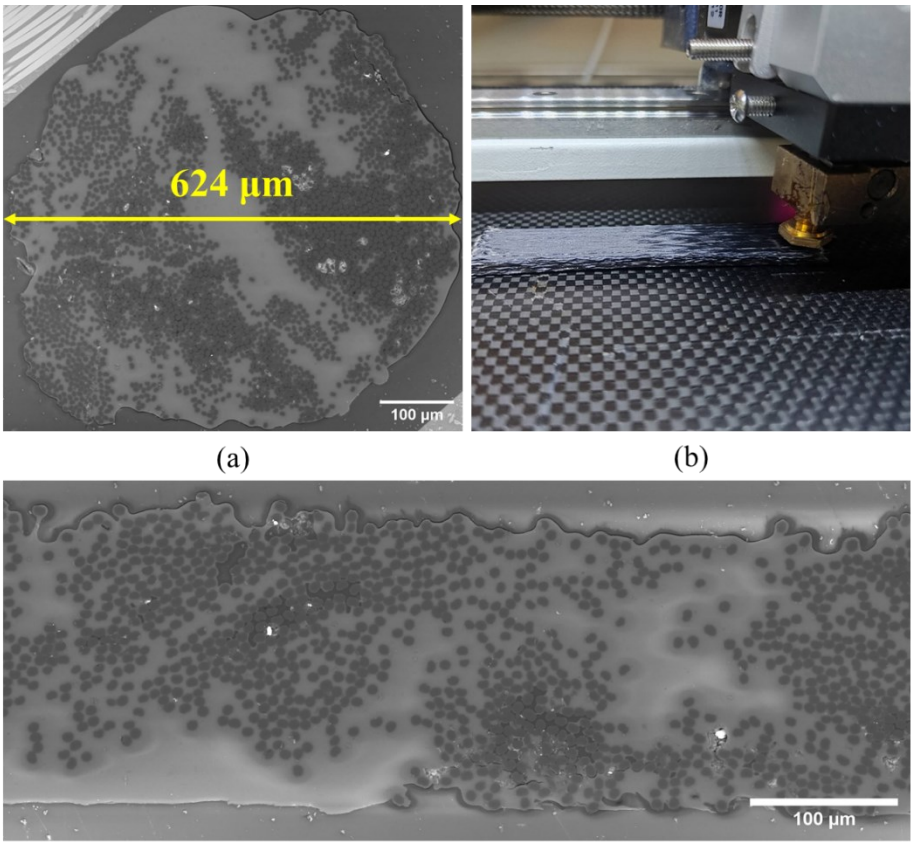

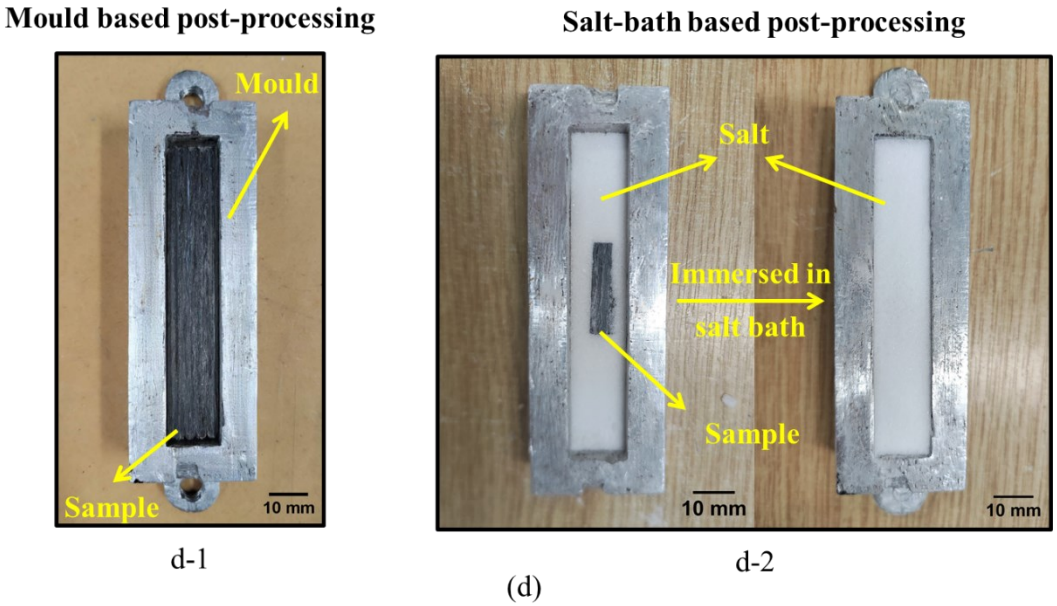

Figure 5-2 (a) Cross-section of produced 3K CCF/PPS filament; (b) printing process of CCF/PPS filament; (c) printed single strip; (d) set-up of mould based post-processing and salt-bath based post-processing.

A high-temperature 3D printer (Creatbot F430) was employed to manufacture CCF/PPS composites from these filaments. For this purpose, a specific fibre placement nozzle with a diameter of 1.3 mm, sourced from Markforged Ltd., United States, was integrated into the 3D printer (see Figure 5-2(b)). This setup allowed for the precise and controlled deposition of the continuous filament during the printing process. The SEM images of printed single stripe is shown in Figure 5-2(c). As expected, the voids within the printing strips are a common defect encountered in the additive manufacturing of continuous carbon fibre filament. To tackle this issure, a detailed post-processing method has been developed and is thoroughly discussed in this chapter. Table 5-1 presents the printing parameters for produced CCF/PPS filament.

Following the 3D printing, the composites underwent a critical post-processing phase, which was conducted using a Pinette Emidecau Industries (P.E.I.) hot-press machine. The hot-press program is depicted in Figure 5-3(a), and the images of as-printed and post-processed specimens are also presented in Figure 5-3(b). This stage was implemented through two distinct hot-press methods (refer to Figure 5-2(d)): mould-based and salt bath-based. In the mould-based post-processing method (Figure 5-2(d-1)), the printed composites were placed within a specially designed mould. They were then subjected to hot-press under elevated temperatures and high pressure. This method ensured a uniform application of heat and pressure, essential for achieving the desired material properties and structural integrity. Alternatively, in the salt bath-based hot press method (Figure 5-2(d-2)), the composites were first immersed in a bath of salt before being hot-pressed. The cuboid mould was filled with ground salt, and the printed object was submerged in the salt. This process enables the salt to act as a support to maintain the detailed features and evenly distribute the pressure in all directions during the hot-pressing procedure. The unique property of the salt, remaining un-melted under high temperatures and pressures, was a crucial aspect of this method. This approach allowed for the successful post-processing of complex two-dimensional structures, including those with holes, and intricate

three-dimensional forms. The salt bath method was particularly effective in reducing void content in the final composites through thickness while maintaining precise dimensions in other directions.

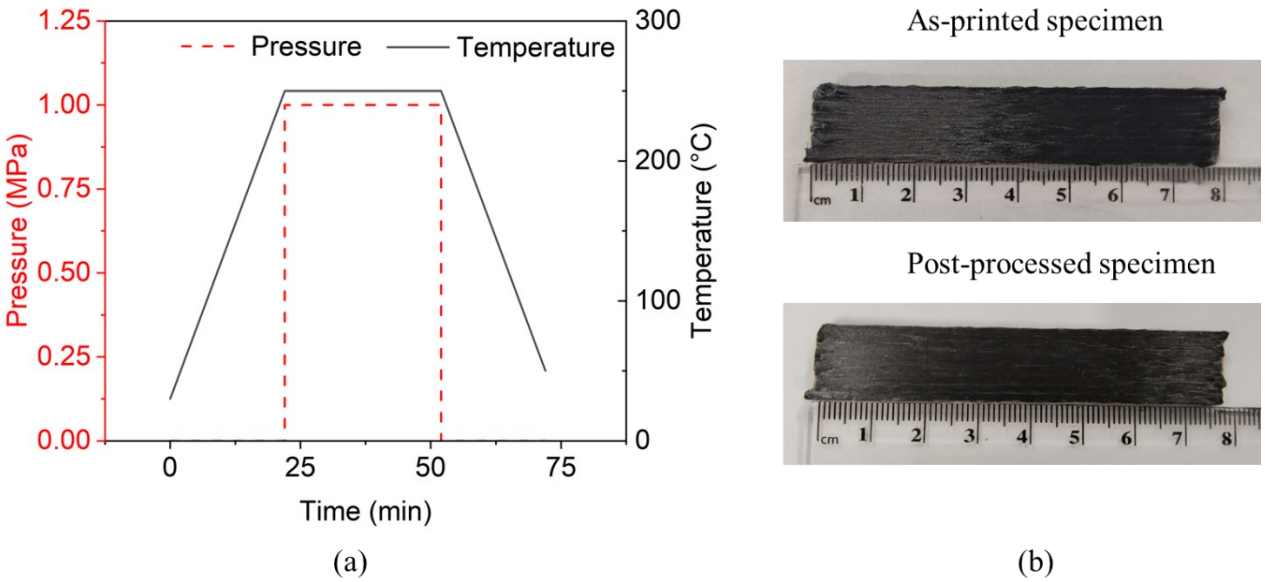

Figure 5-3 (a) Hot-press program; (b) as-printed and post-processed printed specimens.

5.2.5 **Mechanical test of 3D printed CCF/PPS composites**

The mechanical properties of 3D printed CCF/PPS composites were evaluated using a three-point bending test, as detailed in the Section 3.2.3. The sole variation in this test involved the use of a 50 kN load cell. The assessment of interlayer properties was carried out by measuring the interlaminar shear strength (ILSS), as detailed in the Section 4.2.5.

5.2.6 **Nanoindentation tests**

Nanoindentation tests were performed using the NanoTest Vantage system (Micro material) to conduct single fibre push-out tests, as referenced in [185].To prepare the push-out samples, slices of dimensions 13 mm × 4 mm × 2 mm were cut out from 3D printed unidirectional (UD) composite specimens. These slices were then vertically embedded in a polymethyl

methacrylate (PMMA) tube filled with liquid epoxy resin. After curing, the epoxy cylinder was ground and polished by a polisher (ATA Saphir 520). This process involved the use of SiC abrasive paper, with grit sizes ranging 180, 400, 800, 1200 and 2000 grit, ensuring a gradual and uniform abrasion. Subsequently, finer polishing was achieved using the diamond powder with grain size of 3 μm and 1 μm. To ensure uniformity and perpendicular to the polishing plane, the cylinder was secured in an adapter during this procedure. After completing one side, the specimen was flipped, and the opposing side was similarly ground and polished until the composite slice reached an approximate thickness of 100 μm.

Specimens were positioned on a fine mesh featuring a 26 μm diameter groove, ensuring precise alignment during test. Testing parameters included a loading rate set at 20 nm/s, utilising a triangular diamond pyramidal indenter (Berkovich tip) to exert force on the fibres. A series of push-out tests were unloaded at 100 nm/s in the unloading steps. Randomly selected fibres embedded within the PPS matrix were subjected to a maximum load of 100 mN for both untreated composites and treated composites. Subsequently, the cross-sectional areas of these tested samples were examined using Scanning Electron Microscopy (SEM) to assess the interfacial interactions.

The interfacial shear strength (IFSS) is calculated based on the Equation 5-1.

$$\tau_{IFSS} = \frac{F_{max}}{2\pi r_c l_s} \tag{5-1}$$

where F_{max} represents the maximum load at which debonding between fibre and matrix occurs, usually identifiable as the initial peak load in the test data [186]; r_c is the radius of carbon fibre (3.5 μm for T700); and l_s is the sample thickness.

5.2.7 **Thermal properties of 3D printed recycled composites**

Dynamic Mechanical Analysis (DMA) was employed to characterise the viscoelastic properties of 3D printed CCF/PPS composites, described in the Section 3.2.5. In addition, the thermal behaviour of the composites was analysed using Differential Scanning Calorimetry (DSC), as detailed in Section 3.2.4. The degree of crystallinity was calculated by Equation 3-1.

5.2.8 **Microstructure characterisation and morphology analysis**

The microstructure characterisation of printed and post-processing composites was observed by Optical Microscopy and SEM, outlined in Section 3.2.6. Following the ILSS tests, the specimens were entirely torn along the failed layers, and the fractured surface morphologies were examined using SEM. Additionally, the surface morphology of carbon fibres was examined using TEM, as detailed in Section 4.2.3.

The failure mechanisms of the specimens from the short beam tests were investigated using the in-house developed X-ray computed tomography (XCT) facility at the University of Edinburgh. XCT scans were performed at an accelerating voltage of 70 kV and a power of 24 W. To ensure the acquisition of high-quality images, both in terms of contrast and intensity, the exposure time was set to 2 seconds. The raw scan data were then processed and visualised in 3D using the commercial software Avizo. This software's volume rendering and slicing capabilities were particularly used in identifying failure modes at various locations within the specimens. The application of XCT imaging allowed for a capture of the failure modes induced by shear loading within the specimens.

5.3 Molecular dynamics simulation

The interaction between the carbon fibre and the PPS matrix at nano-scale was investigated using molecular dynamic (MD) simulations. These simulations were carried out using the Materials Studio software, employing the Forcite module. The basis for all simulations was the COMPASS (Condensed-phase Optimised Molecular Potential for Atomistic Simulation Studies) force field. This comprehensive force field encompasses valence energy, including both diagonal terms and cross terms, as well as non-bond energy. The diagonal terms cover aspects such as bond, angle, torsion, and inversion, whereas the cross terms include stretch-stretch, stretch-bend-stretch, stretch-torsion-stretch, separated-stretch-stretch, torsion-stretch, bend-bend, torsion-bend-bend, and bend-torsion-bend interactions. The non-bond energy component accounts for van der Waals and electrostatic interactions [187].

5.3.1 Modelling of hybrid layers on CF surface

At the nano-scale, the CF surface is characterised by a highly graphitic arrangement comprising sp2 carbon atoms. The atomic-scale features of the CF surface, however, remain less defined. For the purpose of these simulations, carbon fibre models were constructed based on graphene or graphite crystals, representing an idealised and unsized CF surface, as commonly used in literature [86]. Despite the simplified nature of this graphite carbon fibre surface model, its use in simulations of graphite-polymer composites interfaces, in conjunction with experimental work, is useful in elucidating the molecular-level mechanics of the carbon fibre-matrix interface [188–191]. In this model, four layers of graphite with a density of 1.78 g/cm^3 and an interlayer spacing of 3.4 Å were constructed in a periodic simulation cell.

It is widely accepted that the formation of polydopamine (PDA) molecules stems from the oxidation of dopamine (DPA), along with intramolecular cyclisation and the redistribution of electrons, with oxidation induced by air being crucial to this self-polymerisation process.

Besides the reactions that involve the formation of covalent bonds, the non-covalent self-assembly process also plays a significant role in the synthesis of PDA [95]. Research indicates that the final structure of PDA predominantly comprises oligomers, which are connected through dihydroxy-indole and indole-quinone units via benzene ring linkages [192]. In our simulation system, PDA was therefore considered as a polymer-like aggregate composed of oligomer units connected through tetramer linkages [193].

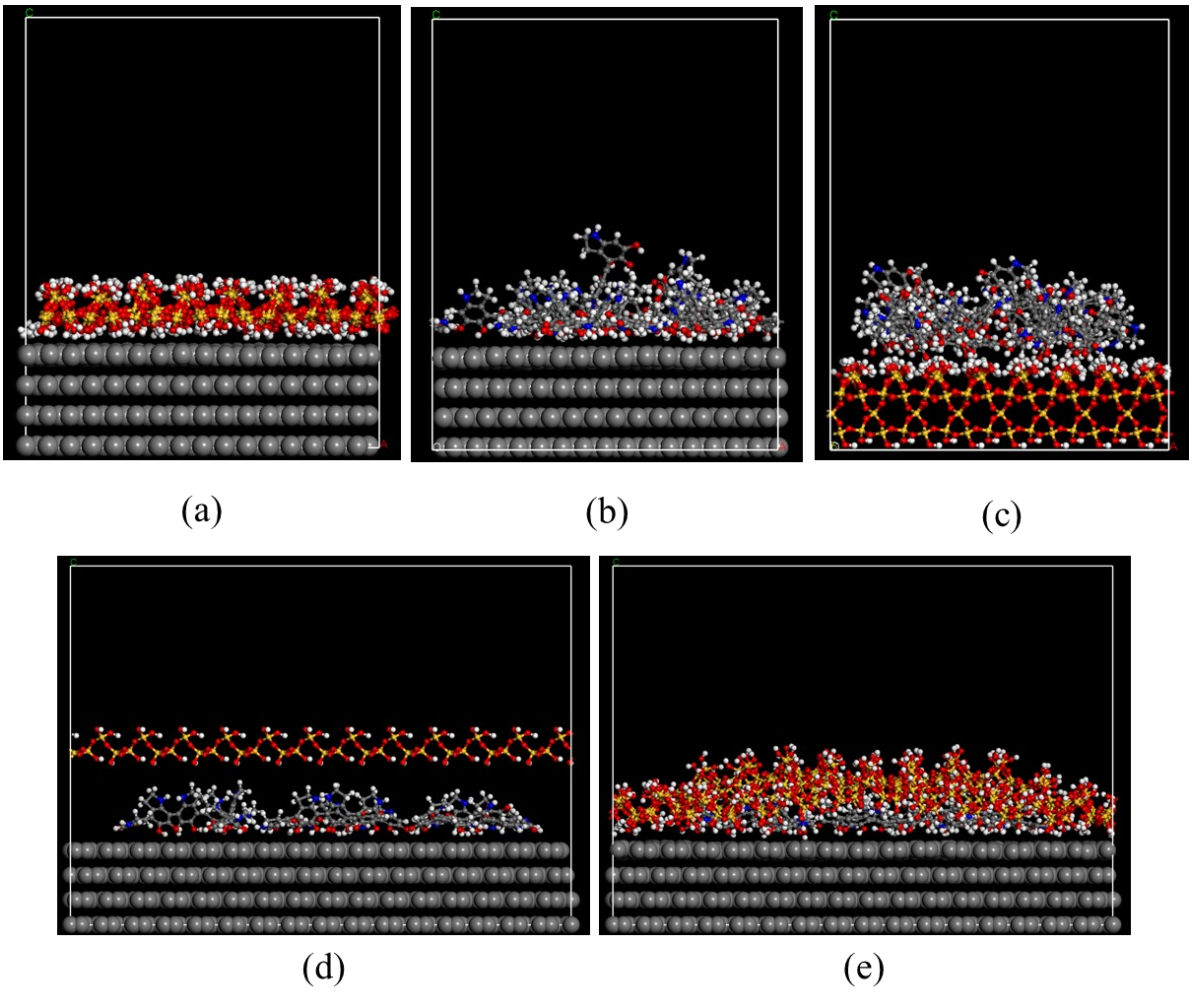

Figure 5-4 Interaction models after equilibration of (a) CF and SiO2; (b) CF and PDA; (c) PDA and SiO2 and (d) initial interaction; (e) equilibrated models of CF, SiO2 and PDA.

Three models representing interactions between CF and SiO_2, CF and PDA, and PDA and SiO_2, respectively, were built to study the adsorption energies and evaluate the interfacial strength.

The geometry of each interface structure was first optimised using the NVT ensemble at 298 K, followed by equilibrium achieved through annealing simulations ranging from 300K to 500K over five cycles. The final frames are presented in Figure 5-4(a-c). Additionally, a multilayer model containing CF, PDA, and SiO_2 was created to investigate the microscopic distribution and geometry configuration of the PDA/NPs hybrid networks on the carbon fibre surface, as shown in Figure 5-4(d). The models underwent equilibration using the aforementioned method, with results presented in Figure 5-4(e).

5.3.2 **Single fibre push-out simulation**

In order to build a model with similar conditions as experiments, PPS polymers model was constructed from an amorphous cell mixed with its monomers at an initial density of 1.3 g/cm^3. This model was designed with periodic boundary conditions (PBC). The PPS polymer matrix layer structures were then established and sufficiently equilibrated to simulate the shear behaviour of the single carbon fibre. The mechanical response at the interface was assessed using push-out MD simulations [189,194]. Here, only CF substrate was pushed out of the polymer matrix to maintain the same contact area, and the change in total system potential energy was monitored. The CF substrate was configurated as an independent rigid body, and laterally pushed out along the x-direction at a constant velocity of 2.5 Å/ps using the NVT ensemble at 298K over 18 ps.

The variation in potential energy is determined by the change in interfacial interaction force between carbon fibre and the PDA/NPs layer, and PDA/NPs layer and PPS polymer. Therefore, we have minimised the thickness of in-depth carbon fibre layer to control the system size and accelerate the computation time [195,196]. The Cartesian position of 50% in-depth atoms of PPS polymer in the cell was fixed to simulate real experimental conditions accurately. Free motion of other atoms in the cell was maintained during the CF pull-out simulation. The

maximum displacement of the substrate was 45 Å, offering valuable insights into the interfacial dynamics and mechanical interactions under simulated shear conditions.

5.4 Results and discussion

5.4.1 Mechanical performance with improved interlaminar properties

To assess the impact of the PDA/NPs hybrid networks and post-processing techniques on the macro-mechanical properties of the composites, we analysed the force-displacement curves and ultimate flexural strength under the three-point bending load (Figure 5-5). This analysis included unidirectional coupons of printed composites with pristine carbon fibre (p-CCF/PPS), printed composites with treated carbon fibres (t-CCF/PPS), as well as their hot-pressed counterparts, *i.e.*, ph-CCF/PPS and th-CCF/PPS. The experimental results revealed notable enhancements in flexural strength following treatments.

Specifically, composites exhibited an increase of 9.3% in flexural strength with the sole application of the PDA/NPs treatment and an increase of 15.9% with only post-processing treatment (using a specially designed mould, refer to the metal mould in Figure 5-2(d-1)). Notably, the parts that underwent post-processing with treated carbon fibre showcased the highest flexural strength, which was 27.0% greater than that of p-CCF/PPS. These findings indicate that the combination of PDA/NPs treatment and post-processing significantly enhanced the mechanical response of CCF/PPS composites, evidencing the efficacy of this two-step treatment approach in enhancing interfacial properties.

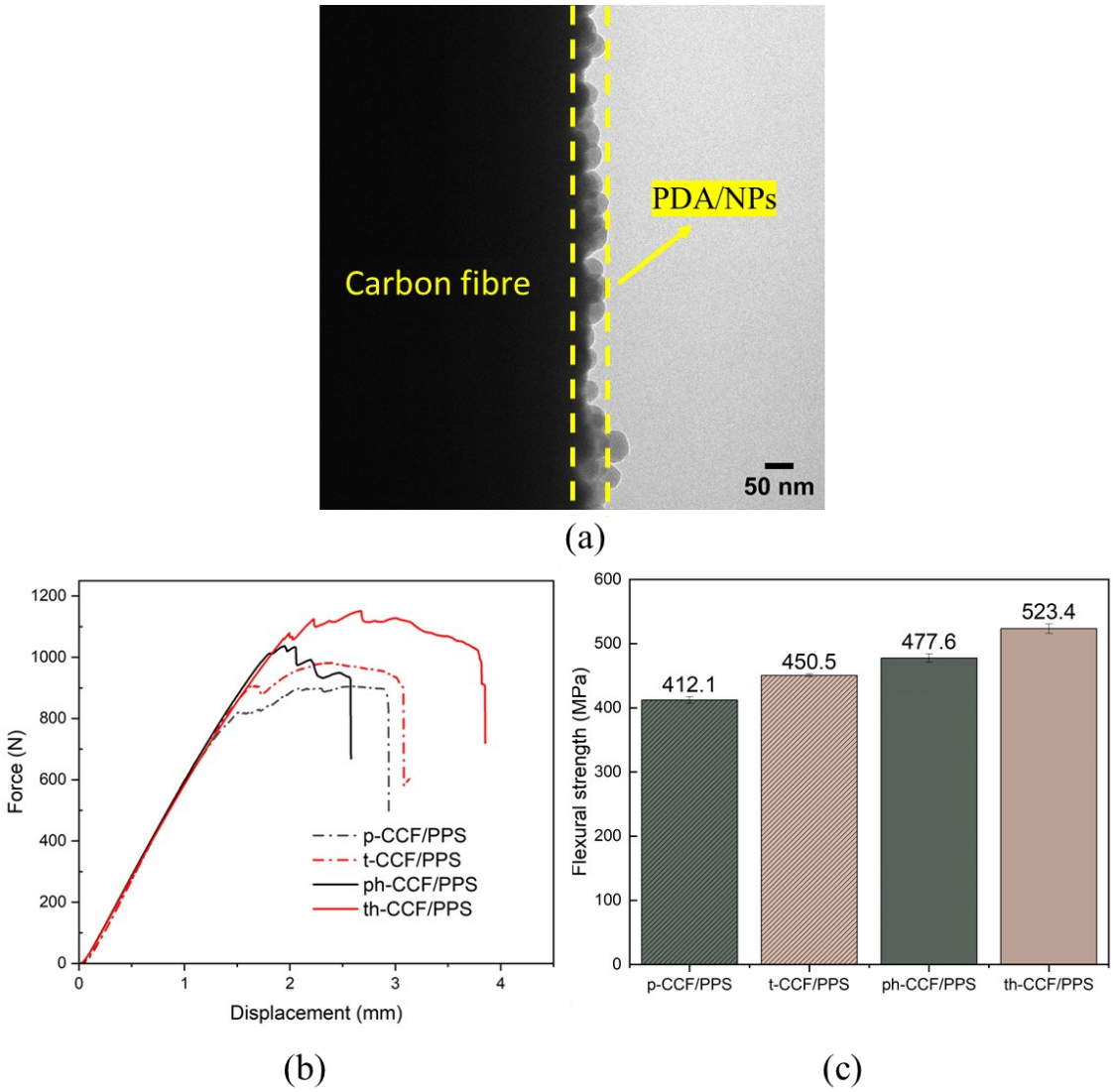

Figure 5-5 (a) TEM images of PDA/NPs layer on the surface of carbon fibre; (b) representative force-displacement curves; (c) flexural strength of p-CCF/PPS, t-CCF/PPS, ph-CCF/PPS and th-CCF/PPS.

Further examination of the interlaminar properties was conducted through the measurement of interlaminar shear strength (ILSS) under a short-beam three-point bending load for the aforementioned four types of composites, as detailed in Figure 5-6. All specimens were maintained at the same displacement during ILSS testing, followed by XCT scans to study the failure mechanisms. Starting with the untreated coupons featuring pristine carbon fibre (p-CCF/PPS), the ILSS was found to be 9.1 MPa, setting a baseline for the subsequent treatments.

When carbon fibres were treated with PDA/NPs, the ILSS values increased significantly by 52.2%, attributing to the effectiveness of the nanoparticle treatment in enhancing the fibre-matrix interface. For samples without post-processing, the curves exhibit delamination after reaching the peak force and have a long plateau stage. The impact of post-processing was even more obvious, with ILSS values effectively doubling, indicating a substantial reinforcement of the interlayer bonds within the composite. This marked ILSS value of 24.73 MPa for composites that underwent both carbon fibre surface treatment and interlayer consolidation. Post-processed samples displayed initial delamination followed by complete failure.

In conclusion, the combination of PDA/NPs and post-processing optimises both flexural and shear strengths, allowing the CCF/PPS composites to sustain higher loads before failure. Interestingly, post-processed composites in ILSS test exhibit steeper initial slopes, while those in 3PB bending maintain consistent elastic properties. This difference occurs because the treatments primarily affect interfacial and interlaminar properties rather than the bulk modulus of the composites. The ILSS test focused more on interlaminar shear strength, where improvements due to these treatments are more directly observable than in 3PB bending.

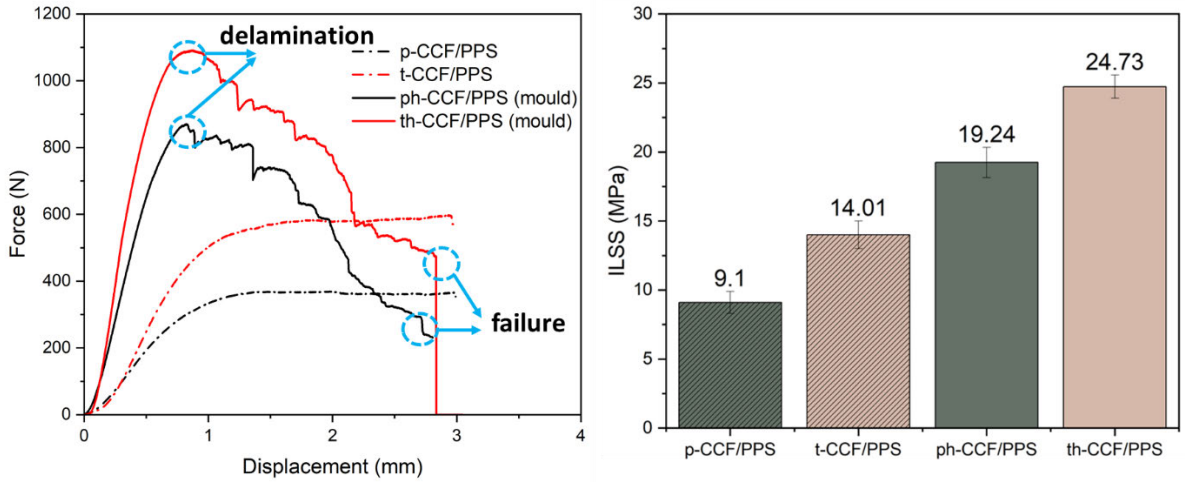

Figure 5-6 (a) Representative force-displacement curves; (b) interlaminar shear strength (ILSS) of p-CCF/PPS, t-CCF/PPS, ph-CCF/PPS and th-CCF/PPS.

The DMA curves depicted in Figure 5-7 provide a comprehensive overview of the thermal-mechanical performance of the various composite configurations across a temperature spectrum from room temperature to 250 °C. The storage modulus, representing the elastic response of the material, typically decreases with an increase in temperature due to the softening of the polymer matrix. This trend is consistent across all composite types, as observed in Figure 5-7(a).

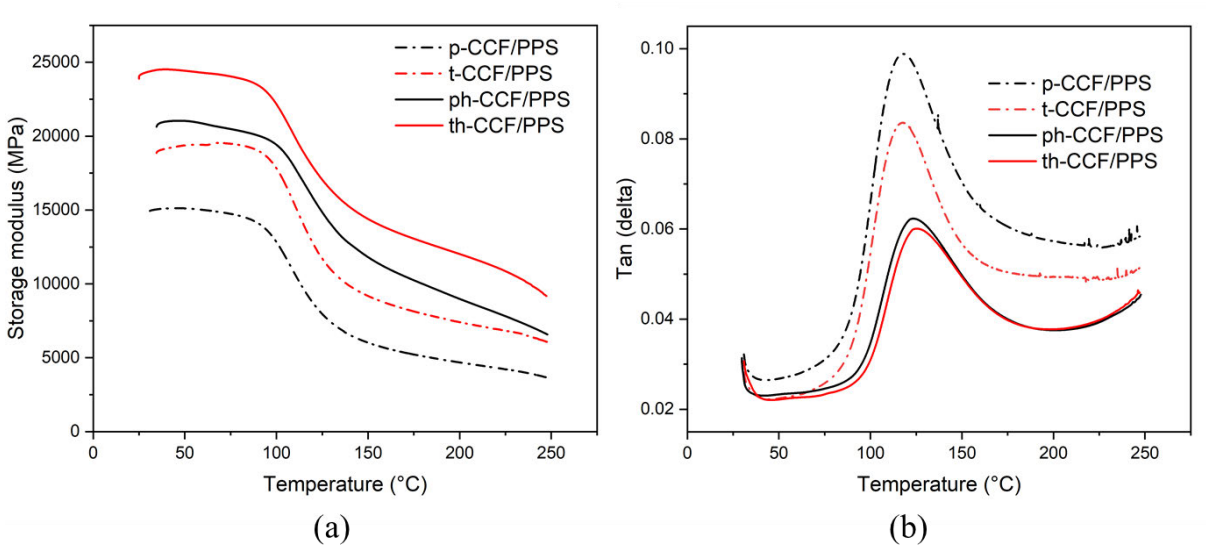

Figure 5-7 (a) Storge modulus and (b) damping factor of p-CCF/PPS, t-CCF/PPS, ph-CCF/PPS and th-CCF/PPS.

For the p-CCF/PPS composites, the modulus begins at a substantial value but experiences a marked decrease as the material transitions through its glass transition region. The t-CCF/PPS composites display a notable increase in the storage modulus at lower temperatures, as a result of the positive impact of the PDA/NPs treatment on the stiffness of the composite. This improvement, quantified at 25.9% at 35 °C, indicating the effectiveness of surface treatment in reinforcing the composite's elastic properties. Upon examining the effects of post-processing, it becomes evident that this treatment plays a vital role in enhancing the thermal stability of the composites. The hot-pressed ph-CCF/PPS and th-CCF/PPS composites demonstrate a less drop

in the storage modulus with increasing temperature, signifying superior performance and stability. In particular, the th-CCF/PPS composites achieve an impressive storage modulus of 24.5 GPa at 35 ℃ and 9.2 GPa at 250 ℃, which is a remarkable 62.7% and 149.4% increment compared to the untreated samples.

Figure 5-7(b) illustrates the tan delta (damping factor) curves, which offer insight into the material's damping characteristics and glass transition temperature (T_g). The p-CCF/PPS composites have a T_g of 117 ℃, while the th-CCF/PPS composites exhibit an increased T_g of 127 ℃. This elevation in T_g for the th-CCF/PPS composites can be attributed to the enhanced fibre/matrix adhesion and the stabilisation of the polymer chains achieved through the synergistic effects of PDA/NPs treatment and post-processing. The shift in T_g also suggests changes in the semi-crystalline structure of the polymer, indicative of melting and recrystallisation processes which occur under the influence of the applied temperature and pressure during post-processing.

5.4.2 **Enhancing mechanism for interlaminar properties**

(1) Effect of PDA/NPs treatment on fibre/matrix interfacial interaction

The calculated adsorption energies for the interfaces of CF-SiO_2, CF-PDA, and PDA-SiO_2 provide a quantitative measure of the interaction strengths. Molecular dynamic simulations under an NVT ensemble at 298 K were carried out via Forcite module for 100 ps, allowed the systems to reach a fully relaxed state. The interfacial structures, as visualised in Figure 5-8, reveal the relaxed configurations between carbon fibre and silica nanoparticles (CF-SiO_2), carbon fibre and polydopamine (CF-PDA), and polydopamine and silica nanoparticles (PDA-SiO_2), respectively.

Upon obtaining stable adsorption configuration, the interaction energy ΔE was computed using the formula:

$$\Delta W = W_{AB} - (W_A + W_B) \quad (5\text{-}3)$$

In this equation, W_{AB} represents the total energy of adsorption system comprising components A and B, while W_A and W_B denote the energies of the isolated component A and component B.

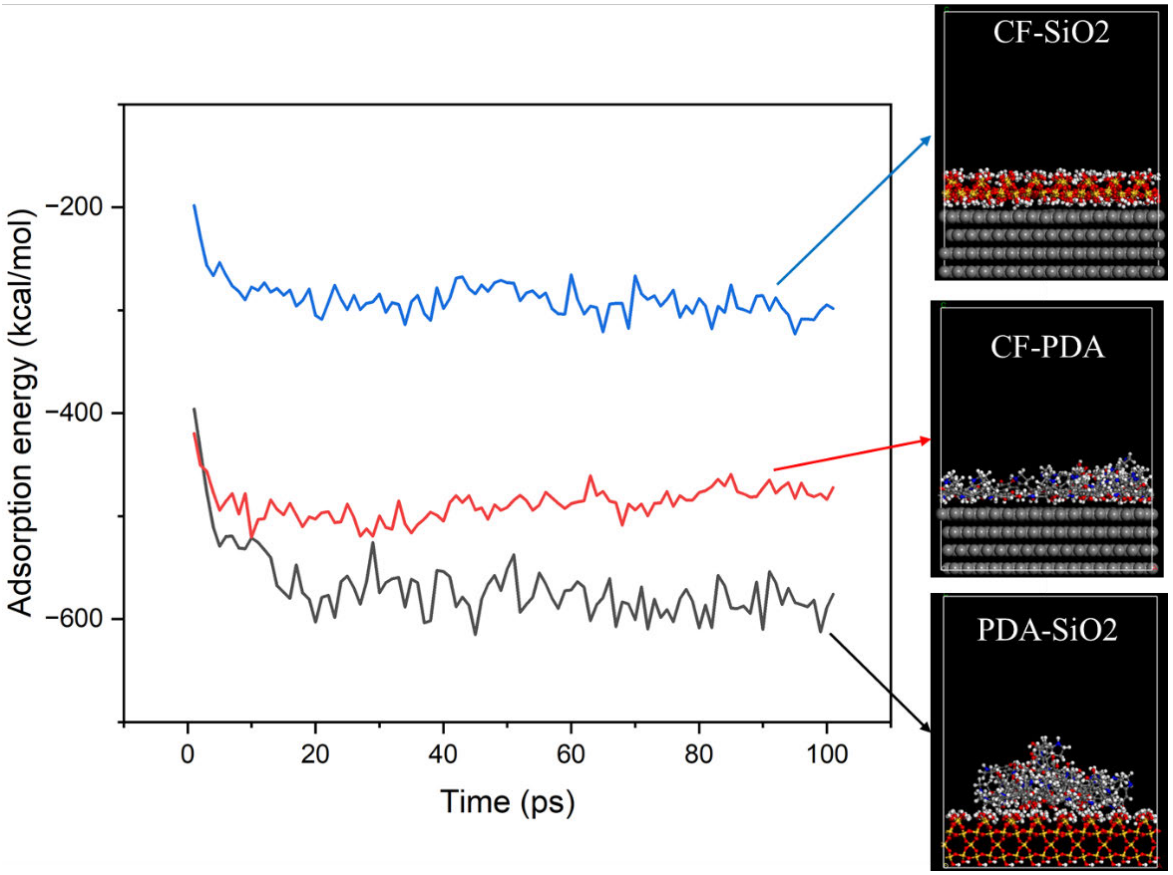

Figure 5-8 Adsorption energy and equilibrated models of CF-SiO2, CF-PDA and PDA-SiO2 in MD simulations.

The adsorption energies data during MD simulations, depicted in Figure 5-8, indicate that CF-PDA interactions (-488 kcal/mol in average) were uniformly stronger than that involving SiO_2 (-287 kcal/mol in average). Notably, PDA displays a higher affinity for SiO_2 with an adsorption energy of -569 kcal/mol in average, suggesting that PDA significantly enhanced the surface interaction between CF and SiO_2. This stronger affinity between PDA and SiO_2 implies that PDA effectively enhanced the interface, leading to better adhesion and thus reinforcing the composite's structure. The energy profiles indicate that the presence of PDA created a more

stable interface, contributing to the improved interlaminar properties observed in the enhanced composites.

A multi-layered system comprising PDA, SiO2, and CF layers was constructed to investigate their stable adsorption configurations. The MD simulation was extended over 100 ps to monitor the adsorption progression and the change in van der Waals energies, which are depicted in Figure 5-9(a). The sequential snapshots show the dynamic adsorption process, highlighting transitions in the interaction structure (refer to Figure 5-9(b)). As shown in Figure 5-9(a), as the simulation time increases, the var der Waals force also increases, indicating stronger bonding within the system. As observed from Figure 5-9(b), as the simulation progresses, the silica nanoparticles layer presents a tendency to curl up. The silica nanoparticles exhibit an obvious affinity towards the PDA layer, progressively establishing a contact with the underlying carbon fibre surface. The role of PDA is crucial, serving as a binding agent that facilitates the adhesion of SiO_2 onto the CF substrate. This bridging effect not only stabilises the nanoparticle deposition but also enhances the surface properties of the carbon fibre, creating a modified interface with potentially superior mechanical attributes.

A detailed evaluation of the van der Waals in non-bonded energy components was also obtained via MD simulations. The simulation in Figure 5-9 reveals a clear pattern: as the van der Waals forces get stronger, so does the bond between the particles. This shows that these forces are the primary driving force to make the combined material stable and strong. Essentially, the PDA acts as a connector, bringing together the silica and carbon fibre parts. The increase in van der Waals forces correlates with the strengthening of the adsorptive bond, suggesting a stronger connection over time. The whole process, captured by the simulation, emphasises the importance of van der Waals forces in explaining the role of PDA in binding the materials together, ultimately leading to a reinforced interface with enhanced material performance.

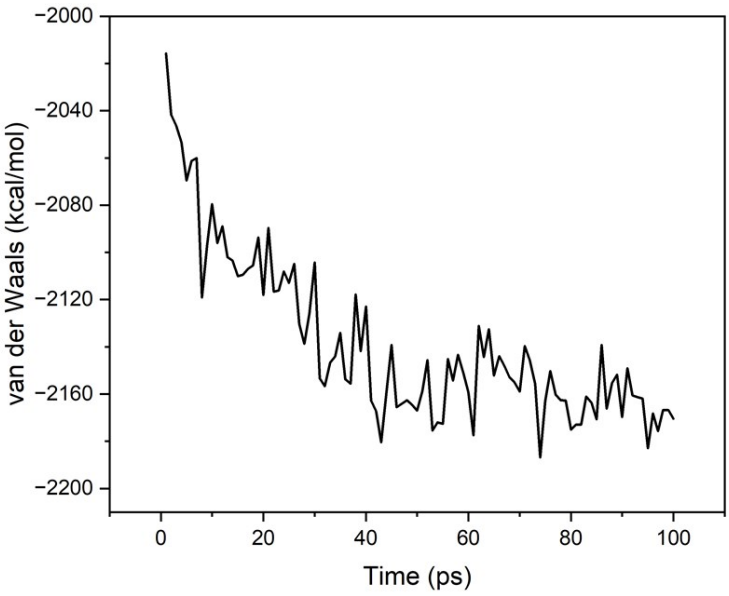

(a)

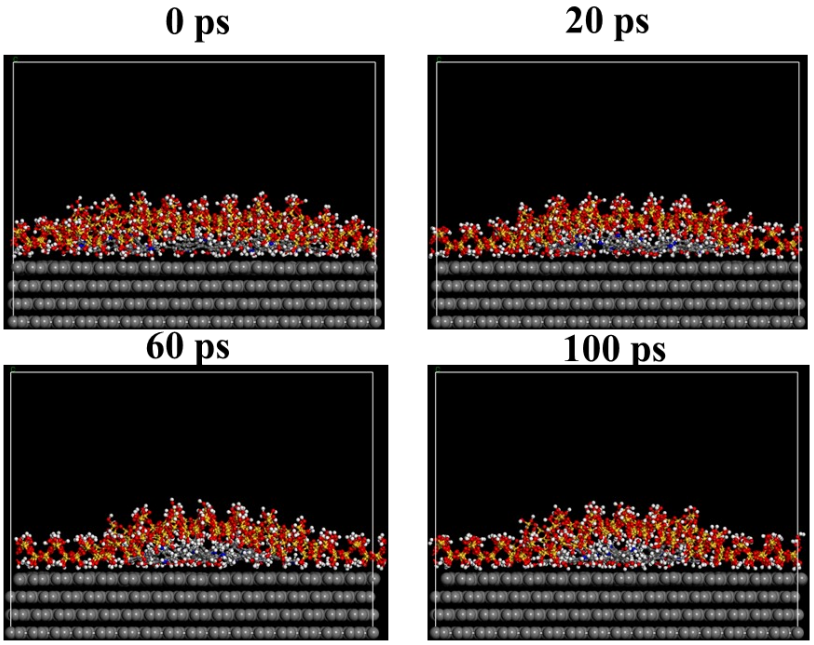

(b)

Figure 5-9 The changes in (a) van der Waals force and (b) morphology of models containing CF, PDA and SiO_2 over time during molecular dynamic adsorption progress in MD simulations.

Figure 5-10 illustrates the dynamic interfacial behaviour observed during fibre push-out simulations, comparing two distinct models: one with untreated carbon fibre and the other with PDA/NPs treated carbon fibre. As the simulations advance, the untreated carbon fibre shows a clean separation from the PPS matrix, indicating minimal adhesion. In contrast, the treated carbon fibre retains a considerable amount of PPS matrix, attributed from the presence of hydroxyl (-OH) functional groups introduced by the PDA/NPs treatment.

The interfacial shear energy, defined as the peak energy required to disrupt the bond between the PPS matrix and the carbon fibre, is a measure of the energy difference throughout the push-out process. Interfacial shear energy (W) is quantified by the energy variation and is given by the equation:

$$W = \frac{W_{max} - W_{min}}{A} \tag{5-4}$$

Here, W denotes the interfacial shear energy, W_{max} and W_{min} are the maximum and minimum potential energies of the total system, and A is the contact area, respectively.

The interfacial shear strength (IFSS) is partially derived from interfacial shear energy, with their relationship formalised as follows [197]:

$$\tau_{IFSS} = kW = \delta[\frac{E_m}{E_f}]^{1/2} W \tag{5-5}$$

In this context, τ_{IFSS} represents the total interfacial shear strength, k is a constant of the proportionality between interfacial shear strength and interfacial shear energy. δ is the coefficient equal to about 2×10^9 m^{-1}, and E_m and E_f are the elastic moduli of PPS matrix and carbon fibre.

This equation reveals a direct linear relationship between the change in energy and the interfacial shear strength. Thus, the shear strength derived from nanoindentation experiments can be matched with the shear energy obtained from MD simulations.

As shown in Figure 5-11(a), the simulated untreated composite displays an interfacial shear energy of 0.21 kcal/mol/Å^2, whereas the treated composite exhibits a significantly higher value of 0.78 kcal/mol/Å^2. Correspondingly, the experimental results of single-fibre push-out tests by nano-indentation were depicted in Figure 5-11(b) and Figure 5-11(c). The representative force-displacement curves (loading/unloading) for composites reinforced with untreated carbon fibres and treated carbon fibres reached a plateau (marked with a dashed square) after an elastic deformation stage, which determines the maximum push-out force during the indenter displacement. The first plateau in force-displacement curves was formed by the initial interface crack, which represents the elastic limits of the fibre/matrix bonding [185]. After the treatment of hybrid PDA/NPs network, the level of IFSS increased by 74.1%.

Figure 5-11(d) presents the SEM images of a typical individual pushed fibre viewed from the bottom side of the sample after the nano-indentation test. The failure occurs at the interface between the carbon fibre and the PPS matrix. The pushed fibre exhibits distinct debonding from the surrounding carbon fibres.

A good consistence of nano-indentation results and MD simulations validates the reasonable simulations on interfacial adsorption and shear behaviour at nanoscale. Both sets of results elucidate the mechanism by which PDA/NPs treatment enhances the fibre/matrix interface through interfacial bonding and prevents interfacial failure via uniform deposition.

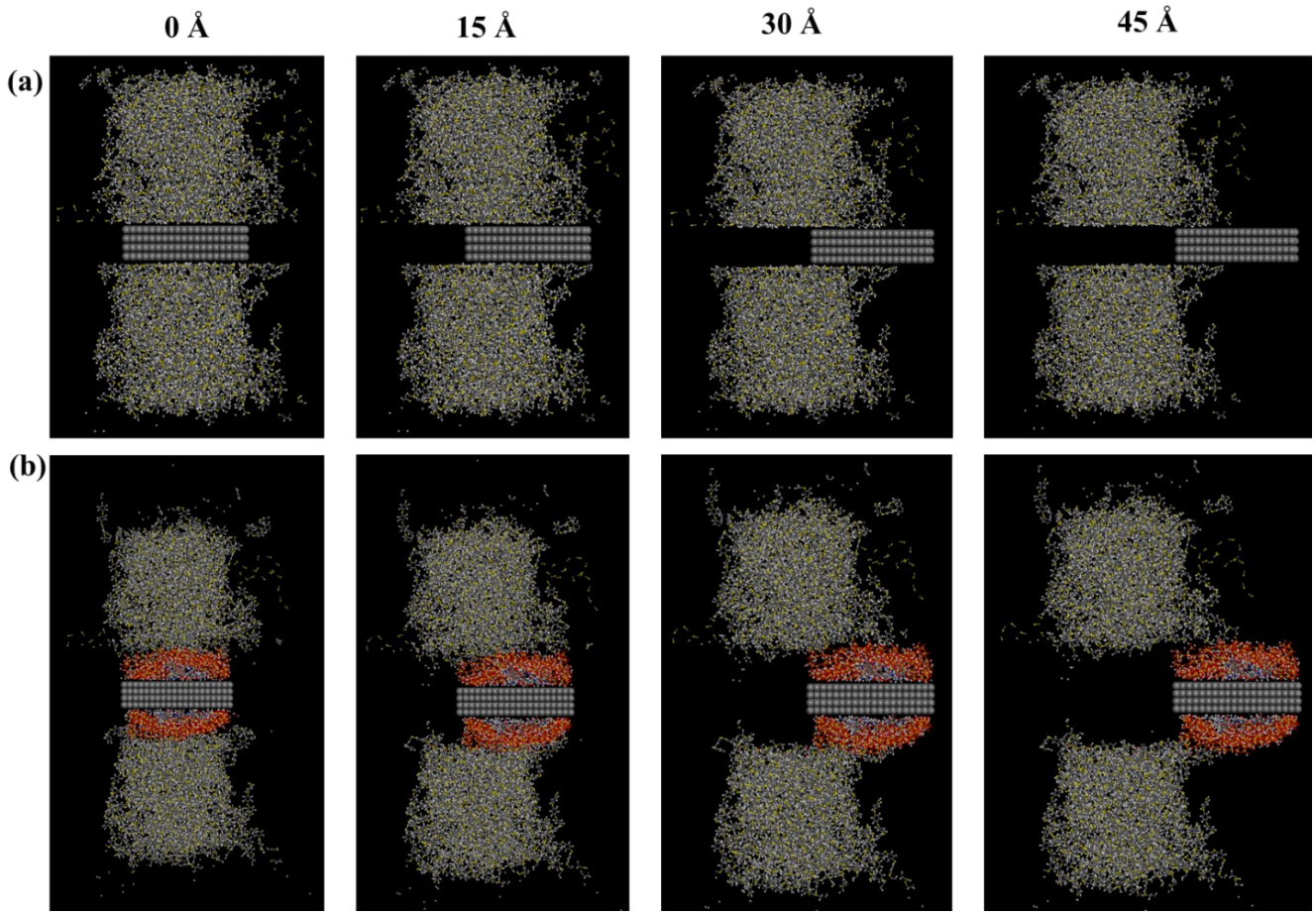

Figure 5-10 The simulation of carbon fibre pull-out in CCF/PPS composites: (a) untreated carbon fibre; (b) treated carbon fibre.

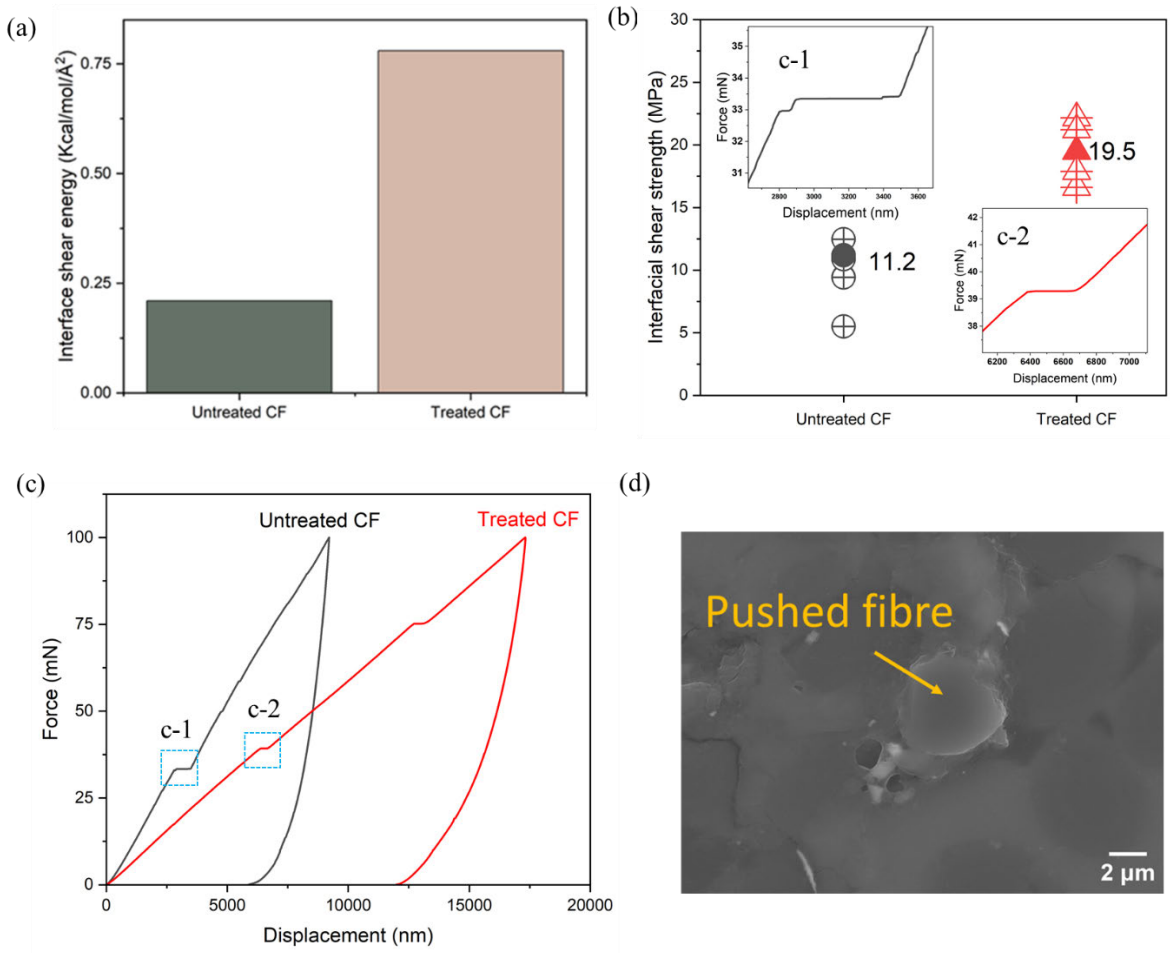

Figure 5-11 (a) Simulated interface interaction energy calculated from the fibre push-out shear simulations; (b) experimental interfacial shear strength (IFSS) from the single fibre push-out test with enlarged force-displacement graphs; (c) representative force-displacement curves in single fibre push-out test of composites reinforced with untreated CF (enlarged graph c-1) and treated CF (enlarged graph c-2); (d) microscopic images of single fibres after the push-out test in treated composites.

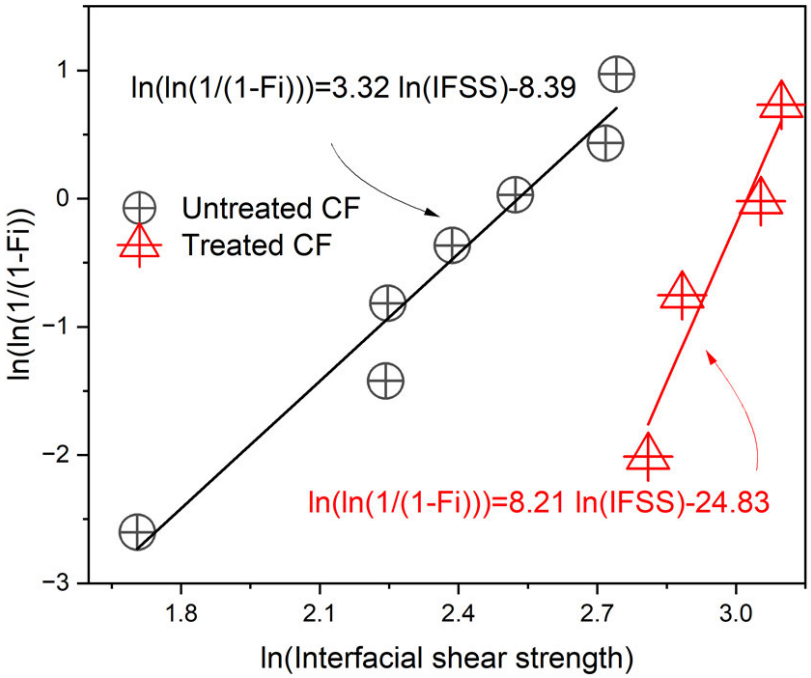

Figure 5-12 Weibull plots of IFSS values for untreated composites and treated composites.

Results indicate that the crack was assumed to propagate directly through the smooth fibre/matrix interface in untreated composites, and the major failure was along the debonding fibre due to the poor fibre/matrix interface. After the treatment, however, the initial crack energy could be absorbed by silica nanoparticles deposited on the carbon fibre surface. The spherical shaped nanoparticles could induce more smaller cracks in the interfacial region, acting as spacer, leading to the stress transfer in the interface region. As a result, the propagation of cracks would be retarded and fibre/matrix debonding would be prevented, contributing to an improved interfacial shear strength (IFSS) and fracture energy. In addition, a lower stiffness at the interface was found in the treated CF, compared with the untreated CF, which indicates that the interface has become more compliant or less rigid due to the treatment of PDA/NPs network. This could be the result of the treatment modifying the surface properties of carbon fibre, making the interface more capable of distributing stresses, which could better accommodate the deformations and contribute a tougher interface.

Weibull plot was performed to get the Weibull modulus α. The presence of manufacturing-induced defects in carbon fibre filaments, such as voids and non-impregnation between the carbon fibre and polymer matrix, contributes to the scattering in IFSS values. Consequently, the Weibull modulus α can be interpreted as a measure of the frequency distribution of these defects. Higher values of α suggest fewer defects and a more uniform distribution within the material. This modulus will give a more convinced value than standard deviation or coefficient of variation to compare the defect level.

The variability in IFSS values is analytically represented by Weibull equation [198].

$$P_F = 1 - exp\left[-\left(\frac{\tau_{IFSS}}{\tau_0}\right)^{\alpha}\right] \tag{5-6}$$

In this equation, P_F is the cumulative probability of interface failure in composite under a given IFSS, α is the Weibull modulus (a shape parameter) and τ_0 is the Weibull scale parameter. By taking the natural logarithm of both sides (twice), the equation transforms to:

$$ln\left[ln\left(\frac{1}{1-F_i}\right)\right] = \alpha ln(\tau_{IFSS}) - \alpha ln(\sigma_0) \tag{5-7}$$

Here, F_i is the probability of failure at the i^{th} ranked specimen (ordered from lowest to highest strength), calculated as:

$$F_i = \frac{i-0.5}{N} \tag{5-8}$$

where *N* represents the total number of specimens. The Weibull plots of interfacial shear strength for composites with untreated CF and treated CF were shown in Figure 5-12, where the calculated Weibull modulus α is 3.32 for untreated CF and 8.21 for treated CF. The presence of manufacturing-induced defects in carbon fibre filaments, such as voids and non-impregnation between the carbon fibre and polymer matrix, contributes to the scattering in IFSS values. Consequently, the Weibull modulus α can be interpreted as a measure of the

frequency distribution of these defects. Higher values of α suggest fewer defects and a more uniform distribution within the composites [186,199]. This implies that composites reinforced with untreated CF exhibited poorer impregnation, leading to greater variability in IFSS. On the contrary, the incidence of defects is reduced by grafting PDA/NPs hybrid network on the carbon fibre surface.

(2) Effect of post-processing on crystallinity and morphology

Figure 5-13 displays the DSC thermograms of specimens pre- and post-thermal processing. Employing Equation 3-1, the percentage crystallinity of both sets of specimens was calculated. The DSC curves reveal notable distinctions in the melting peak profiles: post-processed specimens exhibit broader peaks with a larger integrated area, indicative of heightened crystallinity. This observation is quantified by an increase in the degree of crystallinity, which rises from a 35.6% in the as-printed specimen to a higher percentage of 59.8% following post-processing, showing that more organised crystalline structures are formed. The observed enlargement in peak breadth and area under the curve is indicative of an enhanced degree of order within the polymer matrix, resulting from the post-processing conditions at elevated temperature and pressure. A more organised polymer chains in matrix translates to a stronger interlaminar shear strength, suggesting that the application of specific thermal conditions - onset melting temperature - can improve the modulus of the material. Consequently, this leads to a more robust response under short-beam shear and three-point bending loads.

Additionally, the cross-sectional images observed by optical microscope and SEM are shown in Figure 5-14. The images illustrate a significant reduction in voids after applying a moderate pressure (1 MPa) to the specimens. This consolidation effect has led to a considerable decrease in void content, from 10.22% in the as-printed specimen to 3.42% in the post-processed specimen, as quantified by Image J software analysis. As a result, the reduction in voids

minimises the defects at the layer-layer interfaces, thereby strengthening the interlaminar shear strength. Furthermore, the consolidation process has been shown to further potentially improve the orientation of continuous carbon fibre compared to the as-printed specimens. Overall, post-processing has demonstrably enhanced both the interlaminar properties and the material's resistance to deformation under shear and flexural stresses.

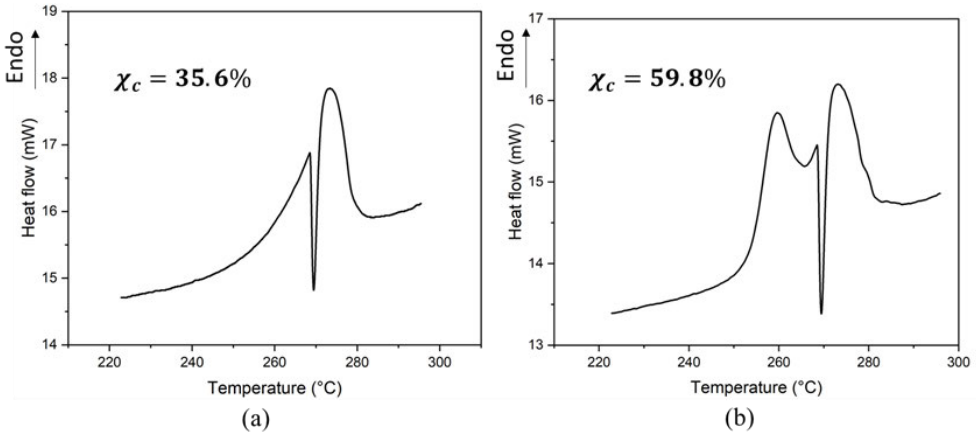

Figure 5-13 DSC curves of CCF/PPS composites: (a) as-printed and (b) post-processed.

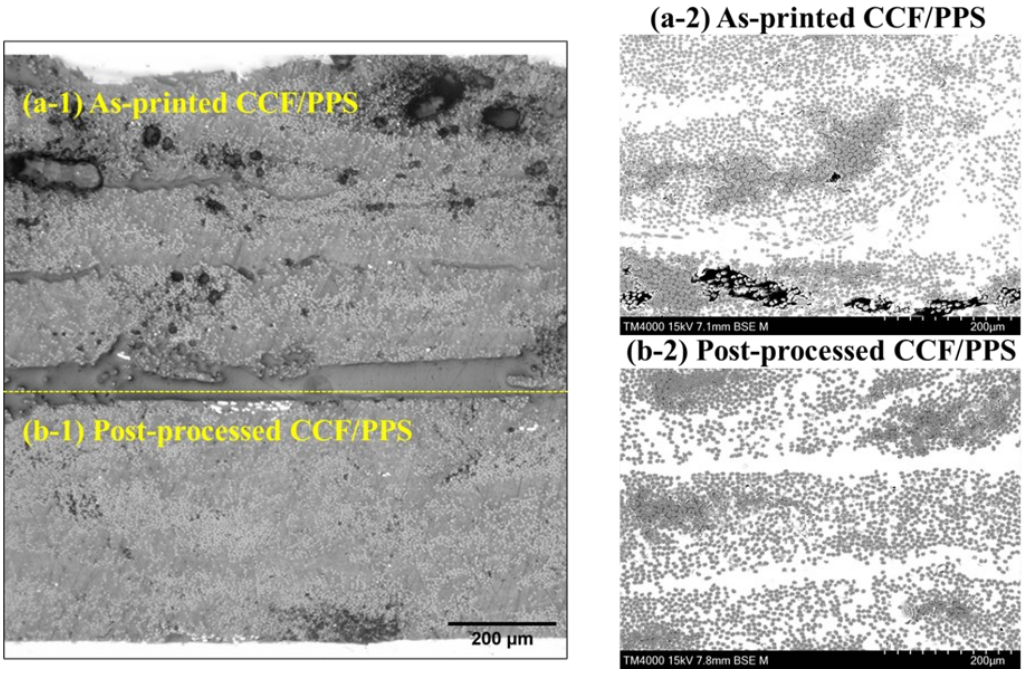

Figure 5-14 Microscopic images of as-printed (a-1: optical microscopy; a-2: SEM image) and post-processed (b-1: optical microscopy; b-2: SEM image) CCF/PPS composites.

(3) Combined effect on the interlaminar properties

To further elucidate the impact of carbon fibre treatment and post-processing on the interlaminar properties, X-ray computed tomography (XCT) images of failure modes following the short-beam shear tests on 3D printed CCF/PPS specimens were presented in Figure 5-15. Generally, the printed parts undergoing testing exhibited significant inelastic deformation and ductility. A prevalent mode of failure identified in the composites was delamination, as evidenced in both composites reinforced with pristine carbon fibre (p-CCF/PPS) and treated carbon fibre (t-CCF/PPS), depicted in Figure 5-15(a) and 5-15(b). In contrast, the post-processed composites demonstrated more intricate failure modes when post-processed at elevated temperatures and pressures. Beyond interlayer delamination, the specimens also exhibited tension and compression failures, as illustrated in Figure 5-15(c) and Figure 5-15(d).

Furthermore, the mechanical response of carbon fibre treatment positively correlated with the failure modes at the interlaminar level. When comparing untreated specimens to treated ones, it was observed that cracks propagated more uniformly through the fibre/matrix interface in the untreated composites. The combined effects of the PDA/NPs network on the carbon fibre surface and the post-processing techniques are promising in enhancing the shear yield stress at the interface layer. Consequently, these improvements lead to significantly enhanced interlaminar properties of the composites.

The fracture surfaces of the CF/PPS composites following the ILSS test were examined in Figure 5-16 to further explore the combined effect of improving the fibre/matrix interfacial and interlayer properties through the incorporation of PDA/NPs network and subsequent post-processing techniques. Upon examining Figure 5-16(a) and its zoomed-in image, it was observed that the untreated carbon fibres were predominantly detached from the PPS matrix across many surface areas, attributing to weaker interfacial adhesion. This was evidenced by

the observation of clean and smooth fibre bundles and gaps aligned with the CF direction, suggesting rapid crack propagation through the CF/PPS interface. Following the integration of the PDA/NPs network (refer to Figure 5-16(b)), an obvious layer of PPS resin was found on the fractured surface, alongside more textured CF surface patterns. In this context, the silica nanoparticles functioned as spacers in the interfacial region, promoting the development of multiple smaller cracks rather than direct debonding between the PPS matrix and carbon fibres.

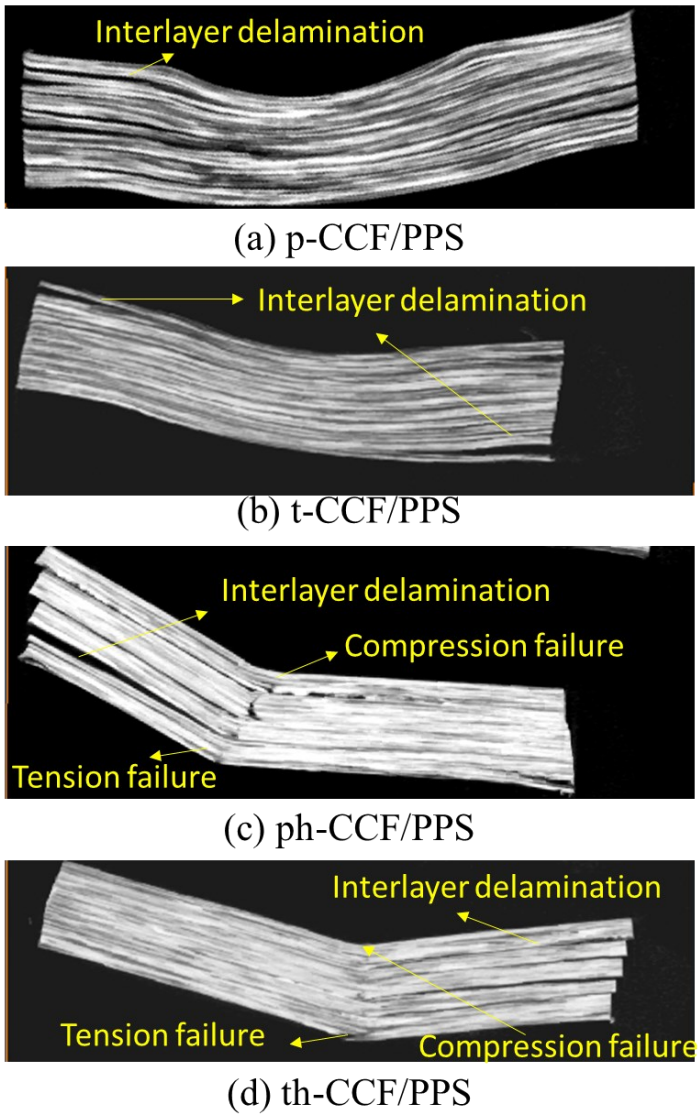

Figure 5-15 XCT imaging of (a) p-CCF/PPS; (b) t-CCF/PPS; (c) th-CCF/PPS; (d) ph-CCF/PPS.

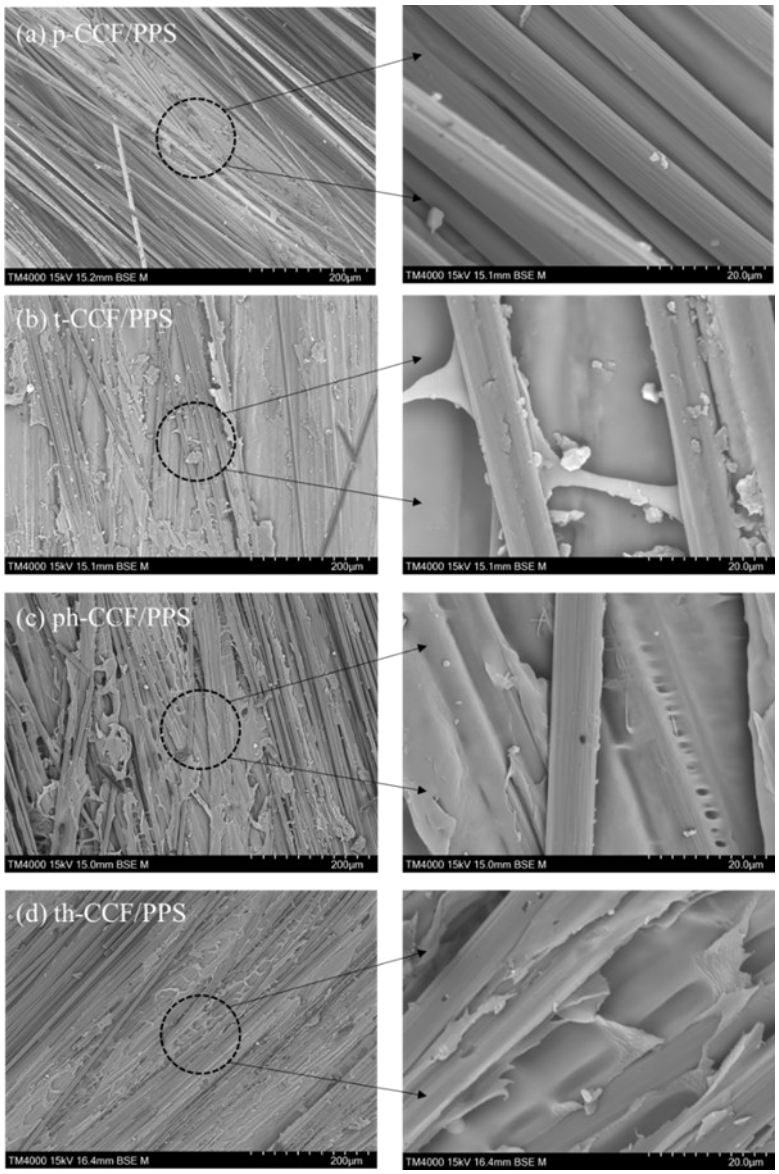

Figure 5-16. SEM images of (a) p-CCF/PPS; (b) t-CCF/PPS; (c) th-CCF/PPS; (d) ph-CCF/PPS (left: ×500; right: ×5000).

Furthermore, an increased impregnation percentage was observed to expand the area of matrix residue present during the separation process. It is noted that the application of hot-pressing treatment results in zigzag fracture patterns between carbon fibres and the PPS matrix, as depicted in Figure 5-16(d). This is indicative of a synergistic effect contributing to the enhancement of the shear yield stress within the interface layer.

5.4.3 **Post-processing of complex structures using a salt-bath**

It is known that 3D printing has the advantages for manufacturing complex structures. Therefore, it is expected that a low-cost post-processing method would benefit its application to more complex structures. Here, we propose a novel post-processing method with salt bath for 3D printed CCF/PPS composite structures with complex geometries. Figure 5-17 presents the force-displacement curves in short-beam bending curves for CCF/PPS composites subjected to different post-processing techniques. The graph compares the peak force of as-printed specimens against those that have undergone post-processing using a specifically designed metal mould and a salt bath method. The ILSS of composites post-processed with the salt bath generally falls below that of the mould-processed counterparts but remains superior to the as-printed composites. This trend holds true for both untreated and treated CCF/PPS composites. Notably, both post-processed curves start with a similar initial modulus, indicating comparable stiffness at the onset of loading. The curves reveal that while the mould-based post-processing technique leads to higher peak values, the salt bath method exhibits a more pronounced plastic deformation beyond the peak, similar to the behaviour of the as-printed specimen. This suggests that the salt bath post-processing not only retains some of the ductility seen in the as-printed composites but also enhances the interlaminar properties.

The use of a salt bath for post-processing is particularly advantageous for complex geometries. During hot pressing, the salt acts as a support, enabling the pressure distribution in all directions of intricate two-dimensional perforated patterns and three-dimensional structures. This technique ensures that even with the application of high temperatures and moderate pressures, the integrity of the complex designs is maintained. In summary, the salt bath post-processing method emerges as an effective alternative to traditional mould methods, offering a balanced improvement in interlaminar properties. It aligns with the strengths of 3D printing in

manufacturing complex structures, allowing for the retention of design intricacies while enhancing material performance.

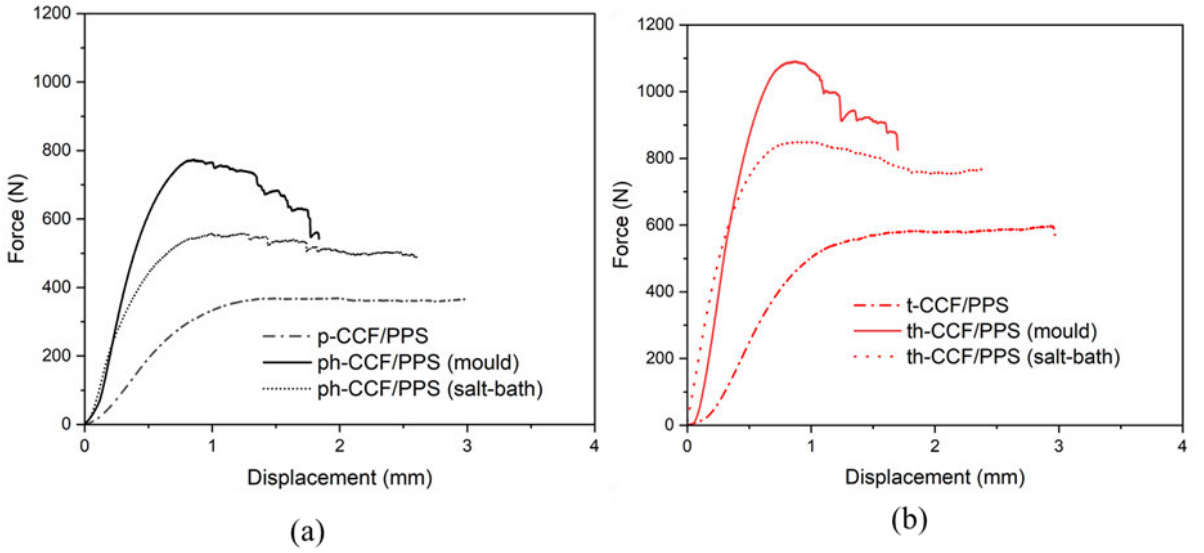

Figure 5-17 Representative force-displacement curves in short beam bending for specimens before and after mould-based hot press and salt-bath based hot press: (a) untreated composites; (b) treated composites.

We further demonstrated the effect of the salt-bath based post-processing on two demonstrative models with complex geometries, a two-dimensional lightweight perforated structure featuring an array of holes (Figure 5-18) and a three-dimensional integrated stiffener structure (Figure 5-19), respectively. The former design, depicted in Figure 5-18, is typically challenging to post-process due to the risk of distorting the delicate features. Figure 5-18(a) shows the printing trajectory of the model. The dimensions of designed model are shown in Table 5-2. The dimensions of components, as-printed part and post-processed part, were quantified using a FARO arm scanner to capture precise geometry and assess dimensional variances (refer to Table 5-2). Observations from Figure 5-18 (c) and Figure 5-18 (d) reveal that the fitting ellipse for the as-printed part measured a major axis of 119.11 mm and a minor axis of 12.88 mm, whereas post-processing dimensions registered a major axis of 119.18 mm and minor axis of

13.22 mm. These corresponding nominal deviations are less than 2%. A notable reduction in thickness by 10.36% in post-pressing samples signifies a decrease in void content within the composites, and the change in the width (labelled in Figure 5-18(b)) have a reduction by 9.35%. The salt-bath based post-processing has been validated to preserve the integrity of these perforations while reducing the defects in all directions due to flexibility of salt.

The other case, shown in Figure 5-19, is a three-dimensional stiffener structure. The complexity of this geometry, with its integrated layers and support elements, often complicates post-processing. The dimensions of components, including designed model, as-printed part and post-processed part, were presented in Table 5-3). For the as-printed part, presented in Figure 5-19(c), the top inner diameter measured 170.29 mm, and the top outer diameter stood at 190.83 mm. Correspondingly, the bottom inner diameter was 200.29 mm, and the bottom diameter measured 165.37 mm. The dimensions of post-processed samples, as shown in Figure 5-19(d), indicated a top inner diameter of 169.80 mm and a top outer diameter of 188.84 mm. Correspondingly, the diameters of bottom inner and bottom outer measured 199.37 mm and 165.38 mm, respectively. All calculated deviations of as-printed part and post-processed part based on nominal dimensions in the top and bottom sections are less than 2%, shown in Table 5-3. An expected reduction in thickness by 13.13% is in the post-processed part, which also validate the void minimisation of the composites. Notably, the top width has decreased by 7.30% due to the reduction of voids as well, which results from the pressure distributed in the in-plane direction. The findings demonstrate that the salt-bath approach effectively mitigates the structural defects in both out-of-plane and in-plane directions.

These two demonstrations illustrate that the salt-bath based post-processing technique is advantageous for complex structures that benefit from the design freedom of 3D printing. This method offers a post-processing solution that upholds the dimensional accuracy and design intricacy of printed objects while delivering an improvement in mechanical performance. In

conclusion, the post-processing techniques applied to 3D printed composites is promising in enhancing the intralaminar properties for both uncomplicated shapes, using a mould-based method and complex structures via the salt-bath technique.

Table 5-2 Designed dimensions and actual dimensions of as-printed and post-processed perforated part.

Perforated part	Designed model (mm)	As-printed part (mm)	Post-processed part (mm)	As-printed deviations (%)	Post-processed deviations (%)	Variations (%)
Major size	120.00	119.11	119.18	0.74	0.68	/
Minor size	13.00	12.88	13.22	0.92%	1.70	/
Thickness	2.00	2.22	1.99	/	/	10.36
Width	3.00	3.21	2.91	/	/	9.35

Table 5-3 Designed dimensions and actual dimensions of as-printed and post-processed stiffener part.

Stiffener part	Designed diameter (mm)	As-printed diameter (mm)	Post-processed diameter (mm)	As-printed deviations (%)	Post-processed deviations (%)	Variations (%)
Top inner	173.00	170.29	169.80	1.57	1.85	/
Top outer	191.00	190.83	188.84	0.09	1.13	/
Bottom inner	164.00	165.37	165.38	0.84	0.84	/
Bottom outer	200.00	200.29	199.37	0.15	0.31	/
Top width	18.00	20.54	19.04	/	/	7.30
Bottom width	36.00	34.92	33.99	/	/	2.67
Thickness	4.00	4.34	3.77	/	/	13.13

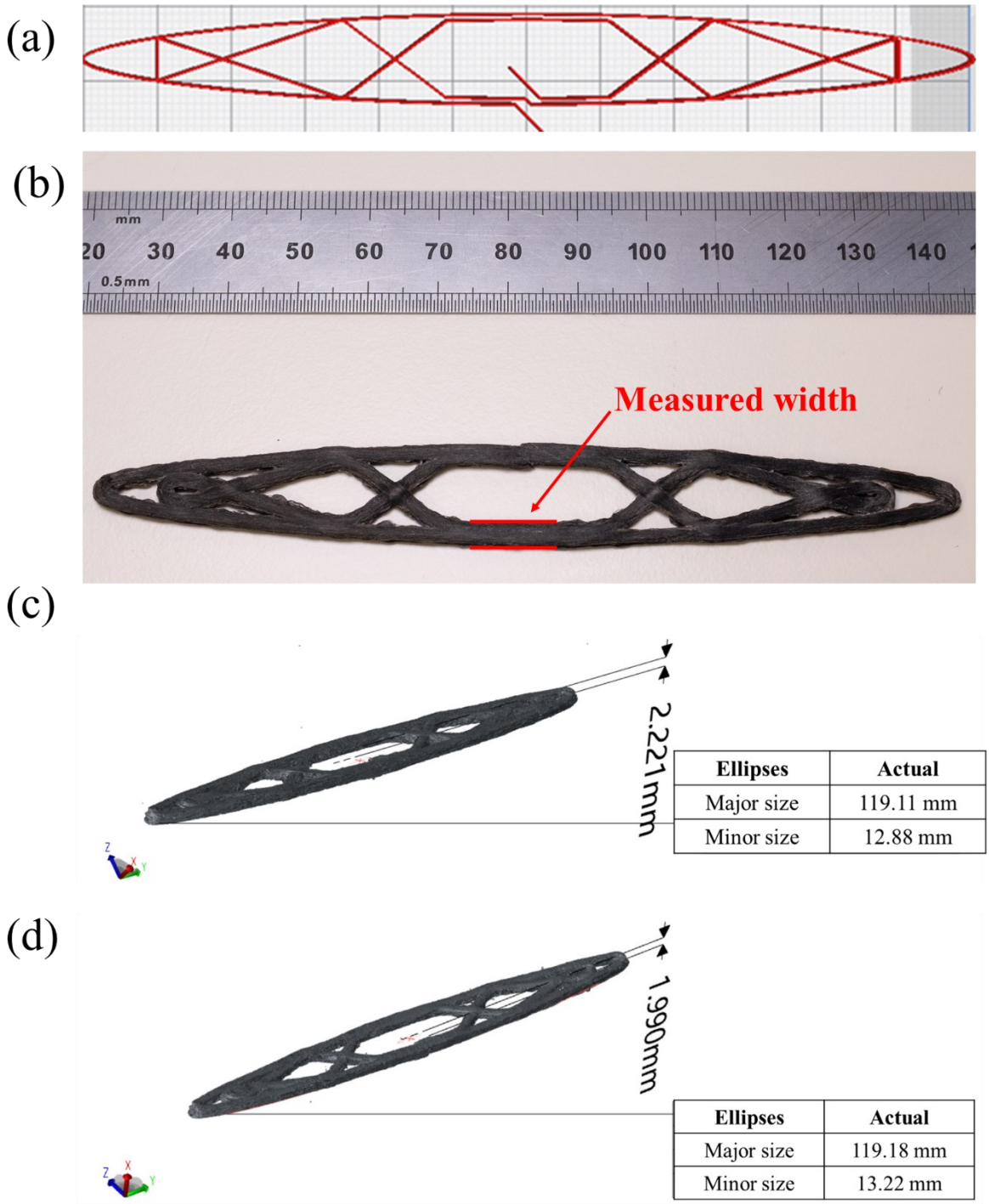

Figure 5-18 Demonstration of a perforated structures using the salt-bath method: (a) designed trajectory of continuous carbon fibre; (b) image of post-processed part; (c) scanning of as-printed part; (d) scanning of post-processed part.

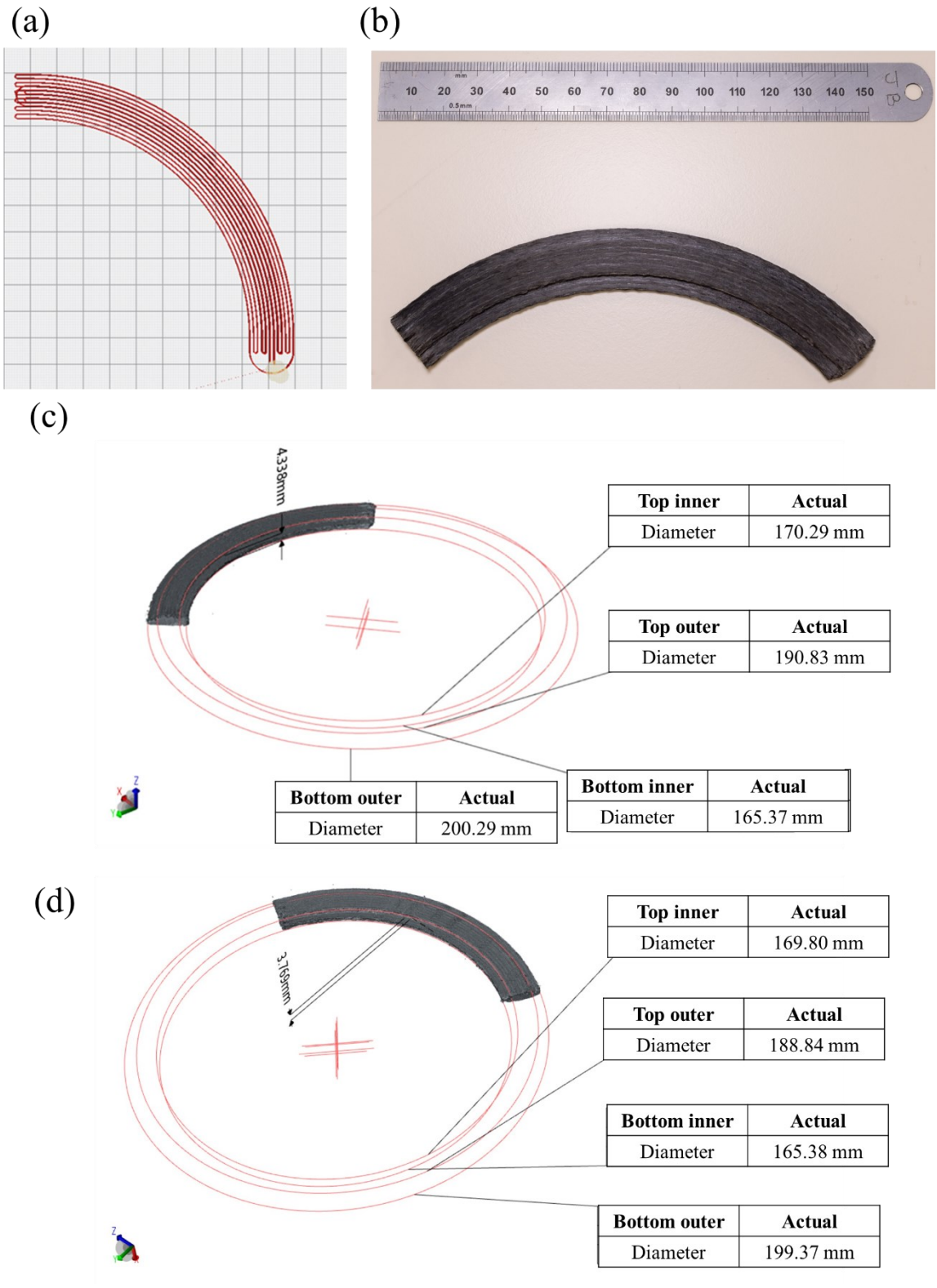

Figure 5-19 Demonstration of integrated stiffener structures: (a) designed trajectory of continuous carbon fibre; (b) post-processed part; (c) scanning of as-printed part; (d) scanning of post-processed part.

5.5 Conclusions

The study elucidates the considerable advantages of PDA/NPs treatment and post-processing techniques on the mechanical properties of CCF/PPS composites. The integration of PDA/NPs network on CCF and post-processing technique has been shown to significantly enhance the interfacial and interlayer properties. This has led to a substantial improvement of 27% in flexural strength and 172% in the interlaminar shear strength (ILSS). For the effect of PDA/NPs treatment, The MD simulations offered further insights into the enhanced adhesion mechanisms, validating the experimental observations in the nano-indentation test. For the effect of post-processing techniques, the DSC analysis and morphological observations confirmed improvements in crystallinity, void content reduction and fibre orientation, which correlated with the superior mechanical performance under shear and flexural loads. Moreover, the salt-bath based post-processing technique was proved to successfully preserve the intricate details of complex 3D printed structures while enhancing their material mechanical performance. These findings not only provide a deeper understanding of the interfacial and interlayer properties of 3D printed CCF/PPS composites but also demonstrates practical enhancements that can be readily applied in aerospace and automotive industries, where high-performance thermoplastic composite materials are advantageous.

Chapter 6 **Overprinting of continuous carbon fibre and recycled discontinuous carbon fibre composites with a stabilised surface treatment for in-situ composites repairing**

Abstract

This study proposes an efficient and convenient in-situ repair approach for thermoplastic composites, incorporating a stable surface treatment. Initially, the mechanical performance of reclaimed carbon fibre from commercial thermosetting composites and reshaped carbon fibre from printed thermoplastic composites was examined. This examination was crucial to assess the thermal stability of the carbon fibre's surface treatment in processing next-generation carbon fibre/polyphenylene sulphide (CF/PPS) composites. Subsequently, the study employed reshaped short carbon fibre reinforced PPS filament (rCF/PPS) alongside continuous carbon fibre reinforced PPS (CCF/PPS) filament to print repair patches on open-hole woven carbon fibre reinforced polyamide (PA6) laminates. The effect of varying interface temperatures throughout the printing process on in-situ bonding quality was evaluated through tensile tests accompanied by Digital Image Correlation (DIC), establishing a process window for optimal interface bonding temperature. The findings indicate that the load-bearing capacity of the open-hole laminates improved by 35.4% when repaired at the optimal interfacial temperature. This study lays the groundwork for a sustainable in-situ remanufacturing system.

Keywords:

Thermoplastic composites; Recycled carbon fibre; 3D overprinting; Composites repair

6.1 Introduction

Carbon fibre reinforced thermoplastic polymer (CFRTP) composites have become increasingly popular, as evidenced by their growing use in industries such as automotive and aerospace [29,200,201]. CFRTP composites typically offer enhanced impact resistance and increased toughness, compared to their thermoset counterparts [202,203]. Additionally, they present advantages like short processing times, potential for recycling and repair, and sustainability due to their ability to be melted, remelted, and reformed [203]. During the service life of CFRTP materials, various forms of damage failures, such as holes and impacts, can occur. These defects can significantly affect the mechanical integrity of composite structures [204]. Therefore, to fully make use of CFRTP in load-bearing structures and reduce replacement cost, developing a systematic methodology for composite repair is crucial.

Although repair methodologies for thermoset matrix composites exist, the methodologies for CFRTP repair remain less clearly defined [117]. Traditional methods such as mechanical fastening and adhesive bonding have been proposed for CFRTP repair. However, mechanical fastening requires a drilling process and can introduce the stress concentration points with the structures, although it is simple to operate [115]. Adhesive bonding, while offering uniform load transfer, poses challenges due to the complex surface treatment required in the thermoplastic repair process [116]. In addition, three most promising fusion bonding techniques (induction, resistance, and ultrasonic welding) have been studied in the previous literature for joining thermoplastic matrix composites [1,118,119]. These methods offer many advantages, including rapid process time and robust repair quality. The principle of this technique is particularly favourable for the repair of thermoplastic composites, facilitating the joining of a repair patch to a prepared structure. The main challenges associated with this

technique involve the accurate control of interface temperature and high consolidation pressures [117].

Additive manufacturing (AM), widely known as 3D printing, holds significant promise for the processing of polymers, particles, and their composites or hybrid materials [175]. This technology offers the advantages of a high degree of customisation, independence from multiple machining tools, and savings in both cost and materials [177,205,206]. Recently, material-extrusion based AM technology has been explored as an innovative solution for hybrid composites repair, involving the separate manufacturing of carbon fibre patches via a 3D printer, followed by adhesive bonding in thermoset or thermoplastic composites repair [24–26].

A more efficient and convenient approach, the 3D overprinting technique, has been applied in previous literature for in-situ bonding of 3D-printed commodity and engineering thermoplastics onto existing laminates [109–111]. While previous research on 3D overprinting of high-temperature polymers is limited, pioneering studies have extended this technique to PEI polymer [112,113] and short carbon fibre reinforced PEEK polymer [114]. This technique shows great potential for in-situ repairs by heating the surface when the extruding nozzle is in close contact with the damaged surface. To utilise this sustainable technique in CFRTP repair, further exploration of in-situ printing of repair patches to CFRTP structures is needed.

In addition, Digital Image Correlation (DIC) has been employed by some scholars to monitor damage modes online during tests on open-hole and repaired composites [26,207,208]. DIC is a non-contact and full-field method that relies on pattern recognition applied to a surface. The surface is randomly sprayed with paint and then observed using a digital camera. The fundamental principle involves correlating sub-images in photographs of the specimens before and after loading, to correlate the two-dimensional (2D) or three-dimensional (3D) surface

displacement vectors. This technique offers a versatile and reliable means of measuring the strain fields on a tested specimen [207], thus enabling the performance assessment of the repaired composites under loading.

This study firstly investigates the mechanical performance of sustainable composites reinforced with recycled commercial thermosetting composites and reshaped composites from previously developed continuous carbon fibre reinforced polyphenylene sulphide (CCF/PPS) filament. The aim is to validate the thermal stability of the hybrid network treated with polydopamine/silica nanoparticles (PDA/NPs) in the recycling process and optimise material performance for repair patches. Subsequently, the study examines the impact of interface temperature on in-situ repair quality. Mechanical properties of open-hole laminate and repaired laminates were tested under tensile loading, and strain fields were monitored using DIC technology. The damage development process under various repair temperatures was analysed and discussed.

6.2 Experimental setup

6.2.1 Materials

Recycled carbon fibre (non-woven mat) and continuous carbon fibre tow (3K) were purchased from Easy composites Ltd, Stoke on Trent, UK. Tetraethoxysilane (TEOS), Dopamine hydrochloride (DP) and Tris (hydroxymethyl)-aminomethane (Tris) were purchased from Merck Life Sciences Ltd, UK. Polyphenylene sulphide (PPS, Torelina A900) was manufactured by Toray Industries, Japan. Acetone, utilised in the desizing process, was obtained from Fisher Scientific Ltd, Leicestershire, UK. All chemicals were employed in their received condition, unless specified otherwise.

6.2.2 3D printing of CF/PPS with reclaimed carbon fibres from thermosetting composites

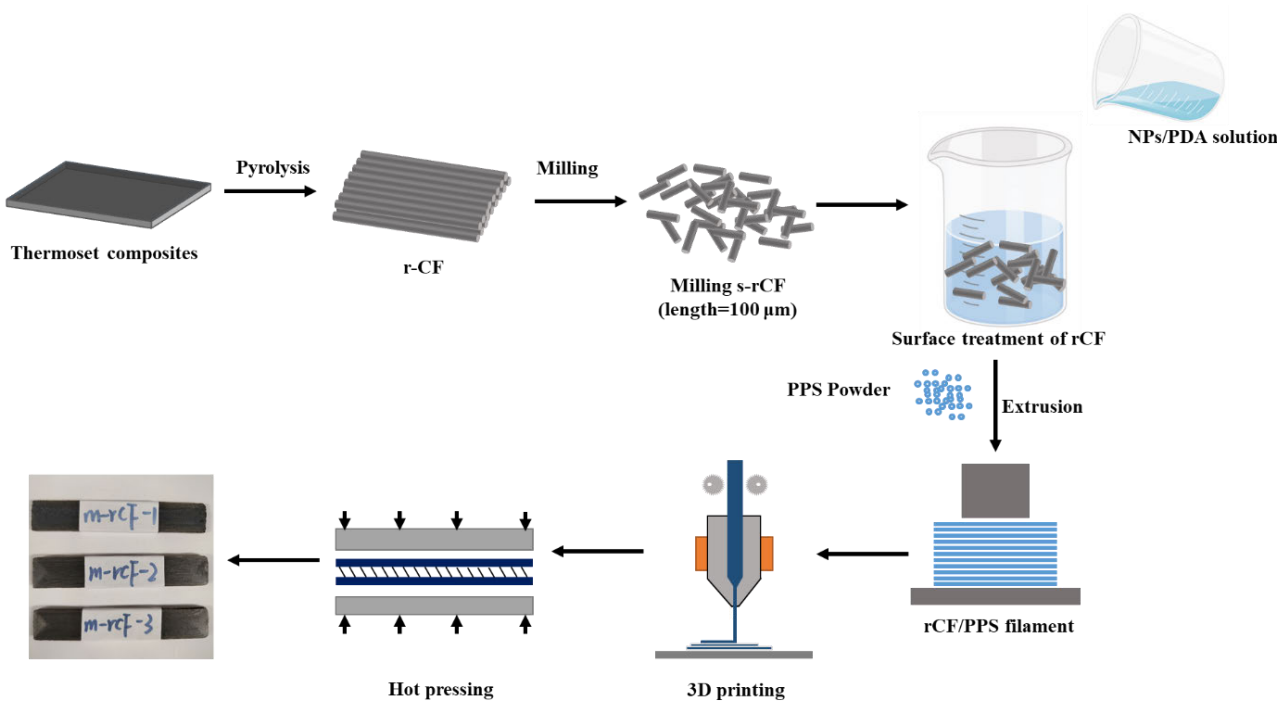

Figure 6-1 Reclaimed and reused process of carbon fibre from commercial thermosetting composites.

Figure 6-1 illustrates the process of reclaiming milled carbon fibre from commercial thermosetting composites. Colloidal silica nanoparticles (NPs) were synthesised using tetraethoxysilane (TEOS) and then dispersed in a buffer solution (0.1% Tris solution, pH=8.5). Recycled woven carbon fibre mats were first milled using a grinder. The carbon fibre and dopamine hydrochloride were simultaneously introduced into the buffer solution at room temperature, employing an ultrasound instrument to reclaim the recycled carbon fibre from the commercial thermoset composites. Subsequently, PPS powder was compounded with the milled carbon fibre using a mixer, producing short recycled carbon fibre (length is around 100 μm) reinforced PPS composites (s-rCF/PPS) and modified carbon fibre-reinforced PPS composites (m-rCF/PPS) respectively. The mixture was then fed into a lab-scale single screw

extruder (Noztek Pro HT) to produce CF/PPS filaments (1.6 ± 0.1 mm in diameter). This filament was subsequently used in a material extrusion-based Creatbot F430 printer (420°C version, Henan, China). The nozzle temperature was set at 320 °C, and the build platform temperature at 90°C. The nozzle diameter was 0.8 mm, and the printing speed was 20 mm/s. The printing direction was aligned with the longitudinal direction of the filament. All specimens were printed with a 100% infill degree. Furthermore, all 3D-printed specimens underwent hot pressing to reduce void content, using a Pinette PEI Lab 450 press machine.

6.2.3 3D printing of CF/PPS with reshaped carbon fibres from thermoplastic composites

Figure 6-2 illustrates the process of reshaping carbon fibre from printed thermoplastic composites. A powder-based tapeline, developed in a previous study [28], was utilised to produce 3K continuous carbon fibre filaments for 3D printing. The continuous carbon fibre tow was tensioned by a wind-up spooler. PPS powder was applied onto the carbon fibre surface and subsequently melted in a nozzle at a high temperature to form a resin bath. The continuous carbon fibre was impregnated with PPS resin as it was drawn through the bath, producing pristine continuous carbon fibre reinforced PPS composites (p-CCF/PPS). The nozzle temperature for this in-nozzle process was maintained at 320 °C.

In the modification process, 3K dry continuous carbon fibre was initially treated with a modification solution containing polydopamine and silica nanoparticles (refer to Figure 5-1(a)). Following immersion, rinsing, and drying, the carbon fibre was coated with PPS powder using tapeline equipment to create the modified continuous carbon fibre reinforced PPS composites (t-CCF/PPS) (refer to Figure 5-1(b)).

Both types of continuous filaments thus produced were then printed using a high-temperature printer to fabricate unidirectional laminate. A fibre placement nozzle (1.3 mm diameter) from

Markforged Ltd, UK, was installed in the 3D printer for printing the continuous filament. In the recycling process, printed specimens were crushed and ground into small pristine composite pieces (p-rCF/PPS) and modified composite pieces (t-rCF/PPS). These recycled pellets were mixed with PPS powder and extruded again to fabricate CF/PPS filament, which was then fed into a printer to create the next generation of composites. To reduce void content during the printing process, a hot press was also applied to the printed specimens before mechanical testing.

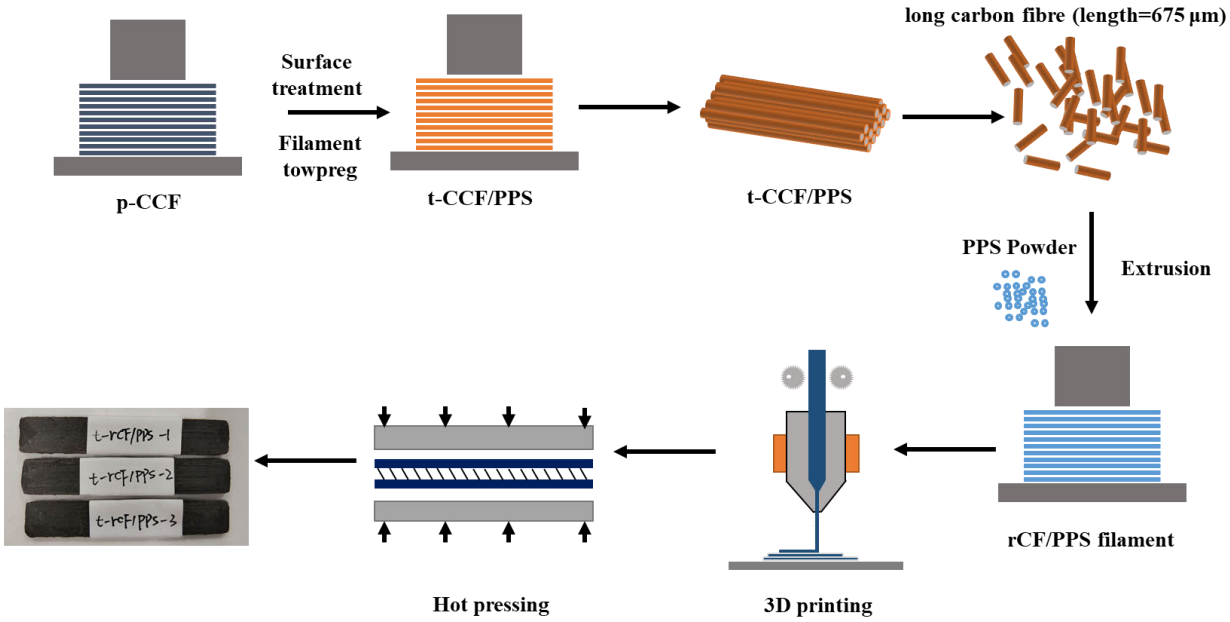

Figure 6-2 Reshaped and reused process of carbon fibre from printed thermoplastic composites.

6.2.4 **Three-point bending test of 3D printed recycled composites**

Three-point bending tests on the printed parts were conducted in accordance with the methodology in Section 3.2.3.

6.2.5 **Dynamic mechanical analysis of 3D printed recycled composites**

Dynamic Mechanical Analysis (DMA) was employed to characterise the viscoelastic properties of 3D printed recycled composites, as detailed in Section 3.2.5.

6.2.6 **Thermal characterisation of polymers**

Differential Scanning Calorimetry (DSC, PerkinElmer 8000) was utilised to characterise the melting behaviour of the PA6 polymer and the crystallisation behaviour of the PPS polymer. The PA6 samples were heated from 30 °C to 250 °C at a ramp rate of 20 °C/min, followed by cooling back down to 30 °C at the same rate. The heat flows from the second heating cycle were recorded and analysed to determine the melting temperature. Similar thermal cycles were performed for the PPS samples, heating from 30 °C to 300 °C and then cooling down to 30 °C again to negate the effects of thermal history. Other details can be found in Section 3.2.4.

6.2.7 **In-situ composites repair and uniaxial tensile test**

Woven carbon fibre reinforced PA6 laminates were mechanically cut into specimens measuring 200 mm × 36 mm × 1.8 mm. To simulate damage cut-outs in composite structures, a hole with a diameter of 14 mm was drilled at the centre of each laminate specimen, in accordance with the ASTM D5766 standard. This process resulted in open-hole laminate specimens. The repair method involved a double-bonded hybrid approach with an external patch. The hybrid patch, comprised of composites reinforced with recycled short carbon fibre and continuous carbon fibre, was adhered on-site to the damaged open-hole specimens using overprinting techniques, as depicted in Figure 6-3. The initial step involves additively manufacturing the continuous carbon fibre reinforced PPS filament onto the damaged surface of the thermoplastic laminates (Figure 6-3(a)). Subsequently, the laminate is positioned with the opposing side facing the printing bed (Figure 6-3(b)). The next step involves filling the hole in the laminate with reshaped composites reinforced with discontinuously treated carbon fibre,

chosen for their comparative mechanical strength and cost-effectiveness (Figure 6-3(c)). The final step is to bond another continuous carbon fibre reinforced PPS patch to the opposite side of the damaged area (Figure 6-3(d)).

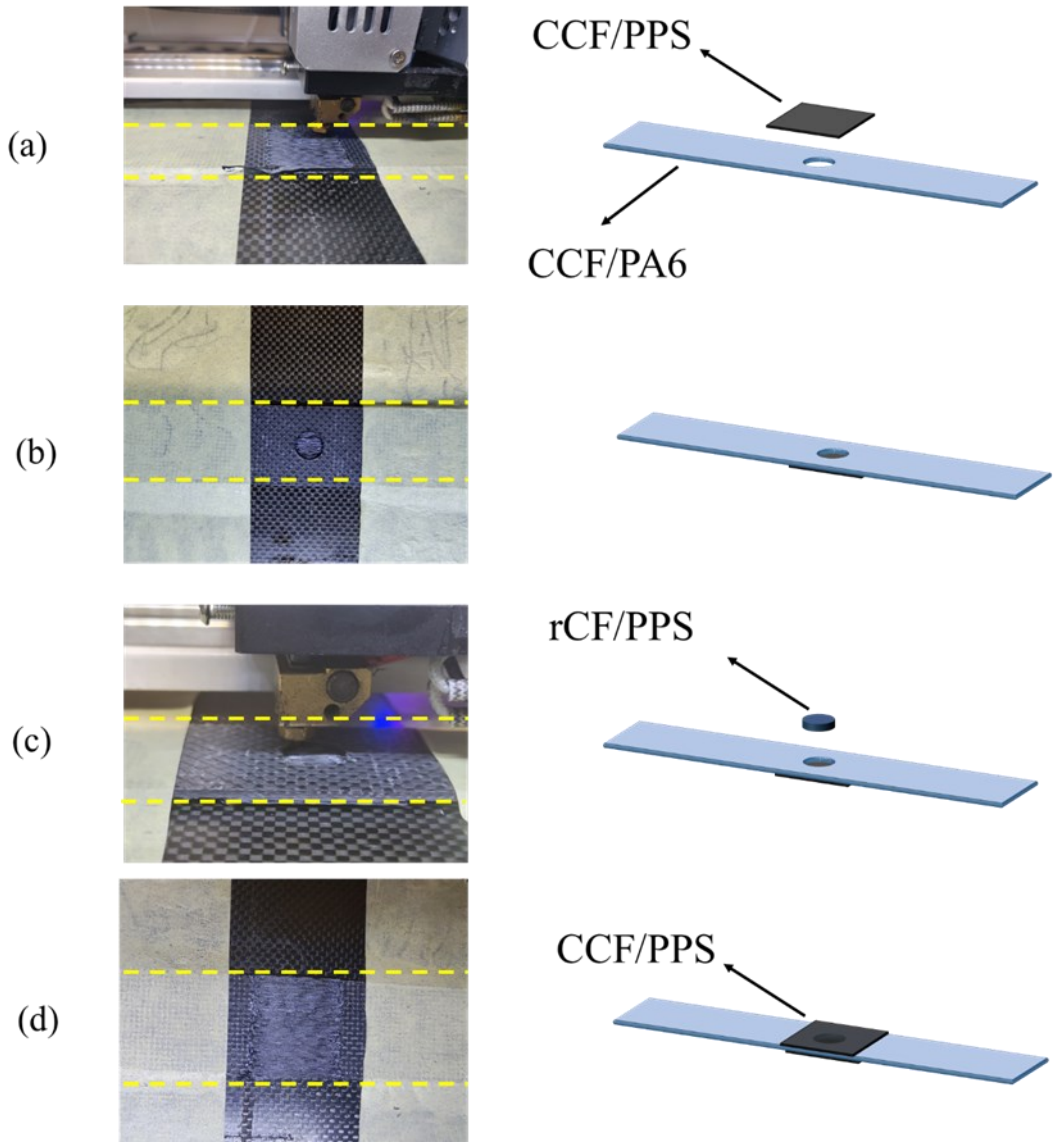

Figure 6-3 In-situ repair procedure of hybrid patch by 3D printer: (a) Overprinting the CCF/PPS unidirectional composites on damaged CCF/PA6 laminate; (b) Positioning the opposite side of CCF/PA6 laminates; (c) Filling the recycled rCF/PPS composites in the damaged hole; (d) Overprinting another CCF/PPS patch on the opposite side.

Mechanical testing of the damaged and repaired specimens was carried out based on ASTM D3026 and ASTM D5766 standards. The tests were conducted at a constant tensile loading velocity of 2 mm/min. Additionally, a full-field measurement technique DIC was employed to monitor the damage process and the strain field. A white pattern was painted on the specimen surface, and two charged-coupled device (CCD) cameras were used for the measurements.

6.2.8 **Microstructure characterisation and morphology analysis**

The microstructure characterisation of printed composites was observed and calculated by the methodology described in Section 3.3.4.

6.3 Results and discussion

6.3.1 **Mechanical performance of 3D printed rCF/PPS composites**

Figure 6-4 illustrates the force-displacement curves of s-rCF/PPS (recycled carbon fibre from thermosetting composites) and m-rCF/PPS (modified recycled carbon fibre from thermosetting composites) in 3PB bending. As depicted in Figure 6-4(a) and 6-4(b), the flexural strength of the composites (167.9 MPa) featuring treated CF, after grafting with the PDA/NPs network, shows a 26.4% increase compared to composites with untreated CF (132.8 MPa). Furthermore, Figure 6-4(c) indicates that the diameter of the extruded filament is 1.72 mm. The average fibre volume fraction was determined to be 14.5%, and the average void content was calculated to be less than 5%, based on the analysis of 5 samples using ImageJ software. Post-pyrolysis of the printed composites, the average fibre length was found to be approximately 100 μm (see Figure 6-4(d)).

Figure 6-5 presents the force-displacement curves of p-rCF/PPS (reshaped carbon fibre from thermoplastic composites) and t-rCF/PPS (modified reshaped carbon fibre from thermoplastic composites) in 3PB bending. As illustrated in Figure 6-5(a) and 6-5(b), following the grafting

of the PDA/NPs network onto the carbon fibre surface, the flexural strength of composites (252.9 MPa) with treated CF increased by 22.4% compared to that of composites with untreated CF (206.7 MPa). Furthermore, Figure 6-5(c) shows that the diameter of the extruded filament is 1.69 mm. The fibre volume fraction is measured to be 11.9%, and the void content is less than 5% calculated using ImageJ software. Five samples were analysed to minimise the uncertainty. Post-pyrolysis of the printed composites revealed an average fibre length of approximately 675 μm (refer to Figure 6-5(d)).

The results indicate that the PDA/NPs network consistently enhances the interfacial adhesion on recycled carbon fibre from both thermosetting and thermoplastic composites, leading to improvements in the flexural strength of the treated composites. By enhancing the intralaminar properties of the composites, the composites exhibit an increased capacity to resist mechanical loads. The findings suggest the PDA/NPs network demonstrates good thermal ability in the processing of composites during mechanical recycling process and through various thermal cycles including extrusion and 3D printing. This highlights the sustainability of the surface treatment methodology in modifying thermoplastic composites.

Compared to milled carbon fibre recycled from thermosetting composites, the reshaped carbon fibre demonstrates a relatively longer length in the composites, contributing to higher flexural strength and modulus. The composite with treated CF from reshaped printed CCF/PPS achieved the best mechanical performance, showing promise for the sustainable printing of recycled composites on damaged thermoplastic laminates for in-situ repair techniques.

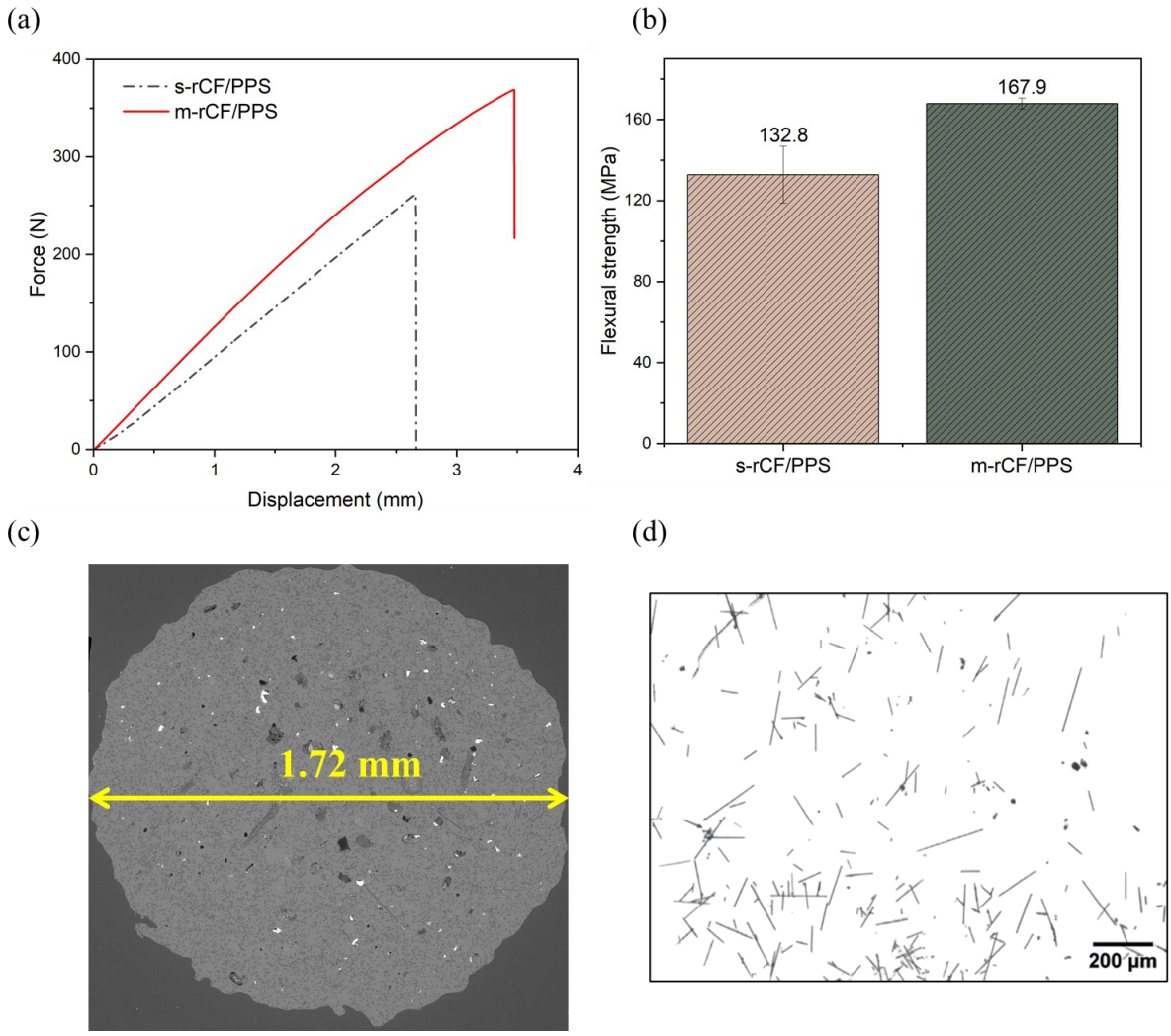

Figure 6-4 (a) Representative force-displacement- curves; (b) flexural strengths of s-rCF/PPS with recycled carbon fibre from thermosetting composites and m-rCF/PPS with modified recycled carbon fibre from thermosetting composites; (c) SEM image of cross-section of extruded filament (diameter is 1.72 mm); (d) optical microscopy of recycled carbon fibre after pyrolysis experiment.

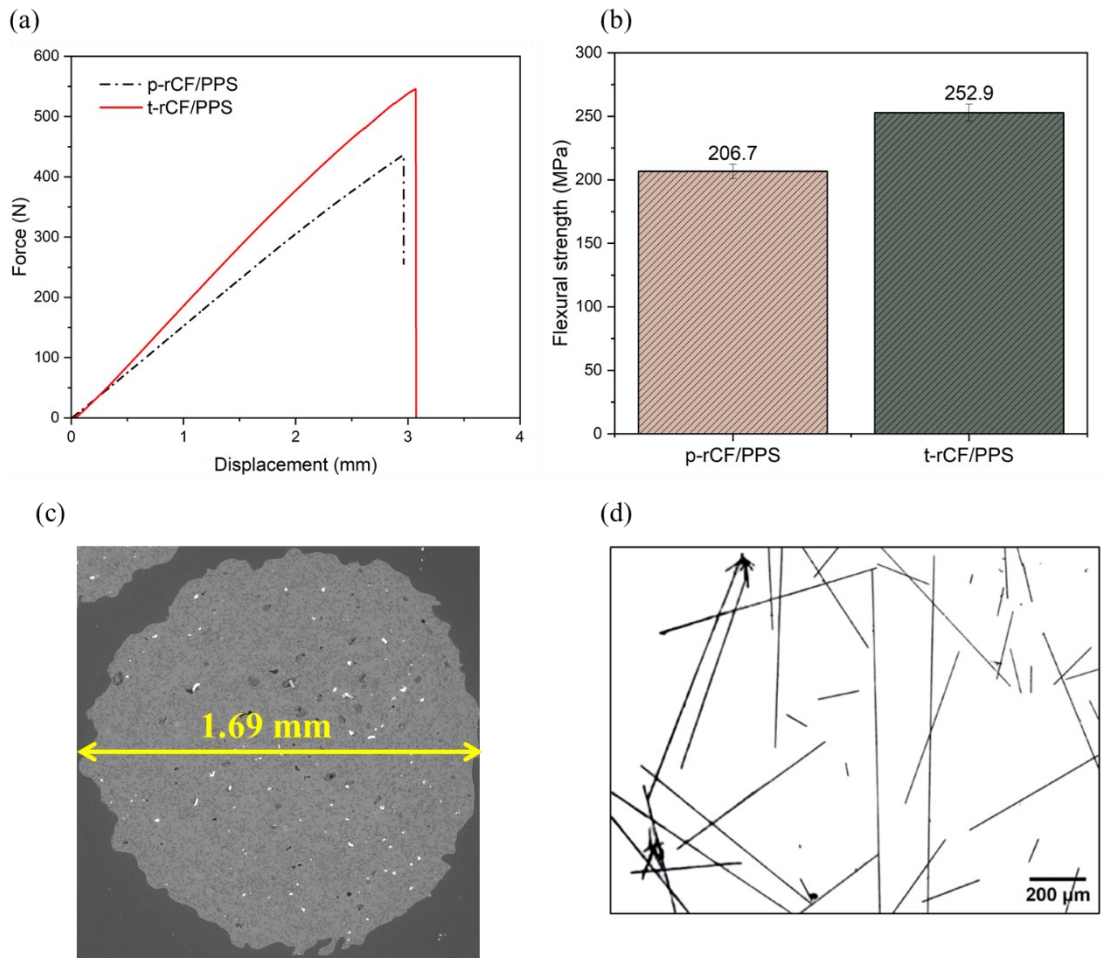

Figure 6-5 (a) Representative force-displacement curves and (b) flexural strengths of p-rCF/PPS with reshaped carbon fibre from thermoplastic composites and t-rCF/PPS with modified reshaped carbon fibre from thermoplastic composites; (c) SEM image of cross-section of extruded filament (diameter is 1.69 mm); (d) optical microscopy of recycled carbon fibre after pyrolysis experiment.

6.3.2 **Process window on the in-situ repair performance**

To identify the process window for in-situ repair, Figure 6-6 provides an enhanced characterisation of the thermal properties of PA6 and PPS polymers using a DSC machine. The analysis reveals that the crystallisation temperature of PPS polymers is established at 227.6 °C during the cooling cycle, while the melting temperature of PA6 polymers is recorded at 216.8 °C. These findings suggest an optimised interface temperature range for the printing process,

spanning from the melting temperature of PA6 polymers to the crystallisation temperature of PPS polymers, which is 216.8 °C to 227.6 °C. If the interface temperature is lower than the melting temperature of the substrate, the substrate polymer fails to melt due to inadequate thermal energy, leading to poor bonding quality. Conversely, if the interface temperature exceeds the crystallisation temperature of the repair polymer, the deposition polymer is unable to form crystals as it moves along the nozzle, leading to compromised printing quality.

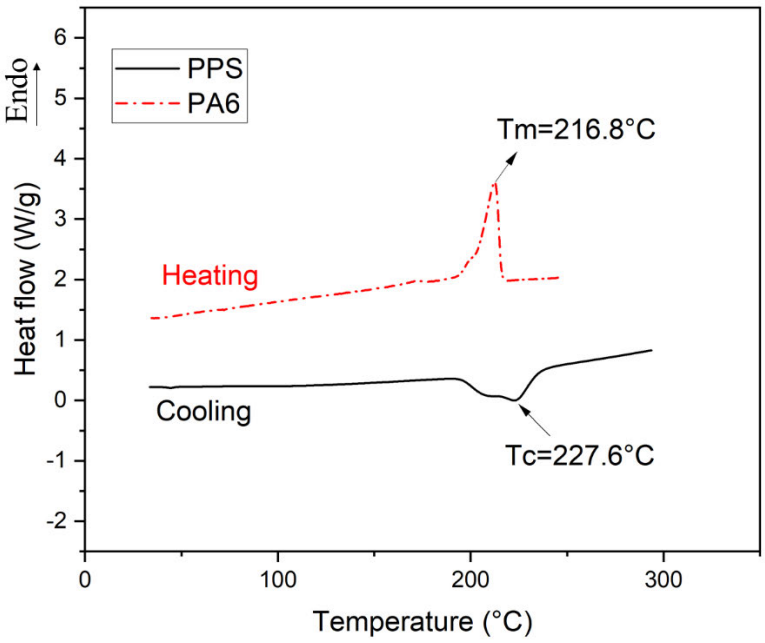

Figure 6-6 DSC heating curves of PA6 polymer and cooling curves of PPS polymer.

It is well established that interface temperature significantly influences the quality of in-situ bonding, thereby impacting the overall in-situ repair performance. In this study, the substrate layer was pre-heated to temperatures of 80 °C, 120 °C, and 140 °C, and these temperatures were maintained consistently. To ensure the attainment of these target temperatures, a thermocouple was positioned on the surface throughout the printing process. The nozzle temperature was set at 320 °C. The interface temperatures were set to be 200 °C, 220 °C, and 230 °C across the identified process window, representing the average values of the nozzle and

bed temperatures. Figure 6-7 presents typical load-crosshead curves of an open-hole sample and samples repaired under different interface temperatures. Figure 6-8 displays the calculated ultimate tensile strength along with images of the repaired patches.

As observed from Figure 6-7, the curve of the open-hole samples serves as the baseline performance for a simulated damaged structure. This curve exhibits elastic behaviour until a sudden drop in force occurs, indicative of brittle failure. The in-situ repaired sample at an interface temperature of 200 °C also displays an initial linear increase, similar to the open-hole sample. However, it withstands a higher peak force compared to the open-hole sample. As the temperature rises to 220 °C, the curve initially mirrors that at 200 °C, but then the force continues to rise, reaching the highest force among all the samples. The drop in force post-peak is sharp but demonstrates a fluctuation stage before complete failure. At 230 °C, the repair performance initially resembles that at 220 °C, but the peak force occurs slightly earlier and at a lower value than the sample repaired at 220 °C. The behaviour after reaching peak force shows less resistance before complete detachment.

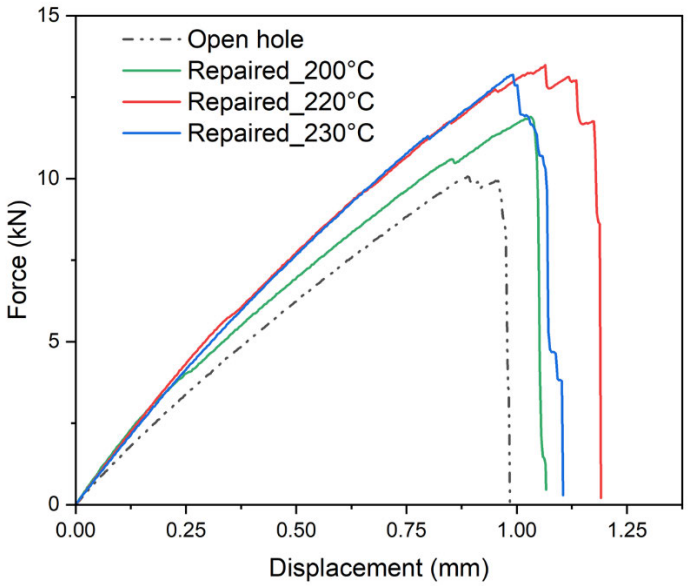

Figure 6-7 Representative force-displacement curves of open-hole sample, repaired samples under interface temperatures of 200 °C, 220°C and 230 °C, respectively.

Figure 6-8 presents the corresponding ultimate tensile strength values for each sample. The open-hole sample exhibits the lowest tensile strength at 153.7 MPa, while the repairs conducted at 200 °C, 220 °C, and 230 °C demonstrate increased tensile strength values of 187.8 MPa, 208.1 MPa, and 203.4 MPa, respectively. The most significant enhancement in tensile strength, a 35.4% improvement in mechanical performance, is observed in the sample repaired at 220 °C. This temperature achieves the optimal repair quality, consistent with the findings from the previous graph. The images offer a visual comparison of the repair patch throughout the repair process at different temperatures. The fibre alignment and matrix distribution appear uniform on the surfaces repaired at 200 °C and 220 °C. However, the samples repaired at 230 °C display poorer fibre alignment, particularly noticeable at the end of each print path when printing filament turns back with a very small curvature radius.

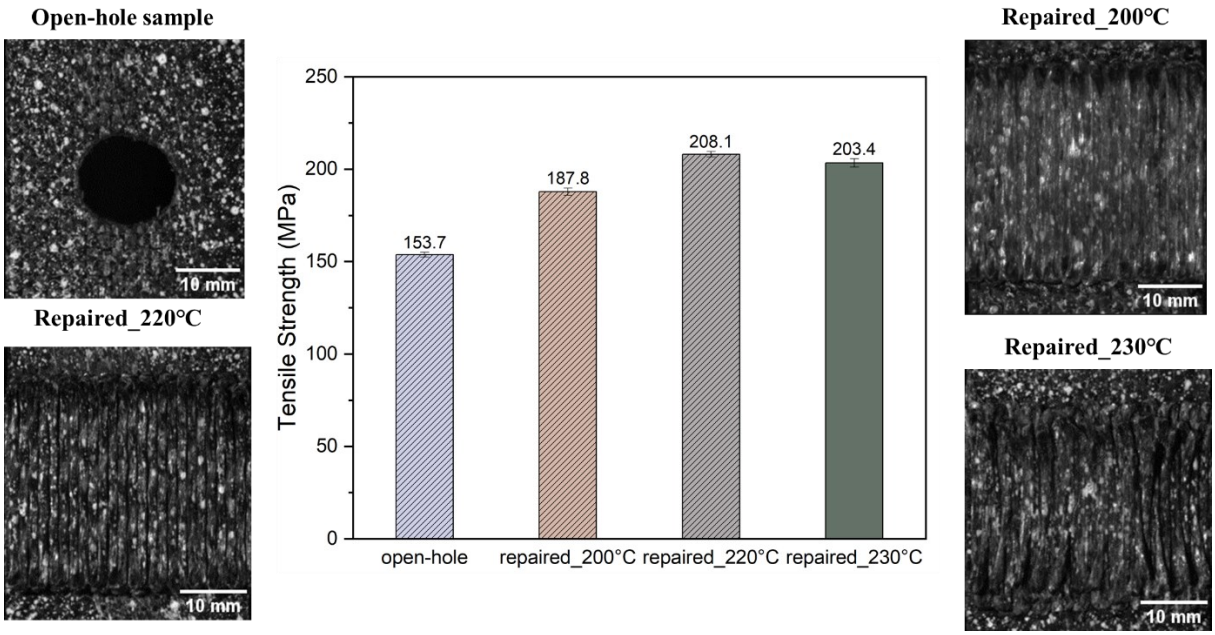

Figure 6-8 Ultimate tensile strength of open-hole sample, repaired samples under interface temperatures of 200 ℃, 220℃ and 230 ℃, respectively and visual images of repaired patch.

The results demonstrate that in-situ bonding of CCF/PPS and rCF/PPS materials to the damaged woven CF/PA6 laminates significantly enhances the performance of composites to

withstand force, indicating that the in-situ repair process is effective in restoring the mechanical integrity of the laminate. The increase in interface temperature from 200 °C to 220 °C leads to a more robust repair, attributable to improved bonding of the repair material at higher temperatures, exceeding the melting temperature of the PA6 polymers. Conversely, the weakened performance observed in repairs conducted at 230 °C, relative to those at 220 °C, may be attributed to delayed crystallisation of CCF/PPS composites. When the interface temperature exceeds the crystallisation temperature of the composites, delayed crystallisation occurs during the printing process, particularly at turning points, leading to poorer attachment of continuous carbon fibre. The poorer fibre alignment is the primary cause for the lower tensile strength. When repaired at 230 °C, this delay potentially compromises the structural integrity of the repair, lowering the tensile strength compared to those repaired at 220 °C. This observation indicates the critical role of optimising temperature parameters to balance melting and crystallisation dynamics to ensure robust and durable repairs.

We have conducted tests on un-notched samples as well, revealing a tensile strength of 424.0 MPa. Samples repaired at the optimal interface temperature demonstrated the capacity to restore approximately 50% of the strength observed in notched samples. Moving forward, our research will focus on further optimising various parameters that significantly affect the adhesion quality of the patch. This will be aimed at enhancing the recovery rate of un-notched samples, thereby improving the overall effectiveness and durability of the repairs.

The progressive failure process of open-hole laminate and repaired structures was monitored using DIC technology. Figure 6-9 illustrates the strain contour during the tensile failure process of the open-hole laminate. As the tensile load increases, strain concentration is observed around the edge of the hole, forming a symmetrical pattern. This pattern is typical for isotropic materials under tension, exhibiting a uniform response. The maximum strain values extend along the vertical axis over time until the failure point of the woven CF/PA6 laminate is

reached. Compared to the open-hole samples, Figure 6-10 depicts the failure process of a sample repaired at an interface temperature of 200 °C. The contour map indicates that the in-situ repair process alters the mechanical response to tensile loading, particularly near the repair patch. A notable strain concentration is observed at the top edge of the repaired area, with less symmetrical strain distribution at the edge of the repair site, suggesting non-uniform bonding quality at this temperature. Figure 6-11 presents the strain contour maps for a sample repaired at an interface temperature of 220 °C under different loading times. In contrast to 200 °C, the strain appears more uniformly distributed in the upper and lower areas of the repair patch. Additionally, the overall strain intensity at 26 seconds is lower than in the samples at 200 °C, indicating that the repair is effectively withstanding the applied load. The strain contours suggest a more effective repair. Figure 6-12 provides further contour maps for a sample repaired at an interface temperature of 230 °C under different loading times. Here, the strain is concentrated on the top edge of the repair patch, similar to the less uniform pattern observed at 200 °C. The contour lines are more intense at both 16 and 26 seconds compared to 220 °C, indicating the compromised performance of the repaired composites at this higher temperature, possibly due to poorer attachment of the continuous CCF/PPS filament at the surface. Moreover, the 220 °C interface temperature proves most effective for the woven CF reinforced PA6 laminate, with a delay in failure initiation compared to both the open-hole sample and other repaired temperatures. Detailed analysis of the strain contours for repairs at various temperatures (200 °C, 220 °C, and 230 °C) suggests that the optimal interface temperature for these specific in-situ repair conditions is 220°C.

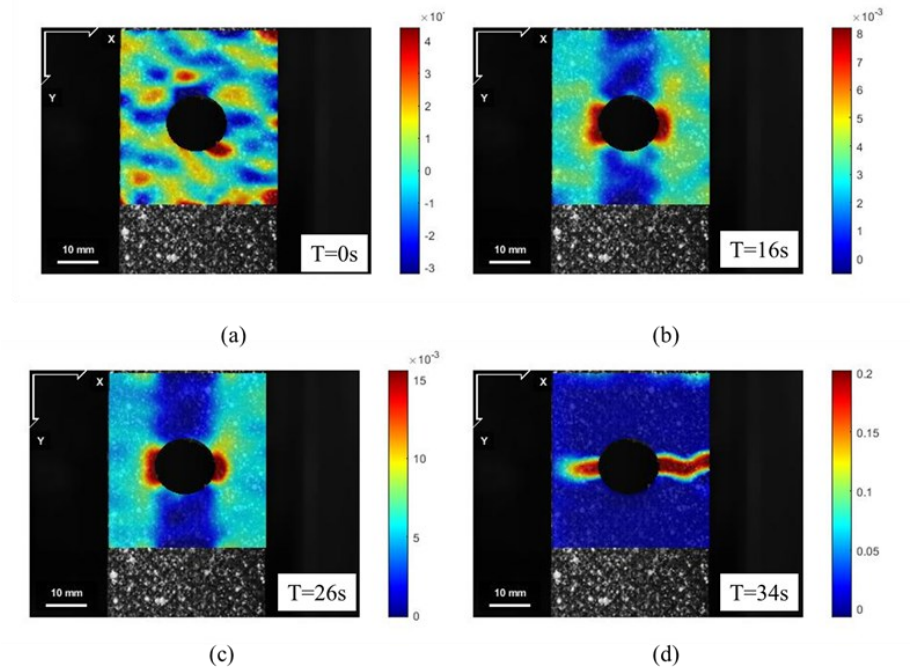

Figure 6-9 Progressive failure process and DIC strain contour (Eyy) of open-hole sample: (a) initial point: T=0s; (b) T=16s; (c) T=26s; (d) failure point: T=34s.

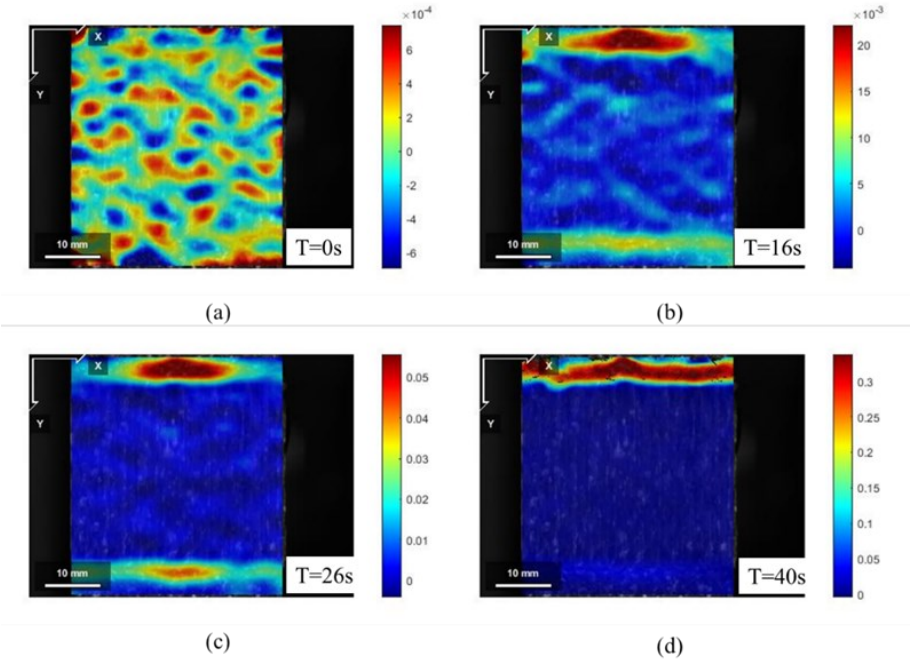

Figure 6-10 Progressive failure process and DIC strain contour (Eyy) of sample repaired at interface temperatures of 200 ℃: (a) initial point: T=0s; (b) T=16s; (c) T=26s; (d) failure point: T=40s.

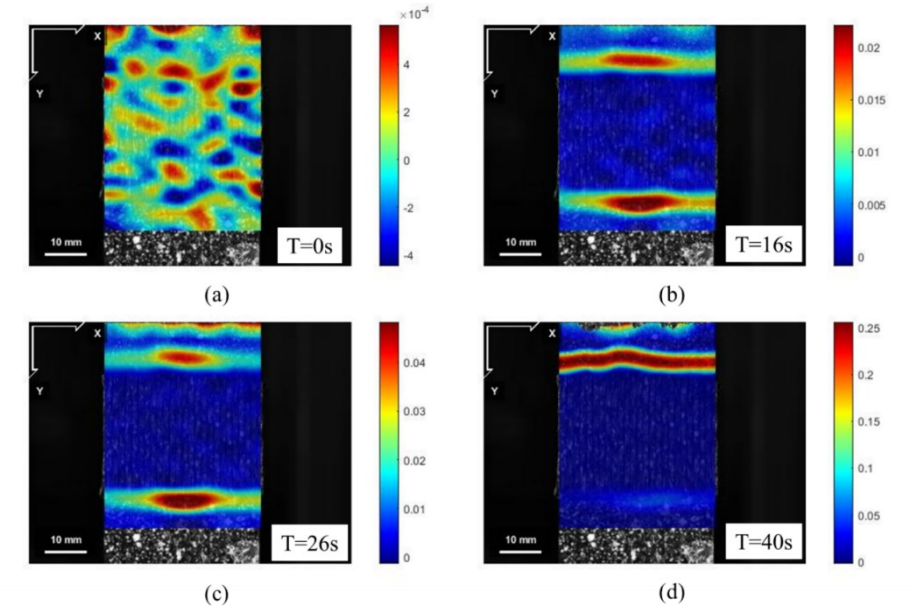

Figure 6-11 Progressive failure process and DIC strain contour (Eyy) of sample repaired at interface temperatures of 220 ℃: (a) initial point: T=0s; (b) T=16s; (c) T=26s; (d) failure point: T=40s.

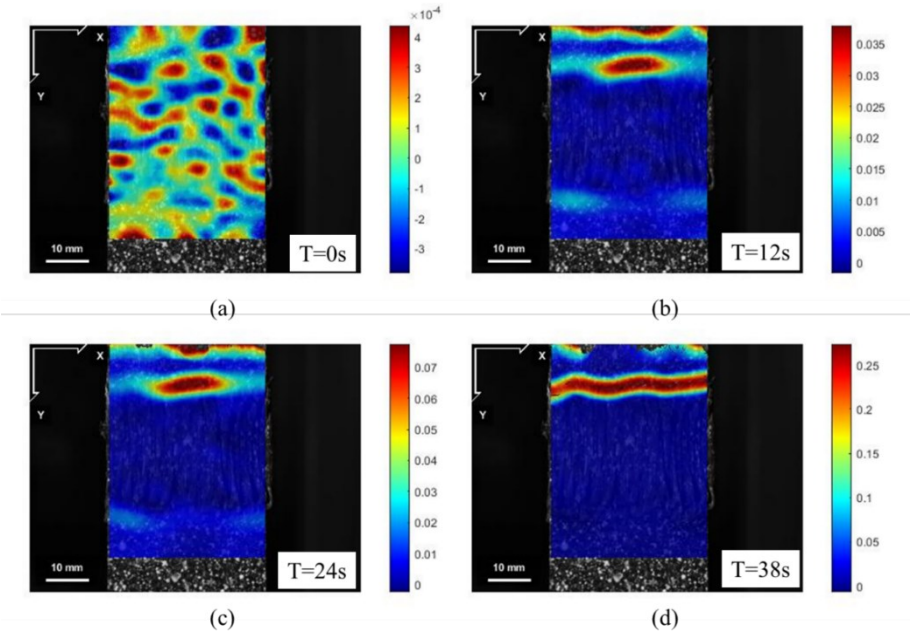

Figure 6-12 Progressive failure process and DIC strain contour (Eyy) of sample repaired at interface temperatures of 230 ℃: (a) initial point: T=0s; (b) T=16s; (c) T=26s; (d) failure point: T=38s.

6.4 Conclusions

In this study we established a basis for a novel in-situ remanufacturing system. We initially examined PPS composites reinforced by two types of recycled carbon fibres: reclaimed carbon fibre from thermosetting composites and reshaped carbon fibre from thermoplastic composites, followed by an exploration of an in-situ composites repair approach using 3D overprinting techniques. The primary conclusions are as follows:

(1) The mechanical performance of 3D printed composites, reinforced with reclaimed and reshaped carbon fibres, improved by 26.4% and 22.4%, respectively, following the surface treatment of carbon fibres. The specimen t-rCF/PPS (modified reshaped carbon fibre from thermoplastic composites) achieved the highest flexural strength at 252.9 MPa, attributed to its longer carbon fibre length, demonstrating promise in restoring the mechanical integrity of damaged thermoplastic laminates.

(2) Within the 3D overprinting repair system, in-situ bonding repair at an interface temperature of 220 °C proved most effective, yielding the highest tensile strength and lowest strain intensity. The optimal mechanical performance of repaired composites could improve by 35.4% of the damaged structure. The process window for the repair conditions was delineated through thermal characterisation of PPS and PA6 polymers, spanning from the melting temperature of PA6 polymer (216.8 °C) to the crystallisation temperature of PPS polymer (227.6 °C).

For future industrial application of this sustainable in-situ repair approach, the typical repair procedure for the hole failure of damaged components is outlined as follows: Firstly, the damaged area is removed, and the path of a repair is designed using finite element analysis. Next, the inner side of the damaged hole is repaired using continuous filament guided and placed by a robotic arm printer, followed by filling the damaged hole with recycled composites

containing short carbon fibre. The outer side of the damaged area is then repaired using the same method. Additionally, in instances where the parts present crack failure due to minor damage accumulated over the service life, it is recommended to use the continuous carbon fibre filament to construct a skin patch, which is precisely placed using a guided nozzle.

Although this approach shows promise in repairing CFRTP, further investigations into the insertion of an amorphous polymer layer and localised heating should be conducted, which may elevate the repair quality to a higher level. In addition, a preliminary result of customise trajectory for printing continuous filament is presented in Appendix and will be discussed in next section.

Chapter 7 Conclusions and future work

7.1 Main conclusions

This thesis has been dedicated to the exploration of extrusion-based additive manufacturing of carbon fibre reinforced polyphenylene sulphide (CF/PPS) composites. A primary objective for high-end applications is the enhancement of the mechanical performance of printed composites. This improvement is anticipated through the optimisation of thermal processing parameters, the improvement of interfacial adhesion, and further enhancement of interlaminar properties. Following these efforts, the thesis has also pioneered an in-situ manufacturing approach employing 3D overprinting technology. Main conclusions drawn from this thesis are as follows:

(1) Effect of different thermal processing conditions on CF/PPS materials via filament fabrication, material extrusion, and annealing treatment:

- The thermal parameters were optimised by reducing the degree of crystallinity in the extruded filament and enhancing the flexural strength of the printed composites. The optimum extrusion temperature was identified as 280 °C, and the printing temperatures were optimised towards 320 °C.
- The crystallisation process of the semi-crystalline PPS was modified through annealing treatment, thereby impacting the mechanical properties of the printed components. It was noted that annealing thermal treatment led to an improvement in the mechanical properties of printed CF/PPS composites with initially poorer properties.
- Oxidation crosslinking reactions between PPS chains were crucial in altering crystallinity, which is a key determinant of mechanical strength in the printed composite at elevated temperatures. It was observed that oxidation crosslinking

impeded crystallisation at higher temperatures due to dominant effects of less ordered polymer chains.

- This study offers valuable insights into the thermal processing conditions and their impact on CF/PPS materials in material extrusion. By optimising the extrusion and printing parameters, we successfully achieved maximised flexural strength in the printed parts.

(2) Introduction of a novel polydopamine/silica nanoparticles layer for enhanced impregnation of carbon fibre and thermoplastic polymers:

- A robust and eco-friendly one-step surface modification strategy was developed for carbon fibres to create a hybrid network on their surface. Optimal self-polymerisation time for polydopamine in treating carbon fibre was determined to be 16 hours, based on SEM microscopic imaging.
- The function of polydopamine in bridging silica nanoparticles and carbon fibres was confirmed through TEM characterisation of the fibre surface morphology. Chemical analyses, including Raman spectroscopy and X-ray photoelectron spectroscopy, provided evidence of successful modification.
- The interfacial bonding between carbon fibres and the high-performance thermoplastic matrix was significantly improved. The interlaminar shear strength (ILSS) of the resulting CF/PPS laminates increased by 28.4% due to the establishment of a PDA/NPS network.
- Dynamic Mechanical Analysis (DMA) revealed that the fibre-matrix interfacial bonding exhibits considerable thermal stability, indicating the network's thermal robustness. The hybrid network comprising polydopamine and silica nanoparticles demonstrated strong resistance to thermal cycling, with the storage modulus after the fifth cycle maintaining 95% of its initial value.

- Grafting polar functional groups onto the carbon fibre surface altered its roughness and wettability, leading to improved fibre/matrix impregnation in the resultant composites. Nanoparticles functioned as spacers, inducing smaller cracks in the cross-sectional area, rather than allowing cracks to extend directly to the surfaces of the carbon fibre. This contributed to the enhanced shear yield stress of the interface layer.

(3) Enhancements interfacial and interlaminar properties of printed CF/PPS through combined pre-processing with enhanced impregnation and post-processing with hot press:

- The integration of PDA/NPs network on CCF, coupled with hot press compaction approach, has significantly enhanced the interlaminar properties. This combination led to obvious enhancements, with flexural strength and interlaminar shear strength (ILSS) of 3D printed CCF/PPS composites increasing by 27% and 172%, respectively.
- Molecular dynamic (MD) simulations offer further insights into the enhanced adhesion mechanisms of the PDA/NPs network. Polydopamine plays a vital role as a binding agent, facilitating the adhesion of SiO_2 onto the CF substrate. This bridging effect not only stabilises nanoparticle deposition but also improves the surface properties of the carbon fibre, resulting in a modified interface with potentially superior impregnation. Additionally, experimental findings from nano-indentation tests of single fibre push-out are consistent with the shear simulations of carbon fibre.
- Regarding the mechanisms of post-processing techniques, Differential Scanning Calorimetry (DSC) analysis and morphological observations confirm an increase in crystallinity to 59.8% and a reduction in void content to 3.42%.

These changes contribute to the composites' superior mechanical performance under shear and flexural loads.

- An innovative salt-bath-based hot press compaction method has been successfully employed to preserve the geometric details of complex 3D printed structures, such as a two-dimensional lightweight perforated structure with an array of holes and a three-dimensional integrated stiffer structure. The nominal deviations in dimensions for both structures were less than 3%, while their thickness could be reduced by 10%-15%.

(4) Overprinting of continuous carbon fibre and recycled discontinuous carbon fibre composites on damaged thermoplastic composites in in-situ composites repairing:

- The surface treatment of carbon fibres leads to a notable improvement in the mechanical performance of 3D printed next-generation composites. Specifically, composites reinforced with reclaimed and reshaped carbon fibres exhibited enhancements of 26.4% and 22.4%, respectively. Among these, the specimen reshaped from thermoplastic composites demonstrated the most significant increase in flexural strength, reaching 252.9 MPa, showcasing potential in recovering the mechanical performance of damaged CFRTP.
- The in-situ bonding repair conducted at an interface temperature of 220°C presents the highest tensile strength and the lowest strain intensity. The optimal mechanical performance of the repaired composites indicated an improvement of 35.4% over the damaged structure. The process window for the repair conditions was defined through thermal characterisation of PPS and PA6 polymers, ranging from the melting temperature of PA6 polymer (216.8 °C) to the crystallisation temperature of PPS polymer (227.6 °C).

7.2 Recommendations to future work

This work on additive manufacturing of high-performance CF/PPS composites demonstrates the technique's potential to produce high-quality, lightweight, and sustainable structural parts for the automotive and aerospace industries. This was achieved by optimising process parameters, improving fibre-matrix adhesion, and enhancing interlaminar adhesion.

(1) *Investigation on the effect of the cooling rate in the printing process on the degree of crystallinity of semi-crystalline polymer composites:*

The cooling rate is known to be crucial in the recrystallisation process for high-temperature semi-crystalline polymers. In 3D printing, the deposition rate is maintained at a relatively high speed to enhance work efficiency. Furthermore, the elevated nozzle temperature means that deposited materials cool rapidly upon contact with the existing layer, potentially leading to insufficient crystallisation. Therefore, controlling the chamber temperature is essential when printing high-performance polymers, particularly for semi-crystalline polymers. Due to limitations in modifying the commercial high-temperature printer used in this thesis, the chamber temperature could not be controlled as desired. Future research should focus on investigating the effect of cooling rate on the mechanical properties of printed high-performance composites.

(2) *Accelerating the self-polymerisation process of polydopamine for industrial applications and scale-up:*

While polydopamine is a robust, eco-friendly, and versatile adhesive for treating carbon fibre to improve impregnation, its typical self-polymerisation process can take nearly a day. Recent research focuses on applying ultrasonic waves during polymerisation, potentially reducing the time to 2 hours through mechanical agitation and increased energy input. Further research is needed to control this chemical reaction, possibly

through the addition of catalysts and increasing oxygen concentration, which could further accelerate the polymerisation rate. Such acceleration could enable the automatic grafting of polydopamine onto commercial continuous carbon fibre tow.

(3) *Enhancing the in-situ bonding for overprinting techniques.*

Improving the interface temperature in the overprinting process can enhance in-situ bonding strength, but current limitations in bed temperature prevent achieving the optimal interface temperature. Additionally, heating the entire laminate could deform existing structures and let the anchored filament detached from in the turning radius the area the due to the delayed cooling. Future studies should focus on designing a localised heating system that concentrates heat on the bonding area near the printer nozzle during the printing process. This approach would address the challenge of insufficient heat energy at the interface. Integrating thermal mapping equipment, such as a thermal camera, on the printer could also monitor heat distribution around the bonding area. For broader industrial applications of 3D overprinting techniques, a localised system would be beneficial for large existing parts. Pressure is another parameter to consider in overprinting techniques for in-situ bonding. Adjusting the nozzle level alters the pressure applied by the nozzle, necessitating further integration of a pressure-monitoring sensor in the printer.

Additionally, a potential improvement for in-situ bonding is the introduction of an amorphous layer between overprinted CF/PPS materials and existing CF/PA6 laminates. Introducing an amorphous layer, such as PEI, could further enhance the in-situ strength. Amorphous layers can diffuse more easily into semi-crystalline polymers and bond multi-materials when the heating temperature is above the glass transition temperature. Inserting an amorphous layer between the extruding materials and existing structures could potentially achieve fusion bonding strength in overprinting techniques.

Appendix

Customised trajectory on the in-situ repair patch

This section further explores the optimisation of a customised trajectory for in-situ repair patches, a collaborative effort that included contributions from my colleague, who led the simulation work. These efforts were aimed at predicting stress distribution and interfacial failure in repaired composites via Finite Element (FE) modelling. Herein, we detail the methodology employed and present preliminary findings:

Methodology

Utilising ABAQUS/Explicit software, a three-dimensional model for Finite Element Analysis (FEA) was developed. This model's purpose was to accurately simulate stress transfer within pure polyphenylene sulphide (PPS) patches and to track the evolution of detachment areas between these patches and the parent laminate, particularly in the context of repaired open-hole laminates. Insights obtained from this analysis were intended to inform the printing paths for patches fabricated from continuous carbon fibre/polyphenylene sulphide (CCF/PPS) filament.

Given the identification of delamination between the patch and parent laminate as the primary failure mechanism in these repair tests, the model was specifically designed to simulate interlaminar failure triggered by delamination, whilst assuming purely elastic behaviour in unaffected regions. To accurately represent the separation between the patch and parent laminate within the FE model, a cohesive cone model (CZM) was implemented by designating cohesive properties to interfaces. The traction-separation response, indicative of linear elastic behaviour, was integrated into the CZM. Considering delamination often occurs under mixed-mode loading conditions, the quadratic-stress failure criterion was employed to predict the onset of delamination, as delineated by Equation A-1. Upon initiation, a linear softening law was applied to simulate damage progression. The interlaminar properties pertinent to the

analysis, including fracture energy, interfacial strength, and penalty stiffness, are summarised in Table A-1 as well, allocated to the composite layers.

$$\left(\frac{t_n}{N}\right)^2 + \left(\frac{t_s}{S}\right)^2 + \left(\frac{t_t}{T}\right)^2 = 1 \quad \text{(A-1)}$$

Where t_n, t_s, t_t are the normal and shear tractions. N, S and T denote normal shear cohesive strengths, respectively.

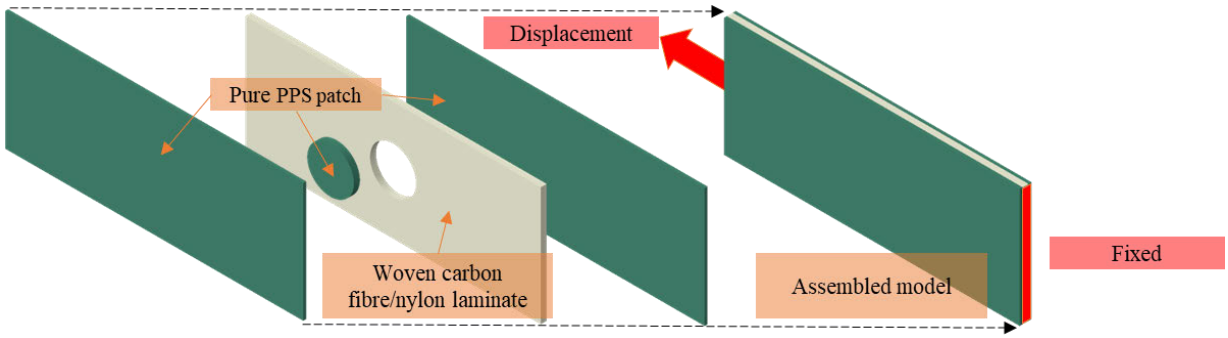

Figure A-1 Used boundary and loading conditions of a repaired woven PA6 laminate.

Table A-1 Materials properties of the woven CF/PA6 laminates

Property	Values	Source
Elastic properties		
Young's moduli, E_1	54.11 GPa	ASTM D3039
Passions' ratio, υ_{12}	0.36	[209]
Shear moduli, G_{12}	5.8 GPa	[209]
Interlaminar properties		
Fracture energy, G_{IC}	0.3 N/mm	[210]
Fracture energy, G_{IIC}	1.0 N/mm	[210]
Interfacial strength, σ_I	45 MPa	[210]
Interfacial strength, σ_{II}	35 MPa	[210]
The penalty stiffness, K_I	3×10^5 N/mm^3	[210]
The penalty stiffness, K_{II}	3×10^5 N/mm^3	[210]

Specimens were modelled with specified dimensions, employing eight-node linear reduced integration solid elements (C3D8R). The boundary and loading conditions, reflective of a repaired woven PA6 laminate, are illustrated in Figure S-1. The dimensions for the open-hole laminate were meticulously set to 200 mm × 36 mm × 2 mm, mirroring the experimental laminate. Cohesive contact properties were assigned to the direct interfaces between the patches (denoted in green in Figure A-1) and the woven carbon fibre/nylon laminate. Figure A-1 also depicts the model assembly and boundary conditions, with displacement and fixed regions clearly marked in red.

Preliminary results

The simulation results, presenting the propagation contour of cohesive surface failure, are presented in Figure A-2(a). Furthermore, the trajectory pattern of load path, obtained from the load path theory (Equation A-2) and the stress components within the pure PPS patch, was generated using Python scripts, as depicted in Figure A-2(b). The final printing path was crafted combining the outer contours of the cohesive surface failure and the load path trajectory, as illustrated in Figure A-2(c).

$$\int V_x \cdot \boldsymbol{n}\, dA = 0 \tag{A-2}$$

Where V_x is the stress vector and $\boldsymbol{n}$ is the unit vector perpendicular to V_x. The vector field of determines the fibre trajectory.

To facilitate a robust comparison, the area of the final continuous fibre printed patches was matched to that of unidirectional (UD) patches (refer in Figure A-3(a)). Moreover, to ensure printability by continuous fibres, the final printing path was processed into a continuous trajectory, as shown in Figure A-3(b).

Figure A-4 presents the tensile response curves for composites repaired using both unidirectional (UD) and customised printing paths. It shows that UD path outperforms the

customised path in terms of ultimate tensile strength. The customised path, whilst initially following a similar trajectory to the UD path, does not sustain the load as effectively, peaking at a lower force. This observation suggests that the customised path repair, despite its strategic design, does not confer the same level of mechanical integrity as the UD path.

Several factors may contribute to this outcome. Notably, the UD path, with its linear fibre orientation, is inherently more suited to withstanding uniaxial tensile stresses, thereby enhancing the repaired composite's performance under such loading conditions. The customised path, which may incorporate multi-directional fibre orientations to accommodate specific stress patterns, does not provide the same level of uniform resistance. Furthermore, the quality of the customised repair can be compromised by overlaps in the printed path, a common issue observed in the second side of the repair patches. Such overlaps can introduce areas of weakness, resulting in reduced tensile strength and potentially leading to early initiation of failure. In essence, while the customised path offers a tailored approach to repair, accounting for specific stress distributions, it does not inherently equate to superior mechanical performance when compared to UD repairs for the open-hole damaged laminate.

Future insights

The efficacy of customised printing paths in the repair process should not be solely gauged on the results of uniaxial tensile loading, especially when considering their potential in addressing more complex and atypically shaped damages such as surface cracks. The promise of customised paths lies in their adaptability and precision, which may prove especially beneficial in scenarios where the damage imparts irregular stress distributions within the composite structure. Additionally, the performance of a customised repair under shear stresses could reveal additional strengths of this tailored approach, potentially offering a more comprehensive restoration when compare to traditional unidirectional repairs.

In future research, there is a significant opportunity to extend the scope of investigation to include a variety of damage types and loading conditions. By doing so, we can enhance our understanding of how customised printing paths can be optimised to exploit the full capabilities of 3D printing technology. This will involve testing and refinement of the printing paths to ensure that they not only conform to the geometric complexities of the damage but also align with the stress contours that emerge during service conditions.

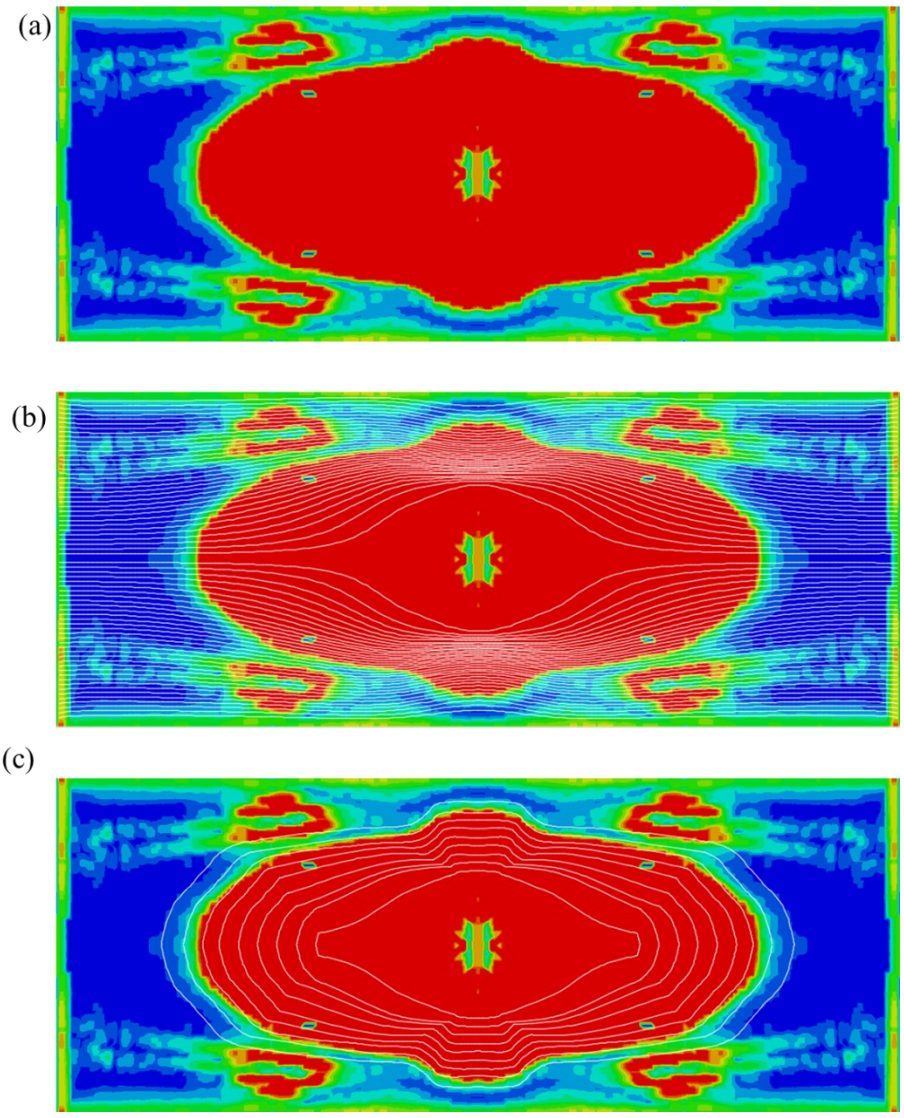

Figure A-2 (a) Cohesive failure contour; (b) mapping of load path trajectories in the cohesive failure contour; (c) novel hybrid printing path through integration of load path trajectories on cohesive failure contour.

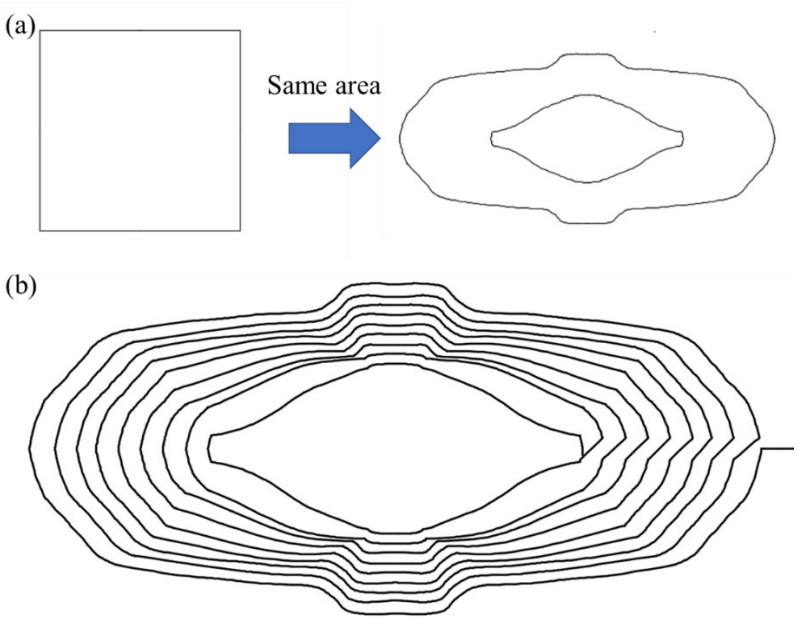

Figure A-3 (a) Determination of size for customised patch; (b) final 3D printing continuous path.

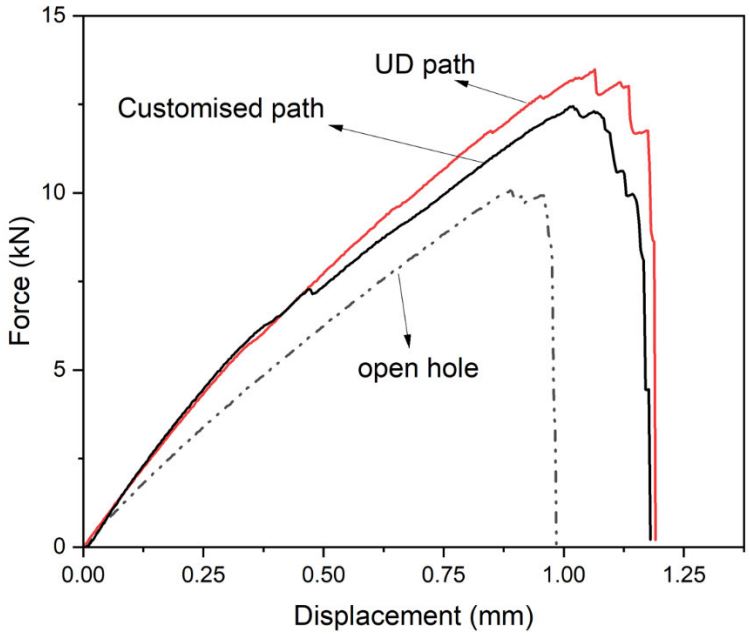

Figure A-4 Force-displacement curves of open hole composites and repaired composites with unidirectional (UD) path and customised path.

Publications

Lyu, Y., Wu, J., Zhang, H., Brádaigh, C. M. Ó., & Yang, D. (2023). Effects of thermal process conditions on crystallinity and mechanical properties in material extrusion additive manufacturing of discontinuous carbon fibre reinforced polyphenylene sulphide composites. *Journal of Composite Materials*, *57*(24), 3775-3787.

Lyu, Y., Koutsos, V., Brádaigh, C. M. Ó., & Yang, D. (2024). Improving the interfacial adhesion between recycled carbon fibres and polyphenylene sulphide by bio-inspired dopamine for advanced composites manufacturing. *Journal of Cleaner Production*, 141855.

References

[1] Ingen V, Wijngaarden V, Iii S. Development of the Gulfstream G650 induction welded thermoplastic elevators and rudder. International SAMPE symposium and exhibition, Seattle, WA, USA: 2010.

[2] Garmabi MM, Shahi P, Tjong J, Sain M. 3D printing of polyphenylene sulfide for functional lightweight automotive component manufacturing through enhancing interlayer bonding. Addit Manuf 2022;56. https://doi.org/10.1016/j.addma.2022.102780.

[3] Kishore V, Chen X, Hassen AA, Lindahl J, Kunc V, Duty C. Post-process annealing of large-scale 3D printed polyphenylene sulfide composites. Addit Manuf 2020;35:101387. https://doi.org/10.1016/j.addma.2020.101387.

[4] Barocio E, Brenken B, Favaloro A, Bogdanor M, Pipes RB. Extrusion deposition additive manufacturing with fiber-reinforced thermoplastic polymers. Structure and Properties of Additive Manufactured Polymer Components, Elsevier; 2020, p. 191–219. https://doi.org/10.1016/B978-0-12-819535-2.00007-7.

[5] Wong KH, Syed Mohammed D, Pickering SJ, Brooks R. Effect of coupling agents on reinforcing potential of recycled carbon fibre for polypropylene composite. Compos Sci Technol 2012;72:835–44. https://doi.org/10.1016/j.compscitech.2012.02.013.

[6] Zhu C, Li S, Cong X, Rudd C, Liu X. Effect of silane coupling agent on the properties of recycled carbon fibers reinforced bio-based epoxy composites. Fibers and Polymers 2021;22:1976–85. https://doi.org/10.1007/s12221-021-0691-9.

[7] Käppler I, Hund RD, Cherif C. Surface modification of carbon fibres using plasma technique. Autex Research Journal 2014;14:34–8. https://doi.org/10.2478/v10304-012-0048-y.

[8] Eyckens DJ, Arnold CL, Simon Ž, Gengenbach TR, Pinson J, Wickramasingha YA, et al. Covalent sizing surface modification as a route to improved interfacial adhesion in carbon fibre-epoxy composites. Compos Part A Appl Sci Manuf 2021;140. https://doi.org/10.1016/j.compositesa.2020.106147.

[9] Dong Y, Yu T, Wang X jun, Zhang G, Lu J hong, Zhang M lin, et al. Improved interfacial shear strength in polyphenylene sulfide/carbon fiber composites via the carboxylic polyphenylene sulfide sizing agent. Compos Sci Technol 2020;190. https://doi.org/10.1016/j.compscitech.2020.108056.

[10] Hu J, Li F, Wang B, Zhang H, Ji C, Wang S, et al. A two-step combination strategy for significantly enhancing the interfacial adhesion of CF/PPS composites: The liquid-phase oxidation followed by grafting of silane coupling agent. Compos B Eng 2020;191:107966. https://doi.org/10.1016/j.compositesb.2020.107966.

[11] Li S, Wang K, Zhu W, Peng Y, Ahzi S, Chinesta F. Contributions of interfaces on the mechanical behavior of 3D printed continuous fiber reinforced composites. Constr Build Mater 2022;340. https://doi.org/10.1016/j.conbuildmat.2022.127842.

[12] Ma S, Li H, Li C, Tian H, Tao M, Fei J, et al. Metal-organic frameworks/polydopamine synergistic interface enhancement of carbon fiber/phenolic composites for promoting mechanical and tribological performances. Nanoscale 2021;13:20234–47. https://doi.org/10.1039/d1nr07104a.

[13] Jin L, Zhang M, Shang L, Liu L, Li M, Ao Y. A nature-inspired interface design strategy of carbon fiber composites by growing brick-and-mortar structure on carbon fiber. Compos Sci Technol 2020;200. https://doi.org/10.1016/j.compscitech.2020.108382.

[14] Sun Z, Guo FL, Li YQ, Hu JM, Liu QX, Mo XL, et al. Effects of carbon nanotube-polydopamine hybridization on the mechanical properties of short carbon fiber/polyetherimide composites. Compos B Eng 2022;236. https://doi.org/10.1016/j.compositesb.2022.109848.

[15] Tian X, Liu T, Yang C, Wang Q, Li D. Interface and performance of 3D printed continuous carbon fiber reinforced PLA composites. Compos Part A Appl Sci Manuf 2016;88:198–205. https://doi.org/10.1016/j.compositesa.2016.05.032.

[16] Chen K, Yu L, Cui Y, Jia M, Pan K. Optimization of printing parameters of 3D-printed continuous glass fiber reinforced polylactic acid composites. Thin-Walled Structures 2021;164. https://doi.org/10.1016/j.tws.2021.107717.

[17] Pyl L, Kalteremidou KA, Van Hemelrijck D. Exploration of specimen geometry and tab configuration for tensile testing exploiting the potential of 3D printing freeform shape continuous carbon fibre-reinforced nylon matrix composites. Polym Test 2018;71:318–28. https://doi.org/10.1016/j.polymertesting.2018.09.022.

[18] Mosleh N, Rezadoust AM, Dariushi S. Determining process-window for manufacturing of continuous carbon fiber-reinforced composite Using 3D-printing. Materials and Manufacturing Processes 2021;36:409–18. https://doi.org/10.1080/10426914.2020.1843664.

[19] Liu T, Tian X, Zhang M, Abliz D, Li D, Ziegmann G. Interfacial performance and fracture patterns of 3D printed continuous carbon fiber with sizing reinforced PA6

composites. Compos Part A Appl Sci Manuf 2018;114:368–76. https://doi.org/10.1016/J.COMPOSITESA.2018.09.001.

[20] Heidari-Rarani M, Rafiee-Afarani M, Zahedi AM. Mechanical characterization of FDM 3D printing of continuous carbon fiber reinforced PLA composites. Compos B Eng 2019;175. https://doi.org/10.1016/j.compositesb.2019.107147.

[21] Mei H, Ali Z, Yan Y, Ali I, Cheng L. Influence of mixed isotropic fiber angles and hot press on the mechanical properties of 3D printed composites. Addit Manuf 2019;27:150–8. https://doi.org/10.1016/j.addma.2019.03.008.

[22] He Q, Wang H, Fu K, Ye L. 3D printed continuous CF/PA6 composites: Effect of microscopic voids on mechanical performance. Compos Sci Technol 2020;191. https://doi.org/10.1016/j.compscitech.2020.108077.

[23] Pascual-González C, San Martín P, Lizarralde I, Fernández A, León A, Lopes CS, et al. Post-processing effects on microstructure, interlaminar and thermal properties of 3D printed continuous carbon fibre composites. Compos B Eng 2021;210. https://doi.org/10.1016/j.compositesb.2021.108652.

[24] Justo J, Moreno F, Jiménez M, Simón F, París F. Experimental study of composite structures repairs using additive manufacturing technologies. ECCM18 - 18th European Conference on Composite Materials, 2018, p. 24–8.

[25] Joosten MW, Neave MB, Rider AN, Varley RJ. 3D printed continuous fibre composite repair of sandwich structures. Compos Struct 2022;290. https://doi.org/10.1016/j.compstruct.2022.115518.

[26] Li L, Liu W, Wang Y, Zhao Z. Mechanical performance and damage monitoring of CFRP thermoplastic laminates with an open hole repaired by 3D printed patches. Compos Struct 2023;303. https://doi.org/10.1016/j.compstruct.2022.116308.

[27] Wang X, Jiang M, Zhou Z, Gou J, Hui D. 3D printing of polymer matrix composites: A review and prospective. Compos B Eng 2017;110:442–58. https://doi.org/10.1016/j.compositesb.2016.11.034.

[28] Ngo TD, Kashani A, Imbalzano G, Nguyen KTQ, Hui D. Additive manufacturing (3D printing): A review of materials, methods, applications and challenges. Compos B Eng 2018;143:172–96. https://doi.org/10.1016/j.compositesb.2018.02.012.

[29] Parandoush P, Lin D. A review on additive manufacturing of polymer-fiber composites. Compos Struct 2017;182:36–53. https://doi.org/10.1016/j.compstruct.2017.08.088.

[30] Yao SS, Jin FL, Rhee KY, Hui D, Park SJ. Recent advances in carbon-fiber-reinforced thermoplastic composites: A review. Compos B Eng 2018;142:241–50. https://doi.org/10.1016/j.compositesb.2017.12.007.

[31] Vaes D, Van Puyvelde P. Semi-crystalline feedstock for filament-based 3D printing of polymers. Prog Polym Sci 2021;118:101411. https://doi.org/10.1016/j.progpolymsci.2021.101411.

[32] Ligon SC, Liska R, Stampfl J, Gurr M, Mülhaupt R. Polymers for 3D Printing and Customized Additive Manufacturing. Chem Rev 2017;117:10212–90. https://doi.org/10.1021/acs.chemrev.7b00074.

[33] Lona Batista N, Anagnostopoulos K, Cocchieri Botelho E, Kim H. Influence of crystallinity on interlaminar fracture toughness and impact properties of polyphenylene

sulfide/carbon fiber laminates. Eng Fail Anal 2021;119. https://doi.org/10.1016/j.engfailanal.2020.104976.

[34] Fitzharris ER, Watanabe N, Rosen DW, Shofner ML. Effects of material properties on warpage in fused deposition modeling parts. International Journal of Advanced Manufacturing Technology 2018;95:2059–70. https://doi.org/10.1007/s00170-017-1340-8.

[35] El Magri A, El Mabrouk K, Vaudreuil S, Ebn Touhami M. Experimental investigation and optimization of printing parameters of 3D printed polyphenylene sulfide through response surface methodology. J Appl Polym Sci 2020;138:1–13. https://doi.org/10.1002/app.49625.

[36] Yeole P, Hassen AA, Kim S, Lindahl J, Kunc V, Franc A, et al. Mechanical characterization of high-temperature carbon fiber-polyphenylene sulfide composites for large area extrusion deposition additive manufacturing. Addit Manuf 2020;34:101255. https://doi.org/10.1016/j.addma.2020.101255.

[37] Geng P, Zhao J, Wu W, Wang Y, Wang B, Wang S, et al. Effect of thermal processing and heat treatment condition on 3D printing PPS properties. Polymers (Basel) 2018;10. https://doi.org/10.3390/polym10080875.

[38] Denardo NM. Additive manufacturing of carbon fiber-reinforced thermoplastic composites. 2016.

[39] Barocio E. Fusion bonding of fiber reinforced semi-crystalline polymers in extrusion deposition additive manufacturing. 2017.

[40] Hassen AA, Lindahl J, Chen X, Post B, Love L, Kunc V. Additive manufacturing of composite tooling using high temperature thermoplastic materials. SAMPE Conference Proceedings, vol. 2016- Janua, Long Beach, CA: 2016, p. 2648–1658.

[41] Liu P, Dinwiddie RB, Keum JK, Vasudevan RK, Jesse S, Nguyen NA, et al. Rheology, crystal structure, and nanomechanical properties in large-scale additive manufacturing of polyphenylene sulfide/carbon fiber composites. Compos Sci Technol 2018;168:263–71. https://doi.org/10.1016/j.compscitech.2018.09.010.

[42] Brenken B, Barocio E, Favaloro A, Kunc V, Pipes RB. Fused filament fabrication of fiber-reinforced polymers: A review. Addit Manuf 2018;21:1–16. https://doi.org/10.1016/j.addma.2018.01.002.

[43] Barocio E, Brenken B, Favaloro A, Pipes RB. Interlayer fusion bonding of semi-crystalline polymer composites in extrusion deposition additive manufacturing. Compos Sci Technol 2022;230. https://doi.org/10.1016/j.compscitech.2022.109334.

[44] Brenken B, Barocio E, Favaloro A, Kunc V, Pipes RB. Development and validation of extrusion deposition additive manufacturing process simulations. Addit Manuf 2019;25:218–26. https://doi.org/10.1016/j.addma.2018.10.041.

[45] Yang C, Tian X, Li D, Cao Y, Zhao F, Shi C. Influence of thermal processing conditions in 3D printing on the crystallinity and mechanical properties of PEEK material. J Mater Process Technol 2017;248:1–7. https://doi.org/10.1016/j.jmatprotec.2017.04.027.

[46] Van de Voorde B, Katalagarianakis A, Huysman S, Toncheva A, Raquez JM, Duretek I, et al. Effect of extrusion and fused filament fabrication processing parameters of recycled poly(ethylene terephthalate) on the crystallinity and mechanical properties. Addit Manuf 2022;50. https://doi.org/10.1016/j.addma.2021.102518.

[47] Bousmina M, Qiu H, Grmela M, Klemberg-Sapieha JE. Diffusion at polymer/polymer interfaces probed by rheological tools. Macromolecules 1998;31:8273–80. https://doi.org/10.1021/ma980562r.

[48] Grewell D, Benatar A. Welding of Plastics: Fundamentals and New Developments. International Polymer Processing 2007;22:43–60.

[49] Iragi M, Pascual-González C, Esnaola A, Lopes CS, Aretxabaleta L. Ply and interlaminar behaviours of 3D printed continuous carbon fibre-reinforced thermoplastic laminates; effects of processing conditions and microstructure 2019. https://doi.org/10.1016/j.addma.2019.100884.

[50] Pokluda O, Bellehumeur CT, Vlachopoulos J. Modification of Frenkel's Model for Sintering. AIChE Journal 1997;43:3253–6. https://doi.org/10.1002/aic.690431213.

[51] Das A, Gilmer EL, Biria S, Bortner MJ. Importance of polymer rheology on material extrusion additive manufacturing: correlating process physics to print properties. ACS Appl Polym Mater 2021;3:1218–49. https://doi.org/10.1021/acsapm.0c01228.

[52] Seppala JE, Migler KD. Infrared thermography of welding zones produced by polymer extrusion additive manufacturing. Addit Manuf 2016;12:71–6. https://doi.org/10.1016/j.addma.2016.06.007.

[53] Sopade PA, Halley P, Bhandari B, D'arcy B, Doebler C, Caffin N. Application of the Williams-Landel-Ferry model to the viscosity-temperature relationship of Australian honeys. J Food Eng 2003;56:67–75.

[54] Rodríguez JF, Thomas JP, Renaud JE. Design of fused-deposition ABS components for stiffness and strength. Journal of Mechanical Design 2003;125:545–51. https://doi.org/10.1115/1.1582499.

[55] Yan Y, Zhang R, Hong G, Yuan X. Research on the bonding of material paths in melted extrusion modeling. Mater Des 2000;21:9399.

[56] Ning F, Cong W, Qiu J, Wei J, Wang S. Additive manufacturing of carbon fiber reinforced thermoplastic composites using fused deposition modeling. Compos B Eng 2015;80:369–78. https://doi.org/10.1016/J.COMPOSITESB.2015.06.013.

[57] Jiang D, Smith DE. Anisotropic mechanical properties of oriented carbon fiber filled polymer composites produced with fused filament fabrication. Addit Manuf 2017;18:84–94. https://doi.org/10.1016/j.addma.2017.08.006.

[58] Ferreira RTL, Amatte IC, Dutra TA, Bürger D. Experimental characterization and micrography of 3D printed PLA and PLA reinforced with short carbon fibers. Compos B Eng 2017;124:88–100. https://doi.org/10.1016/j.compositesb.2017.05.013.

[59] Liao G, Li Z, Cheng Y, Xu D, Zhu D, Jiang S, et al. Properties of oriented carbon fiber/polyamide 12 composite parts fabricated by fused deposition modeling. Mater Des 2018;139:283–92. https://doi.org/10.1016/j.matdes.2017.11.027.

[60] Wu J, Zhang K, Yang D. Material extrusion additive manufacturing of recycled discontinuous carbon fibre reinforced thermoplastic composites with different fibre lengths: Through-process microstructural evolution and mechanical property loss. Addit Manuf 2023;78. https://doi.org/10.1016/j.addma.2023.103839.

[61] Mortazavian S, Fatemi A. Effects of fiber orientation and anisotropy on tensile strength and elastic modulus of short fiber reinforced polymer composites. Compos B Eng 2015;72:116–29. https://doi.org/10.1016/j.compositesb.2014.11.041.

[62] Kelly A, Tyson AW. Tensile properties of fibre-reinforced metals: copper/tungsten and copper/molybdenum. J Mech Phys Solids 1965;13:329–50.

[63] Yan X, Yang Y, Hamada H. Tensile properties of glass fiber reinforced polypropylene composite and its carbon fiber hybrid composite fabricated by direct fiber feeding injection molding process. Polym Compos 2018;39:3564–74. https://doi.org/10.1002/pc.24378.

[64] Purslow D. The shear properties of unidirectional carbon fibre reinforced plastics and their experimental determination. HM Stationery Office. 1976.

[65] Der Klift F Van, Koga Y, Todoroki A, Ueda M, Hirano Y, Matsuzaki R. 3D printing of continuous carbon fibre reinforced thermo-plastic (CFRTP) tensile test specimens. Open Journal of Composite Materials 2016;06:18–27. https://doi.org/10.4236/ojcm.2016.61003.

[66] Matsuzaki R, Ueda M, Namiki M, Jeong TK, Asahara H, Horiguchi K, et al. Three-dimensional printing of continuous-fiber composites by in-nozzle impregnation. Sci Rep 2016;6:1–7. https://doi.org/10.1038/srep23058.

[67] Li N, Li Y, Liu S. Rapid prototyping of continuous carbon fiber reinforced polylactic acid composites by 3D printing. J Mater Process Technol 2016;238:218–25. https://doi.org/10.1016/j.jmatprotec.2016.07.025.

[68] Parker M, Inthavong A, Law E, Waddell S, Ezeokeke N, Matsuzaki R, et al. 3D printing of continuous carbon fiber reinforced polyphenylene sulfide: Exploring printability and importance of fiber volume fraction. Addit Manuf 2022;54. https://doi.org/10.1016/j.addma.2022.102763.

[69] Parker M, Ezeokeke N, Matsuzaki R, Arola D. Strength and its variability in 3D printing of polymer composites with continuous fibers. Mater Des 2023;225. https://doi.org/10.1016/j.matdes.2022.111505.

[70] Caltagirone PE, Ginder RS, Ozcan S, Li K, Gay AM, Stonecash J, et al. Substitution of virgin carbon fiber with low-cost recycled fiber in automotive grade injection molding polyamide 66 for equivalent composite mechanical performance with improved sustainability. Compos B Eng 2021;221:109007. https://doi.org/10.1016/j.compositesb.2021.109007.

[71] Stoeffler K, Andjelic S, Legros N, Roberge J, Schougaard SB. Polyphenylene sulfide (PPS) composites reinforced with recycled carbon fiber. Compos Sci Technol 2013;84:65–71. https://doi.org/10.1016/j.compscitech.2013.05.005.

[72] Drzal LT, Rich MJ, Lloyd PF. Adhesion of graphite fibers to epoxy matrices: I. The role of fiber surface treatment. J Adhes 1983;16:1–30. https://doi.org/10.1080/00218468308074901.

[73] Huang S, Fu Q, Yan L, Kasal B. Characterization of interfacial properties between fibre and polymer matrix in composite materials – A critical review. Journal of Materials Research and Technology 2021;13:1441–84. https://doi.org/10.1016/j.jmrt.2021.05.076.

[74] Wolff D, Geiger S, Ding P, Staehle HJ, Frese C. Analysis of the interdiffusion of resin monomers into pre-polymerized fiber-reinforced composites. Dental Materials 2012;28:541–7. https://doi.org/10.1016/j.dental.2011.12.001.

[75] Zhang K, Zhang G, Liu B, Wang X, Long S, Yang J. Effect of aminated polyphenylene sulfide on the mechanical properties of short carbon fiber reinforced polyphenylene sulfide composites. Compos Sci Technol 2014;98:57–63. https://doi.org/10.1016/j.compscitech.2014.04.020.

[76] Gassan J, Gutowski VS. Effects of corona discharge and UV treatment on the properties of jute-fibre epoxy composites. Compos Sci Technol 2000;60:2857–63.

[77] Mohammed M, Rasidi MSM, Mohammed AM, Rahman R, Osman AF, Adam T, et al. Interfacial bonding mechanisms of natural fibre-matrix composites: An Overview. Bioresources 2022;17:7031–90. https://doi.org/10.15376/BIORES.17.4.MOHAMMED.

[78] Liu D, Song J, Anderson DP, Chang PR, Hua Y. Bamboo fiber and its reinforced composites: Structure and properties. Cellulose 2012;19:1449–80. https://doi.org/10.1007/s10570-012-9741-1.

[79] Montes-Moran MA, Young RJ. Raman spectroscopy study of high-modulus carbon fibres: effect of plasma-treatment on the interfacial properties of single-fibre-epoxy composites Part II: Characterisation of the fibre-matrix interface. Carbon N Y 2002;40:857–75.

[80] Tiwari S, Sharma M, Panier S, Mutel B, Mitschang P, Bijwe J. Influence of cold remote nitrogen oxygen plasma treatment on carbon fabric and its composites with specialty polymers. J Mater Sci 2011;46:964–74. https://doi.org/10.1007/s10853-010-4847-z.

[81] Montes-Morán MA, Martínez-Alonso A, Tascón JMD, Paiva MC, Bernardo CA. Effects of plasma oxidation on the surface and interfacial properties of carbon fibres/polycarbonate composites. Carbon N Y 2001;39:1057–68. https://doi.org/10.1016/S0008-6223(00)00220-7.

[82] Da Silva LLG, Alves LG, Tóth A, Ueda M. A study of the effect of nitrogen and air plasma immersion ion implantation treatments on the properties of carbon fiber. IEEE Transactions on Plasma Science 2011;39:3067–71. https://doi.org/10.1109/TPS.2011.2160293.

[83] Jang J, Yang H. Effect of surface treatment on the performance improvement of carbon fiber/polybenzoxazine composites. J Mater Sci 2000;35:2297–303. https://doi.org/10.1023/A:1004791313979.

[84] Li R, Ye L, Mai YW. Application of plasma technologies in fibre-reinforced polymer composites: A review of recent developments. Compos Part A Appl Sci Manuf 1997;28:73–86. https://doi.org/10.1016/S1359-835X(96)00097-8.

[85] Solís-Fernández P, Paredes JI, Cosío A, Martínez-Alonso A, Tascón JMD. A comparison between physically and chemically driven etching in the oxidation of graphite surfaces. J Colloid Interface Sci 2010;344:451–9. https://doi.org/10.1016/j.jcis.2010.01.018.

[86] Eyckens DJ, Stojcevski F, Hendlmeier A, Randall JD, Hayne DJ, Stanfield MK, et al. Carbon fibre surface chemistry and its role in fibre-to-matrix adhesion. J Mater Chem A Mater 2021;9:26528–72. https://doi.org/10.1039/d1ta07151c.

[87] Song B, Wang T, Wang L, Liu H, Mai X, Wang X, et al. Interfacially reinforced carbon fiber/epoxy composite laminates via in-situ synthesized graphitic carbon nitride (g-C3N4). Compos B Eng 2019;158:259–68. https://doi.org/10.1016/j.compositesb.2018.09.081.

[88] Yao H, Zhou G, Wang W, Peng M. Silica nanoparticle-decorated alumina rough platelets for effective reinforcement of epoxy and hierarchical carbon fiber/epoxy composites. Compos Part A Appl Sci Manuf 2018;110:53–61. https://doi.org/10.1016/j.compositesa.2018.04.017.

[89] Yang Y, Lu C, Su X, Wang X. Effects of emulsion sizing with nano-SiO2 on interfacial properties of carbon fibers/epoxy composites. J Mater Sci 2007;42:6347–52. https://doi.org/10.1007/s10853-006-1198-x.

[90] Yamamoto T, Yabushita S, Irisawa T, Tanabe Y. Enhancement of bending strength, thermal stability and recyclability of carbon-fiber-reinforced thermoplastics by using silica colloids. Compos Sci Technol 2019;181. https://doi.org/10.1016/j.compscitech.2019.05.022.

[91] Liu L, Yan F, Li M, Zhang M, Xiao L, Shang L, et al. Improving interfacial properties of hierarchical reinforcement carbon fibers modified by graphene oxide with different bonding types. Compos Part A Appl Sci Manuf 2018;107:616–25. https://doi.org/10.1016/j.compositesa.2018.02.009.

[92] Zhang M, Liu L, Jin L, Sun L, Li M, Shang L, et al. Catechol-based co-deposited carbon fiber surfaces for enhancement of fiber/epoxy composites. Polym Compos 2020;41:3817–29. https://doi.org/10.1002/pc.25679.

[93] Wu Q, Wan Q, Liu Q, He J, Zhao R, Yang X, et al. Synergistic strengthening and toughening the interphase of composites by constructing alternating “rigid-and-soft” structure on carbon fiber surface. Adv Mater Interfaces 2019;6:1–11. https://doi.org/10.1002/admi.201900970.

[94] Wu Q, Wan Q, Yang X, Wang F, Bai H, Zhu J. Remarkably improved interfacial adhesion of pitch-based carbon fiber composites by constructing a synergistic hybrid network at interphase. Compos Sci Technol 2021;205:108648. https://doi.org/10.1016/j.compscitech.2021.108648.

[95] Liu Y, Ai K, Lu L. Polydopamine and its derivative materials: Synthesis and promising applications in energy, environmental, and biomedical fields. Chem Rev 2014;114:5057–115. https://doi.org/10.1021/cr400407a.

[96] Gao B, Du W, Hao Z, Zhou H, Zou D, Zhang R. Bioinspired modification via green synthesis of mussel-Inspired nanoparticles on carbon fiber surface for advanced

composite materials. ACS Sustain Chem Eng 2019;7:5638–48. https://doi.org/10.1021/acssuschemeng.8b03590.

[97] Lee H, Dellatore SM, Miller WM, Messersmith PB. Mussel-inspired surface chemistry for multifunctional coatings. Science (1979) 2007;318:426–30. https://doi.org/10.1126/SCIENCE.1147241.

[98] Sun N, Zhu B, Gao X, Qiao K, Zhang Y, Wang B, et al. Improved the interfacial characteristics of carbon fiber/polyamide 6 composites by synthesizing polydopamine rapidly on the carbon fiber surface with ultrasound-assisted. Compos Sci Technol 2023;234. https://doi.org/10.1016/j.compscitech.2023.109950.

[99] Chabaud G, Castro M, Denoual C, Le Duigou A. Hygromechanical properties of 3D printed continuous carbon and glass fibre reinforced polyamide composite for outdoor structural applications. Addit Manuf 2019;26:94–105. https://doi.org/10.1016/j.addma.2019.01.005.

[100] Papon EA, Haque A, Mulani SB. Process optimization and stochastic modeling of void contents and mechanical properties in additively manufactured composites. Compos B Eng 2019;177. https://doi.org/10.1016/j.compositesb.2019.107325.

[101] Safari F, Kami A, Abedini V. 3D printing of continuous fiber reinforced composites: A review of the processing, pre- and post-processing effects on mechanical properties. Polymers and Polymer Composites 2022;30. https://doi.org/10.1177/09673911221098734.

[102] Luo H, Tan Y, Zhang F, Zhang J, Tu Y, Cui K. Selectively enhanced 3D printing process and performance analysis of continuous carbon fiber composite material. Materials 2019;12. https://doi.org/10.3390/ma12213529.

[103] Dickson AN, Barry JN, McDonnell KA, Dowling DP. Fabrication of continuous carbon, glass and Kevlar fibre reinforced polymer composites using additive manufacturing. Addit Manuf 2017;16:146–52. https://doi.org/10.1016/j.addma.2017.06.004.

[104] Mohammadizadeh M, Imeri A, Fidan I, Elkelany M. 3D printed fiber reinforced polymer composites - Structural analysis. Compos B Eng 2019;175. https://doi.org/10.1016/j.compositesb.2019.107112.

[105] Yu T, Zhang Z, Song S, Bai Y, Wu D. Tensile and flexural behaviors of additively manufactured continuous carbon fiber-reinforced polymer composites. Compos Struct 2019;225. https://doi.org/10.1016/j.compstruct.2019.111147.

[106] Shang J, Tian X, Luo M, Zhu W, Li D, Qin Y, et al. Controllable inter-line bonding performance and fracture patterns of continuous fiber reinforced composites by sinusoidal-path 3D printing. Compos Sci Technol 2020;192. https://doi.org/10.1016/j.compscitech.2020.108096.

[107] Ueda M, Kishimoto S, Yamawaki M, Matsuzaki R, Todoroki A, Hirano Y, et al. 3D compaction printing of a continuous carbon fiber reinforced thermoplastic. Compos Part A Appl Sci Manuf 2020;137. https://doi.org/10.1016/j.compositesa.2020.105985.

[108] Zhang J, Zhou Z, Zhang F, Tan Y, Tu Y, Yang B. Performance of 3D-printed continuous-carbon-fiber-reinforced plastics with pressure. Materials 2020;13. https://doi.org/10.3390/ma13020471.

[109] Boros R, Kannan Rajamani P, Kovács JG. Combination of 3D printing and injection molding: Overmolding and overprinting. Express Polym Lett 2019;13:889–97. https://doi.org/10.3144/expresspolymlett.2019.77.

[110] Morales U, Esnaola A, Iragi M, Aretxabaleta L, Aurrekoetxea J. Over-3D printing of continuous carbon fibre composites on organo-sheet substrates. AIP Conf Proc, vol. 2113, AIP Publishing; 2019. https://doi.org/10.1063/1.5112520.

[111] Maier J, Vogel C, Lebelt T, Geske V, Behnisch T, Modler N, et al. Adhesion studies during generative hybridization of textile-reinforced thermoplastic composites via additive manufacturing. Materials 2021;14. https://doi.org/10.3390/ma14143888.

[112] Caprais I, Joyot P, Duc E. Bonding between high-performance polymer processed by fused filament fabrication and PEEK/carbon fiber laminate. ESAFORM 2021 - 24th International Conference on Material Forming, 2021. https://doi.org/10.25518/esaform21.2335.

[113] Caprais I, Joyot P, Duc E. Bonding between thermostable polymers processed by FFF and PEEK/carbon fiber laminate. ADDFABCOMP—Additive Fabrication of Composite (2), online conference, 2021, p. 23–4.

[114] Hümbert S, Atzler F, Voggenreiter H. Mechanical characterisation of bond formation during overprinting of PEEK laminates. Materials 2023;17:161. https://doi.org/10.3390/ma17010161.

[115] Chan WS, Vedhagiri S. Analysis of composite bonded/bolted joints used in repairing. J Compos Mater 2001;35:1045–61. https://doi.org/10.1106/9R5D-9G62-YLDA-FU9Y.

[116] Davies P, Courty C, Xanthopoulos N, Mathieu H-J. Surface treatment for adhesive bonding of carbon fibre-poly(etherether ketone) composites. J Mater Sci Lett 1991;10:335–8.

[117] Barroeta Robles J, Dubé M, Hubert P, Yousefpour A. Repair of thermoplastic composites: an overview. Advanced Manufacturing: Polymer and Composites Science 2022;8:68–96. https://doi.org/10.1080/20550340.2022.2057137.

[118] Ageorges C, Ye L, Hou M. Advances in fusion bonding techniques for joining thermoplastic matrix composites: a review. Compos Part A Appl Sci Manuf 2001;32:839–57.

[119] Yousefpour A, Hojjati M, Immarigeon JP. Fusion bonding/welding of thermoplastic composites. Journal of Thermoplastic Composite Materials 2004;17:303–41. https://doi.org/10.1177/0892705704045187.

[120] Zhang H, Yang D, Sheng Y. Performance-driven 3D printing of continuous curved carbon fibre reinforced polymer composites: A preliminary numerical study. Compos B Eng 2018;151:256–64. https://doi.org/10.1016/j.compositesb.2018.06.017.

[121] Zhang H, Dickson AN, Sheng Y, McGrail T, Dowling DP, Wang C, et al. Failure analysis of 3D printed woven composite plates with holes under tensile and shear loading. Compos B Eng 2020;186. https://doi.org/10.1016/j.compositesb.2020.107835.

[122] Zhang H, Zhang K, Li A, Wan L, Robert C, Ó Brádaigh CM, et al. 3D printing of continuous carbon fibre reinforced powder-based epoxy composites. Composites Communications 2022;33. https://doi.org/10.1016/j.coco.2022.101239.

[123] Zhang H, Wang S, Zhang K, Wu J, Li A, Liu J, et al. 3D printing of continuous carbon fibre reinforced polymer composites with optimised structural topology and fibre orientation. Compos Struct 2023;313. https://doi.org/10.1016/j.compstruct.2023.116914.

[124] Zhang H, Wu J, Robert C, Ó Brádaigh CM, Yang D. 3D printing and epoxy-infusion treatment of curved continuous carbon fibre reinforced dual-polymer composites. Compos B Eng 2022;234. https://doi.org/10.1016/j.compositesb.2022.109687.

[125] Blok LG, Longana ML, Yu H, Woods BKS. An investigation into 3D printing of fibre reinforced thermoplastic composites. Addit Manuf 2018;22:176–86. https://doi.org/10.1016/j.addma.2018.04.039.

[126] Geng P, Zhao J, Gao Z, Wu W, Ye W, Li G, et al. Effects of printing parameters on the mechanical properties of high-performance polyphenylene sulfide three-Dimensional printing. 3D Print Addit Manuf 2021;8:33–41. https://doi.org/10.1089/3dp.2020.0052.

[127] Zuo P, Tcharkhtchi A, Shirinbayan M, Fitoussi J, Bakir F. Overall investigation of poly (phenylene sulfide) from synthesis and process to applications—A Review. Macromol Mater Eng 2019;304:1–27. https://doi.org/10.1002/mame.201800686.

[128] McLouth TD, Severino J V., Adams PM, Patel DN, Zaldivar RJ. The impact of print orientation and raster pattern on fracture toughness in additively manufactured ABS. Addit Manuf 2017;18:103–9. https://doi.org/10.1016/j.addma.2017.09.003.

[129] Bhandari S, Lopez-Anido RA, Gardner DJ. Enhancing the interlayer tensile strength of 3D printed short carbon fiber reinforced PETG and PLA composites via annealing. Addit Manuf 2019;30. https://doi.org/10.1016/j.addma.2019.100922.

[130] Love LJ, Kunc V, Rios O, Duty CE, Elliott AM, Post BK, et al. The importance of carbon fiber to polymer additive manufacturing. J Mater Res 2014;29:1893–8. https://doi.org/10.1557/jmr.2014.212.

[131] Van de Werken N, Tekinalp H, Khanbolouki P, Ozcan S, Williams A, Tehrani M. Additively manufactured carbon fiber-reinforced composites: State of the art and

perspective. Addit Manuf 2020;31:100962. https://doi.org/10.1016/j.addma.2019.100962.

[132] Luo W, Liu Q, Li Y, Zhou S, Zou H, Liang M. Enhanced mechanical and tribological properties in polyphenylene sulfide/polytetrafluoroethylene composites reinforced by short carbon fiber. Compos B Eng 2016;91:579–88. https://doi.org/10.1016/j.compositesb.2016.01.036.

[133] Blok LG, Longana ML, Woods BKS. Fabrication and characterisation of aligned discontinuous carbon fibre reinforced thermoplastics as feedstock material for fused filament fabrication. Materials 2020;13:1–26. https://doi.org/10.3390/ma13204671.

[134] Magri A El, Vaudreuil S, Mabrouk K El, Touhami ME. Printing temperature effects on the structural and mechanical performances of 3D printed Poly-(phenylene sulfide) material. IOP Conf Ser Mater Sci Eng, vol. 783, 2020. https://doi.org/10.1088/1757-899X/783/1/012001.

[135] El Magri A, El Mabrouk K, Vaudreuil S, Ebn Touhami M. Experimental investigation and optimization of printing parameters of 3D printed polyphenylene sulfide through response surface methodology. J Appl Polym Sci 2020;138. https://doi.org/10.1002/app.49625.

[136] Slonov A, Musov I, Rzhevskaya E, Zhansitov A, Khashirova S. Investigation of the effect of the length and content of carbon fibers on the properties of polyphenylene sulfide. Key Eng Mater 2020;869:474–80. https://doi.org/10.4028/www.scientific.net/KEM.869.474.

[137] Batista NL, Olivier P, Bernhart G, Rezende MC, Botelho EC. Correlation between degree of crystallinity, morphology and mechanical properties of PPS/carbon fiber

laminates. Materials Research 2016;19:195–201. https://doi.org/10.1590/1980-5373-MR-2015-0453.

[138] Deng S, Hou M, Ye L. Temperature-dependent elastic moduli of epoxies measured by DMA and their correlations to mechanical testing data. Polym Test 2007;26:803–13. https://doi.org/10.1016/j.polymertesting.2007.05.003.

[139] Paciornik S, ́dAlmeida J. Digital microscopy and image analysis applied to composite materials characterization. Revista Materia 2010;15:183–91. https://doi.org/10.1590/s1517-70762010000200013.

[140] Lian D, Zhang R, Lu J, Dai J. Performances and structure changes of neat PPS fiber and nano Ti-SiO2-modified PPS fiber after over-temperature oxidation. High Perform Polym 2018;30:328–38. https://doi.org/10.1177/0954008317696346/FORMAT/EPUB.

[141] Lee S, Kim D-H, Park J-H, Park M, Joh H-I, Ku B-C. Effect of curing poly(p-phenylene sulfide) on thermal properties and crystalline morphologies. Advances in Chemical Engineering and Science 2013;03:145–9. https://doi.org/10.4236/aces.2013.32017.

[142] Wang L, Yu H, Chi Y, Lu A, Liu T, Luo S. Influence of thermal cross-Linking temperature on the crystallization behavior of poly(phenylene sulfide). Advances in Polymer Technology 2015;34. https://doi.org/10.1002/adv.21498.

[143] Scobbo JJ, Hwang CR. Annealing effects in poly (phenylene sulfide) as observed by dynamic mechanical analysis. Polym Eng Sci 1994;34:1744–9.

[144] Liu Y, Zhou X, Wang Z. Effect of isothermal heat treatment on crystallinity, tensile strength and failure mode of CF/PPS laminate. High Perform Polym 2021;33:497–508. https://doi.org/10.1177/0954008320969843.

[145] Fan ZZ, He HW, Yan X, Zhao RH, Long YZ, Ning X. Fabrication of ultrafine PPS fibers with high strength and tenacity via melt electrospinning. Polymers (Basel) 2019;11. https://doi.org/10.3390/polym11030530.

[146] Durani SMA, Khawaja EE, Masoudi HM, Bastl Z, Šubrt J, Galíková A, et al. IR laser ablative desulfurization of poly(1,4-phenylene sulfide). J Anal Appl Pyrolysis 2005;73:145–9. https://doi.org/10.1016/j.jaap.2005.01.005.

[147] Jian L, Tao S. The mechanical and tribological properties of CF/PPS composite filled with PA6. Journal of Thermoplastic Composite Materials 2014;27:594–602. https://doi.org/10.1177/0892705712453152.

[148] Pan S, Shen H, Zhang L. Effect of carbon nanotube on thermal, tribological and mechanical properties of 3D printing polyphenylene sulfide. Addit Manuf 2021;47:102247. https://doi.org/10.1016/j.addma.2021.102247.

[149] Park M, Park JH, Yang BJ, Cho J, Kim SY, Jung I. Enhanced interfacial, electrical, and flexural properties of polyphenylene sulfide composites filled with carbon fibers modified by electrophoretic surface deposition of multi-walled carbon nanotubes. Compos Part A Appl Sci Manuf 2018;109:124–30. https://doi.org/10.1016/j.compositesa.2018.03.005.

[150] Karuppannan Gopalraj S, Kärki T. A review on the recycling of waste carbon fibre/glass fibre-reinforced composites: fibre recovery, properties and life-cycle analysis. SN Appl Sci 2020;2. https://doi.org/10.1007/s42452-020-2195-4.

[151] Pimenta S, Pinho ST. Recycling carbon fibre reinforced polymers for structural applications: Technology review and market outlook. Waste Management 2011;31:378–92. https://doi.org/10.1016/j.wasman.2010.09.019.

[152] Yuan Y, Sun Y, Yan S, Zhao J, Liu S, Zhang M, et al. Multiply fully recyclable carbon fibre reinforced heat-resistant covalent thermosetting advanced composites. Nat Commun 2017;8. https://doi.org/10.1038/ncomms14657.

[153] Hadigheh SA, Wei Y, Kashi S. Optimisation of CFRP composite recycling process based on energy consumption, kinetic behaviour and thermal degradation mechanism of recycled carbon fibre. J Clean Prod 2021;292:125994. https://doi.org/10.1016/j.jclepro.2021.125994.

[154] Tian Z shang, Wang Y qi, Hou X lin. Review of chemical recycling and reuse of carbon fiber reinforced epoxy resin composites. New Carbon Materials 2022;37:1021–41. https://doi.org/10.1016/S1872-5805(22)60652-8.

[155] Chen CH, Chiang CL, Wang JX, Shen MY. A circular economy study on the characterization and thermal properties of thermoplastic composite created using regenerated carbon fiber recycled from waste thermoset CFRP bicycle part as reinforcement. Compos Sci Technol 2022;230. https://doi.org/10.1016/j.compscitech.2022.109761.

[156] Yu B, Jiang Z, Tang XZ, Yue CY, Yang J. Enhanced interphase between epoxy matrix and carbon fiber with carbon nanotube-modified silane coating. Compos Sci Technol 2014;99:131–40. https://doi.org/10.1016/j.compscitech.2014.05.021.

[157] Wang S, Yang Y, Mu Y, Shi J, Cong X, Luan J, et al. Synergy of electrochemical grafting and crosslinkable crystalline sizing agent to enhance the interfacial strength of carbon fiber/PEEK composites. Compos Sci Technol 2021;203:108562. https://doi.org/10.1016/j.compscitech.2020.108562.

[158] Corujeira-Gallo S, Dong H. Effect of microstructure on the plasma surface treatment of carbon fibres. J Compos Mater 2017;51:3239–56. https://doi.org/10.1177/0021998316684935.

[159] Eyckens DJ, Jarvis K, Barlow AJ, Yin Y, Soulsby LC, Athulya Wickramasingha Y, et al. Improving the effects of plasma polymerization on carbon fiber using a surface modification pretreatment. Compos Part A Appl Sci Manuf 2021;143:106319. https://doi.org/10.1016/j.compositesa.2021.106319.

[160] Wu Q, Ye Z, Bai H, Deng H, Xiao B, Zhu J. Two-dimensional polydopamine nano-protrusion-modified graphene oxide encapsulation of cylindrical carbon fiber by vacuum filtration to strengthen the interphase of epoxy composites. Appl Surf Sci 2022;598. https://doi.org/10.1016/j.apsusc.2022.153797.

[161] Wu Q, Xiao B, Liu Q, Deng H, Ye Z, Li Y, et al. New strategy for enhancing interfacial adhesion between carbon fiber and epoxy by using mussel-inspired polydopamine-Fe complex nanospheres. Compos B Eng 2023;266. https://doi.org/10.1016/j.compositesb.2023.111032.

[162] Feinberg H, Hanks TW. Polydopamine: a bioinspired adhesive and surface modification platform. Polym Int 2022;71:578–82. https://doi.org/10.1002/pi.6358.

[163] Ibrahim IAM, Zikry AAF, Sharaf MA, Zikry A. Preparation of spherical silica nanoparticles: Stober silica. Journal of American Science 2010;6:985–9.

[164] Grouve WJB, Akkerman R. Consolidation process model for film stacking glass/PPS laminates. Plastics, Rubber and Composites 2010;39:208–15. https://doi.org/10.1179/174328910X12647080902457.

[165] Ech-Chamikh E, Essafti A, Ijdiyaou Y, Azizan M. XPS study of amorphous carbon nitride (a-C:N) thin films deposited by reactive RF sputtering. Solar Energy Materials and Solar Cells 2006;90:1420–3. https://doi.org/10.1016/j.solmat.2005.10.007.

[166] Yang D, Velamakanni A, Bozoklu G, Park S, Stoller M, Piner RD, et al. Chemical analysis of graphene oxide films after heat and chemical treatments by X-ray photoelectron and Micro-Raman spectroscopy. Carbon N Y 2009;47:145–52. https://doi.org/10.1016/j.carbon.2008.09.045.

[167] Shallenberger JR, Cole DA, Novak SW. Characterization of silicon oxynitride thin films by x-ray photoelectron spectroscopy. Journal of Vacuum Science & Technology A: Vacuum, Surfaces, and Films 1999;17:1086–90. https://doi.org/10.1116/1.582038.

[168] SudarshanRao K. Dynamic mechanical behavior of unfilled and graphite filled carbon epoxy composites. IOP Conf Ser Mater Sci Eng, vol. 1126, IOP Publishing; 2021, p. 012033. https://doi.org/10.1088/1757-899x/1126/1/012033.

[169] Zangmeister RA, Morris TA, Tarlov MJ. Characterization of polydopamine thin films deposited at short times by autoxidation of dopamine. Langmuir 2013;29:8619–28. https://doi.org/10.1021/la400587j.

[170] Dreyer DR, Miller DJ, Freeman BD, Paul DR, Bielawski CW. Elucidating the structure of poly(dopamine). Langmuir 2012;28:6428–35. https://doi.org/10.1021/la204831b.

[171] Panwar K, Jassal M, Agrawal AK. In situ synthesis of Ag-SiO2 Janus particles with epoxy functionality for textile applications. Particuology 2015;19:107–12. https://doi.org/10.1016/j.partic.2014.06.007.

[172] Jiang J, Zhu L, Zhu L, Zhu B, Xu Y. Surface characteristics of a self-polymerized dopamine coating deposited on hydrophobic polymer films. Langmuir 2011;27:14180–7. https://doi.org/10.1021/la202877k.

[173] Wang F, Cai X. Improvement of mechanical properties and thermal conductivity of carbon fiber laminated composites through depositing graphene nanoplatelets on fibers. J Mater Sci 2019;54:3847–62. https://doi.org/10.1007/s10853-018-3097-3.

[174] Zhang Z, Long Y, Yang Z, Fu K, Li Y. An investigation into printing pressure of 3D printed continuous carbon fiber reinforced composites. Compos Part A Appl Sci Manuf 2022;162. https://doi.org/10.1016/j.compositesa.2022.107162.

[175] Xu W, Jambhulkar S, Zhu Y, Ravichandran D, Kakarla M, Vernon B, et al. 3D printing for polymer/particle-based processing: A review. Compos B Eng 2021;223. https://doi.org/10.1016/j.compositesb.2021.109102.

[176] Kumar V, Alwekar SP, Kunc V, Cakmak E, Kishore V, Smith T, et al. High-performance molded composites using additively manufactured preforms with controlled fiber and pore morphology. Addit Manuf 2021;37:101733. https://doi.org/10.1016/j.addma.2020.101733.

[177] Tekinalp HL, Kunc V, Velez-Garcia GM, Duty CE, Love LJ, Naskar AK, et al. Highly oriented carbon fiber-polymer composites via additive manufacturing. Compos Sci Technol 2014;105:144–50. https://doi.org/10.1016/j.compscitech.2014.10.009.

[178] Tambrallimath V, Keshavamurthy R, D S, Koppad PG, Kumar GSP. Thermal behavior of PC-ABS based graphene filled polymer nanocomposite synthesized by FDM process. Composites Communications 2019;15:129–34. https://doi.org/10.1016/j.coco.2019.07.009.

[179] Yin J, Lu C, Fu J, Huang Y, Zheng Y. Interfacial bonding during multi-material fused deposition modeling (FDM) process due to inter-molecular diffusion. Mater Des 2018;150:104–12. https://doi.org/10.1016/j.matdes.2018.04.029.

[180] de Toro EV, Sobrino JC, Martínez AM, Eguía VM, Pérez JA. Investigation of a short carbon fibre-reinforced polyamide and comparison of two manufacturing processes: Fused Deposition Modelling (FDM) and polymer injection moulding (PIM). Materials 2020;13. https://doi.org/10.3390/ma13030672.

[181] Araya-Calvo M, López-Gómez I, Chamberlain-Simon N, León-Salazar JL, Guillén-Girón T, Corrales-Cordero JS, et al. Evaluation of compressive and flexural properties of continuous fiber fabrication additive manufacturing technology. Addit Manuf 2018;22:157–64. https://doi.org/10.1016/j.addma.2018.05.007.

[182] Wu S, Shan Z, Chen K, Liu X, Jiang X, Wang S, et al. Investigation of bending properties of continuous fiber reinforced resin T-beams made by 3D printing. Structures 2023;50:835–41. https://doi.org/10.1016/j.istruc.2023.01.034.

[183] Gao X, Qi S, Kuang X, Su Y, Li J, Wang D. Fused filament fabrication of polymer materials: A review of interlayer bond. Addit Manuf 2021;37. https://doi.org/10.1016/j.addma.2020.101658.

[184] Lyu Y, Koutsos V, Ó Brádaigh CM, Yang D. Improving the interfacial adhesion between recycled carbon fibres and polyphenylene sulphide by bio-inspired dopamine for advanced composites manufacturing. J Clean Prod 2024;449:141855. https://doi.org/10.1016/j.jclepro.2024.141855.

[185] Zhang L, Ren C, Zhou C, Xu H, Jin X. Single fiber push-out characterization of interfacial mechanical properties in unidirectional CVI-C/SiC composites by the nano-

indentation technique. Appl Surf Sci 2015;357:1427–33. https://doi.org/10.1016/j.apsusc.2015.10.018.

[186] Yan MA. Mechanical characterization and fracture behavior of thermosetting and thermoplastic polymer based carbon fiber reinforced composites. 2017.

[187] Sun H, Ren P, Fried JR. The COMPASS force field: parameterization and validation for phosphazenes. Computational and Theoretical Polymer Science 1998;8:229–46.

[188] Yan Y, Xu J, Zhu H, Xu Y, Wang M, Wang B, et al. Molecular dynamics simulation of the interface properties of continuous carbon fiber/ polyimide composites. Appl Surf Sci 2021;563. https://doi.org/10.1016/j.apsusc.2021.150370.

[189] Wang H, Jin K, Wang C, Guo X, Chen Z, Tao J. Effect of fiber surface functionalization on shear behavior at carbon fiber/epoxy interface through molecular dynamics analysis. Compos Part A Appl Sci Manuf 2019;126. https://doi.org/10.1016/j.compositesa.2019.105611.

[190] Jiao W, Zheng T, Liu W, Jiao W, Wang R. Molecular dynamics simulations of the effect of sizing agent on the interface property in carbon fiber reinforced vinyl ester resin composite. Appl Surf Sci 2019;479:1192–9. https://doi.org/10.1016/j.apsusc.2019.02.157.

[191] Jiao W, Hou C, Zhang X, Liu W. Molecular dynamics simulation of the influence of sizing agent on the interfacial properties of sized carbon fiber/vinyl ester resin composite modified by self-migration method. Compos Interfaces 2021;28:445–59. https://doi.org/10.1080/09276440.2020.1788305.

[192] Liebscher J, Mrówczyński R, Scheidt HA, Filip C, Haìdade ND, Turcu R, et al. Structure of polydopamine: A never-ending story? Langmuir 2013;29:10539–48. https://doi.org/10.1021/la4020288.

[193] Zhang W, Wang Z, Lv S, Zhan W, Bai G, Zhou A, et al. Molecular simulation of different structure dopamine-modified graphene oxide and its effects on thermal and mechanical properties of the epoxy resin system. Polymer (Guildf) 2021;212. https://doi.org/10.1016/j.polymer.2020.123120.

[194] Yang P, Sun Y, Li G, Yang X, Zuo X. Tailored rigid-flexible interphase of M40X composites via block copolymers: A combined method of experimental analysis and molecular dynamic simulation. Compos B Eng 2023;257. https://doi.org/10.1016/j.compositesb.2023.110674.

[195] Wang C, He X, Tong L, Peng Q, Wang R, Li Y, et al. Theoretical prediction and experimental verification of pulling carbon nanotubes from carbon fiber prepared by chemical grafting method. Compos Part A Appl Sci Manuf 2013;50:1–10. https://doi.org/10.1016/j.compositesa.2013.03.008.

[196] Wang H, Jin K, Tao J. Improving the interfacial shear strength of carbon fibre and epoxy via mechanical interlocking effect. Compos Sci Technol 2020;200. https://doi.org/10.1016/j.compscitech.2020.108423.

[197] Nardin M, Schultz J. Relationship between fibre-matrix adhesion and the interfacial shear strength in polymer-based composites. Compos Interfaces 1993;1:177–92. https://doi.org/10.1163/156855493x00068.

[198] Weibull W. A statistical distribution function of wide applicability. J Appl Mech 1951.

[199] Naito K, Tanaka Y, Yang JM, Kagawa Y. Tensile properties of ultrahigh strength PAN-based, ultrahigh modulus pitch-based and high ductility pitch-based carbon fibers. Carbon N Y 2008;46:189–95. https://doi.org/10.1016/j.carbon.2007.11.001.

[200] Almushaikeh AM, Alaswad SO, Alsuhybani MS, AlOtaibi BM, Alarifi IM, Alqahtani NB, et al. Manufacturing of carbon fiber reinforced thermoplastics and its recovery of carbon fiber: A review. Polym Test 2023;122. https://doi.org/10.1016/j.polymertesting.2023.108029.

[201] Ge J, Catalanotti G, Falzon BG, Higgins C, McClory C, Thiebot J-A, et al. Process characteristics, damage mechanisms and challenges in machining of fibre reinforced thermoplastic polymer (FRTP) composites: A review. Compos B Eng 2024;273:111247. https://doi.org/10.1016/j.compositesb.2024.111247.

[202] Nishida H, Carvelli V, Fujii T, Okubo K. Quasi-static and fatigue performance of carbon fibre reinforced highly polymerized thermoplastic epoxy. Compos B Eng 2018;144:163–70. https://doi.org/10.1016/j.compositesb.2018.03.002.

[203] Carvelli V, Nishida H, Fujii T, Okubo K. Low velocity impact and CAI of woven carbon fibre reinforced highly polymerized thermoplastic epoxy modified with submicron diameter glass fibres. Compos Struct 2020;236. https://doi.org/10.1016/j.compstruct.2019.111835.

[204] Zhou W, Ji X long, Yang S, Liu J, Ma L hua. Review on the performance improvements and non-destructive testing of patches repaired composites. Compos Struct 2021;263. https://doi.org/10.1016/j.compstruct.2021.113659.

[205] Zhang H, Chen J, Yang D. Fibre misalignment and breakage in 3D printing of continuous carbon fibre reinforced thermoplastic composites. Addit Manuf 2021;38. https://doi.org/10.1016/j.addma.2020.101775.

[206] Lyu Y, Wu J, Zhang H, Brádaigh CMÓ, Yang D. Effects of thermal process conditions on crystallinity and mechanical properties in material extrusion additive manufacturing of discontinuous carbon fibre reinforced polyphenylene sulphide composites. J Compos Mater 2023. https://doi.org/10.1177/00219983231194391.

[207] Caminero MA, Lopez-Pedrosa M, Pinna C, Soutis C. Damage monitoring and analysis of composite laminates with an open hole and adhesively bonded repairs using digital image correlation. Compos B Eng 2013;53:76–91. https://doi.org/10.1016/j.compositesb.2013.04.050.

[208] Caminero MA, Pavlopoulou S, Lopez-Pedrosa M, Nicolaisson BG, Pinna C, Soutis C. Analysis of adhesively bonded repairs in composites: Damage detection and prognosis. Compos Struct 2013;95:500–17. https://doi.org/10.1016/j.compstruct.2012.07.028.

[209] Arhant M, Le Gac PY, Le Gall M, Burtin C, Briançon C, Davies P. Effect of sea water and humidity on the tensile and compressive properties of carbon-polyamide 6 laminates. Compos Part A Appl Sci Manuf 2016;91:250–61. https://doi.org/10.1016/j.compositesa.2016.10.012.

[210] Ali Kouka M, Abbassi F, Demiral M, Ahmad F, Soula M, Al Housni F. Behaviour of woven-ply PPS thermoplastic laminates with interacting circular holes under tensile loading: An experimental and numerical study. Eng Fract Mech 2021;251. https://doi.org/10.1016/j.engfracmech.2021.107802.